Faculty of Science and Engineering

WA School of Mines: Minerals, Energy and Chemical Engineering

Department of Petroleum Engineering

Gas Hydrates Investigation: Flow Assurance for Gas Production and Effects on Hydrate-bearing Sediments

Dhifaf Jaafar Sadeq

This thesis is presented for the Degree of
Doctor of Philosophy
of
Curtin University

November 2018

DECLARATION OF ACADEMIC INTEGRITY

To the best of my knowledge and belief, this thesis contains no material previously published by any other person except where due acknowledgment has been made.

This thesis contains no material, which has been accepted for the award of any other degree or diploma in any university.

Signature:

Date: 07/11/2018

COPYRIGHT

I warrant that I have obtained, where necessary, permission from the copyright owners to use any third-party copyright material reproduced in the thesis (e.g. questionnaires, artwork, unpublished letters), or to use any of my own published work (e.g. journal articles) in which the copyright is held by another party (e.g. publisher, co-author).

Signature:

Date: 07/11/2018

DEDICATION

I would like to dedicate my thesis to the memory of my father, Jaafar Sadeq who would have been proud to see me follow his way as an educated person

To my dear mother, for her encouragement, sincere wishes and her prayers

To my lovely husband Omar and my children Maryam and Jaafar who have supported me and believed that I would do it

To my brothers and all family members for their love and support

ACKNOWLEDGMENTS

ABSTRACT

In recent years, the importance of gas hydrates has significantly increased because of their role as the main flow assurance problem in the oil and gas industry and as a potential energy resource. In addition, carbon dioxide capture geo-sequestration into sediments in the form of gas hydrates has been proposed as a promising approach to reduce anthropogenic greenhouse gas emissions. In this context, gas hydrates formation/dissociation in bulk and porous media have been evaluated. Thus, the work presented in this thesis constitutes three main parts, all related to gas hydrates. In the first part, we examined the formation and dissociation of different gas mixtures containing methane, carbon dioxide and nitrogen in bulk. Hydrate equilibrium data were measured using a stirred cryogenic sapphire cell together with recording of the motor current changes during the hydrate formation/dissociation process. The results showed that the hydrate equilibrium conditions vary depending on the composition of the mixtures. The van der Waals-Platteeuw thermodynamic theory coupled with the Peng-Robinson equation of state and the Langmuir adsorption model were used to correlate the hydrate equilibrium data. The calculated values were compared with the obtained experimental results and discussed in terms of cage occupancies and the possibility of structural transformation. A new empirical correlation for the prediction of gas hydrate equilibrium temperatures was developed, which showed a good agreement with the experimental measurements.

In the second part, the effects of hydrate formation on the compressional wave velocities of sandstone were investigated experimentally. Hydrate was formed using tetrahydrofuran (THF, as a liquid hydrate former) through CO_2 injection into partially brine-saturated sandstone. Noticeable differences were recorded due to hydrate formation in sandstone. The behaviour and interaction of both hydrates (THF and CO_2) with the host sediments are discussed focusing on the effect of different pore space fillings on the measured acoustic velocities.

In the last part, we imaged the distribution of CO_2 hydrate in sandstone, and investigated the hydrate morphology and cluster characteristics via X-ray micro-computed tomography at high resolution in 3D in-situ. A substantial amount of gas hydrate (~17% saturation) was observed, and the stochastically distributed hydrate clusters followed power-law relations in terms of their size distributions and surface

area-volume relationships. These fundamental insights will aid large-scale implementation of industrial carbon dioxide geo-sequestration projects via the hydrate route.

PUBLICATIONS

Journal Publications

1. **Sadeq, D.**, Iglauer, S., Lebedev, M., Smith, C., and Barifcani, A. (2017) "Experimental determination of hydrate phase equilibrium for different gas mixtures containing methane, carbon dioxide and nitrogen with motor current measurements", *Journal of Natural Gas Science and Engineering*, 38, 59-73. (https://doi.org/10.1016/j.jngse.2016.12.025)

2. **Sadeq, D.**, Iglauer, S., Lebedev, M., Rahman, T., Zhang, Y. and Barifcani, A. (2018) "Experimental Pore-scale Analysis of Carbon Dioxide Hydrate in Sandstone via X-Ray Micro-Computed Tomography", *International Journal of Greenhouse Gas Control*, 79, 73-82. (https://doi.org/10.1016/j.ijggc.2018.10.006)

3. **Sadeq, D.**, Alef, K., Iglauer, S., Lebedev, M. and Barifcani, A. (2018) "Compressional Wave Velocity of Hydrate-Bearing Bentheimer Sediments with Varying Pore Fillings", *International Journal of Hydrogen Energy,* 43(52), 23193-23200. (doi.org/10.1016/j.ijhydene.2018.10.169)

Conferences Publications

1. **Sadeq, D.**, Iglauer, S., Lebedev, M., Smith, C., and Barifcani, A. (2017) "Hydrate Equilibrium Model and Cage Occupancies for $N_2 + CH_4$ and $N_2 + CO_2$ Gas Mixtures", One Curtin International Postgraduate Conference, At Miri, Sarawak, Malaysia, 10-12 December.

2. **Sadeq, D.**, Iglauer, S., Lebedev, M. and Barifcani, A. (2018) "Prediction of Hydrate Phase Equilibrium Conditions for Different Gas Mixtures", Offshore Technology Conference Asia held in Kuala Lumpur, Malaysia, 20-23 March 2018.

NOMENCLATURE

N_2 Nitrogen gas

CH_4 Methane gas

CO_2 Carbon dioxide gas

THF   Tetrahydrofuran

Q_1 Lower quadruple point

Q_2 Upper quadruple point

LNG   Liquefied natural gas

HFZ   Hydrate formation zone

GHSZ Gas hydrate stability zone

R_o Resistivity of the water saturation sediments

R_t Resistivity of hydrate-bearing sediments

NMR   Nuclear Magnetic Resonance

MRI   Magnetic resonance imaging

μCT   Micro-computed tomography

NaCl   Sodium chloride

NaI   Sodium iodine

DI   Deionized

MEG   Mono-ethylene glycol

V_p Compressional wave velocity

V_s	Shear velocity
ρ	Density
K	Bulk modulus
P	Pressure (or equilibrium pressure)
T	Temperature (or equilibrium temperature)
n	Number of moles or number of data points
m	Mass
M_i	Molecular weight
V	Vapour or volume
I	Ice
μ	Chemical potential or shear modulus
C	Langmuir adsorption constant
f	Fugacity
θ	The fractional occupancy of each hydrate former
k	Boltzmann constant
r	Distance between the guest molecule and the centre of the cavity
R	Radius of cavities
a	Kihara Potential Parameter or Klein-Nishina coefficient
σ	Kihara Potential Parameter
e	Kihara Potential Parameter

A, B   Salufu correlation constants

a_1 to a_5 Coefficient values of the new correlation

Sg   Gas specific gravity

R^2 Squared correlation coefficient

AAPE Average absolute percentage error

AAD   Average absolute deviation

SD   Standard deviation

RMS   Root mean square errors

μ_x X-ray mass attenuation coefficient

ρ_b Bulk density

Z   effective atomic number

E   Energy beam

Superscripts

H   Hydrate

L   Liquid

W   Water

HC   Liquid hydrocarbon

β Hypothetical empty hydrate lattice

i   Gas component

j   Cavity type

s   Small cavities

l   Large cavities

exp   Experimental data

cal   Calculated data

μ_x X-ray mass attenuation coefficient

TABLE OF CONTENTS

LIST OF FIGURES

LIST OF TABLES

Chapter 1   Introduction

1.1   Introduction

Natural gas hydrates in the petroleum and gas industry often have negative connotations as they are most commonly encountered in their bulk form as a flow assurance problem. Gas hydrate formation is responsible for obstructing flow lines and gas production equipment which poses catastrophic economic and safety risks. The oil and gas industry spends millions of dollars each day on inhibiting and preventing unwanted gas hydrates (Max et al. 2005). Once hydrate blockage has occurred, safe dissociation could take weeks or even months with complicated operations required to remove the blockage (Kelkar et al. 1998).

Extensive research projects have been performed for better mitigating the complications caused by hydrate formation. Figure 1-1 shows the growing number of gas hydrate-related publications over the past 20 years and demonstrates the increasing interest in gas hydrate research.
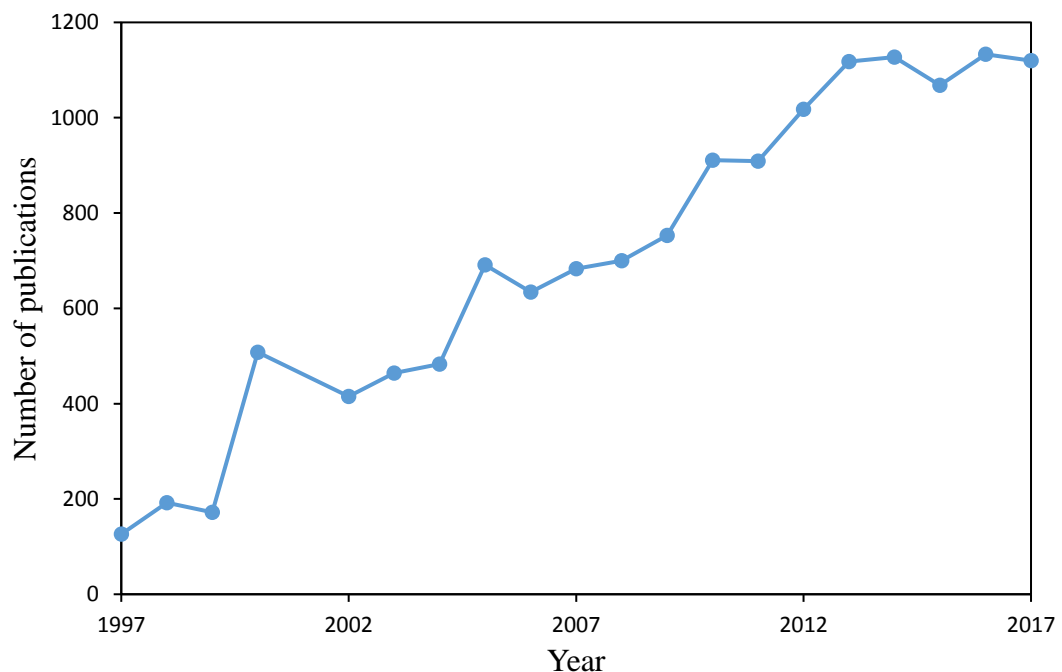
Figure 1-1 Gas hydrate-related publications over the past 20 years (Library catalogue database, Curtin University)

Attention is now growing towards the potentially huge energy resource stored in the naturally occurring hydrate deposits. Because of their ability to concentrate and store gases, the estimated reserves of methane stored in natural gas hydrate deposits are vast and huge (Kvenvolden 1988), which exceeds the entire combined world reserves of oil, natural gas and coal (Makogon et al. 2007, Moridis 2008), as shown comparatively in the resource triangle in Figure 1-2. Simultaneously, the demand for energy sources (e.g. for natural gas) is increasing (Dudley 2013, Al-Fatlawi et al. 2017) especially in countries who are heavily dependent on energy imports due to the lack of their own natural resources, such as China, Japan, and India (Takeishi 2014). Therefore, the oil and gas industry is now looking towards commercial production of gas from hydrate-bearing sediments, and preferably to combine this process with the sequestration of carbon dioxide. The importance of hydrate as a prospective source of energy has been estimated by identifying the distribution and concentration of hydrates in their host sediments (Priest et al. 2009). The occurrence of gas hydrates can be detected using seismic surveys and well-logging data (Jones et al. 2008), which must to be calibrated using laboratory acoustic velocity measurements.
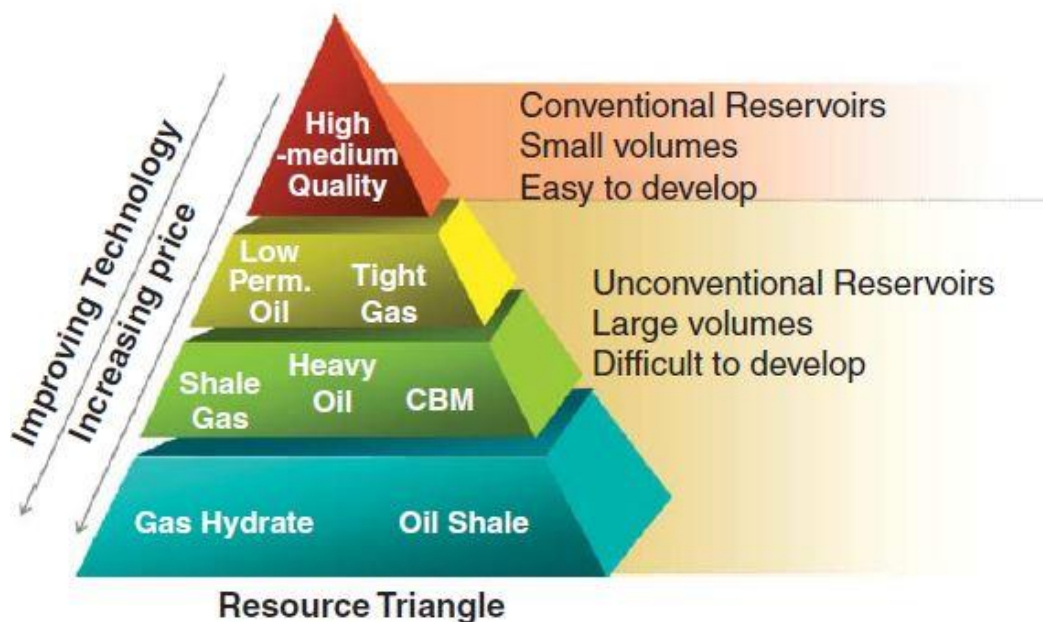
Figure 1-2 Relative volumes of hydrocarbon resources (Dong et al. 2012)

Gas hydrate formation in porous media is of essential importance for understanding the properties of the hydrate-bearing sediments and for its potential role in seafloor stability, drilling hazard, and mitigating climate changes by decreasing CO_2 emissions. Because of the metastable behaviour of natural gas hydrates, the description of their in-situ occurrence via the retrieved real samples has been a challenge. Maintaining the actual equilibrium temperature and pressure is not feasible due to the possibility of hydrate dissociation during core sample recovery. Thus, gas hydrate occurrence and distribution in sedimentary matrices is still not sufficiently explained, and thus their microstructures and morphology remain unclear.

1.2   Thesis Scope and Objectives

Research relating to gas hydrates in bulk and sediments is of the utmost importance to the energy industry. Gas hydrates have been identified as a flow assurance problem that threaten natural gas production facilities and transport pipelines causing high economic losses and safety risks. Therefore, an accurate measurement and estimation of gas hydrate equilibrium conditions for different gas mixtures is of significant importance to avoid these transport complications. In contrast, gas hydrate has been proposed as a promising energy source (Chong et al. 2015). Thus, the increasing demand for energy resources (e.g. for natural gas) encourages the research on the production of natural gas (the main gas here is methane) from hydrate deposits.

Simultaneously, CO_2 emissions into the atmosphere have increased significantly (Pachauri et al. 2014), which has led to increasing global temperatures (global warming) and thus climate change (Houghton et al., 2001). Thus, decreasing the level of CO_2 emissions is essential for mitigating climate change. One solution suggested for achieving this is to capture and sequester CO_2 in the form of gas hydrates (Orr, 2009; White et al., 2003; Yamasaki, 2003). This process may be combined with methane production via CO_2-CH_4 replacement in methane hydrate-bearing sediments (Ohgaki et al. 1994, Graue et al. 2008). In addition, hydrate morphology, distribution and saturation in a porous medium significantly affect seismic velocities (compressional and shear velocities) and other petro-physical properties (Waite et al. 2009).

3

Consequently, the pore-scale characterisation of hydrates in their host sediments and knowledge of their physical properties are vitally essential for exploration, monitoring, implementation of hydrate-carbon dioxide geo-sequestration (CGS) and hydrate exploitation as an energy source. However, experimental data for hydrate formation and existence in bulk and sediments is limited despite their vital importance (Tohidi et al. 2010, Ta et al. 2015).

The main aim of this research study was to establish a good fundamental understanding of gas hydrate formation/dissociation, quantification and detection in bulk and porous media. The following points describe the specific objectives of this research:

1. Obtaining new experimental data of gas hydrate formation from various gas mixtures and investigating the effect of each gas composition on gas hydrate equilibrium conditions.
2. Developing a thermodynamic model and empirical correlation for the prediction of gas hydrate equilibrium conditions.
3. Investigating the distribution and morphology of gas hydrate in sandstone samples via X-ray micro-computed tomography in 3D in-situ and analysing the corresponding hydrate microstructures.
4. Studying the effect of pore volume and hydrate saturation on the acoustic velocity of the hydrate-bearing sediments.

1.3   Structure of the Thesis

The structure of the presented thesis comprises eight chapters, including the introduction, an extensive literature review, results and discussion (experimental and computational studies), conclusions and recommendations. The structural framework of the thesis is presented in Figure 1-3.

Chapter 1 – Introduction provides a summarised introduction of the background and general issues encountered with solutions regarding gas hydrate formation in bulk and sediments. This chapter also includes the research scope, objectives and thesis structure.

Chapter 2 – Literature Review presents a comprehensive review and basic knowledge of the various aspects of gas hydrates including the historical background, structure

and thermodynamics of hydrate formation, gas hydrate applications, natural occurrence of hydrate and hydrate in sediments.

Chapter 3 – Experimental Methods outlines the experimental systems, procedures and materials used to achieve the aims and objectives of the study.

Chapter 4 – Experimental Determination of Hydrate Phase Equilibrium for Different Gas Mixtures Containing Methane, Carbon Dioxide and Nitrogen with Motor Current Measurements. Journal of Natural Gas Science and Engineering, 38, 59-73 measures gas hydrate equilibrium conditions for different gas mixtures using PVT cryogenic sapphire cell and assesses the motor current as a criterion for gas hydrate formation and dissociation.

Chapter 5 – Thermodynamic Modelling and Empirical Correlation for the Prediction of Gas Hydrate Equilibrium Conditions. OCPC-RE0023-2017 and OTC-28478-MS develops a thermodynamic model and empirical correlation for the prediction of gas hydrate equilibrium conditions.

Chapter 6 – Experimental Pore-scale Analysis of Carbon Dioxide Hydrate in Sandstone via X-Ray Micro-Computed Tomography. International Journal of Greenhouse Control, 79, 73-82 shows imaged CO_2 hydrate distribution in sandstone, and investigates the hydrate morphology and cluster characteristics via X-ray micro-computed tomography in 3D in-situ.

Chapter 7 – Ultrasonic Measurements of Hydrate-bearing Sandstone. Accepted in the International Journal of Hydrogen Energy measures the compressional wave velocity (P-wave velocity) of consolidated sediments (sandstone) with and without tetrahydrofuran and carbon dioxide hydrate-bearing pore fillings using the pulse transmission method.

Chapter 8 – Conclusions and Recommendations presents complete conclusions with significant results from this thesis and provides recommendations for potential future work.

Thesis Outline

Gas hydrates investigation: Flow assurance for gas production and effects on hydrate-bearing sediments

Chapter 1
Introduction

1.1 Introduction
1.2 Thesis Objectives and Scope
1.3 Structure of the Thesis

Chapter 2
Literature review

2.1 Historical Background of Gas Hydrate   2.2 Gas Hydrate Structures and Properties
2.3 Thermodynamics of Hydrate Formation and Equilibrium
2.4 Gas Hydrates Formation and Dissociation
2.5 Application of Gas Hydrates (Importance of Gas Hydrates)   2.6 Gas Hydrate Occurrence in Nature
2.7 Hydrates in Sediments

Chapter 3
Experimental Methods

3.1 PVT Cryogenic Sapphire Cell for Determination Equilibrium Conditions of CH_4+CO_2, CH_4+N_2, CO_2+N_2 Hydrates
3.2 Ultrasonic Measurement System for Determination Compressional Wave Velocities of Hydrate-bearing Sediments
3.3 X-Ray Micro Computed- CO_2 Hydrate formation system for analysing pore-scale of Hydrate in Sandstone

Chapter 4
Experimental Determination of Hydrate Phase Equilibrium for Different Gas Mixtures Containing Methane, Carbon Dioxide and Nitrogen with Motor Current Measurements

4.1 Chapter Summary   4.2 Introduction
4.3 Experimental methodology: 4.3.1 Materials and gas preparation
4.3.2 Experimental apparatus and procedure
4.4 Results and discussion: 4.4.1 Gas hydrate equilibrium conditions
4.4.2 Current as an indication of hydrate plug and dissociation

4.5 Conclusion

Chapter 5
Thermodynamic modelling and Empirical correlation for prediction gas hydrate equilibrium conditions

5.1 Chapter Summary 5.2 Introduction
5.3 Methodology: 5.3.1 Theoretical model prediction
5.3.2 Empirical correlation Prediction
5.4 Results and discussion: 5.4.1 Theoretical model prediction
5.4.2 Empirical correlation Prediction

5.5 Conclusion

Chapter 6
Experimental Pore-scale Analysis of Carbon Dioxide Hydrate in Sandstone via X-Ray Micro-Computed Tomography

6.1 Chapter Summary   6.2 Introduction
6.3 Experimental methodology: 6.3.1 Materials and Experimental Set-up   6.3.2 Experimental Procedure
6.4 Results and discussion: 6.4.1 Visualization and Morphology of CO_2 Hydrate   6.4.2 Hydrate Saturation in the Core Sample   6.4.3 Gas Hydrate Statistics - Cluster Size Distributions and Surface Area-Volume Relationships

6.5 Conclusion

Chapter 7
Ultrasonic measurements of hydrate-bearing sandstone

7.1 Chapter Summary   7.2 Introduction   7.3 Experimental methodology
7.4 Results and discussion: 7.4.1 THF hydrate in sandstone   7.4.2 CO_2 hydrate in sandstone

7.5 Conclusion

Chapter 8
Conclusions and Recommendations
8.1 Conclusions
8.2 Recommendations

Figure 1-3 Structural framework of thesis

Chapter 2   Literature Review

This chapter presents the basic knowledge related to gas hydrates concentrating on the aspects related to this research work. A brief historical background involving hydrate discovery and the important steps in the development of gas hydrates research are presented in section 2.1. The description of different hydrate structures and some properties of gas hydrate are summarized in section 2.2. Thermodynamics of hydrate formation and dissociation are presented in section 2.3. The gas hydrates importance and applications are discussed in section 2.5. The natural occurrence of hydrates in sediments are discussed regarding the gas hydrates morphology, their effects on the physical properties of gas hydrate deposits and the visual observation of hydrates in their host sediments are presented in sections 2.6 and 2.7.

2.1   Historical Background of Gas Hydrates

Gas hydrates (clathrate hydrates) are solid ice-like, non-stoichiometry crystalline structures that exist naturally in the presence of water and certain guest (gas or liquid) molecules such as methane, carbon dioxide, nitrogen, ethane, propane or butane for gases (Sloan and Koh 2008), and ethylene oxide and tetrahydrofuran (THF) for liquids (Koh 2002). Gas hydrates are typically formed and are stable under elevated pressure conditions at temperatures above the freezing point of water and up to 25 °C if hydrate former molecules (i.e. gas or liquid) and sufficient amounts of water are available (Sloan and Koh 2008). The water molecules are known as "cage" whereas the hydrate former molecules are called "guest". Figure 2-1 shows the ice-like appearance of methane hydrate.

Figure 2-1 Ice-like appearance of methane hydrate; after (Giavarini and Hester 2011)

Historically, the first observation of gas hydrates was made by Joseph Priestley in 1778 while he was bubbling sulfur dioxide (SO_2) through water at low room temperature and atmospheric pressure (Koh 2002). This discovery was the first identification of gas hydrates; however, it was not officially documented until 1810 when Sir Humphrey Davy noticed a similar crystal structure, now called gas hydrates while he was working with chlorine mixtures (Faraday and Davy 1823). The hydrocarbon hydrates were proven in 1888 by Villard (1896) who discovered several hydrocarbon gases that formed hydrates such as methane, ethane and propane. By the end of the century, many researchers had studied gas hydrates particularly in terms of their discovery and observation of hydrates of various gases (Roozeboom 1885, Villard 1888, Pickering 1893, Villard 1896). The industrial importance of gas hydrates was established in 1934 due to the discovery that the formation of hydrates was responsible for plugging gas-transmission pipelines (Hammerschmidt 1934).

Since then, a considerable amount of research has been focused on studying the formation conditions, composition, kinetics and structures of gas hydrates to inhibit and prevent the blockage of pipelines. Extensive efforts in this area have demonstrated how to manage flow assurance issues and to consider the initial applications of gas hydrate inhibitors. The next era of the history of gas hydrate studies begun in the 1960s when the first occurrence of natural gas hydrates was discovered in Siberia (Makogon

8

1997). Since then, gas hydrates have been highlighted as a potential energy resource and prospective fuel reserves. This important discovery pushed researchers towards studying the formation and dissociation kinetics in their natural environments and interactions with their host sediments to investigate the possibility of the safe production of gas hydrate. Later, it was found that gas hydrate formation required specific thermodynamic conditions (i.e. high pressure and low temperature) that widely exist in many regions worldwide such as in oceanic sediments and permafrost area (Kvenvolden 1998, Kvenvolden and Rogers 2005). Recently, extensive research on gas hydrates has been conducted to investigate the potential production of natural gas hydrates. Many countries such as Japan, Canada, the United States and India have started to fund programs for commercial gas production from gas hydrate-bearing sediments (Lu 2015). The progress and development stages of research on gas hydrates are outlined in Table 2-1.

Table 2-1 The progress and development of gas hydrates research since 1778

Year	Source	Achievements
1778	Priestly (1778)	Discovery of SO_2 hydrate
1810	Davy (1811)	Chlorine (Cl_2) hydrate determination
1823	Faraday and Davy (1823)	Chlorine (CI_2) hydrate formula inference as $Cl_2.10H_2O$
1828	Löwig (1828)	Discovery of bromine hydrates
1829	De la Rive (1829)	Inference of SO_2 hydrates formula as $SO_2.7H_2O$
1856	Berthelot (1856)	First formation of organic hydrates
1882	Wróblewski (1882)	CO_2 hydrate reported
1882	Cailletet and Bordet (1882)	CO_2+PH_3 and H_2S+PH_3 mixed hydrate system formation
1888 1890	Villard (1888) Villard (1890)	Hydrates of methane, ethane, ethylene, acetylene, nitrous oxide and propane hydrate discovered
1896	Villard (1896)	Nitrogen and oxygen proposed as hydrate formers

Year	Source	Achievements
1897	de Forcrand and Thomas (1897)	Exploring hydrates of several halohydrocarbons found mixed with acetylene, carbon dioxide and ethane
1902	De Forcrand (1902)	Utilisation of Clausius-Claypeyron equation for the first time to estimate gas hydrate enthalpies and compositions
1925	De Forcrand (1925)	Discovery and measurement of xenon hydrates
1934	Hammerschmidt (1934)	Detection that the formation of natural gas hydrates in transmission lines was responsible for pipeline blockages
1940	Fowler et al. (1940)	Identification of semi-clathrate hydrates of tetra alkylammonium salts
1941	Wilcox et al. (1941)	Development of the K-factor charts for predicting hydrate formation conditions.
1942	Benesh (1942)	Using gas hydrates for the first time as a means for gas storage and transportation
1946	Deaton and Frost Jr (1946)	Presenting summarised data on gas hydrates and providing methods for their prevention
1946	Strizhov and Khodanovich (1946)	Initial prediction of the potential presence of natural hydrate deposits
1949	Unruh and Katz (1949)	Three phase (L-H-V) hydrate data for CH_4-CO_2 reported
1954	Von Stackelberg (1954)	Identification of sI and sII hydrate structures using X-ray diffraction
1957	(Barrer and Stuart 1957)	Development of a statistical approach for determining the properties of gas hydrates
1959	van der Waals and Platteeuw (1959)	Statistical thermodynamic model depending on structure was proposed for calculating hydrate equilibrium conditions
1965	Saito and Kobayashi (1965)	Applying the van der Waals-Platteeuw theory to mixtures

Year	Source	Achievements
1965	Makogon (1965)	First observation of in-situ natural gas hydrates in permafrost regions
1969	Ginsburg (1969)	Hydrates in geology studied for the first time
1972	Parrish and Prausnitz (1972)	Applying van der Waals-Platteeuw theory to natural gas hydrates and mixed hydrates
1972	ARCO–Exxon	First successful attempt to recover core samples containing hydrates from an Alaskan well on the North Slope
1974	Claypool and Kaplan (1974)	Confirmation that gas hydrates exist naturally in deep sea and shallow marine environments
1976	Ng and Robinson (1976)	Performing measurements on two-phase hydrate equilibrium conditions, three-phase, and four-phase liquid hydrocarbons
1980	Kvenvolden and McMenamin (1980)	Publishing a geological survey of worldwide gas hydrate distribution
1984	Handa et al. (1984)	Employing a temperature-scanning calorimeter to investigate the thermal properties of gas hydrates
1985	John et al. (1985)	Extending the van der Waals-Platteeuw theory based on higher order coordination of hydrate water shells
1987	Ripmeester et al. (1987)	Discovery of new hydrate structure (sH)
1988	(Kvenvolden 1988)	Estimation of the volume of gas within gas hydrates to be $\sim 10^{16}$ m^3
1994	Mehta and Sloan Jr (1994)	First reporting of sH hydrate equilibria formed from methane and liquid hydrocarbon system.
1994	Mehta and Dendy Sloan (1994)	Applying van der Waals-Platteeuw theory to the mixtures containing methane and larger molecules
1996	Sum et al. (1997)	Measurements of the hydration number and hydrate composition using Raman spectroscopy

Year	Source	Achievements
1997	Kuhs et al. (1997)	Double occupancy of N_2 molecules was reported for the first time in the large cages of sII gas hydrate using neutron diffraction
1997	Udachin et al. (1997)	First X-ray diffraction study reported for sH hydrate structure
1999	Dyadin et al. (1999)	Discovery that H_2 and neon gases can form hydrates at conditions of elevated pressure (~ 1.5 GPa)
2000	Kang and Lee (2000)	Proposal of new process for the recovery of CO_2 using gas hydrate
2000	Uchida et al. (2000)	Confirming the occurrence of natural gas hydrates below the permafrost region by imaging the first hydrate sample recovered from Mallik 2L-28 well using the X-ray CT.
2004	Camargo et al. (2004)	"Cold flow" technique introduced to prevent gas hydrate blockage in flowlines.
2006	Hester et al. (2007)	First measurement of oceanic gas hydrates using Raman spectrometer at Vancouver Island
2006	Collett et al. (2008)	Collecting of 493 hydrate core samples during the first Expedition of the Indian National Gas Hydrate Program
2011-2012	Boswell et al. (2014)	Testing the production of methane from hydrates via CO_2-CH_4 exchange
2013	Yamamoto et al. (2014)	Conducting the first attempt for methane production from hydrate deposits in Japan via the depressurisation technique

2.2   Gas Hydrate Structures and Properties

Clathrate hydrates are fundamentally composed of two components; guest molecules (typically gas or liquid) and host molecules (water). The term clathrate hydrates is generated from the Latin origin word *clatratus*, meaning latticed or encaged. When the guest molecules and host molecules exist together under elevated pressure and low temperature, the hydrogen-bonded water molecules tend to organise themselves in frameworks of polyhedral structures surrounding the small gas molecules (Figure 2-2). The water molecules create a structure "cage" that contain the gas molecules. The resulting structures (non-stoichiometric ice-like components) are known as gas hydrates or gas clathrates. Within the crystalline structure, there are no chemical bonds occurring between the water molecules (cage) and the gas molecule whose diameter is normally less than that of the cage diameter. Figure 2-3 shows the five different types of hydrate cages that are the pentagonal dodecahedron (5^{12}), tetrakaidecahedron ($5^{12}6^2$), hexakaidecahedron ($5^{12}6^4$), irregular dodecahedron ($4^35^66^3$) and icosahedron ($5^{12}6^8$) (Sloan and Koh 2008). Those cavities become stabilised when they are filled with gas molecules within the hydrate structure (Tse et al. 1993).
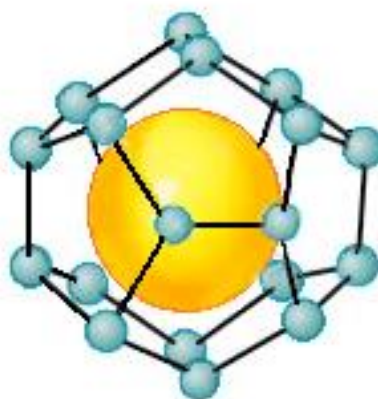
Figure 2-2 A stabilising gas molecule (yellow ball) enclosed by a framework of water molecules

5^{12} $5^{12}6^2$ $5^{12}6^4$ $5^{12}6^8$ $4^3 5^6 6^3$
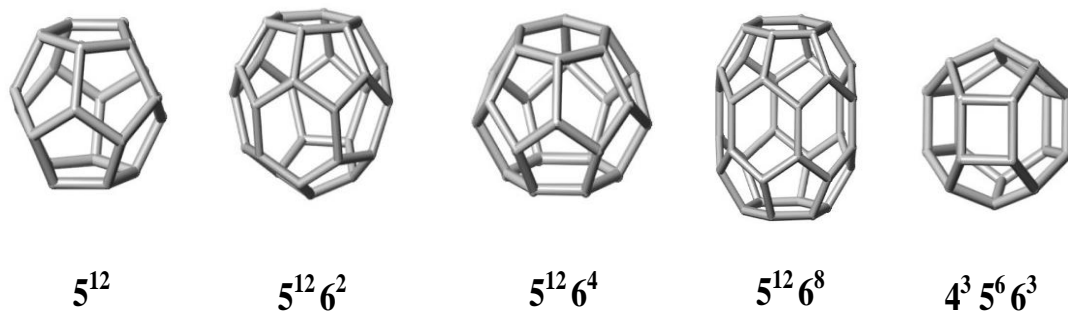
Figure 2-3 Various types of natural gas hydrate cages (adapted from Koh and Sloan 2007)

The experimental observation of gas hydrate and ice has revealed that there are several distinct differences between them regarding the chemical and physical properties even though they have almost the same appearance (Koh and Sloan 2007). However, the most distinct property is that hydrate could be stable at a temperature greater than the freezing point of water. In addition, hydrate submerges in water due to its higher density whereas ice floats on water (Giavarini and Hester 2011). Furthermore, unlike ice, the stored gases in the form of hydrates can be flammable when exposed to an excessive heat source (Figure 2-4) (Suess et al. 1999).

Figure 2-4 Flame of gas hydrate (methane) (Suess et al. 1999)

Generally, the majority of hydrates exist in three distinct structures depending on the size of the guest molecules (Sloan and Koh 2008). To date, three different crystal structures have been identified in natural hydrates as follows: cubic structure I (sI), cubic structureII (sII) and hexagonal structure (sH). First, von Stackelberg and Müller (1954) identified the sI and sII structures using the X-ray diffraction testing methods conducted at Bonn University. The third hydrate structure, sH was discovered later by Ripmeester et al. (1987) using magnetic resonance imaging and X-ray powder diffraction techniques. Small guest molecules (size range 0.4–0.550 nm, e.g. methane, ethane, hydrogen sulfide and carbon dioxide) form sI hydrate. sII hydrate is generally formed from larger guest molecules of sizes ranging from 0.6 to 0.7 nm, for instance, propane and isobutane (Sloan 2003). sH gas hydrates can be formed from both large and small guest molecules (size range 0.8–0.9 nm). Methane and some additives including THF and cycloheptane are examples of sH hydrates formers (Sloan 2003). These types of hydrate exhibit structural transitions between different structures (Sloan 2003). Details of each hydrate structure including the number of cavities, crystal structures and hydrate formers for each type are listed in Table 2-2 and demonstrated in Figure 2-5.

Table 2-2 Description of each hydrate structure (number of cavities, crystal structure and hydrate formers (adapted from Sloan 2003)

Hydrate Structure	I	II	H
Cavity	5^{12}, $5^{12}6^2$	5^{12}, $5^{12}6^4$	5^{12}, $4^35^66^3$, $5^{12}6^8$
Cavities / Unit cell	2,6	16,8	3,2,1
Average cavity radius (Å)	3.95,4.33	3.91,4.73	3.91,4.06,5.71
Water molecules/ Unit Cell	46	136	34
Variation in radius (%)	3.4,14.4	5.5,1.73	4.0,15.1
Type of crystal	cubic	cubic	hexagonal
Example of hydrate former	CH_4, CO_2, C_2H_6, H_2S,Xe	H_2, N_2,O_2, C_3H_8,THF	CH_4+ THF CH_4+ cycloheptane
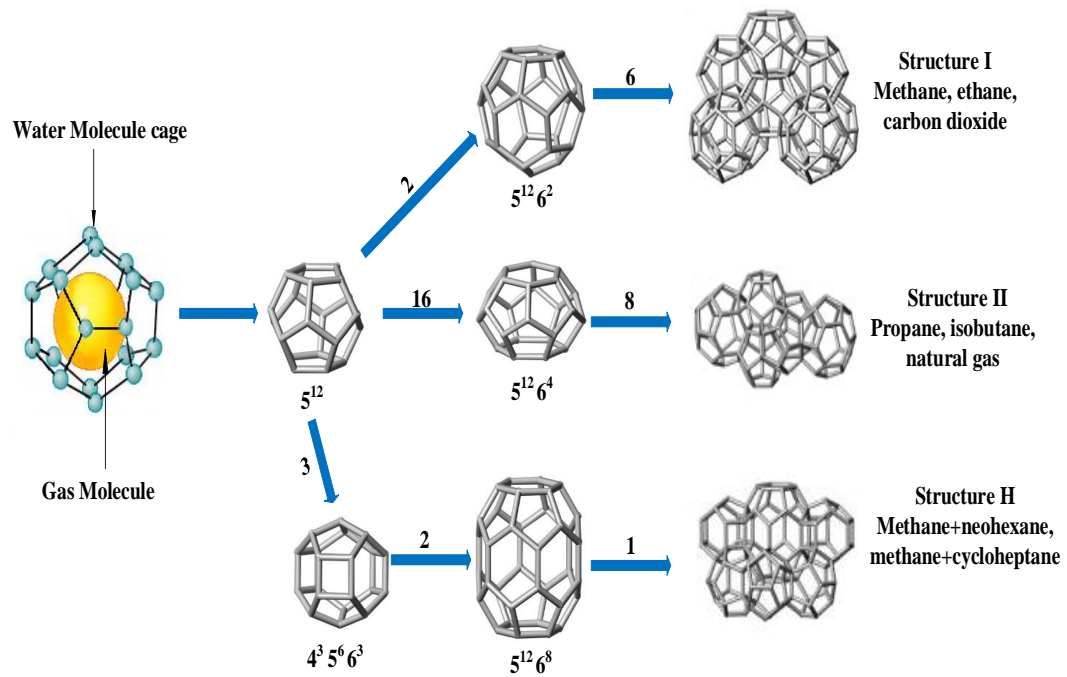
Figure 2-5 Three common types of hydrate network unit structures. The term $5^{12}6^2$ characterises a water cage consisting of twelve pentagonal and two hexagonal faces. The arrows characterise the number of unit cells of the various cavities. Figure modified from Koh and Sloan (2007)

If a single type of guest molecule occupies the cavities within the hydrate structure, the resulting hydrate is named a pure hydrate. Examples of the most common guest molecules in nature and the corresponding hydrate structures are listed in Table 2-3. Methane can stabilise both the small and large cages of sI, whereas molecules larger than methane (e.g. propane) are able to considerably stabilise only the large cages of sII, and thus form sII hydrates (Koh et al. 2011). However, other large guest molecules can be incorporated in sII and sH hydrate structures in the presence of a so-called help-gas (e.g. CH_4) to stabilise the 5^{12} and $4^35^66^3$ cages (Giavarini and Hester 2011). In this context, the equilibrium conditions for the existence of hydrate vary depending on the types of forming gases (Sadeq et al. 2017).

Furthermore, gas hydrates could also be formed from binary, ternary and multi-component gas systems. The composition of mixed gas hydrates has a significant influence on the thermodynamic stability of hydrates and increasing the concentration

of higher hydrocarbons (e.g. CO_2) compared to pure methane that shifts the equilibrium conditions to lower pressures and higher temperatures (Sadeq et al. 2017). A mixture of methane and carbon dioxide forms only sI hydrate, whereas the binary mixture of methane and ethane can form sI or sII hydrates (each one forms sI hydrate) based on the temperature, pressure and concentration of each gas in the mixture (Sloan and Koh 2008).

Table 2-3 The most common guest molecules found in gas hydrates (Sloan and Fleyfel 1991)

Guest Molecules	Formula	Hydrate Structure	Cavities
Methane	CH_4	sI	5^{12}, $5^{12}6^8$
Ethane	C_2H_6	sI	$5^{12}6^2$
Propane	C_3H_8	sII	$5^{12}6^4$
Butane	C_4H_{10}	sII	$5^{12}6^4$
Methylcyclohexane	C_7H_{14}	sII	$5^{12}6^8$
Carbon Dioxide	CO_2	sI	5^{12}, $5^{12}6^2$
Nitrogen	N_2	sII	5^{12}, $5^{12}6^4$
Hydrogen Sulfide	H_2S	sI	5^{12}, $5^{12}6^2$

In addition, certain materials that are in the liquid status at room temperature can form hydrates at conditions of low temperatures and atmospheric pressure (Ohmura et al. 1999). These types of chemicals are of special interest for studying gas hydrates experimentally due to their ability to form the same hydrate structures that some of the gas molecules can do without the need for high-pressure conditions. Examples of such

materials are THF (C_4H_8O) and cyclopentane (C_5H_{10}), which both form sII hydrates at atmospheric pressures and temperature above 0 °C.

2.3   Thermodynamics of Hydrate Formation and Equilibrium

Understanding the thermodynamics of gas hydrate formation is essential before undertaking any effort in the field of gas hydrate. Without fundamental knowledge regarding the thermodynamics, driving forces and solubilities cannot be fully comprehended or the correct operating conditions determined.

Knowing the minimum pressure necessary for the formation of a small amount of gas hydrate at a specified temperature is fundamental in deciding the operating conditions. These minimum conditions are commonly referred to as the incipient hydrate formation conditions and have been extensively studied.

Incipient hydrate formation conditions are commonly measured in the laboratory using three different types of experimental procedures as follows: the isothermal method, the isobaric method and the isochoric method (Sloan and Koh 2008).

In the isothermal method, the temperature of the system is decreased to a certain value. Then, the experiment is started at a constant temperature and pressure above the hydrate formation point. Throughout the isobaric method, the system pressure is kept constant while the volume varies. During the isochoric method, the volume is kept constant while the pressure changes. According to Mohebbi et al. (2012), the gas diffusion rates by the isochoric and isobaric approaches are approximately the same because the gas consumption rates are equal. These experiments can be repeated over a range of conditions to obtain a partial phase diagram. Researchers have known the conditions required to form the gas hydrate (e.g. methane) since 1946. Figure 2-6 illustrates the phase-diagram for methane; the solid line represents the H-Lw-V line that connects a series of three-phase (solid hydrate, liquid water and vapour) equilibrium points. Hydrates will not form below this line, and the system will consist of liquid water and gas in equilibrium. Above this line, hydrates start to form causing hydrate-liquid water equilibrium. At any point on the line, the three phases exist in equilibrium.
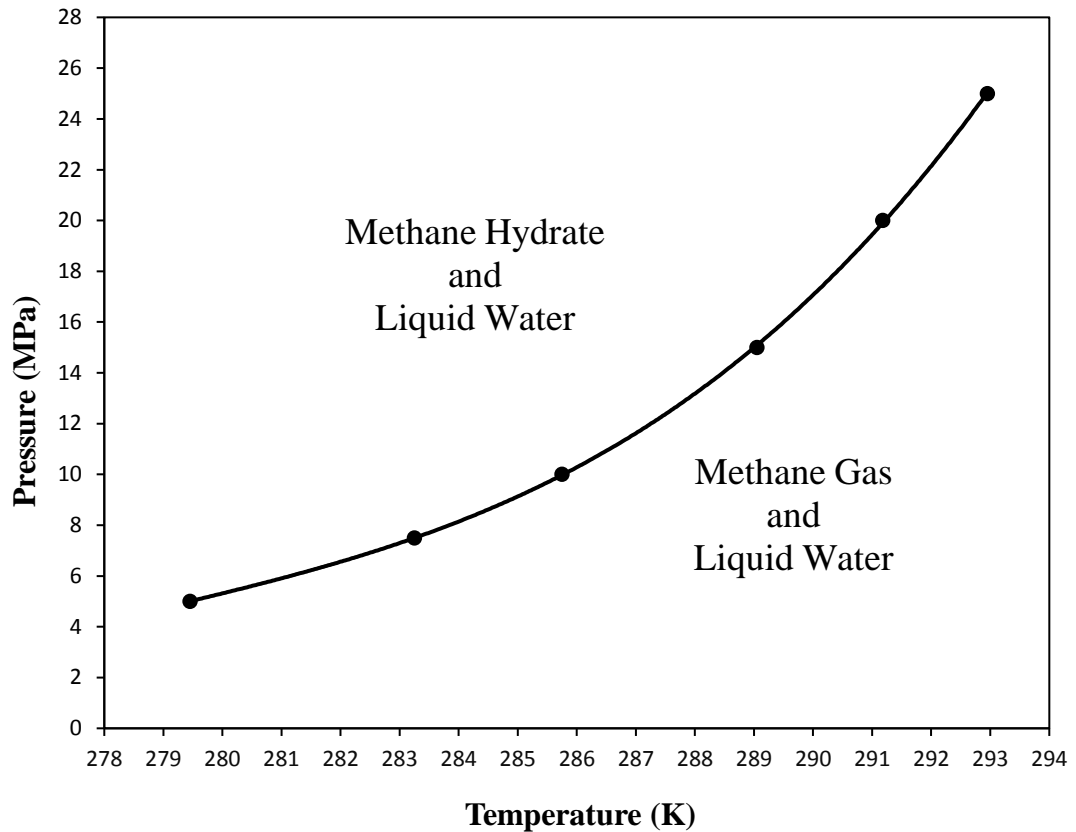
Figure 2-6 Phase diagram for methane-water (our work)

2.4   Formation and Dissociation of Gas Hydrates

The formation of gas hydrates is mainly determined by the availability of the following fundamental elements: low temperature, high pressure and sufficient amount of hydrate former with the existence of free water. However, the requirement for free water was later debated by Kobayashi in his experimental studies from 1973 to 2000, which demonstrated that gas hydrates can form in the absence of free water (Sloan and Koh 2008). In addition, it has been found that other factors enhancing hydrate formation include a turbulence source (agitation), nucleation site and water history (memory effect) (Moon et al. 2003, Wenji et al. 2009, Obanijesu et al. 2014). Moreover, acid gases such as carbon dioxide and hydrogen sulfide are also known to promote hydrate formation because they are more soluble in water than the hydrocarbon gases (Adeleke 2010). Gas hydrate formation (or crystallisation) is an exothermic reaction (i.e. releases heat) and typically includes nucleation and growth processes. However, dissociation of gas hydrates is an endothermic activity (i.e.

absorbs heat) that causes hydrate to decompose to water and guest molecules (hydrate former).

2.4.1 Gas Hydrates Formation

The formation process of hydrates can be typically characterised by the following three phases: gas dissolution, hydrate nucleation and growth. During the dissolution stage, the gas dissolves in the liquid phase until it reaches the point of supersaturation. Then, the nucleation period starts at time = t_{eq} as shown in Figure 2-7. During nucleation, liquid and guest molecules constantly react and vibrate to form small hydrate nuclei (clusters). These hydrate nuclei remain unstable until they reach the critical nucleation size necessary for continual hydrate growth to proceed. Hydrate nucleation is an inherently stochastic process and it is reflected by the induction time required to form the nuclei. Standard induction times are dependent on the supersaturation and the degree of temperature reduction during the formation process (You et al. 2015).
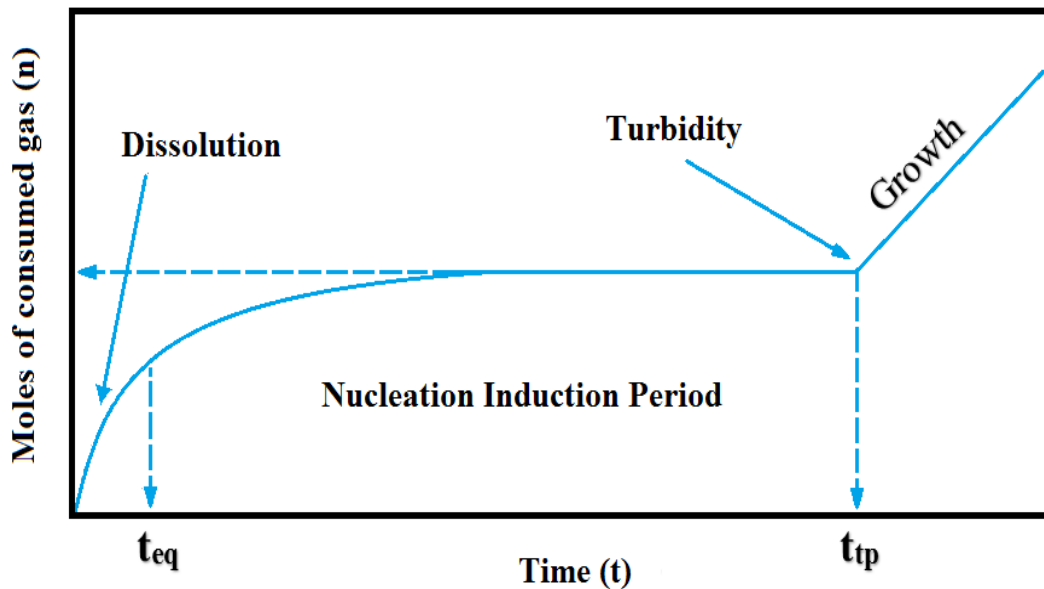
Figure 2-7 Typical hydrate formation stages

Hydrate growth then begins once the critical nuclei size is accomplished. The point at which the hydrate clusters become visible is referred to as turbidity point (t_{tp}) as shown in Figure 2-7. The time between nucleation and turbidity is known as the induction

time. During the growth period, the stable hydrate nuclei that formed during the induction time will grow and progressively agglomerate until completion of the formation process.

To date, two major hypotheses for hydrate nucleation have arisen through experimental and modelling studies, i.e. labile cluster nucleation and local structuring nucleation (Sloan and Koh 2008). In the labile cluster mechanism, which is the more accepted conception, nucleation is controlled by the dissolving of gas in the liquid phase along the liquid-gas interface where the gas molecules create local structuring of the neighbouring liquid molecules into clusters. Such clusters arrange themselves and agglomerate because of the reduction in free energy. The number of coordinated labile clusters varies based on the type of dissolved gas in the aqueous solution (Sloan and Fleyfel 1991). When the labile clusters come in contact with each other, they start to agglomerate through the face or/and vertices sharing. As discussed above, when these clusters achieve a critical size, the hydrate nucleus is formed as a larger and more stable structure and are able to start the growth period (Sloan and Fleyfel 1991). Figure 2-8 shows the stages of nucleation according to the labile cluster mechanism.

(a)	(b)	(c)	(d)
Initial state	**Labile clusters**	**Agglomeration**	**Primary nucleation**
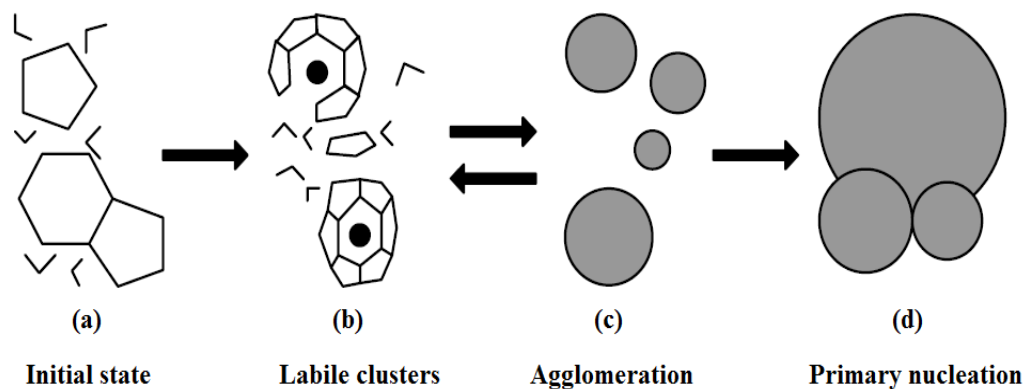
Figure 2-8 Labile cluster nucleation model (adapted from Sloan and Koh 2008)

In the local structuring nucleation, the gas molecule is absorbed in the aqueous phase surface instead of dissolving in water. This hypothesis assumes that nucleation occurs on the vapour side of the liquid-vapour interface (Long 1994). This process leads to

building half a cage by water molecules (local structuring). The gas will then migrate through surface diffusion until it enters the cage and then a complete enclosure will be formed. This hypothesis is clearly presented in Figure 2-9.
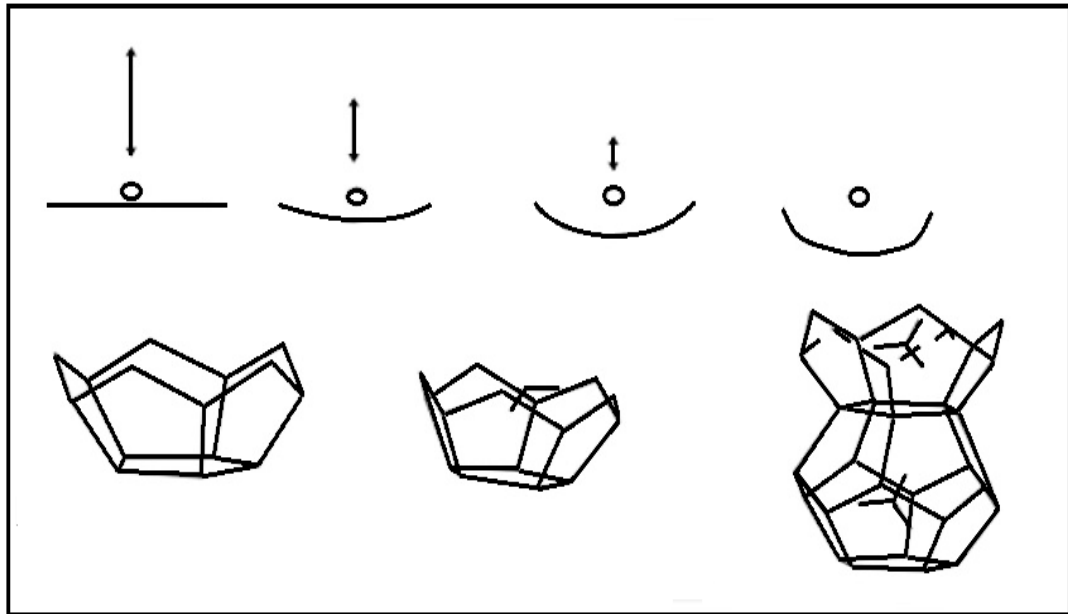
Figure 2-9 Adsorption of gas molecules onto hydrate cavities based on the local structuring nucleation mechanism Long (1994)

2.4.2   Dissociation of Gas Hydrates

Hydrate dissociation requires considerable external energy to break the intermolecular bonding between the water and guest molecules (hydrate cage) and the decomposed hydrates (Sloan and Koh 2008). To induce hydrate dissociation, the equilibrium conditions (pressure and temperature) have to be shifted to a lower pressure or a higher temperature.

Generally, in the oil and gas industry, several methods have been suggested for hydrate dissociation including thermal stimulation, depressurisation and thermodynamic inhibitor injection, which are also proposed as techniques for natural gas production (Makogon and Makogon 1997).

A typical pressure-temperature (P-T) phase diagram for different gas hydrate formers is shown in Figure 2-10. Two quadruple points are shown in this figure, the lower quadruple point, Q_1 (I-Lw-H-V) and the upper quadruple point, Q_2 (Lw-H-V-L$_{HC}$). Q_1 refers to the point at which the four phases (ice, liquid water, hydrate and hydrocarbon vapour) exist in equilibrium with lowering temperature. Conversely, Q_2 represents the point at which water liquid, hydrocarbon liquid, hydrocarbon vapour and hydrate coexist in an equilibrium state showing the upper-temperature limit for gas hydrate formation. Q_1 and Q_2 are unique for each hydrate former.
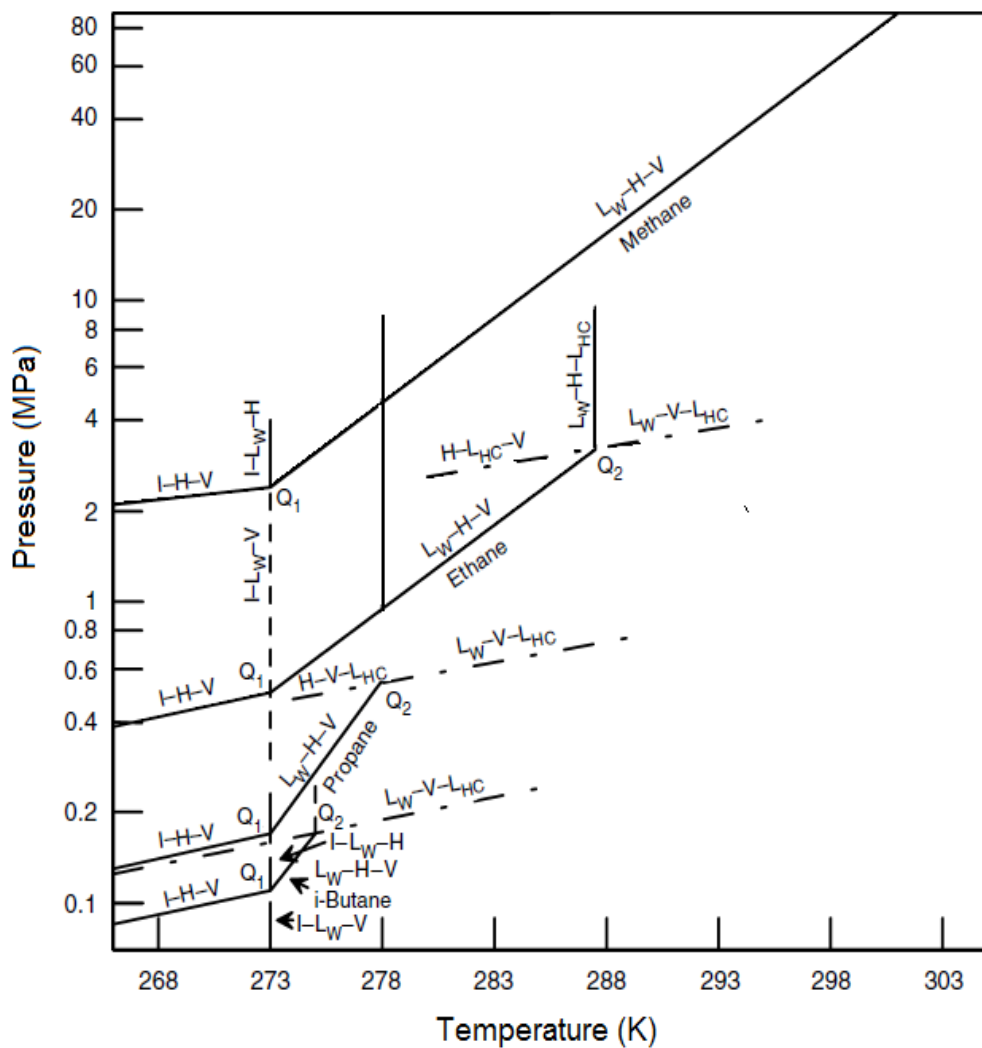
Figure 2-10 Pressure-temperature phase diagram for various natural component gases that form hydrates (adapted by Sloan and Koh 2008 from a figure developed by Katz 1959). H refers to hydrate; V for vapour; I for ice; L$_{HC}$ for liquid hydrocarbon and Lw for water. Q_1 and Q_2 are lower and upper quadruple points

2.5 Application of Gas Hydrates (Importance of Gas Hydrates)

Gas hydrates have unique physical and chemical properties as non-flowing structures that have a higher density than other fluids and a high volume of gas contents (Sloan 2003). These unique properties produce the proposal that gas hydrates can be applied in various industrial applications including potentially flow assurance, carbon dioxide capture to reduce carbon dioxide emissions, gas storage, gas transportation and separation, potential energy resource and others. The applications of gas hydrates worldwide are summarised in the following sections.

2.5.1 Flow Assurance

Since the discovery by Hammerschmidt (1934) that gas hydrates could block the gas production and transportation pipelines, gas hydrates have been highlighted as the main flow assurance and safety issue. Currently, the formation of solid hydrates in pipelines represents a concern for the oil and gas industry (Macintosh 2000) due to their significant threat to the safe and economical operation of production facilities. Hydrate plugs can stop the flow of natural gas and can be difficult to remove (Figure 2-11). Methane hydrate is often hard to decompose even at temperatures and pressures above equilibrium conditions.

Figure 2-11 Natural gas hydrate plug in a transmission pipeline (Zarinabadi and Samimi 2012)

Consequently, extensive studies have been conducted to investigate how to avoid hydrate blockage in pipelines. Many techniques have been suggested to reduce the potential threats from gas hydrates. The conventional solution depends on eliminating one of the required elements for the formation of gas hydrates, such as removing water from the production system using the dehydration process. Another solution is to prevent hydrate blockage by shifting the hydrate formation conditions to elevated pressures and lower temperatures using thermodynamic inhibitors such as methanol and mono-ethylene glycol. The thermodynamic inhibitor shifts the three-phase equilibrium curve; therefore, the system can tolerate lower temperatures and higher pressures.

It has been revealed that other types of inhibitors such as low-dosage inhibitors (e.g. kinetic hydrate inhibitors and anti-agglomerates) can be utilised to decrease the hydrate nucleation and growth rate at very low amounts during the liquid phase compared to thermodynamic inhibitors (Kelland 2006). The low-dosage inhibitors work either by delaying the initial hydrate formation or by preventing the agglomeration of hydrate particles (Perrin et al. 2013).

2.5.2 Gas Storage and Transportation

Gas hydrate technology has been proposed as a promising method for natural gas storage and transportation. Utilising such technology was first proposed by Benesh in 1942 who studied the unique properties of the hydrate structure (i.e. up to 180 m^3 of gas can be stored in 1 m^3 of hydrate). However, such a process is often hindered by some restriction such as unfavourable kinetics and low conversion of water to hydrates (Lee, Zhang, et al. 2007). Hydrate promoters can increase the hydrate formation rate by increasing the solubility of gas in the aqueous phase (King 2004).

The gas hydrate technique for gas storage and transportation is favourable in terms of safety and economics compared to other storage and transportation methods (e.g. liquefied natural gas (LNG)) (Byk and Fomina 1968). The LNG process requires high pressure (up to 4 MPa) and temperature lower than -160 °C (Thomas and Dawe 2003). In addition, LNG production facilities require huge construction costs (Gudmundsson and Borrehaug 1996), which is reflected negatively in natural gas prices. However, gas storage in the hydrate form could be transported at atmospheric pressure and much

higher temperature (~ -20 °C) than those required for LNG storage and transportation (Nakajima et al. 2002). Consequently, research is being conducted on hydrate promoters, which may increase the viability of hydrate as a medium for storage and transportation.

2.5.3 Gas Hydrate as a Potential Energy Resource

The demand for energy sources (e.g., for natural gas) is increasing with the growing population and is fast depleting conventional energy resources (Dudley 2013, Al-Fatlawi et al. 2017). To meet such increasing demand, natural gas hydrates (the main gas here is methane) have been proposed as one of the most potential energy resources (Collett 2000, Makogon 2010, Arora and Cameotra 2015). Moreover, hydrates are a massive reservoir of natural gas because 1 m^3 of methane hydrate contains up to 180 m^3 of methane gas under standard conditions (Max et al. 2005, Sloan and Koh 2008). Estimates of the global natural gas volume contained in hydrates range from 10^{14} m^3 to 10^{18} m^3 (Kvenvolden 1988, Moridis et al. 2009, Dawe and Thomas 2007). These estimates exceed the entire combined world reserves of conventional energy resources (Makogon et al. 2007, Moridis 2008). In the present energy consumption situation, production of 15% of these reserves will cover the global energy needs for the coming 200 years (Makogon et al. 2007). It has been stated that methane hydrates alongside renewable energy and hydrogen are the most significant substitution energy resources for the next few years (Demirbas 2010a). Thus, attention towards the commercial recovery and production of natural gas from hydrate-bearing sediments is on the rise to become another aspect of industrial interest in deposits of gas hydrates.

Several techniques have been suggested for the production of gas from natural hydrate sediments (Collett 2000). These techniques rely on inducing hydrate dissociation through:

(1) Thermal stimulation by heating the hydrate-bearing sediments to a temperature outside the gas hydrate stability conditions (Zhao, Zhu, et al. 2015). Heat sources such as steam or hot water can be utilised for heat stimulation and then gas production (Sloan and Koh 2008). This method has been suggested as the most attractive option for reservoirs with high permeability and those under saline aquifers (McGuire 1981). Thermal stimulation has been conducted in a production test at the Mallik site in

Canada, which showed a poor and insufficient production efficiency as only 470 m^3 of gas was produced over 5 days (Song et al. 2015). Following the idea that a significant amount of heat was getting lost during the injection of the hot fluids into the targeted layer, Schicks et al. (2011) developed a counter-current heat-exchange reactor to produce heat in the target zone. In the laboratory scale testing, thermal stimulation could be applied using water/air bath. The hydrate-bearing samples were heated by increasing the surrounding temperature without contacting the heating source (hot water) to ensure that the water produced from hydrate dissociation did not mix with the injected water (Mekala et al. 2014). This technique has also been conducted by electromagnetic heating (Islam 1994), constant heat flux (Misyura 2013) and in-situ combustion (Castaldi et al. 2007).

 (2) **Depressurisation technique** by reducing the pressure to a point under the hydrate stability pressure to disturb the mechanical equilibrium. This technique is conducted by placing a pump into the borehole and continuously producing fluid due to decreasing reservoir pressure to initiate hydrate dissociation. This method was successfully used to produce a total 4×10^6 cubic feet of gas (0.7×10^6 cubic feet /day) in the Nankai Area (Japan) from 12 to 18 March 2013 (Johnson 2013). Production by depressurisation is considered the most economical and feasible option among the other production methods due to its high production capability (Moridis et al. 2009). However, gas recovery may be restricted by ice generation and hydrate reformation during the depressurisation process because of the endothermic behaviour of the hydrate dissociation (Collett 2000, Song et al. 2015).

(3) **Inhibitor injection** by injecting the system with chemicals (e.g. methanol, glycol and NaCl) to disrupt the hydrate equilibrium conditions beyond the hydrate stability conditions, and thus assist the dissociation of the hydrate to gas and water. Typically, the dissociation rate is controlled by the concentration of the inhibitor, the injection rate, pressure and interfacial area between the hydrate and the inhibitor (Sira et al. 1990). However, this method is not economically feasible due to the high cost of these types of chemicals. This technique could also be used alongside other methods to enhance the production efficiency due to the lower heat required for hydrate dissociation (Fan et al. 2006).

Of these three main techniques for gas production, it has been found that depressurisation technique combined with thermal stimulation could be the most practical method for gas extraction from gas hydrate reservoirs (Demirbas 2010b). Figure 2-12 illustrates a scheme of the three main techniques for gas production from natural gas hydrate deposits.
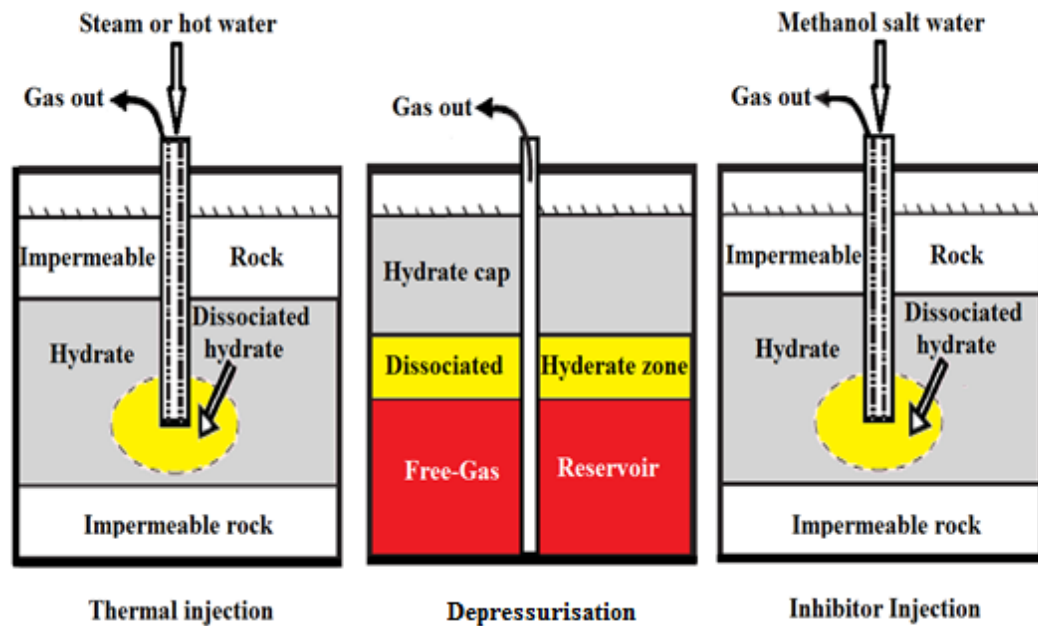
Figure 2-12 Scheme explaining the three main techniques (thermal injection, depressurisation and inhibitor injection) for gas production from hydrate deposits (Collett 2002)

Recently, a new technique has been suggested for methane production from gas hydrates via CO_2-CH_4 exchange (Kvamme et al. 2007, Graue et al. 2008). This method involves methane extraction from hydrates by carbon dioxide injection into existing hydrate reservoirs and subsequent exchange of methane molecules by CO_2 molecules in which CO_2 is sequestered in the form of hydrates (Baldwin et al. 2009). Both carbon dioxide and methane can form sI hydrate (Sloan and Koh 2008); however, carbon dioxide hydrate is thermodynamically more stable than that of methane hydrate under the prevailing conditions (Ohgaki 1994, Ersland et al. 2009). Therefore, injection of

carbon dioxide into hydrate reservoirs causes the exchange of methane hydrate by carbon dioxide hydrate and simultaneously releasing trapped natural gas (Kvamme et al. 2007). Such a technique has considerable advantages compared with the conventional production techniques, e.g. maintaining the mechanical stability of the sediments during the production process via CO_2 hydrate formation, controlling the water and sand production to a minimum level, and providing a cleaner environmental method for carbon dioxide storage, and thus contributing to reduce carbon dioxide emissions into the atmosphere.

Most of the above recovery methods have specific limitations when applied individually. Thus, gas production efficiency could be improved using a combination of these methods. The huff and puff technique is one of the suggested approaches to combine the thermal stimulation and depressurisation methods (Wang et al. 2014). An increase of 3.6 times has been reported in gas production using the combined thermal stimulation-depressurisation method (Falser et al. 2012).

2.5.4 Gas Hydrates as an Environmental Hazard and Factor in Climate Change

Natural gas hydrates in reservoirs are generally vulnerable because they are sensitive to certain conditions of pressure and temperature as discussed earlier. Therefore, small changes in these conditions can disturb the hydrate stability zone causing the dissociation of hydrates to water and gas. Two serious implications can result from uncontrolled hydrate dissociation: geological hazard and contribution to global climate change (Kvenvolden 1993, 1999). It is recognised that the existence of gas hydrates in the submarine and permafrost regions results in cementation of the sediments and reduction in its permeability, which leads to restriction of the pore fluids. Therefore, when hydrates dissociate to gas and liquid, the sediments become unconsolidated and overpressured due to the release of gas. This phenomenon leads to lowering of the shear strength of the zone, which could cause structural failure and landslides. The slope failure issue related to hydrate dissociation is one of the main topics of ongoing gas hydrate studies.

Most of the natural hydrate-bearing sediments, where the hydrate is stable, are already occupied by hydrate and gas causing continuous sedimentation and more hydrate burial. The deep hydrate burial produces a temperature increase in the bottom section of the hydrate zone, which affects the hydrate stability causing gas release.

Moreover, small changes in subsurface ocean temperatures due to global warming could shift the hydrate stability zone by meters, thus causing gas hydrate dissociation with a severe geo-hazard in the future (Maslin et al. 2010). Therefore, in terms of climate issues, the release of methane from hydrate reservoirs because of hydrate dissociation could increase the methane concentration in the atmosphere. This is contributing significantly to climate change because methane has a greenhouse effect that is 25 times stronger than that of carbon dioxide (Beget and Addison 2007). In 2010, methane emissions contributed to 16% of all other greenhouse gas emissions (Blanco et al. 2014), and the total concentration of atmospheric methane rose to 1.82 ppm by volume in 2013 (Hartmann et al. 2013). Furthermore, there is a huge amount of methane trapped in a relatively small volume of gas hydrate, as mentioned above. Therefore, releasing even a small percentage of methane could have a catastrophic effect on climate warming over a relatively short time. A diagram demonstrating submarine slope failure and gas release due to hydrate dissociation is shown in Figure 2-13.
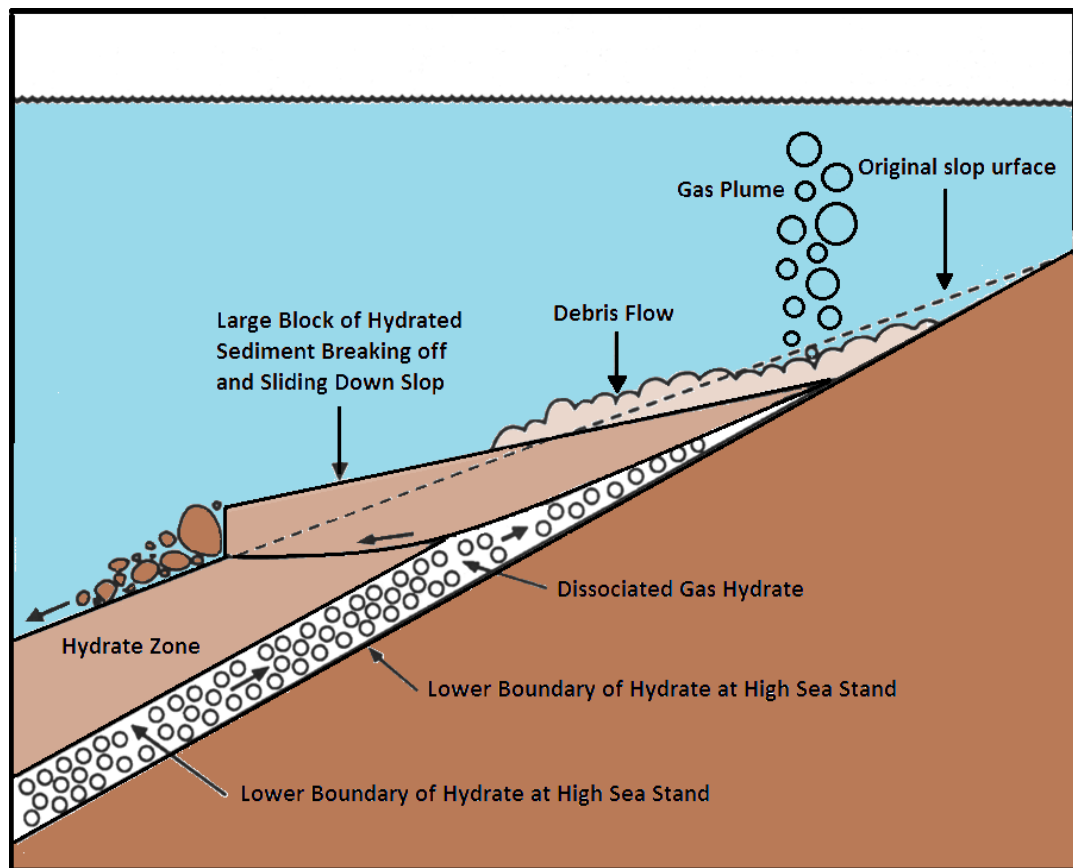
Figure 2-13 Scheme illustrating the effects of changes in temperature and pressure on gas hydrate deposits and the subsequent gas release with seafloor failures (adapted from Kvenvolden 1998)

Several studies related to environmental issues have revealed that the main reason for global warming and climate change is elevated anthropogenic carbon dioxide emissions to the atmosphere (Houghton et al. 2001). CO_2 emissions into the atmosphere have increased significantly (IPCC 2005, Pachauri et al. 2014). This is coupled with the massive growth in fossil fuel consumption, where carbon dioxide is emitted (IEA 2016). Consequentially, such high CO_2 concentrations lead to increasing global temperatures (global warming), and thus climate change. Indeed, CO_2 contributes to approximately 60% of this global warming (Yang et al. 2008). Decreasing CO_2 concentration in the atmosphere is thus crucial for mitigating climate change.

One of the methods suggested to reduce such emissions is carbon dioxide geo-sequestration and capture in deep ocean sediments (Yamasaki 2003, Orr 2009). The

prevalent thermodynamic conditions in such marine environments are suitable for hydrate formation as they are located within the stability zone of the CO_2 hydrates (Clennell et al. 1999, Tohidi et al. 2010). Simultaneously, hydrate formation within the porous medium blocks the pore space and causes a decrease in the permeability of sediments to gases and liquids, thus providing a second seal in the system by self-sealing (House et al. 2006, Kvamme et al. 2007, Kwon and Cho 2009, Tohidi et al. 2010). Therefore, CO_2 geo-sequestration and capture via hydrate formation is proposed as a promising new technology to reduce carbon emissions, and thus mitigate the harmful influences of global warming and climate change.

2.6   Gas Hydrate Occurrence in Nature

Natural gas hydrate accumulation has been reported in several locations over the last decades. The geological areas in which hydrate deposits have been discovered are specified according to the substantial elements of hydrates formation (low temperature and elevated pressure in the presence of water and forming gases). Thus, hydrate deposits have been discovered mostly in polar regions (onshore and offshore permafrost) and in the sediments of marine continental slopes (Kvenvolden 1993). Figure 2-14 shows a map of worldwide locations of found and inferred gas hydrate deposits.
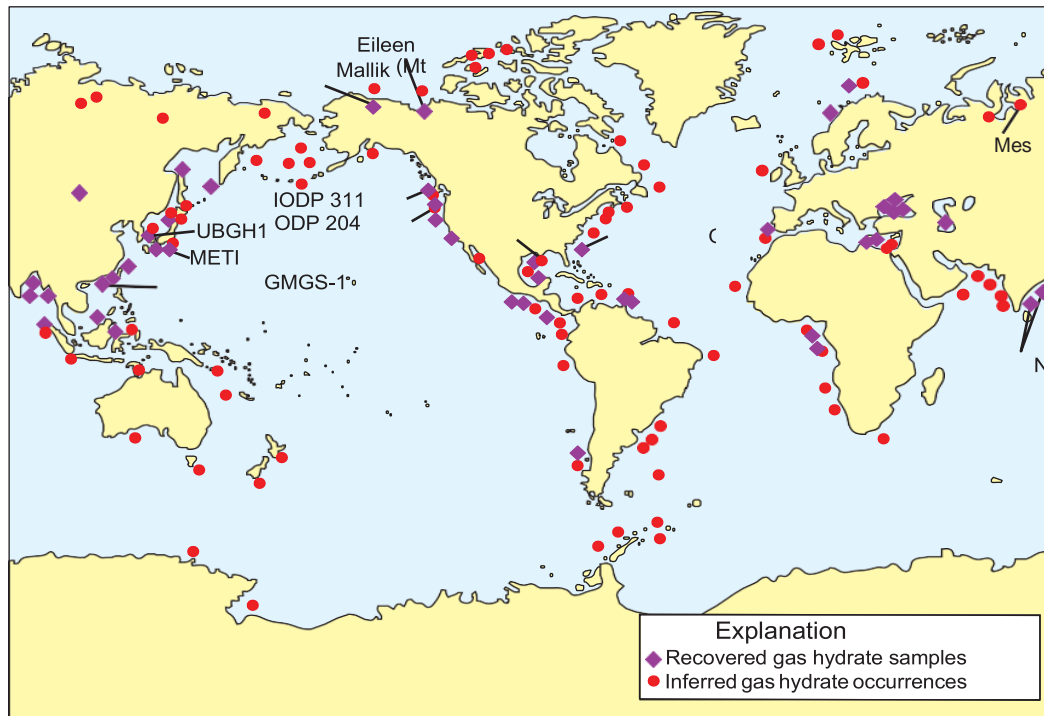
Figure 2-14 Locations of natural gas hydrate deposits worldwide (Paull et al. 2010)

In the polar region, hydrates accumulate in shallow water as the low-temperature environment is dominant. In such environments, gas hydrates form in depths below 150 m because the hydrostatic pressure and low ambient temperatures (below freezing) control the stability of the hydrate (Figure 2-15 (a)). Permafrost region hydrates comprise approximately ~ 1% of global gas hydrate reserves. However, approximately 99% of the gas hydrate reserves are located in the deep oceanic environment. The sub-zero temperature of the bottom water and the high pressures secure the hydrate formation and stability. In these environments, hydrates exist at depths beneath 300 m with the maximum lower limit of ~ 2000 m (Figure 2-15 (b)).
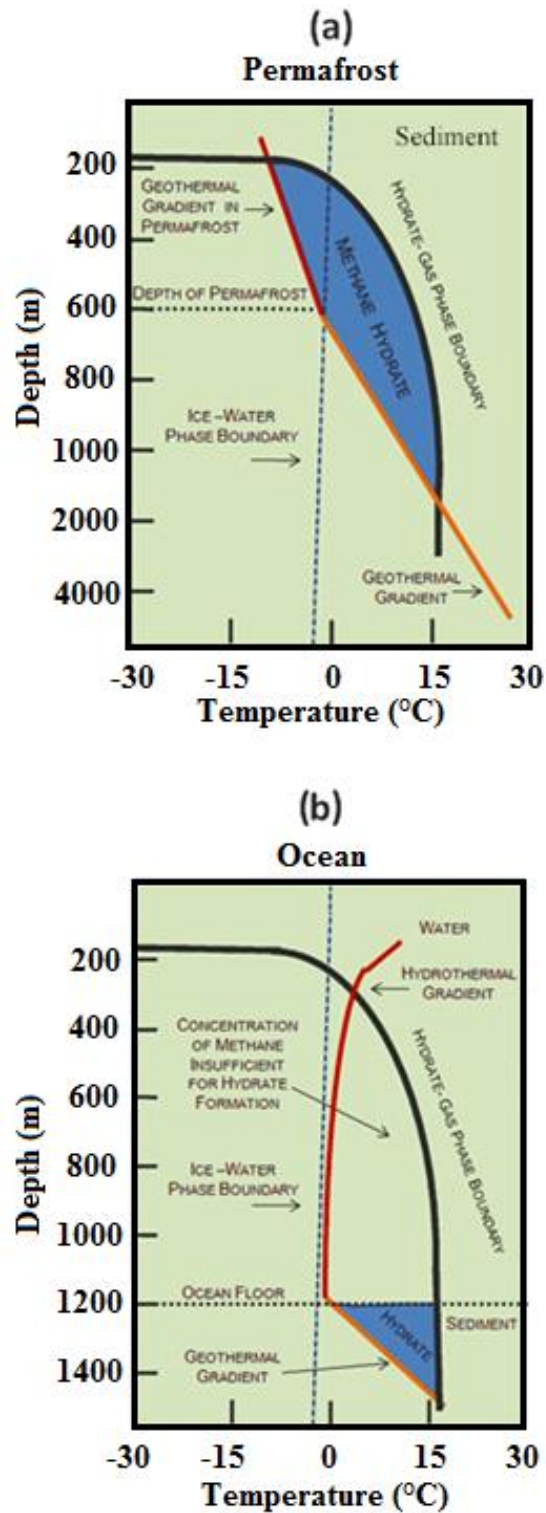
Figure 2-15 Depth-temperature stability zone for gas hydrates (a) in the permafrost environment and (b) in deep oceanic (marine continental slops) adapted after (Kvenvolden 1988)

2.7 Hydrates in Sediments

2.7.1 Naturally Occurring Gas Hydrate in Porous Medium (Reservoir System)

In nature, a gas hydrate system could be considered similar to a conventional hydrocarbon system, which is determined by the fundamental elements required for gas hydrate formation in sediments (Collett et al. 2009). Four significant elements are required for the formation of gas hydrate in sediments as follows (Max et al. 2013):

(a) Thick hydrate stability zone appropriate for hydrate formation.

(b) Adequate gas sources.

(c) Migration pathways to the seabed.

(d) High-quality host reservoir sediments.

The substantial main changes between the two systems (gas hydrate and conventional hydrocarbon) are determined by the structure and timing regarding the accumulations themselves. Table 2-4 contains some of the similarities and changes between the two systems.

Table 2-4 Similarities and differences between gas hydrate deposits and the conventional hydrocarbon system (Max et al. 2013)

Similarities	Differences
• High-quality reservoirs have high porosity and permeability. • Early exploration is dependent on seismic surveys.	• Not necessary to connect reservoir to the fixed source beds. • In general, the geological position cannot be changed by deposits and geological trap. • Hydrate deposits required less detailed measurements and less costly assessments of resources. • Focus on the co-existence of the required elements for gas hydrate formation and stability • long-standing basin history and thermal history of sediments are less significant in analysis.

2.7.1.1 Gas Hydrate Stability Zone

As discussed previously, hydrate formation is generally reliant on the correct thermodynamic equilibrium conditions and accessibility of sufficient concentration of hydrate formers (natural gas), which mix and react with the pore water. The hydrate formation zone (which is also known as a gas hydrate stability zone (GHSZ)) refers to a sedimentary zone and depth of bed that is saturated with gas and water under suitably thermodynamic P-T conditions for hydrate formation (Makogon 1982). GHSZ thickness is governed by pressure, temperature, gas composition and pore water. The optimal GHSZ is located at relatively elevated pressures and low temperatures (e.g. pressure higher than 14–20 MPa and temperatures range from 4 to 17 °C across the Andaman Deep Sea and Krishna-Godavari Basin, India), with the presence of a relatively sufficient volume of natural gas and low salinity pore water. Figure 2-16 illustrates the worldwide range of GHSZ conditions by showing the thermodynamic conditions (pressure and temperature) and the equivalent water depth for several collected hydrate samples including the methane-hydrate equilibrium curve.

The equilibrium pressure (for a given subsurface area) is identified by gravity and mass of overlying geological layers (overburden). This pressure increases almost linearly with increasing depth. In the same manner, the low-temperature environment is the result of decreasing bottom water temperature with depth (because of differential density effects). Consequently, the changes in pressure and temperature conditions in the underground can provide the required thickness of GHSZ (Max et al. 2013). This thicker zone is favourable for concentrating more natural gas hydrates in the subsurface.
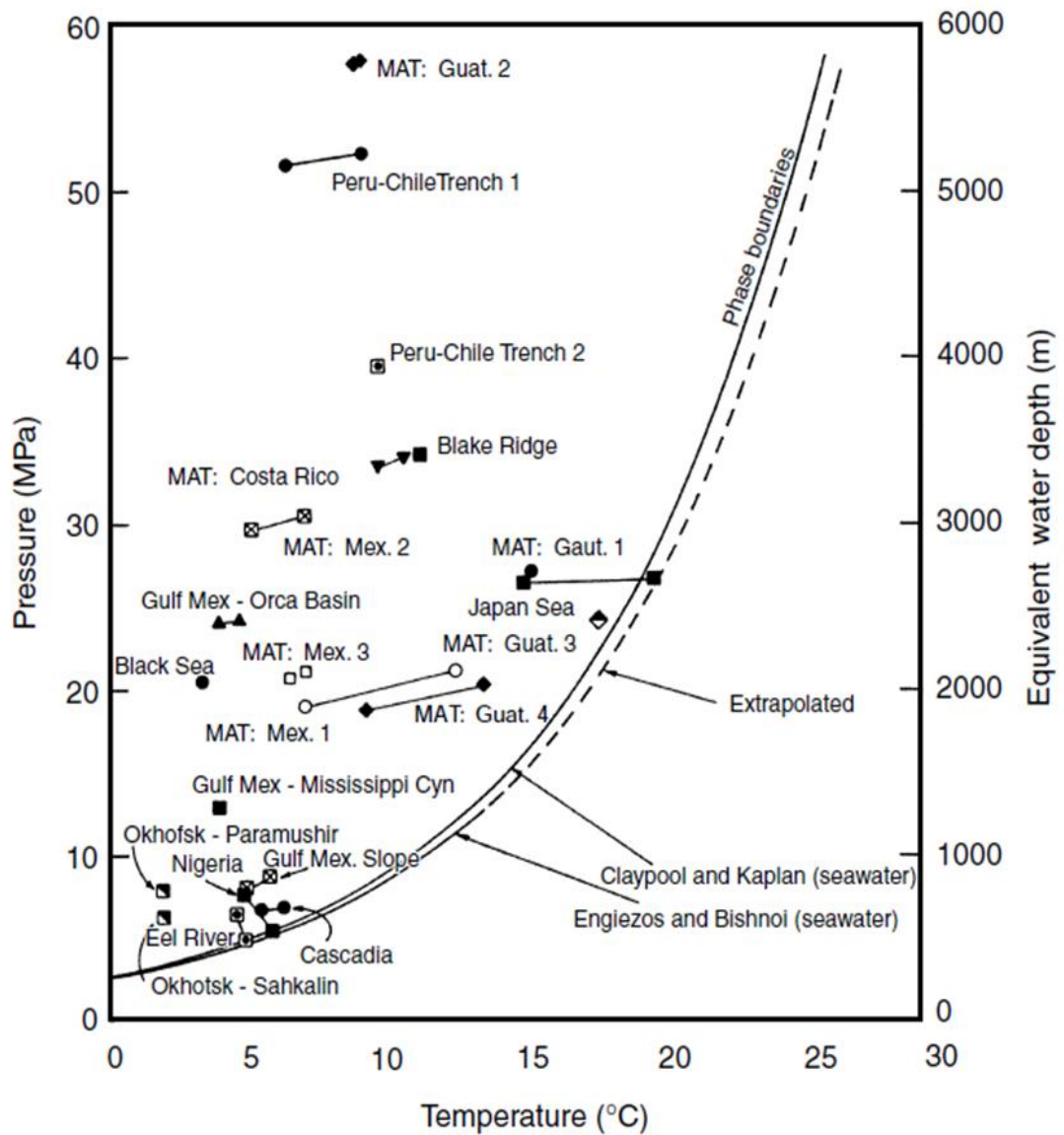
Figure 2-16 Pressure-temperature equilibrium conditions and water depth recorded for collected hydrate samples (Sloan and Koh 2008)

2.7.1.2 Gas Sources Availability

The availability of a sufficient amount of gas sources is a substantial factor controlling the location of natural gas hydrate formation and distribution (Kvenvolden 1988, Collett 1993). Many areas provide P-T conditions that allow for hydrate formation, and yet they do not have any hydrate formation at all. The reason for this is mostly due to insufficient gas supply (Giavarini and Hester 2011).

The most common natural hydrate deposits are of sI methane hydrates, which widely exceed other hydrate deposits. However, sII and sH gas hydrates have also been found naturally in the upper continental slope of the Gulf of Mexico (Sassen and MacDonald 1994, Sassen et al. 2001).

Methane gas that forms gas hydrates can be generated from both biogenic and thermogenic sources. Biogenic methane (microbial) is created by the biological activity of anaerobic bacteria breaking down organic matter (Whiticar et al. 1986). This process is performed at low temperatures in relatively shallow sediments extending from the seabed to a few hundred meters below the seafloor (Claypool and Kvenvolden 1983, Parkes et al. 1990). The biogenic methane is then ready for the formation of sI gas hydrate in sediment (Bohrmann and Torres 2006). Approximately 99% of all gas hydrates existing in nature are composed of this microbial methane (Kvenvolden and Lorenson 2001). Consequently, the availability of a sufficient source of methane into the sediments at present and in the immediate-geological past represents the required precursors for the formation of gas hydrates in nature (Max et al. 2013).

Conversely, thermogenic gas is produced in the deepest buried sediments more than 1 km below the seabed via the thermal decomposition of organic materials (e.g. kerogen) under relatively high temperature and pressure conditions (Floodgate and Judd 1992). This type of gas includes a broader variety of hydrocarbons in addition to methane (e.g. ethane, propane, butane, pentane and hexane). Most of the naturally occurring gas hydrates are generated from biogenic gas sources. This type of hydrates has been observed in shallow deposits (Kvenvolden and Barnard 1982). However, thermogenic gases may also form hydrates such as the natural hydrates in the Black Sea and in Northern Alaska (Collett 2002). Moreover, a mixture of both biogenic and thermogenic gas sources have been proposed for Nigeria and the Gulf of Mexico (Booth et al. 1996).

2.7.1.3 Migration Pathways

Studies on gas hydrate deposits demonstrate the great importance of the gas migration pathway in terms of the formation of hydrates in reservoirs. In most instances, the amount of biogenic gas created in-situ within the sediment pore space is not enough for hydrate formation, or the reservoir sediment is not buried deep enough for the generation of thermogenic gas (Kvenvolden 1993, Collett et al. 2009). Therefore, it is necessary for gas to have an upwards migration pathway to enter the GHSZ. Various strategies have been suggested for gas migration through the sedimentary layers into the GHSZ such as diffusion, gas dissolving in the migrating water and gas migration as a continuous bubble phase. The gas diffusion process is considered relatively slow and may not contribute to concentrating hydrate deposits (Xu and Ruppel 1999). The other strategies require permeable paths that allow fluids to migrate through them. Channels such as faults and salt diapirs are considered fundamental pathways for gas migration (Sloan and Koh 2008, Collett 2013). Generally, natural gas hydrate accumulations can be determined by tracking formation water from a free gas source under the hydrate stability zone. Such a process represents a substantial factor in the formation of natural hydrate accumulations. In passive margins, water drive is generally because of the compaction of gravity on the sedimentary layers, whereas tectonics and fractures are more controlling in active margins (Max et al. 2013).

2.7.1.4 High-quality Host Sediments

Substantial amounts of natural gas hydrates have been found within coarse-grained, fine-grained and fractured reservoirs (Trehu et al. 2004, Waite et al. 2009). Examples of such reservoirs are sandy sediments close to the margins of deep oceans in Japan (Egawa et al. 2013), sediments in continental slopes in the Gulf of Mexico (Boswell et al. 2012) and turbidite sands in the Ulleung Basin offshore of Korea (Lee 2011). Recent estimations of hydrate reservoirs in Japan and the US show that high-quality hydrate-bearing sands (i.e. with high permeability and porosity) are more prevalent in methane hydrate systems than previously thought (Collett et al. 2014). However, regarding the global volume of gas hydrates, accumulation of gas hydrates in fine-grained marine sediments is larger than that in coarse-grained deposits because up to

90% of global hydrate accumulations are hosted in fine-grained sediments (Boswell and Collett 2006).

Hydrate-bearing sediments in Alaska have demonstrated low permeability, having a range of 0.01–0.1 mD compared to the same hydrate-free sediments that have a permeability of 1 D (Collett 2013). The lower permeability is due to the existence of gas hydrates within the sediment, which blocks the pores of the sediments and causes a reduction in their permeability. Studies on sedimentary samples recovered from Alaska indicate that the high permeability is substantial for the formation of high hydrate saturation in sediments. This is consistent with high hydrate saturation (~ 80%) observed in coarse-grained sediments at the Mallik permafrost site in Canada and high permeability reservoirs in the Nankai Trough in offshore Japan (Dallimore 2005, Fujii et al. 2009, Winters et al. 2011).

2.7.1.5   Hydrate Growth in Sediments

Typically, three main steps summarise the hydrate growth process in sediments (Figure 2-17). Gas hydrate within the pore space of sediments grows in discrete steps contrary to that of hydrate plugs, which grow gradually (Jung and Santamarina 2012).

Hydrate growth rate, which is known as an increase in hydrate thickness with time, was previously identified by gas diffusion. However, experimental studies have demonstrated that the rapid formation of the first hydrate particles is faster than that which can be explained by the diffusion of gas (Jung and Santamarina 2012). Simultaneously, the hydrate growth rate in the meniscus between water-wet surfaces is greater than that in oil-wet surfaces.
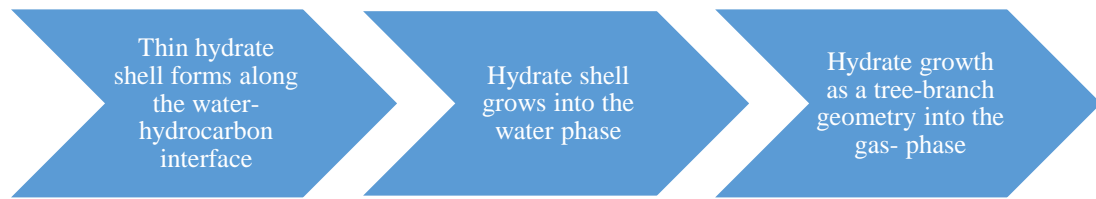
Figure 2-17 Steps of hydrate growth in sediments (modified from Jung and Santamarina 2012)

In addition, X-ray micro-computed tomography studies on hydrate growth within a pore space show that hydrates nucleate randomly causing grain particles (sediment) movements during hydrate formation. Patchy hydrate growth and distribution in sediments significantly affect the seismic velocities (compressional and shear velocities) and petro-physical properties such as permeability, electrical conductivity and shear strength (Waite et al. 2009).

2.7.2 Gas Hydrate Morphology and Distribution in Sediments

When formed in sediments, natural gas hydrate as a solid crystalline structure grows as a configuration (Figure 2-18). Generally, two scales describe the hydrate configuration in sediments, which are macro-scale morphology and micro-scale morphology (Clayton et al. 2010). The macro-scale morphology describes the structure of large-scale hydrate formation within the host sediments, while the micro-scale indicates the interactions of the hydrates with their host sediments.

Figure 2-18 Examples of gas hydrates found in the natural environment: (a) bulk; (b) nodules; (d) layered and (e) laminae (Worthington 2010)

Four distinct forms (modes) in which hydrates exist in marine sediments are shown in Figure 2-19. These forms are disseminated, nodules, veins or layered, and bulk or massive.

Disseminated hydrates refer to the hydrates that distribute homogeneously in the pore space of the macro-structure of the sediments (Booth et al. 1998, Clennell et al. 1999, Gabitto and Tsouris 2010). This type of hydrate preferentially exists in coarse-grained sediments such as sand due to low capillary pressure (Kleinberg et al. 2003, Torres et al. 2008). Through such sediments, gas and fluid can flow smoothly with the availability of many nucleation sites, which allows for the formation of hydrates throughout the sediment. The other three types typically exist in fine-grained sediments such as clay, carbonates and silts. Nodules and veins types have been observed in large accumulations that can potentially grow into massive hydrate types in the presence of a sufficient source (high flux) of gas and water (Malone 1985). In

addition, veins (layered) may grow in sediments with planes of weakness and pre-existing fracture planes (Collett et al. 2008).
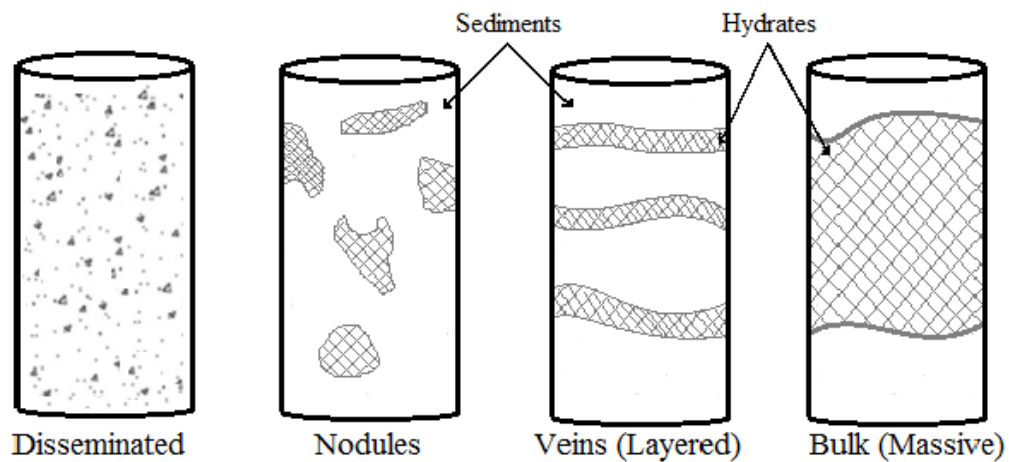
Figure 2-19 The four morphological modes of hydrates in sediments (adapted from Dangayach et al. 2015)

Recently, another classification of gas hydrate morphology has been proposed to describe them in the pore space depending on the interaction of hydrates with the host sediments (micro-scale morphology) (Clennell et al. 1999, Dvorkin et al. 2000). According to the pore filling or cementing morphology, gas hydrates can form in sediments in four pore habit patterns (Helgerud et al. 1999, Lee, Yun, et al. 2007, Waite et al. 2009); Figure 2-20:

(a) **Pore filling:** Hydrates nucleate within the pore space and grow freely without contacting or bridging grains. The hydrate is considered to be part of the pore fluid (not the matrix); thus, only the bulk modulus of the pore water and the electrical resistivity will be affected (Helgerud et al. 1999, Spangenberg and Kulenkampff 2006), whereas the permeability will decrease (Kleinberg et al. 2003).

(b) **Load bearing:** As the formed hydrate cluster grows, it bridges the space between adjacent grains and acts as part of the load-bearing structure increasing the mechanical strength of the sediments. Hydrates are considered to be a part of the sediment matrix, increasing the seismic velocities higher than that of the pore filling type (Helgerud et al. 1999). The pore filling hydrate

grows to a load bearing hydrate when the hydrate saturation exceeds 40% (Priest et al. 2009).

(c) **Cementing:** Hydrate forms preferentially at the grain contacts. It performs as a consolidation item, bonding adjacent grains together, significantly affecting the shear and the bulk stiffness of the sediment even in small quantities (Dvorkin et al. 1999) and rapidly increasing the seismic velocities (Dai et al. 2012).

(d) **Grain coating:** The hydrate forms as a uniform layer coating the surface of the grains. The formed hydrate shell can clog pore throats and then cut parts of the pore space from the interconnected pore network (Kumar et al. 2010). This hydrate the same effect as the cementing type when the hydrate saturation exceeds 30%.
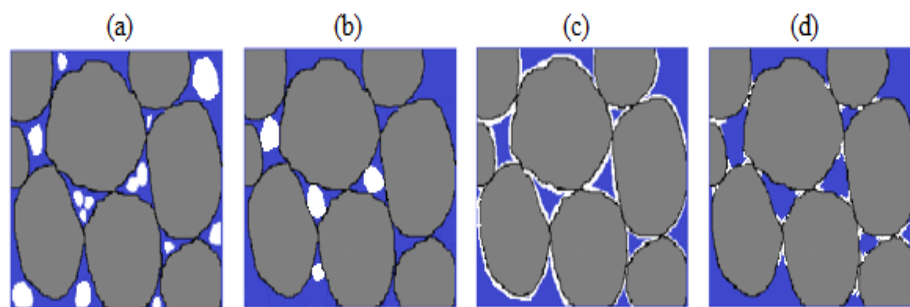
Figure 2-20 Morphological patterns of gas hydrates (white) in sediment (grey) saturated with pore fluid (blue); (a) pore filling, (b) load-bearing, (c) cementing and (d) grain coating

It is difficult to determine the hydrate growth patterns from field core samples owing to the difficulty in maintaining the hydrate in the samples during the coring process. Therefore, most of the hydrate morphological observations depend on experimentally formed hydrates and modelling studies.

2.7.3   Physical Properties of Hydrate-bearing Sediments

The presence of gas hydrate in the pore space of any geological layer can have a substantial effect on its physical properties. Hydrate morphological habits and saturation define the main physical properties of hydrate-bearing sediments. The

difference in the physical properties of free-hydrate sediments and those containing hydrates is mainly influenced by hydrate saturation. The most affected physical properties are the seismic velocities, electrical resistivity and hydraulic permeability.

The seismic velocities describe the relationship between the elastic properties of a medium to its density regarding the elastic wave speed moving through a body of that medium. The body waves can be classified into two types: compressional waves (P-waves) and shear waves (S-waves) (Crampin 1977). These two types have propagation velocities (compressional velocity (V_P) and shear velocity (V_S)) that are determined by the bulk modulus (K), shear modulus (μ) and density (ρ) of the medium they are travelling through (Rabbel 2006). Those two velocities are defined as follows:

$$V_P = \sqrt{\frac{K + \frac{4}{3}\mu}{\rho}}$$

$\qquad$ 2-1

$$V_S = \sqrt{\frac{\mu}{\rho}}$$

$\qquad$ 2-2

The seismic velocities are a common tool used to classify materials or to assess properties of the pore fill. The presence of gas hydrates in sediments is known to cause an increase in the seismic velocities because some of the pore fluids will be replaced by the hydrates. This could cement the sediment grains, increasing their stiffness, and thus increasing the bulk modulus and shear modulus. Typically, the degree of increase in seismic velocities is related to the volume of hydrates formed and their morphological habits. The seismic velocities of hydrate-bearing sediments can be severely changed based on the type of hydrate growth habit even for the same sediments and degree of hydrate saturation (Dvorkin and Nur 1996, Helgerud et al. 1999).

In addition to influencing the seismic velocities of sediments, electrical properties are also affected by the formation of gas hydrates. The electrical resistivity or its inverse electrical conductivity are widely used parameters to characterise electrical charge

transportation through a given medium. Because gas hydrates and most rocks are electrical insulators (Pearson et al. 1983), the charge transport in natural sediments and rocks is generally provided by the conductive pore water. Therefore, when the hydrate forms in the pore space of sediments replacing the pore water, the bulk resistivity of the sediments increases. This increase in resistivity represents the fundamental tool for the detection of hydrate-bearing sediments using resistivity logs (Collett 2001, Boswell et al. 2012). The variance between the resistivity of the water saturation sediments (without hydrate) (R_o) and the measured resistivity of hydrate-bearing sediments (R_t) represents the increase in the bulk resistivity. Formations with R_t greater than R_o give an indication of gas hydrate occurrence in the sediments.

Changes in the seismic and electrical properties due to the presence of gas hydrates are mainly used to map and explore natural gas hydrate accumulations. The transition of sediments pore filling from free gas and water to hydrates is accompanied by an intense acoustic impedance (wave velocity $\times$ density) variation, which results in significant seismic reflection (Berndt et al. 2004). These seismic reflections generally crosscut sedimentary layers and follow the topography of the seabed, which is why they are indicated as bottom simulating reflectors (Kvenvolden et al. 1983).

To investigate the physical properties of gas hydrate reservoirs on a laboratory scale, studies are generally kept uncomplicated by considering it as a homogenous sediment sample. Medium and coarse sand (quartz) are most favourably used as hydrate-bearing sediments due to their high permeability that gives the most promising gas production rates in the case of economical gas production from hydrate-bearing sediments. Table 2-5 lists the seismic velocities and electrical resistivities of materials, which are frequently considered in sand gas hydrate reservoirs. The various materials cover a wide range of each physical property and the large disparity between these properties allows the physical detection of the process of hydrate formation and dissociation.

Table 2-5 Seismic and electrical properties of materials that are generally considered in natural gas hydrate reservoirs

Material	V_P, m/s	V_s, m/s	Resistivity, Ωm
Ice	3900 (Shaw 1986)	1900 (Shaw 1986)	$\sim 4 \times 10^3$ (Du Frane et al. 2011)
Methane gas	412 (Waite et al. 2009)	0 (Waite et al. 2009)	$\rightarrow \infty$
3 wt% brine	1412 (Mavko et al. 2009)	0 (Mavko et al. 2009)	3.77 (Mavko et al. 2009)
Bulk methane hydrate	3369 (Whiffen et al. 1982)	-	$\sim 2 \times 10^3$ (Du Frane et al. 2011)
Sediment (quartz)	6040 (Helgerud et al. 1999)	4120 (Helgerud et al. 1999)	$\sim 2 \times 10^{14}$ (Schon 1998)

2.7.4   Visual Observation of Hydrates in Sediments

Previously, considerable attempts have been conducted to observe hydrate formation and morphology (macro and micro scale) in the pore space of sediments. One of these attempts was conducted by Brewer et al. (1997) who investigated the hydrate formation process by bubbling gas into two types of sediments (coarse-grained and fine-grained) at a depth of 910 m in the ocean. It was observed that in the coarse-grained matrix, gas hydrates filled the pore space in a dispersed nature, whereas in the fine-grained sediments, gas hydrates were formed in channels (veins) and grew until large masses formed. These findings have been confirmed by hydrate core sampling. The observation of actual hydrate growth directly represents the first concept of the formation mechanism.

Since then, various characterisation methods have been applied to study the gas hydrate microstructure and growth pattern in sediments such as direct microscopy

observation (Tohidi et al. 2001), nuclear magnetic resonance (NMR) (Mork et al. 2000, Kleinberg et al. 2003), magnetic resonance imaging (MRI) (Baldwin et al. 2003, Zhao et al. 2011) and high resolution X-ray micro-computed tomography (μCT) (Kerkar et al. 2014, Chaouachi et al. 2015).

The first direct observation of hydrate formation at the pore scale was conducted by Tohidi et al. (2001). They formed CO_2 and CH_4 hydrates in a 2D synthesised micromodel. Their results showed that hydrates formed from the free gas beginning at the gas-liquid interface and hydrates mainly existed in the pores without contacting the grain surface. However, grains could be cemented by hydrates if they were small, or in the case of pores were almost filled with hydrates.

NMR-related technologies have also been used to study inclusion complexes since the 1960s (Brownstein et al. 1967). However, this technique was developed afterwards for utilisation in a variety of gas hydrate studies. Using NMR, Kleinberg et al. (2003) suggested that hydrate formed mainly in the large pores of sediments without coating the grain surface. Cheng et al. (2013) investigated the formation and dissociation of carbon dioxide hydrate in porous media using MRI and also measured the induction time and hydrate saturation. Their findings demonstrated that the free pore water was identified by a strong MRI signal; however, the solid hydrate was not detected due to the background noise. Daraboina et al. (2013) used MRI to investigate the kinetics of CH_4-C_2H_6-C_3H_6 hydrate formation in the presence of a kinetic inhibitor. Their study confirmed the efficiency of MRI as a technique for visualisation and valuation of the performance of the inhibitor on gas hydrate formation.

Recently, high-resolution X-ray computed tomography has shown an advantage for characterising gas hydrate-bearing sediments. The first discovery of X-ray was in 1895 by the German engineer and physicist Wilhelm Röntgen (Röntgen 1896). X-ray is a type of electromagnetic waves with high frequency. They are similar to normal light but have more energy and shorter wavelengths (~ 10^{-10} m) (Hau-Riege 2012). Such waves have the ability to pass through opaque objects. Thus, the X-ray technique presents a non-destructive tool for imaging the microstructure features within the interior of solid materials, and it is considered to be a significant contributor to the understanding of gas hydrates in sediments. This technology offers a fine spatial resolution that is easy to adapt and apply to various experimental studies (Akin and

Kovscek 2003). Various studies have been performed to observe the microstructure of hydrate-bearing sediments via the X-ray technique. Examples of these research studies are presented in Table 2-6.

Table 2-6 Examples of research studies observing the hydrate microstructure in sediments via the X-ray technique

Research	Hydrate	Porous media	Description
Mork et al. (2000)	THF	Quartz sand	Investigating the hydrate formation and mechanical strength measurement of hydrate-bearing samples. They could not gain useful information via computed tomography (CT) scanner due to the difficulties in differentiation between the THF hydrate and liquid mixture.
Jin et al. (2004, 2006)	CH_4	Sand	Direct determination of porosity and hydrate saturation of hydrate sediments without destroying the sample.
Waite et al. (2008)	CH_4	Sand	Investigating the physical properties of hydrate-bearing sediments
Kneafsey et al. (2007)	CH_4	Silica sand	Observation of the hydrate system behaviour during the formation and dissociation of methane hydrate. The results showed that the hydrate formation rate was not constant but occurred mainly at the starts. The percentage of water converted to hydrate was 65% depending on a hydration number of 5.75.

Research	Hydrate	Porous media	Description
Kerkar et al. (2009)	THF	Glass spheres	Imaging the THF hydrate patches in regular sized glass spheres; the results showed random formation and growth with grain movements but without being affected by the cell wall.
Kneafsey et al. (2011)	CH_4	Sand, sand/silt	Observation of location-specific density variation resulting from hydrate formation and water flowing; the images showed a heterogeneity formation of hydrate within the host sediments.
Seol and Myshakin (2011)	CH_4	Sand	Prediction of porosity and distribution of the water phase in samples containing hydrates; quantifying the influence of grains size distribution during the formation and dissociation of methane hydrate.
Rees et al. (2011)	CH_4	Natural cores collected from drilling sites	Obtaining detailed 3D images of the internal structure of natural samples containing gas hydrates.
Zhao, Yang, et al. (2015)	CH_4	Different sized sands	Investigating the microstructure and distribution of hydrates forming in a porous medium. The results showed that hydrates are randomly distributed in the pores without contacting the grains.

Research	Hydrate	Porous media	Description
Chaouachi et al. (2015)	Xenon	Different types of sand and glass beads	Observation of the crystallisation and growth processes of xenon hydrate in various sediments; hydrate was formed using juvenile water and metastable gas-enriched water.
Schindler et al. (2017)	THF	Glass beads	Obtaining information about hydrate distribution in the pore space. The images indicate that the formed hydrates followed the pore-filling model.

2.7.5   Laboratory Techniques for Hydrate Formation in Sediments

Hydrate formation in sediments is a long-time process that depends mainly on the degree of gas solubility in the liquid phase. Several laboratory techniques have been suggested that aim to balance smooth formation with achieving hydrate distribution resembling natural samples. Different formation techniques result in diverse hydrate patterns and distribution, and consequentially influence the physical properties of hydrate-bearing sediments, as discussed previously. Sediments with the same hydrate saturation but various pore filling patterns may produce several degrees of variation in their physical properties (Dai et al. 2012).

The successful laboratory formation methods are summarised below.

2.7.5.1   Hydrate Formation by Dissolved Gas

The hydrate formation by this method is achieved by circulating liquid containing dissolved gas as a hydrate former through sediment under hydrate stability conditions. As mentioned above, gas solubility in the liquid phase governs the hydrate concentration and influences the formation time. Thus, gases with high solubility (e.g. CO_2) are generally used in such methods (Tohidi et al. 2001, Katsuki et al. 2006). In addition, it has been reported that the hydrate formation process from dissolved

methane requires a long duration time (up to a few weeks) and advanced equipment, making such approach an experimental challenge (Spangenberg et al. 2005, Waite and Spangenberg 2013).

Typically, the saturation of hydrate formed by this method does not exceed 70% (Waite et al. 2009), and it nucleates heterogeneously within the coarse-grained sediments on the grain surface and grows into the pore space (Yun et al. 2005). Acoustic velocity measurements for sediments containing hydrate formed by this method suggest that the hydrate follows the load-bearing behaviour at saturation levels above 40% but follows pore-filling behaviour at levels below that (Spangenberg et al. 2005).

2.7.5.2   Hydrate Formation by the Partial Saturation Method

In this method, the hydrate is formed with partially water-saturated sediments by pressurising the system with the former gas under controlled pressure-temperature conditions (Waite et al. 2004). Then, the sample is cooled to the hydrate equilibrium temperature. In sandy sediments, the hydrate formed by this method produces a grained cementing hydrate because the hydrate forms at the grain contact areas. The cemented hydrate could bond sand particles at low hydrate saturation, thus producing sediment with a stiffer skeleton higher than that of pore-filling hydrates (Priest et al. 2005). Typically, the hydrate formed in the high gas flux regions represents most of this hydrate distribution pattern (Bohrmann et al. 1998).

A successful experiment was conducted to form CO_2 hydrate in partially saturated clay-silt sediments with different hydrate saturations (Kim et al. 2013). The authors described the hydrate behaviour as 'weak cementation', which was identified as transitional behaviour between load-bearing and grain-cementing patterns. This behaviour was assumed to be because of weak connections between hydrate clusters and the mineral surface due to the existence of the water film on the mineral grains.

2.7.5.3   Hydrate Formation by Excess Water Method

Recently, the excess water method has been introduced as another approach for gas hydrate formation at the laboratory scale (Priest et al. 2009, Clayton et al. 2010, Falser et al. 2013). In this method, a known volume of hydrate former (gas) is introduced to the sedimentary sample and then accompanied by an excess water injection (Priest et al. 2009). The gas is allowed to exist as small bubbles within the sediment pore space. This hydrate formation process is considered an analogue to the conditions for natural hydrates formed within the water-saturated sediments in nature (Winters et al. 2004, Lee and Waite 2008). Hydrates formed by this method are not restricted to exist at the inter-grain contacts; thus, the cementing behaviour has not been observed for hydrate saturation below 20% (Priest et al. 2009, Spangenberg et al. 2014). In addition, it has been reported that there are large differences in seismic wave velocities of sediments containing hydrates formed via this method and other methods (Best et al. 2013).

2.7.5.4   Hydrate Formation from Soluble Hydrate Former (Tetrahydrofuran)

Another technique for laboratory hydrate formation involves forming hydrate using soluble hydrate former (e.g. THF, C_4H_8O as shown in Figure 2-21 (a)). THF is a hydrate former (liquid at room temperature) that is colourless and is fully mixable with water. THF has been widely employed for laboratory synthesising of hydrate in sediments and provides specific control of hydrate saturation and a rapid hydrate formation process compared to the long process of methane hydrate formation (Lee, Yun, et al. 2007). THF forms sII hydrate as only the large cavities are occupied as shown in Figure 2-21 (b). It has been found that a solution composed of THF and water in a molar ratio of 1:17 can form THF hydrates at ~ 4 °C under atmospheric pressure (Leaist et al. 1982).

In similar behaviour to that of hydrates formed from dissolved gas, THF hydrate forms on grain surfaces and grows toward the sediment pore space (Waite et al. 2009). THF hydrate dissociation does not produce free gas; thus, there is no significant change in the volume resulting from dissociation compared to that of the gas hydrate**.**

Yun et al. (2007) studied THF hydrate formation in silt, clay and sand sediments at 50% and 100% hydrate saturation. They conducted their experimental study by

saturating the dry samples with THF and water mixture, applying the effective stress to the specimen and then cooling. Several other studies have been conducted to form THF hydrate following the same procedure such as Lee et al. (2010) and Santamarina and Ruppel (2010).

(a)   (b)
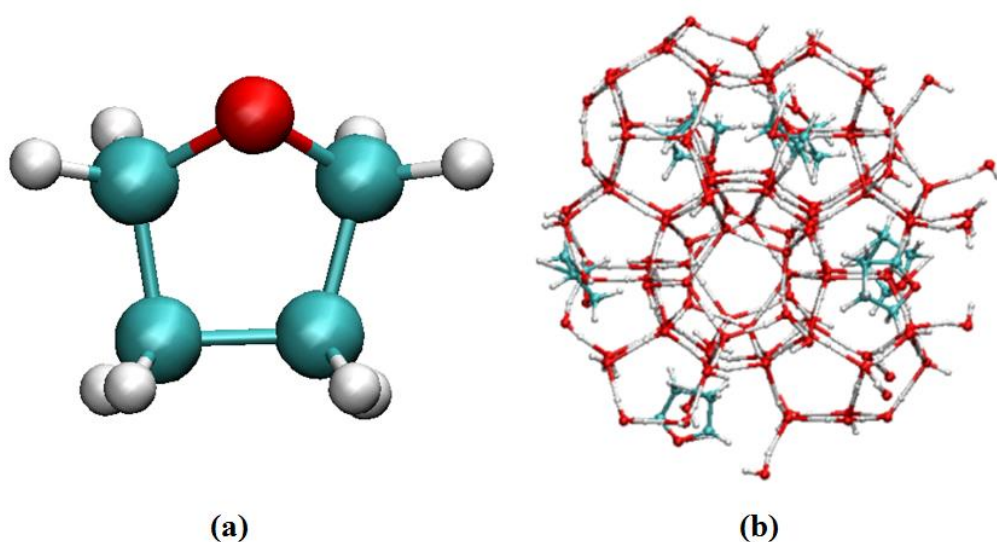
Figure 2-21 Scheme illustrating (a) Tetrahydrofuran molecule and (b) Tetrahydrofuran hydrate. Green is carbon atoms, white is hydrogen atoms, and red is oxygen atoms (Conrad 2009)

Chapter 3   Apparatuses and Experimental Methods

This chapter introduces comprehensive characterisation of the experimental systems, procedures and materials utilised to accomplish the aims and objectives of this research. The three systems discussed are the PVT cryogenic sapphire cell for determination of the equilibrium conditions of hydrates, the ultrasonic measurement system for the determination of the compressional wave velocities of hydrate-bearing sediments and the μCT-CO_2 hydrate formation system for analysing the pore-scale of hydrate in sandstone.

3.1   PVT Cryogenic Sapphire Cell for the Determination of Equilibrium Conditions of CH_4+CO_2, CH_4+N_2 and CO_2+N_2 Hydrates

The PVT cryogenic sapphire cell system was employed to determine the hydrate equilibrium data for different gas mixtures. This system was manufactured and supplied by Sanchez Technologies (France) and is installed at the Clean Gas Technology Australia research centre. The PVT sapphire cell apparatus has the ability to analyse the behaviour of the fluid, determining hydrates and evaluating the efficiency of hydrate inhibitors under various operating conditions.

3.1.1 PVT Cryogenic Sapphire Cell System

Figure 3-1 shows the PVT sapphire cell apparatus. The entire system is comprised of the following:

(a)   A cylindrical PVT sapphire cell unit with a total inner volume of 60 mL, as shown in Figure 3-2, and that is placed inside a controlled air bath at working temperatures varying from -160 °C to 100 °C. The cell itself is made of protected sapphire material designed for high pressure up to 500 bar and is isolated from the outside environment by a strengthened glass window. The cell is equipped with a magnetic stirrer (rotating at different velocities by a motor drive) that provides the required agitation for hydrate formation.

(b) A series of pumps including a vacuum pump (Edwards Rotation pump, Model E2M2), positive displacement pump and pneumatic gas booster pump (Haskel, model AA-30).

(c) A cooling/heating system: the unit is connected to a chiller (R2G2 Series Cooler-*AQUA*) providing cooling during the hydrate formation process. The cooling and heating processes are enhanced using a fan that circulates the cold or hot air through the bath surrounding the cell.

(d) Various thermocouples (RTD PT100 sensors, Model TC02 SD145; Hinco) and pressure monitoring sensors (Sanchez).

(e) Gas supplying and transporting lines of 6.4 mm (1/4 inch) size equipped with all associated valves and fittings (all provided by Swagelok Western Australia).

(f) Digital displays and computer software for monitoring the pressure and temperature during the experiments. Two colour video cameras, Sony HYPER HAD (5× magnifying lens), placed against the cell window for visual observation of the behaviour of the cell contents. These cameras are of great importance for hydrate equilibrium and formation experiments owing to the reliance on visual indications and changes.

(g) Gas injection manifold installed to allow several gas sample bottles (canisters) to connect and feed gas into the system.

Figure 3-1 PVT Cryogenic Sapphire Cell Apparatus
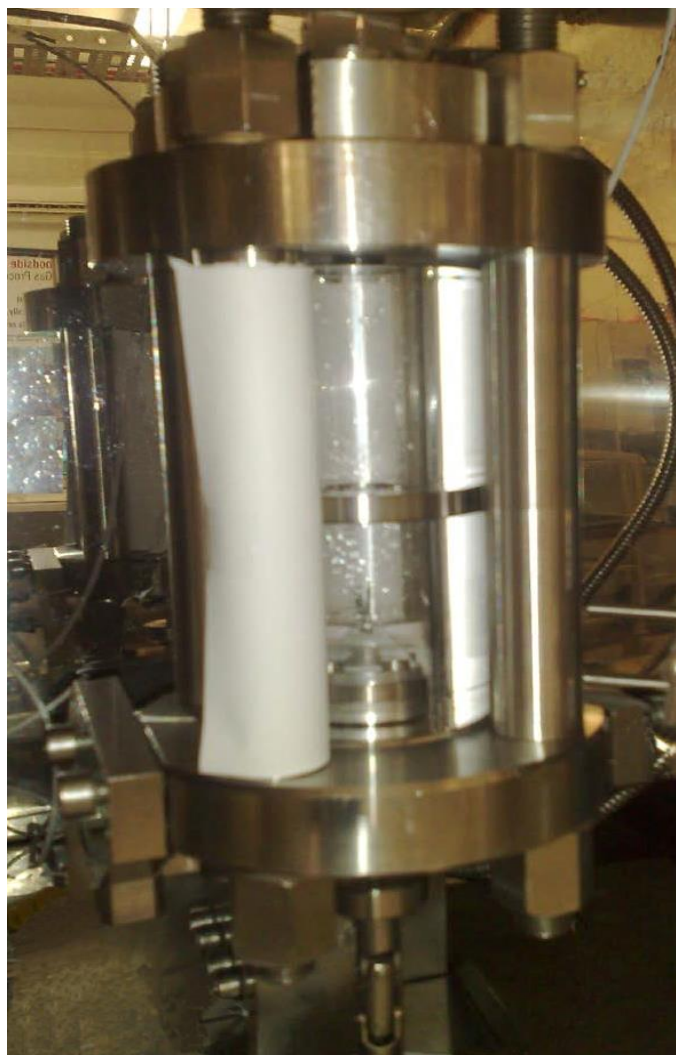
Figure 3-2 Cylindrical Sapphire Cell

3.1.2 Materials and Gas Mixtures Preparation

Deionised water (electrical resistivity of 18 MΩ.cm at 25 °C) from David Gray was used as the liquid. Methane, carbon dioxide and nitrogen, all supplied by BOC Australia and of high purity (99.95 mol.% to 99.99 mol.%), were used as a pure gas or gas mixtures The preparation of gas mixtures at the desired composition was conducted on a weight basis using 500 mL stainless sample bottles as follows:

1- Vacuuming the residual gas and air from all the sample bottles using the vacuum pump.

2- Weighing each individual bottle using a high accuracy electrical balance from Shimadzu, model UW6200H (accuracy of ± 0.01 g).

3- Supplying the bottles with the required gas from the main gas cylinders and reweighing.

4- Determining the gas quantity and concentration when mixed by the following equations:

$$n_i = \frac{\Delta m_i}{M_i}$$ 3-1

$$X_i = \frac{n_i}{n_t}$$ 3-2

where, n_i and m_i are moles and mass of component (i) gas, respectively; M_i is the molecular weight of gas (i); and X_i is the gas (i) mole fraction. All compositions of gas mixtures used in this PVT sapphire cell experiment are listed in Table 4-2 (chapter 4). Prior to each experiment, the CO_2 and CH_4 compositions in the gas mixtures were verified by sample testing using two gas sensors (Gas Alarm Systems, PolyGard manufactured by MSR model MGC-03) with a standard accuracy of ± 0.05.

3.1.3   Set-up and Experimental Procedure

A schematic of the experimental set-up is depicted in Figure 4-1, and a detailed description of the apparatus is given in chapter 4. This apparatus was used to procure the hydrate dissociation conditions by employing the temperature research method at constant pressure (isobaric method) (Kim et al. 2011, Loh et al. 2012, Smith et al. 2015, AlHarooni et al. 2015, Smith et al. 2016). This method includes stimulating the cell content (fluids) by cooling and heating processes to enhance the hydrate formation and dissociation by maintaining a constant pressure.

Before the beginning of each experiment, the apparatus was cleaned and purged with nitrogen to remove any impurities that could affect the results. The gas sample bottles were connected to the gas manifold to allow the gases to be mixed and transferred via the piston pump to the sapphire cell. Then, deionised water (5 mL) was syringed into the evacuated sapphire cell through the upper inlet. The nitrogen and air were

vacuumed from the entire system using the vacuum pump, following the pressurisation of the cell with the prepared gas mixtures via a pneumatic pump in combination with the piston pump. When the prescribed pressure was achieved, the stirrer was switched on, and the cooling of the sapphire cell contents (fluids) was initiated at a rate of 2 K/h for gas hydrate formation. After completing the hydrate crystallisation, which was visually observed via the control PC, the cooling was stopped. The sapphire cell was then heated at a rate of 2 K/h to start the hydrate dissociation. During each experiment, the hydrate dissociation conditions (pressure and temperature) and stirrer currents were determined.

Finally, the PVT sapphire cell was depressurised and the fluids were evacuated through the cell outlet on the bottom cell base followed by flushing of the cell with deionised water several times and cleaning it for the next experiment.

3.2 Ultrasonic Measurement System for the Determination of Compressional Wave Velocities of Hydrate-bearing Sediments

The compressional wave velocities for THF and CO_2 hydrate-bearing sandstone samples were measured using an experimental set-up consisting of the following essential parts:

(a) High-pressure cell (Figure 3-3 and Figure 3-4), which was designed for simultaneous acoustic measurements and hydrate formation in a sample of 3.8 cm (1.5″) in diameter. This cylindrical cell was composed of a polyether ether ketone with a base for attaching two piezo-electric transducers to the outside wall. A thermocouple was attached to the cell to monitor the temperature during the experiment with a precision of ± 0.5 K.

(b) Various pumps were used for fluid injections and to confine the pressure. In the THF hydrate experiments, a high-performance liquid chromatography (HPLC) pump (LC-20AT Shimadzu Ltd.) was used for liquid injection (THF + brine) whereas the confining pressure was applied using a hand oil pump. Three syringe pumps (ISCO 500D) with high accuracy of 0.1% were used in the CO_2 hydrate formation experiment; the first two pumps were used for CO_2 and brine injection, and the third pump was used to apply the confining pressure by compressing the deionised water.

(c) A thermo-refrigerated bath (Alpha RA8, Lauda, Germany) was used to circulate a coolant antifreeze liquid containing ethylene glycol via a copper coil wrapped around the flowing cell. This bath provided the cooling temperature required for the hydrate formation process.
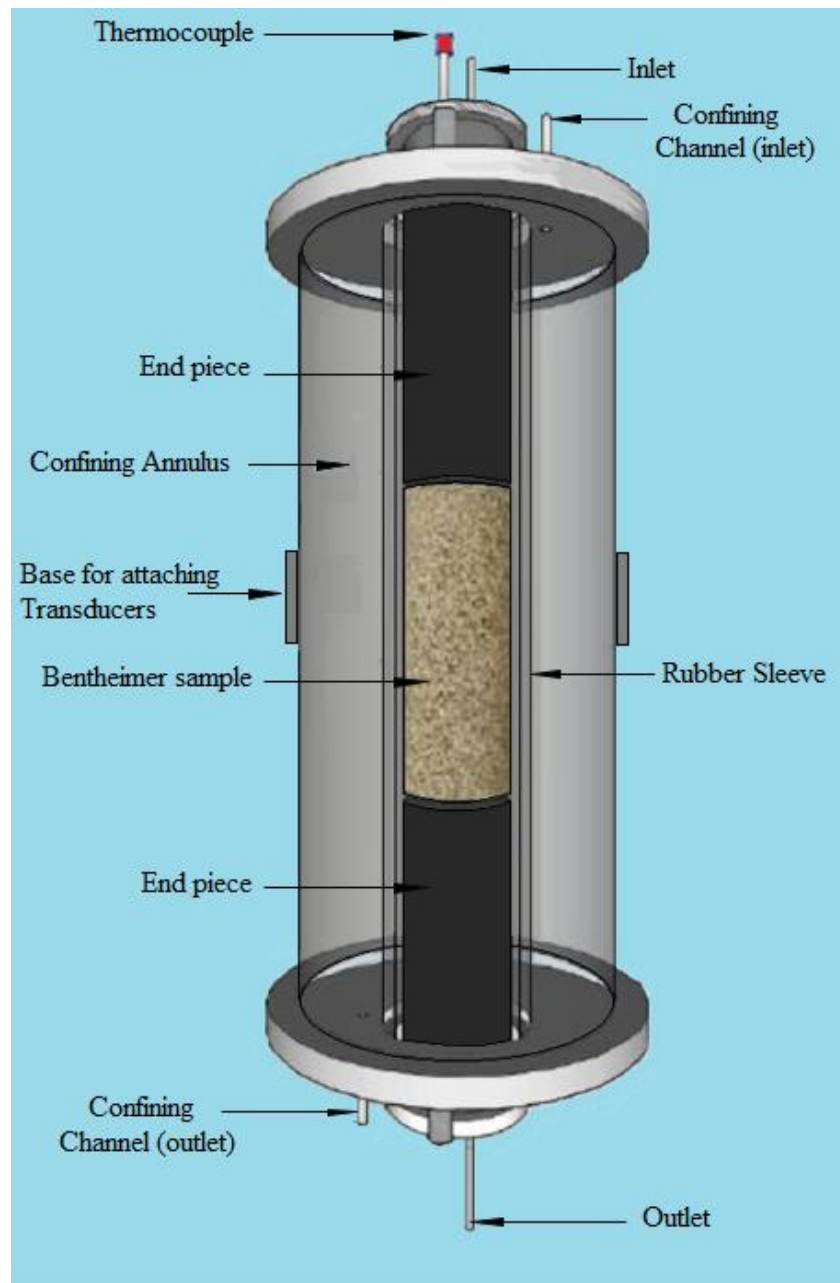
Figure 3-3 High-pressure cell (core holder) used in ultrasonic measurements for determining the compressional velocities of hydrate-bearing sediments
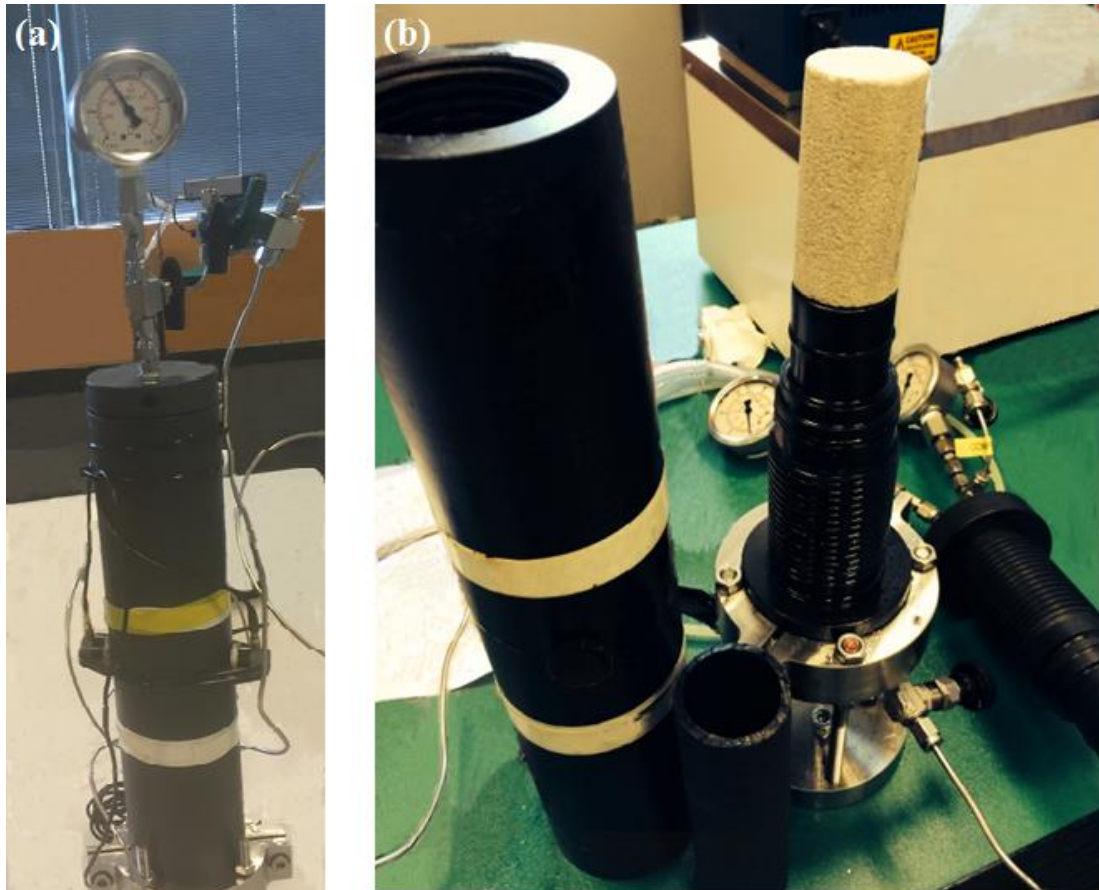
Figure 3-4 Photograph showing (a) high-pressure cell and (b) a sandstone sample placed in the middle of the high-pressure core holder

(d) An ultrasonic measurements system comprised of a Pulser-receiver (model 5072PR, OLYMPUS), digital oscilloscope (model DS4022, RIGOL) and two piezo-electric transducers (1 MHz, model A114S, OLYMPUS) as shown in Figure 3-5. This system was used to determine the compressional velocities through the sample before, during and after hydrate formation.
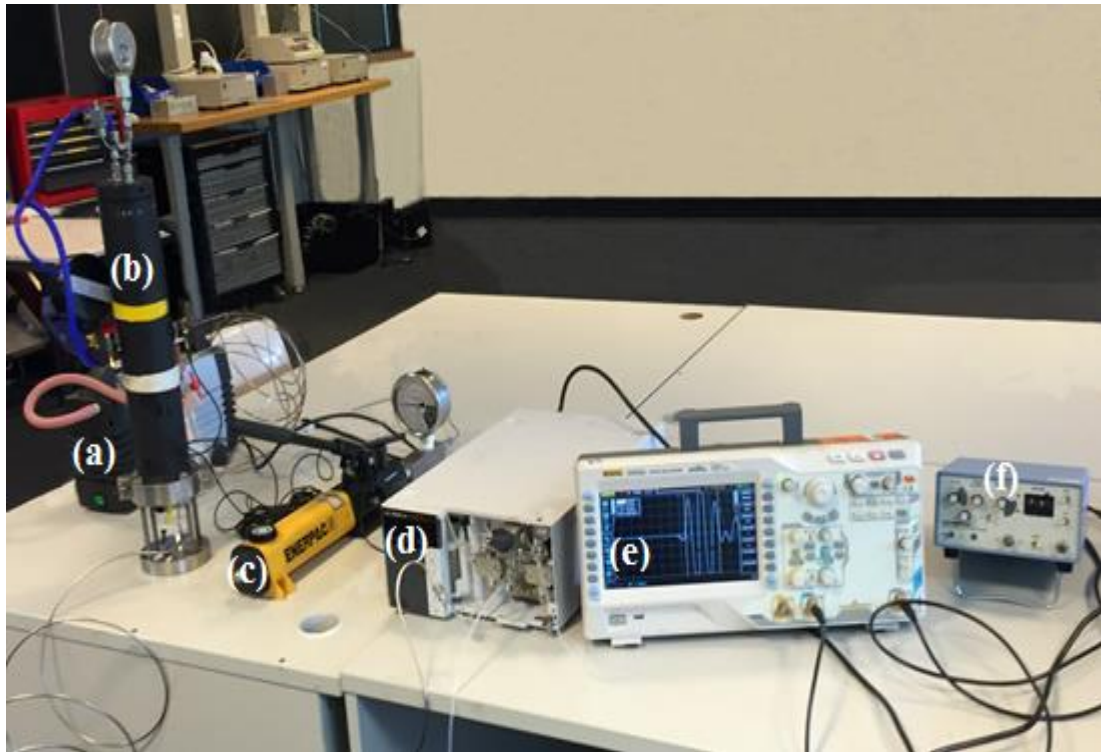
Figure 3-5 Photograph showing the experimental set-up for the determination of compressional wave velocities of hydrate-bearing sediments: (a) vacuum pump; (b) high-pressure cell; (c) hand oil pump; (d) HPLC injection pump; (e) oscilloscope and (f) pulser/receiver

3.2.1 Materials and Sample Preparation

The cylindrical Bentheimer sandstone core samples (3.8 cm in diameter and 8.1 cm in length) from Kocurek Industries were used as an experimental hydrate-bearing porous medium. Bentheimer is a clean, homogeneous sandstone consisting mainly of quartz (99 wt%) with high permeability and porosity (Rahman et al. 2016). Figure 3-6 shows an example of the Bentheimer sandstone cores used in this study. The petrophysical properties (porosity and permeability) of the Bentheimer samples were determined experimentally using a nitrogen automated permeameter-porosimeter (AP-608 with an accuracy of $\pm$ 0.1%). THF (purity of 99.9 mol%) from Sigma-Aldrich Germany and carbon dioxide (purity 99.9 mol%) supplied by BOC Australia were used as hydrate formers. The aqueous solution (brine) used was prepared by mixing sodium chloride (NaCl) or sodium iodine (NaI) both obtained from Rowe Scientific with purity $\geq$ 99.5

mol% into deionised water from David Gray. The salts were dissolved in deionised water to achieve the desired concentrations.
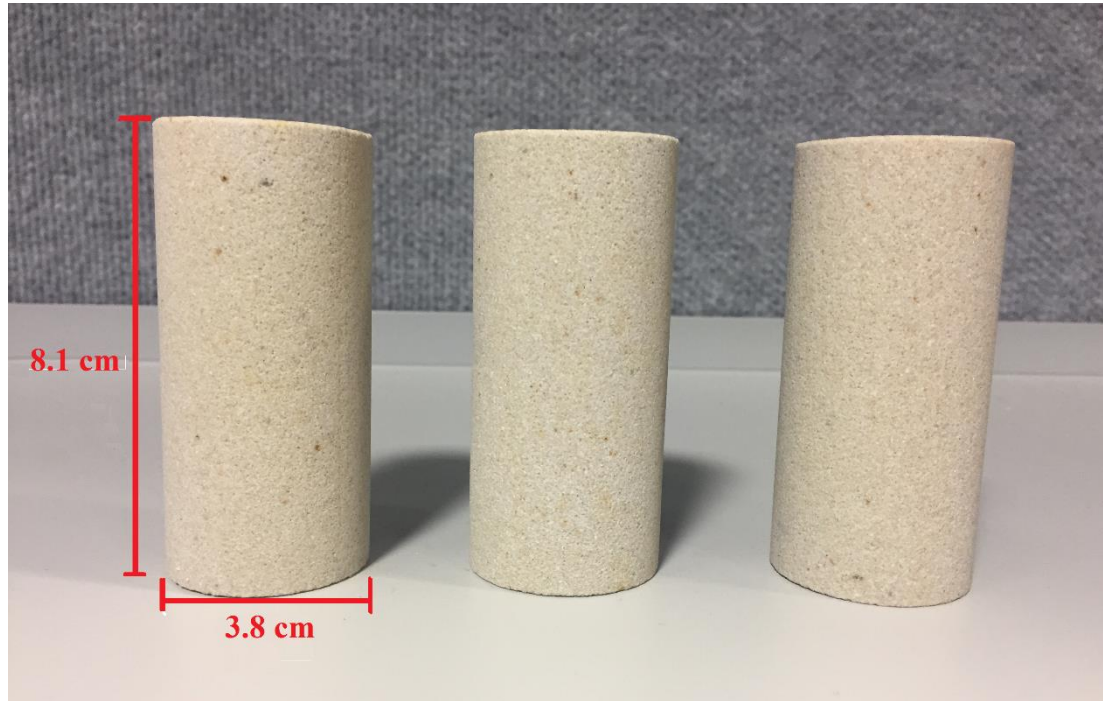
Figure 3-6 Bernheimer sandstone core samples used for compressional velocities experiments

3.2.2 Experimental Procedure

To protect the rubber sleeve from the injected fluids, first, clean dry samples were wrapped in a layer of plastic foil before they were placed inside the high-pressure cell. Then, the cell was connected to the experimental system through the fluids line. The cell was placed inside the cooling bath, and the injection pumps, confinement pump and transducers were connected. Then, the entire system including the core sample were vacuumed for 24 h using the vacuum pump to remove any air from the system, and the confining pressure was raised to 8 MPa. The sample was then fully saturated with brine by injecting more than 1000 pore volumes (PV) of brine into the cell via the inlet tube connected to the top of the cell. Subsequently, the hydrate former (THF testing solution or CO_2 gas) was injected into the cell at the same conditions and the desired flow rate. The hydrate formation process was then started by decreasing the

temperature to the hydrate forming temperature. The THF hydrate can form at atmospheric pressure and temperature below 277 K whereas the CO_2 hydrate forming conditions are 3 MPa and 274 K. During this process, the P-wave velocity measurements were recorded while maintaining a constant temperature. Increasing the P-wave velocities indicated that hydrate was formed. The hydrate formation process was completed when there was no change in the compressional velocities. Consequentially, P-waves were recorded as a function of a series of confining pressure (2–20 MPa). Details of both THF and CO_2 hydrate formation procedures are presented in chapter 7.

3.3   X-Ray Micro Computed-CO_2 Hydrate Formation System for Analysing Pore-scale of Hydrate in Sandstone

Here, the experimental system included the following two parts: the CO_2 hydrate formation system and the μCT imaging instrument. The experimental set-up for the CO_2 hydrate formation in sandstone is the same as described in section 3.2. However, a smaller high-pressure cell (Lebedev et al. 2017, Iglauer and Lebedev 2017) was used for CO_2 hydrate formation and μCT imaging of small Bentheimer plugs (diameter = 5mm) as shown in Figure 3-7. The main body of the cell was made from polyether ether ketone (diameter = 21 mm, length = 300 mm) supplied by RS Components. The plug was fitted in a hole of 8 mm in diameter. The confinement pressure was supplied via union fittings (1/4″) passing through stainless steel fluid tubing (1/8″) inside the high-pressure cell. A high-resolution μCT instrument (3D X-ray Microscope VersaXRM 500; XRadia-Zeiss) was used to image the CO_2 hydrate-bearing plug at a high resolution of 3.43 μm^3. A detailed description of the experimental set-up is given in Chapter 6.

Figure 3-7 High-pressure cell for CO$_2$ hydrate formation in small plugs and CT imaging

3.3.1 Materials and Sample Preparation

The experiments were performed on a small cylindrical Bentheimer sandstone plug (diameter = 5 mm, length = 15 mm) as shown in Figure 3-8; this plug was drilled from a clean homogenous Bentheimer block from Kocurek Industries and was used as the host porous medium for carbon dioxide hydrate in this study. Carbon dioxide with a purity of 99.9 mol% supplied by BOC Australia was used as the hydrate-forming gas. The aqueous solution used in this study was sodium iodide (NaI) brine prepared by dissolving 6 wt% of NaI salt into deionised water. The iodide was used in this experiment to ensure sufficient X-ray contrast during the imaging process.

Figure 3-8 Photograph of the small cylindrical Bentheimer plug using µCT imaging experiment

3.3.2 Experimental Procedure

The clean small Bentheimer plug was jacketed in the rubber sleeve and connected to the fluid lines inside the pressure-cell (core holder), and the core holder was then connected to the hydrate formation system (see Figure 6-1). The experimental system including the core holder and flow lines were vacuumed for 24 h to remove air from the entire system. Then, the cell was pressurised by increasing the confining pressure and the pore pressure to 8 MPa and 3 MPa, respectively. The cooling process was achieved by decreasing the temperature to 274 K. These conditions were maintained for 24 h to allow hydrate to form and grow inside the core sample. After completing the hydrate formation process, the cell was placed inside the µCT instrument, and an image of the hydrate-bearing core was acquired at a high resolution of $(3.43 \ \mu m)^3$.

The cell including the core sample was then left in the μCT scanner for 24 h at room temperature (294 K), and the core sample was again imaged using μCT at the same high resolution. More details of the experimental set-up, procedure and segmentation of the μCT images are discussed in chapter 6.

Chapter 4 Experimental Determination of Hydrate Phase Equilibrium for Different Gas Mixtures Containing Methane, Carbon Dioxide and Nitrogen with Motor Current Measurements*

4.1   Summary

Hydrate dissociation equilibrium conditions for carbon dioxide + methane with water, nitrogen + methane with water and carbon dioxide + nitrogen with water were measured using a cryogenic sapphire cell. Measurements were performed for the temperature range of 275.75 K to 293.95 K and for pressures ranging from 5 MPa to 25 MPa. The resulting data indicated that as the carbon dioxide concentration was increased in the gas mixture, the gas hydrate equilibrium temperature increased. In contrast, increasing the nitrogen concentration in the gas mixtures containing methane or carbon dioxide decreased the gas hydrate equilibrium temperatures.

In addition, the motor current changes during the hydrate formation and dissociation processes were measured by keeping the rotation speed of the magnetic stirrer constant, which was connected to a DC motor. The motor current measurements were reported and showed that the hydrate plug formation and dissociation could be predicted by the changes in the motor current.

4.2   Introduction

In recent years, the importance of gas hydrates has significantly increased in the energy sector. Large amounts of natural gas hydrate deposits have been discovered beneath the permafrost areas and in deep oceanic sediments (Buffett 2000, Kim et al. 2005, Sloan and Koh 2008). These deposits present an enormous fuel resource (Makogon 2010), with ~2.1×10^{16} m^3 methane gas reserves estimated (Kvenvolden 1988), which is more than double the entire combined world reserves of oil, natural gas and coal (Makogon et al. 2007, Moridis 2008, Sloan and Koh 2008). Therefore, the oil and gas industry are now looking into commercially producing gas from these deposits, and preferably combining this production with the sequestration of carbon dioxide (Goel 2006, Eslamimanesh et al. 2012, Wood 2015). In addition, gas hydrates have received

growing attention because of their role in carbon dioxide capture to reduce carbon dioxide emissions (Adeyemo et al. 2010, Dashti et al. 2015), gas storage (Sun et al. 2003, Taheri et al. 2014), transportation (Taheri et al. 2014), cool-energy storage (Xie et al. 2010, Wood 2015) and water desalination (Park et al. 2011, Eslamimanesh et al. 2012). Thus, such low temperature, high-pressure reservoirs are a potential sink for anthropogenic carbon dioxide storage and climate change may be mitigated via this route (Kvamme et al. 2007). Second, gas hydrate formation presents the main flow assurance problem in the oil and gas industry (Englezos 1993, Sloan and Koh 2008, Haghighi et al. 2009). Here, gas hydrate particles can agglomerate and build-up gradually so that a large mass of hydrate is formed, which can block flowlines, valves, chokes and other production equipment (Najibi et al. 2009, Sloan et al. 2010).

Natural gas hydrates (clathrate hydrates) are solid ice-like, non-stoichiometric structures that consist of water and small gas molecules such as methane, carbon dioxide, nitrogen, ethane, propane or butane (Bishnoi and Natarajan 1996, Sloan and Koh 2008, Delli and Grozic 2014). Clathrate hydrates are classified into the following three categories based on the arrangement of the water molecules in the crystal structure and the size of the gas molecules: sI, sII and sH (Sloan 2003, Sloan and Koh 2008, Carroll 2014). Typically, gas hydrates are formed and are stable under high-pressure conditions at temperatures above the freezing point of water up to 25 °C if a gas hydrate former (i.e. a gas) and a sufficient amount of water are available (Sloan and Koh 2008).

In this context, several experimental studies have reported hydrate equilibrium data for various gas mixtures, including for methane, nitrogen and carbon dioxide (Unruh and Katz 1949, Adisasmito et al. 1991). Later, Ohgaki et al. (1993), Fan and Guo (1999), Seo et al. (2000), Kang et al. (2001), Seo et al. (2001), Bruusgaard et al. (2008) and Sun et al. (2015) measured hydrate equilibrium data for CO_2 and CH_4 or N_2, whereas the N_2-CH_4 hydrate data were reported by Jhaveri and Robinson (1965), Lee et al. (2006) and Mei et al. (1996). A summary of the experimental hydrate equilibrium data reported in the literature for the CH_4+CO_2, CH_4+N_2 and CO_2+N_2 gas mixtures in the presence of water are listed in Table 4-1.

Most of the existing experimental data are limited to low and medium pressure conditions, while gas hydrates naturally exist in a high-pressure environment.

Moreover, natural gas production from deep reservoirs requires hydrate prevention at high pressures; thus, reliable and accurate hydrate equilibrium measurements are essential to formulate and validate thermodynamic models for predicting the hydrate-forming conditions.

We thus measured hydrate equilibria for various gas mixtures (methane + carbon dioxide), (methane + nitrogen) and (nitrogen + carbon dioxide) for a wide range of temperatures and pressures.

Table 4-1 Review of the Gas Hydrate Equilibrium for CH₄+CO₂, CH₄+N₂, and CO₂+N₂ and Water Systems

System	Reference	T/K	P/MPa
CH₄+CO₂	Unruh and Katz (1949)	275.5 – 285.7	1.99 – 7.00
	Adisasmito et al. (1991)	273.7 – 287.4	1.45 – 10.95
	Dholabhai and Bishnoi (1994)	277.56-284.84	3.41 – 17.90
	Ohgaki et al. (1993)	280.3	3.04 – 5.46
	Fan and Guo (1999)	273.5 – 282.3	1.10 – 4.80
	Servio et al. (1999)	273.5-283.1	1.7-5.070
	Seo et al. (2001)	274.3 – 283.5	1.5 – 5.0
	Beltrán and Servio (2008a)	275.1 –285.3	1.92 –7.47
	Belandria et al. (2011)	279.1–289.9	2.96 –13.06
	Belandria et al. (2011)	277.9 –285.5	2.72–8.27
	Herri et al. (2011)	277.15	2.04 – 3.90
	Sabil et al. (2014)	272.15 –290.15	1.10 –15.29
CH₄+N₂	Jhaveri and Robinson (1965)	282.8 – 294.4	7.40 – 35.96
	Mei et al. (1996)	273.2 – 279.8	2.64 – 32.42
	Lee et al. (2006)	273.30 –285.05	8.325 –20.70
CO₂+N₂	Fan and Guo (1999)	273.1 – 280.2	1.22 – 3.09
	Kang et al. (2001)	273.75 – 284.25	1.56 – 32.308
	Linga et al. (2007)	273.7	1.6 –7.7
	Bruusgaard et al. (2008)	275.00 – 283.00	2.0 – 22.4
	Kim et al. (2011)	276.88 –285.41	5.0 –20.0
	Herri et al. (2011)	273.40 –281.10	5.60 – 6.10
	Sfaxi et al. (2012)	278.1–285.3	3.24 –29.92
	Sun et al. (2015)	273.4 – 278.4	5.28 – 17.53

4.3 Experimental Methodology

4.3.1 Materials and Gas Preparation

Methane (purity 99.995 mol%), carbon dioxide (purity 99.9 mol%) and nitrogen (purity (99.99 mol%), all supplied by BOC Australia, were used as the received or gas mixtures prepared by mass balance as follows: empty 500 mL stainless steel bottles (Whitey DOT-3E1800 12EK082) were vacuumed using an Edwards Rotation pump (Model E2M2) for 30 min and then weighed using a high-precision electronic balance (Shimadzu model UW6200H, accuracy = 0.01 g). The vacuumed bottles were then filled with the gas(es) from the main cylinders and reweighed. The weight of the empty bottle was 1350 g. The weight difference was then converted into a mole percentage (Table 4-2). Two gas sensors (PolyGard manufactured by MSR) measured CO_2 and CH_4 concentrations in the gas mixtures with a standard uncertainty of $\pm$ 0.05. Deionised water (electrical resistivity of 18 MΩ.cm at 25 °C) was used as the aqueous phase.

Table 4-2 Gas mixtures used in the present study

Component Mol%	Mixture No.									
	1	2	3	4	5	6	7	8	9	10
CH_4%	100	90	84	80	90	80	69	64		
CO_2%		10	16	20					26	36
N_2%					10	20	31	36	74	64

4.3.2 Experimental Apparatus and Procedure

A high-pressure apparatus (Sanchez Technology, France) comprising of a sapphire cell (60 mL inner volume), piston pump and pneumatic booster pump (Haskel, model AA-30), valves and connection tubing was employed for the experiments (Figure 4-1). The temperature of the cell was carefully controlled with a chiller (R2G2, Model R130A3-

P4) and electric heater. Furthermore, two thermometers (RTD PT100 sensor with three core Teflon tails, Model TC02 SD145) were positioned in contact with the liquid and gas at the top and bottom of the sapphire cell, and thus measured the liquid and gas temperatures. The pressure inside the sapphire cell was measured with a pressure sensor (Sanchez). The maximum uncertainty of the pressure and temperature measurements were ± 0.05 MPa and 0.1 K, respectively. All cell contents were continuously mixed with an electric stirrer (550 rpm) driven by a DC motor (equipped with a variable speed drive). By magnetic coupling, the load on the motor was decreased when solid hydrate formed in the cell. The electrical current required to maintain a constant motor speed was measured and it was found to be proportional to the torque load on the impeller.

Hydrate formation and dissociation processes in the sapphire cell were observed visually using two Sony Digital cameras (Model SSS-DC 18P, 1/3-inch colour DSP CCD with 470TV lines of horizontal resolution) located outside the cell. Cooling and heating cycles were started by operating the refrigeration compressor or electrical heater, respectively. During each experiment, pressure, temperature and motor current were continuously recorded at a rate of 12 points per minute.

In all experiments, the gas steel bottles were fitted into the gas manifold to transfer the gas through the piston pump to the PVT sapphire cell. Then, approximately 5 mL of deionised water was initially charged into the evacuated clean sapphire cell. Subsequently, the gas mixture was introduced into the sapphire cell from the fitted steel bottles via the piston pump. The cell was then pressurised by a pneumatic pump (Haskel, model AA-30) in combination with a piston pump (Sanchez). Once the prescribed pressure was reached, the stirrer was switched on, and cooling was started at a rate of approximately 2 K/h until hydrate (formation) was visually observed. The cooling process was stopped when complete hydrate crystallisation was achieved. The cell was then heated at a rate of 2 K/h to start the hydrate dissociation process. The gas hydrate dissociation temperatures, pressures and stirrer currents were measured during the experiments. All experiments were repeated for each gas mixture at 5, 7.5, 10, 15, 20 and 25 MPa and for the temperature range of 275.75K to 293.95K. Moreover, the repeatability of the hydrate experimental data was determined by performing the experiment three times for the methane hydrate and two times for some randomly

selected experiments, with closely matching results obtained. The statistical analysis of the obtained experimental data showed a maximum experimental error of 1.65%.
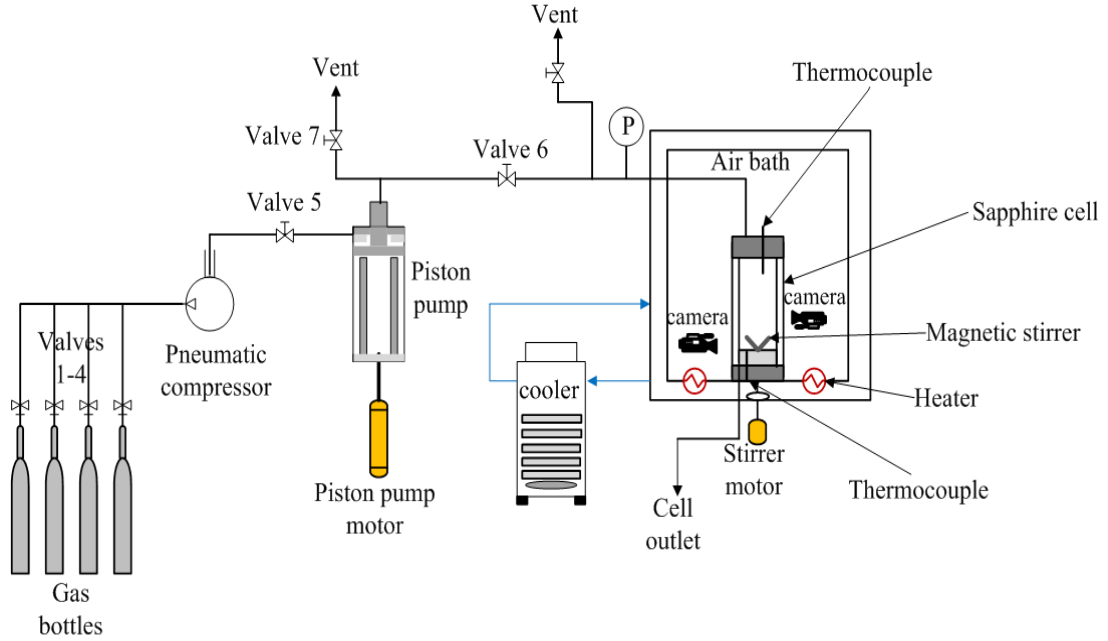
Figure 4-1 Schematic of the PVT Sapphire Cell

The PVT sapphire cell apparatus was used to measure the hydrate dissociation conditions by employing the temperature search method as an experimental determination technique (Kim et al. 2011, Loh et al. 2012, AlHarooni et al. 2015, Smith et al. 2015, 2016). Experimentally, the PVT cell was maintained at a constant pressure using the piston pump and keeping the valve to the PVT cell open. Because of that, the hydrate formation conditions depended on various factors (induction time, rate of cooling and memory effect), had a high degree of variance compared to the dissociation conditions and represented a fixed thermodynamic property, thus the dissociation was considered as the hydrate equilibrium conditions (Tohidi et al. 2000). Hydrate dissociation conditions for the carbon dioxide + methane, nitrogen + methane and carbon dioxide + nitrogen gas mixtures were measured for the temperature and pressure ranges of 275.75K to 293.95K and 5 MPa to 25 MPa, respectively. In addition, motor current measurements were used as an indication of gas hydrate plug formation and dissociation.

4.4 Results and Discussion

4.4.1 Gas Hydrate Equilibrium Conditions

Initially, the accuracy of the experimental results was checked by measuring the equilibrium conditions for pure methane and the gas mixture containing 20 mol% CO_2 and 80 mol% CH_4 (Figure 4-2 and Figure 4-3), with our data in good agreement with the literature data (Jhaveri and Robinson 1965, Adisasmito et al. 1991, Dholabhai and Bishnoi 1994, Servio et al. 1999, Seo et al. 2001, Nakamura et al. 2003, Mohammadi et al. 2005, Lu and Sultan 2008, Beltrán and Servio 2008a, Sabil et al. 2014). The measured hydrate data are listed in Table A-1, Table A-2 and Table A-3 and plotted in Figure 4-4, Figure 4-5 and Figure 4-6.

Figure 4-4 shows the equilibrium conditions for the CO_2+CH_4 gas mixture. As expected, the CO_2+CH_4 hydrate equilibrium curves are located between the equilibrium curves of pure CO_2 and pure methane (Ohgaki et al. 1993, Sloan and Koh 2008). Furthermore, as the CO_2 concentration increased in the CO_2-CH_4 mixture, the equilibrium temperature also increased, approaching the curve for pure CO_2. Figure 4-4 shows that the measured CO_2+CH_4 hydrate data in the present study showed a similar trend with the data available in the literature (Adisasmito et al. 1991, Ohgaki et al. 1993, Fan and Guo 1999).

An analogue scenario was observed for the N_2+CH_4 system (Figure 4-5). Again the equilibrium curves of the N_2+CH_4 mixture are located in between the curves for pure N_2 (Van Cleeff and Diepen 1960) and pure CH_4, and the gas hydrate equilibrium temperature decreased with increasing N_2 concentration, approaching the N_2 curve. Jhaveri and Robinson (1965), Mei et al. (1996) and Lee et al. (2006) observed similar behaviour. This is due to the dilution effect of nitrogen, which leads to a lower hydrate temperature.

This behaviour was again observed for the carbon dioxide + nitrogen mixtures (Figure 4-6), i.e. the presence of CO_2 in the CO_2+N_2 mixture led to an increased hydrate equilibrium temperature. The equilibrium curve of 64 mol% nitrogen (36 mol% carbon dioxide) is closer to the pure carbon dioxide curve than the pure nitrogen curve. This phenomenon was also observed by Seo et al. (2000), who explained that this behaviour was due to the competition of CO_2 and N_2 molecules for optimum occupancy of the

hydrate structure. Mechanistically, during the hydrate formation process, CO_2 molecules occupy small and large cavities in the hydrate structure whereas N_2 molecules fill the other unoccupied cavities.

Figure 4-6 shows that the $N_2 + CO_2$ data reported in the present study are incomparable to the behaviour of those in the literature (Kang et al. 2001). Figure 4-7, Figure 4-8 and Figure 4-9 show plots of ln P vs 1/T for the experimental data obtained in the present study, which show a good linear relationship.
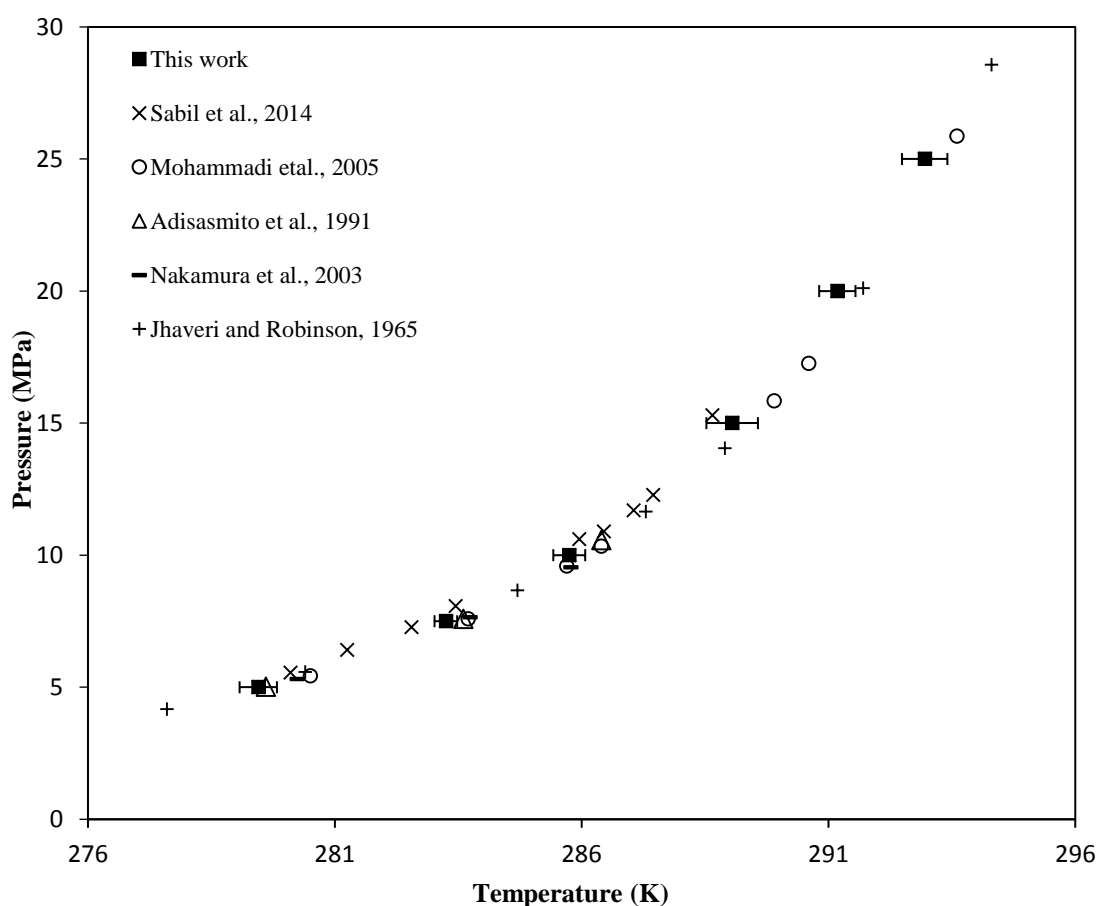
Figure 4-2 Comparison of CH₄ hydrate dissociation points (black squares: experimental data; open symbols: literature data (Jhaveri and Robinson 1965, Adisasmito et al. 1991, Nakamura et al. 2003, Mohammadi et al. 2005, Sabil et al. 2014)
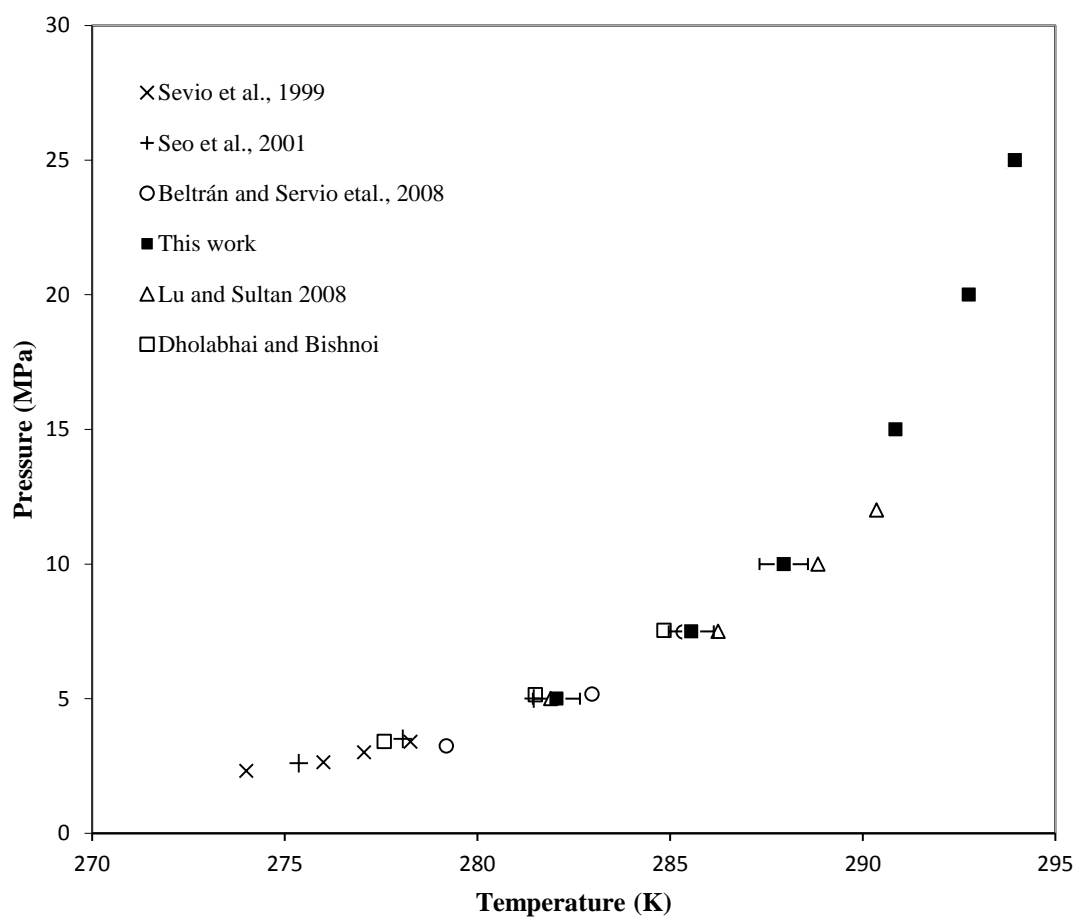
Figure 4-3 Comparison of 80 mol% methane and 20 mol% carbon dioxide hydrate dissociation points (black squares: experimental data; open symbols: literature data (Dholabhai and Bishnoi 1994, Servio et al. 1999, Seo et al. 2001, Lu and Sultan 2008, Beltrán and Servio 2008a)
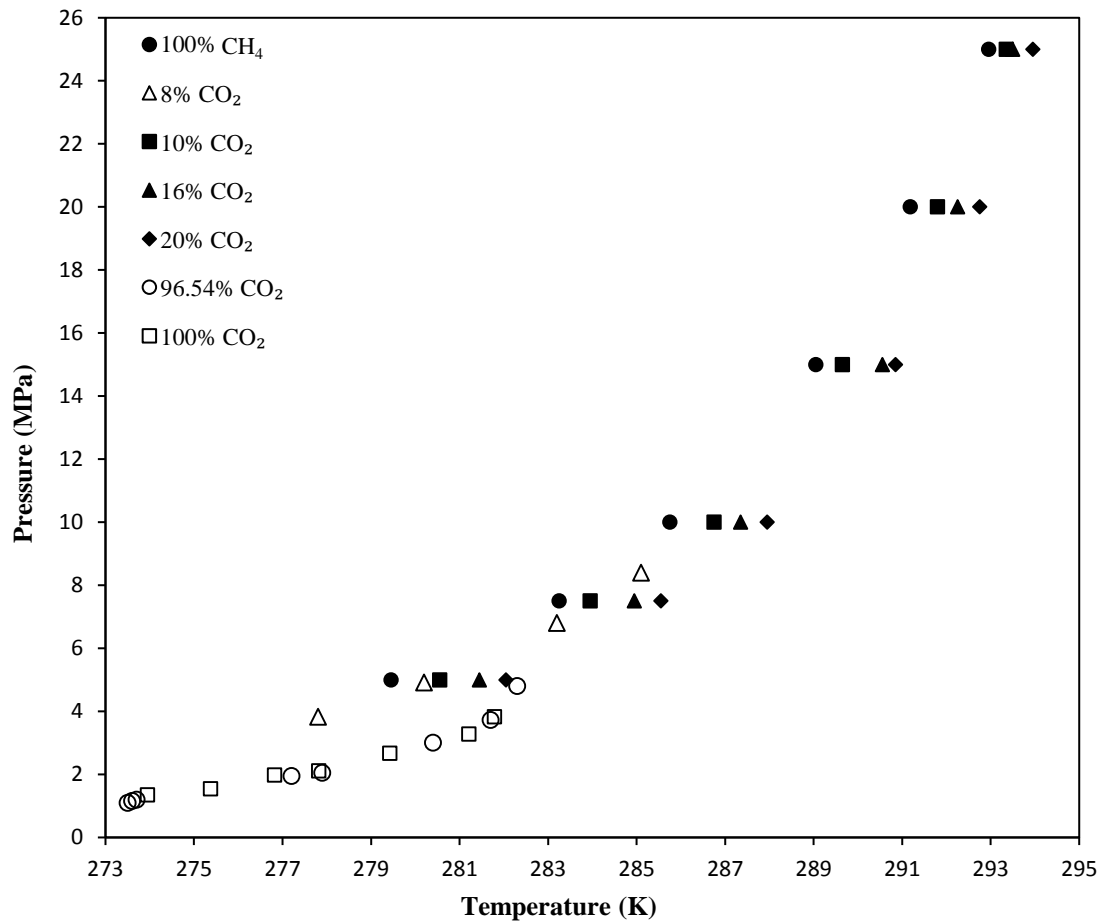
Figure 4-4 CH₄ hydrate equilibrium curves. Closed symbols represent our experimental data and open symbols represent the literature data: Pure carbon dioxide reported by Ohgaki et al. (1993), 8% carbon dioxide reported by Adisasmito et al. (1991) and 96.54% carbon dioxide reported by Fan and Guo (1999). Numbers indicate gas mole in the mixture
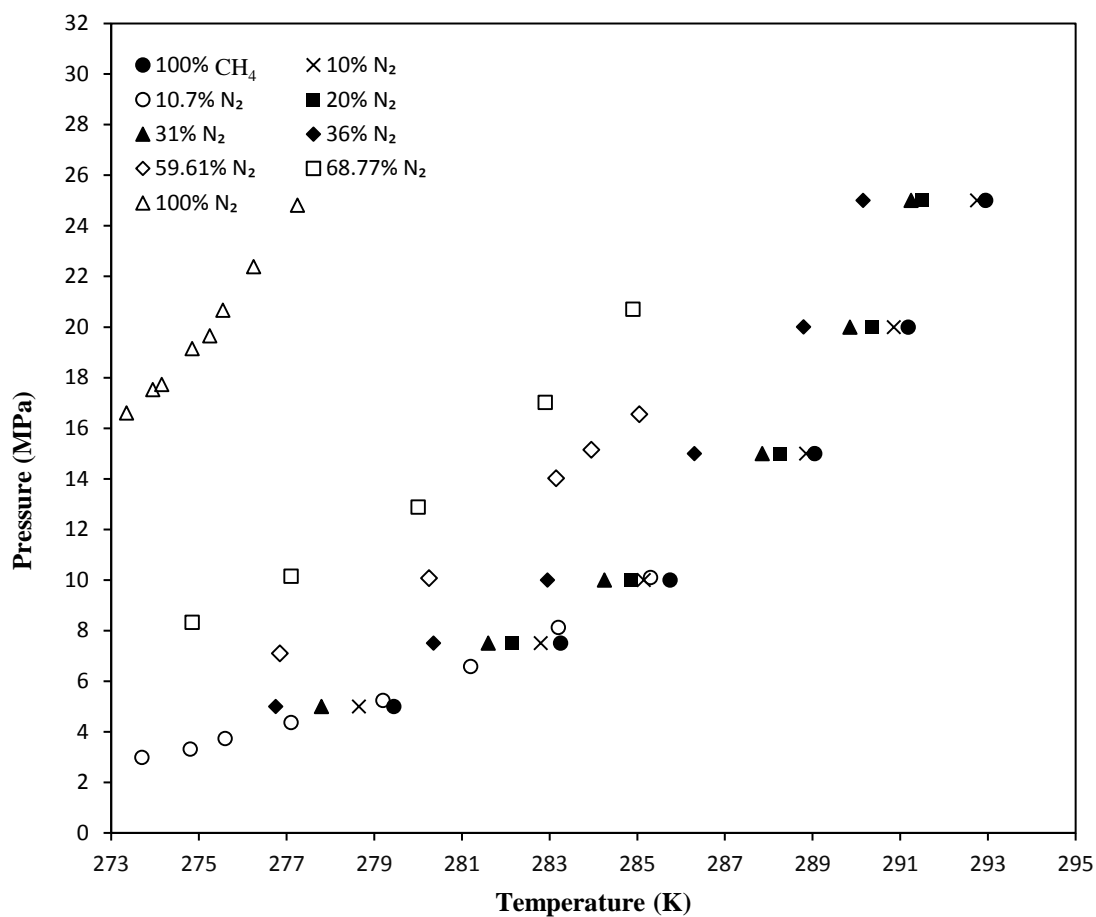
Figure 4-5 N₂-CH₄ hydrate equilibrium curves. Closed symbols represent experimental data and open symbols represent literature data: pure nitrogen reported by Van Cleeff and Diepen (1960), 10.7% nitrogen reported by Mei et al. (1996), 59.61% nitrogen reported by Lee et al. (2006) and 68.77% nitrogen reported by Lee et al. (2006). Numbers indicate gas mole in the mixture
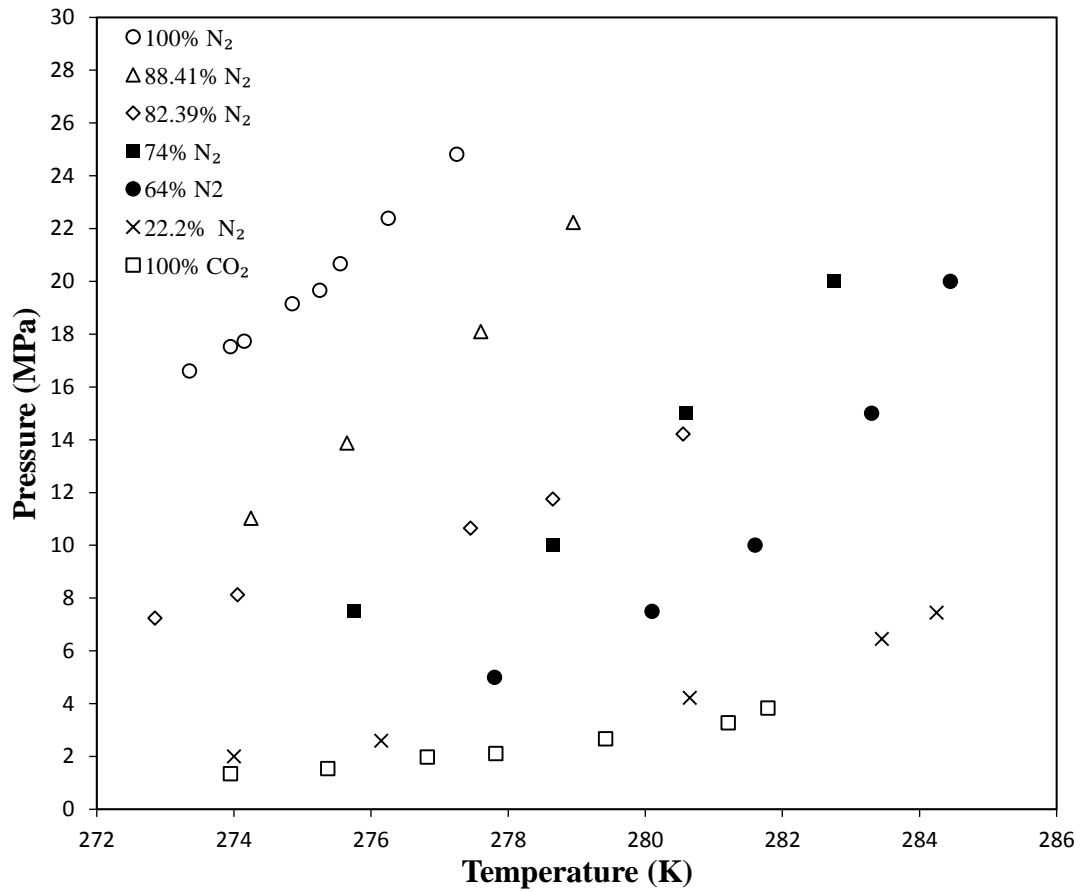
Figure 4-6 CO₂-N₂ hydrate equilibrium curves. Closed symbols represent experimental data and open symbols represent the literature data: pure nitrogen reported by Van Cleeff and Diepen (1960), pure carbon dioxide reported by Ohgaki et al. (1993), 88.41% nitrogen reported by Kang et al. (2001), 82.39% nitrogen reported by Kang et al. (2001) and 22.2% nitrogen reported by Kang et al. (2001). Numbers indicate gas mole in the mixture
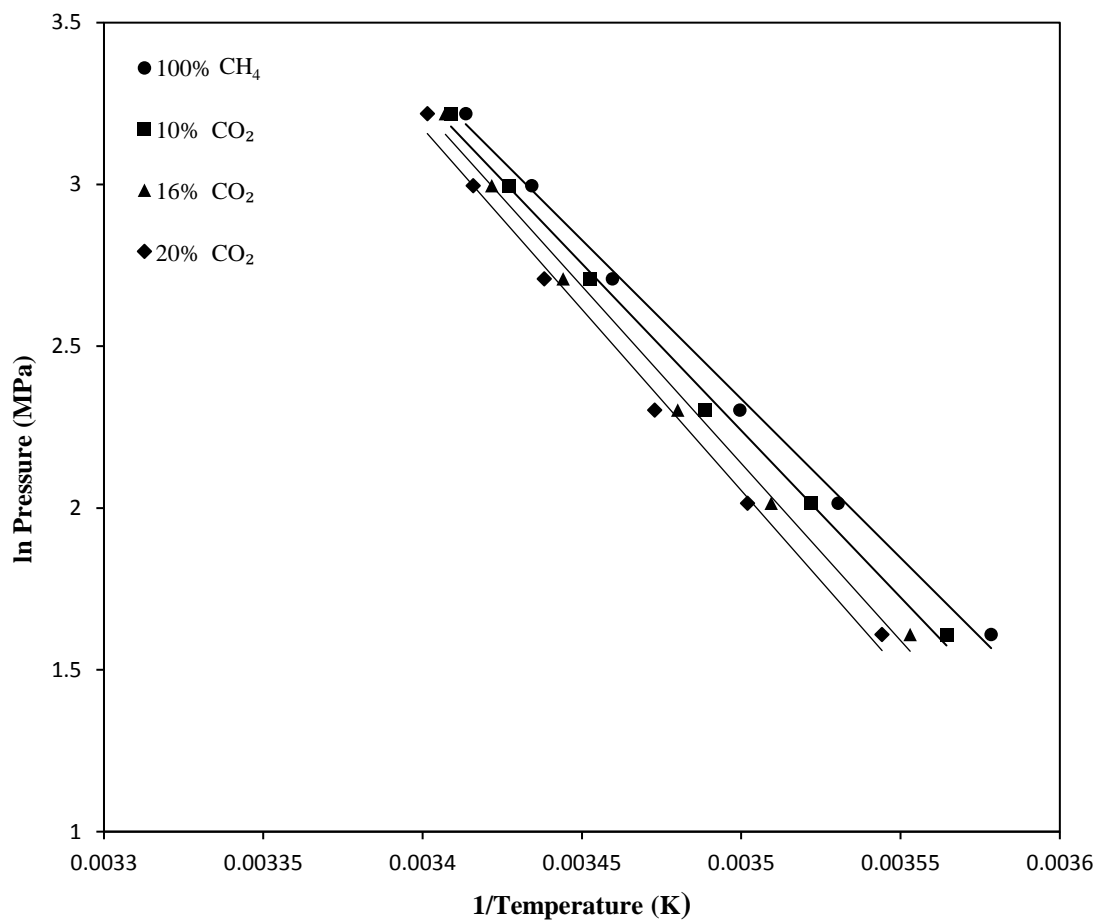
Figure 4-7 Experimental CO_2-CH_4 hydrate equilibrium data in ln Pressure versus 1/Temperature plot. Numbers indicate gas mole percentages in the mixture used in this study
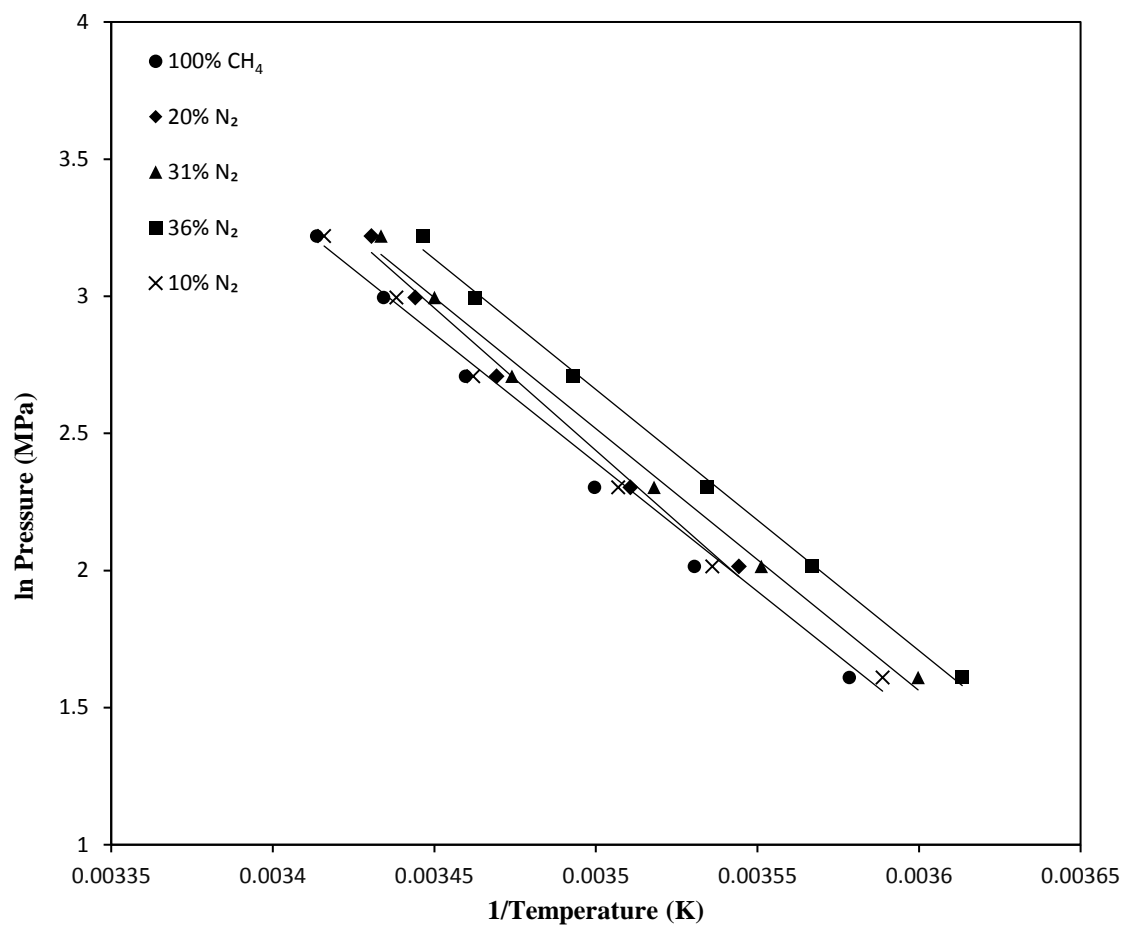
Figure 4-8 Experimental N₂-CH₄ hydrate equilibrium data in ln Pressure versus 1/Temperature. Numbers indicate gas mole percentages in the mixture used in this study
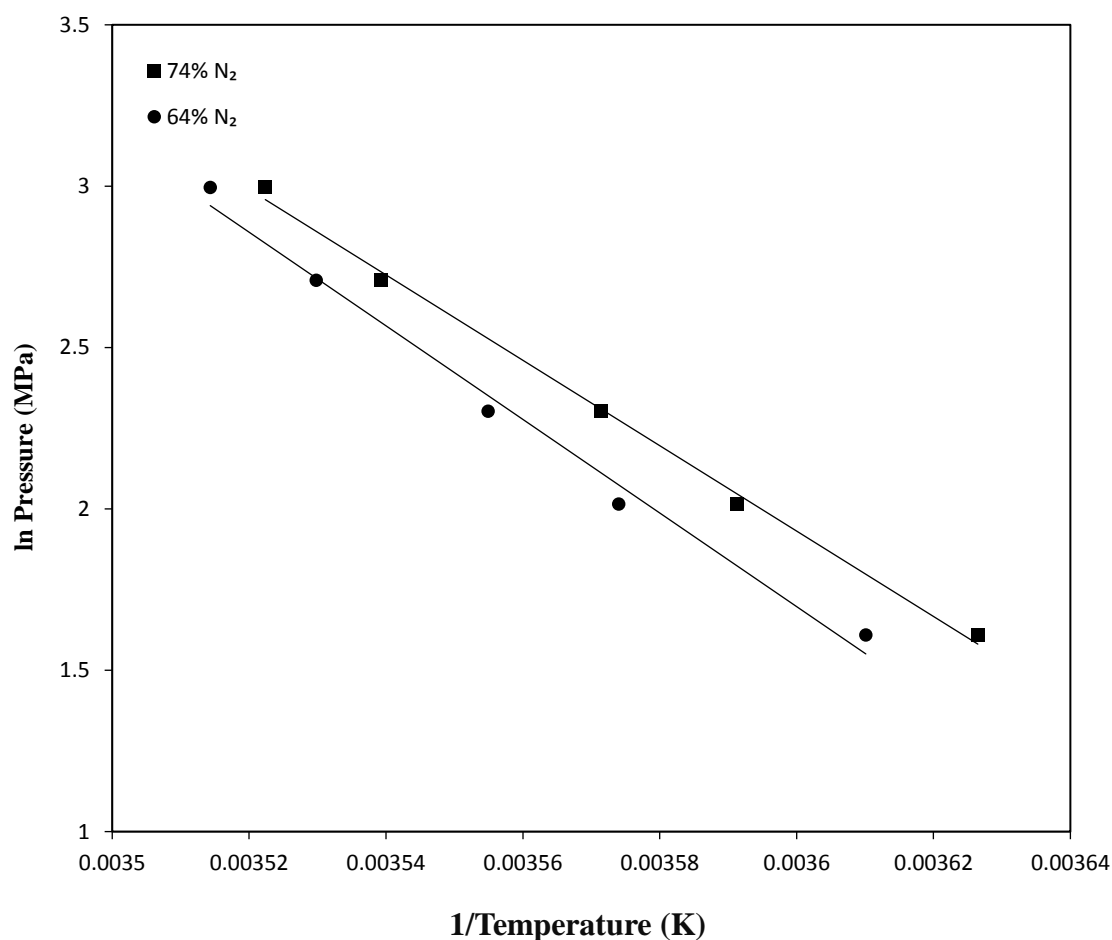
Figure 4-9 Experimental CO_2-N_2 hydrate equilibrium data in ln Pressure versus 1/Temperature. Numbers indicate gas mole percentages in the mixture used in this study

4.4.2   Current as an Indication of Hydrate Plug and Dissociation

In the present study, visual observation was employed to measure the hydrate dissociation condition. In some experiments, this technique was not available, especially where the experimental cell is not visual. Therefore, the motor current changes during the hydrate formation/dissociation process could be related to the hydrate plug formation and dissociation. The motor current is a function of the torque required to mix the sapphire cell contents; once a hydrate plug is formed, the torque and thus the motor current increases due to the increasing load on the stirrer.

The stirrer motor current as a function of experimental time was measured in a set of experiments as shown in Figure 4-10, Figure 4-11, Figure 4-12 and Figure 4-13. Clearly, the motor current changes during hydrate formation and dissociation. Initially, the motor current remains constant but then increases dramatically until it reaches a maximum. This maximum indicates the presence of the full plug of the gas hydrate. However once the solid plug hydrate was formed, the motor current decreased rapidly due to slippage of the stirrer on the magnetic coupling. After dissociation began, the stirrer started rotating again due to the magnetic stirrer being reconnected to the motor and a small spike in the motor current was observed. Therefore, there was no significant current change before hydrate plug formation, whereas the current changed significantly once the full hydrate plug was formed. The hydrate behaviour as indicated by the motor current was consistent with independent visual observations. Therefore, the motor current can be used as a hydrate formation and dissociation criterion.
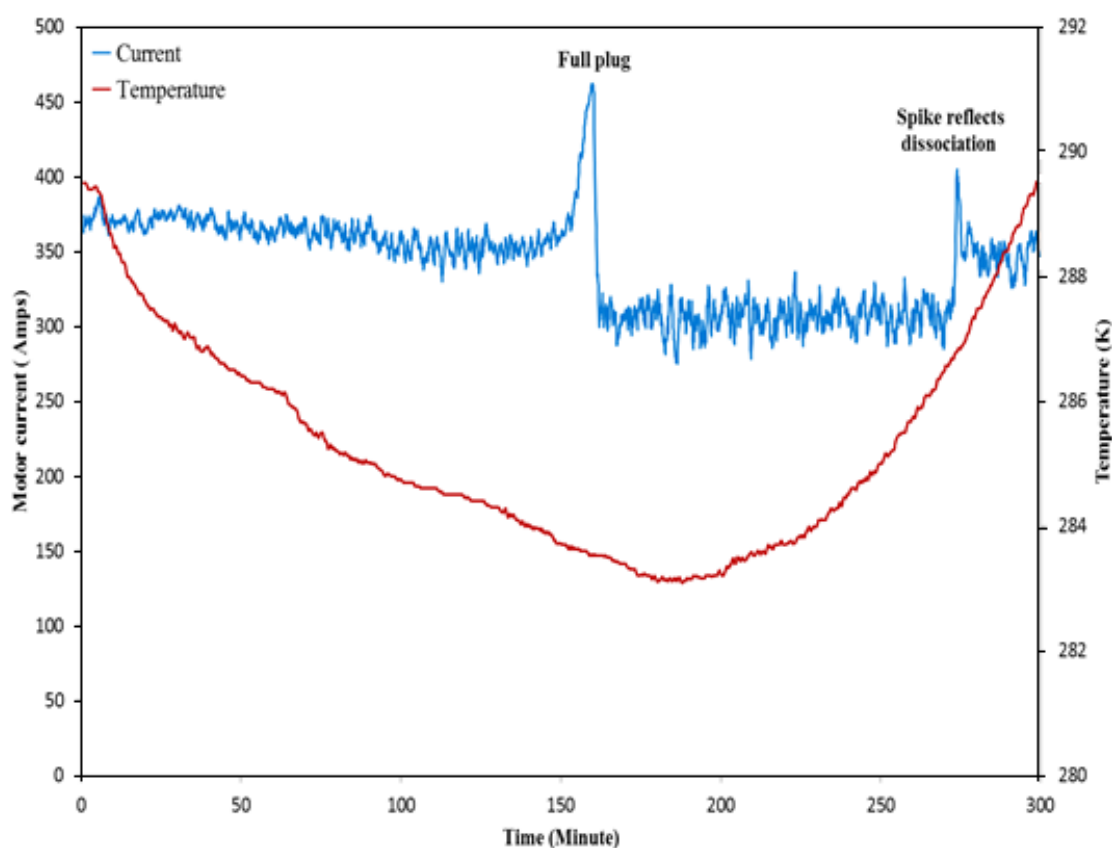
Figure 4-10 Motor current and temperature vs time during hydrate formation/dissociation process for pure CH₄ at a pressure of 10 MPa
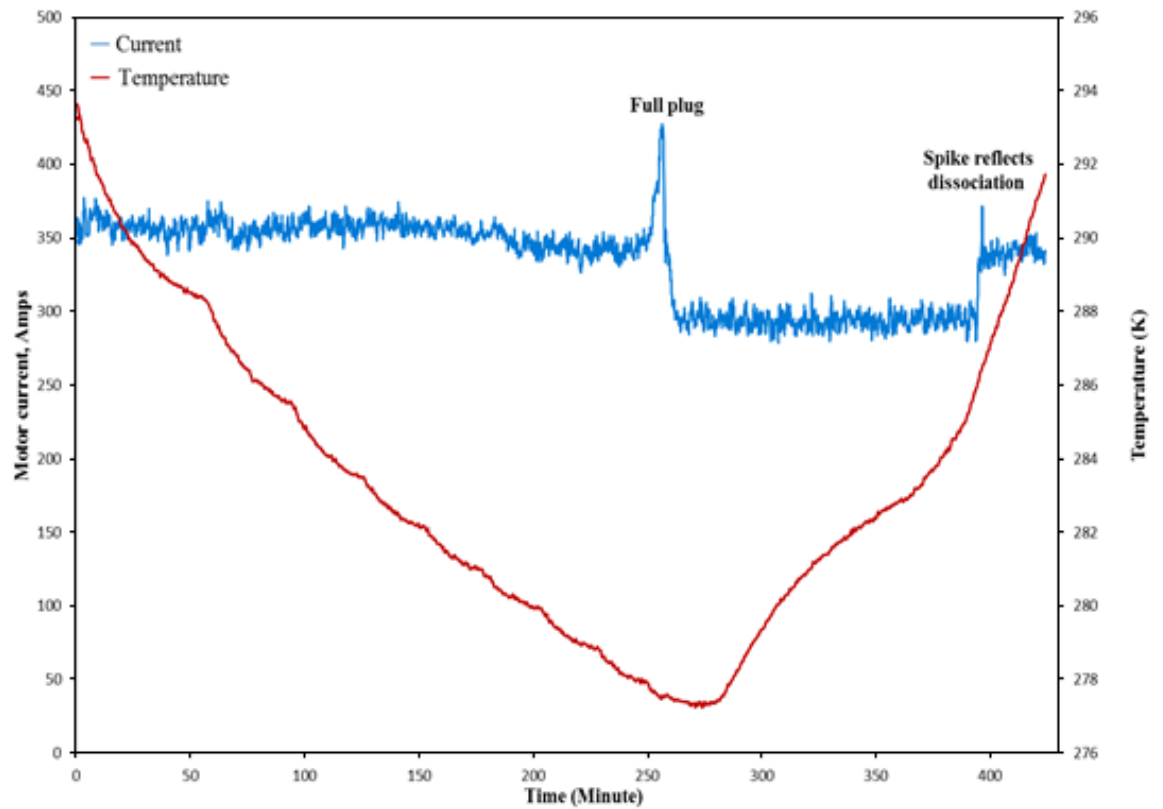
Figure 4-11 Motor current and temperature vs time during hydrate formation/dissociation process for a 10% CO_2 + 90% CH_4 gas mixture at a pressure of 10 MPa
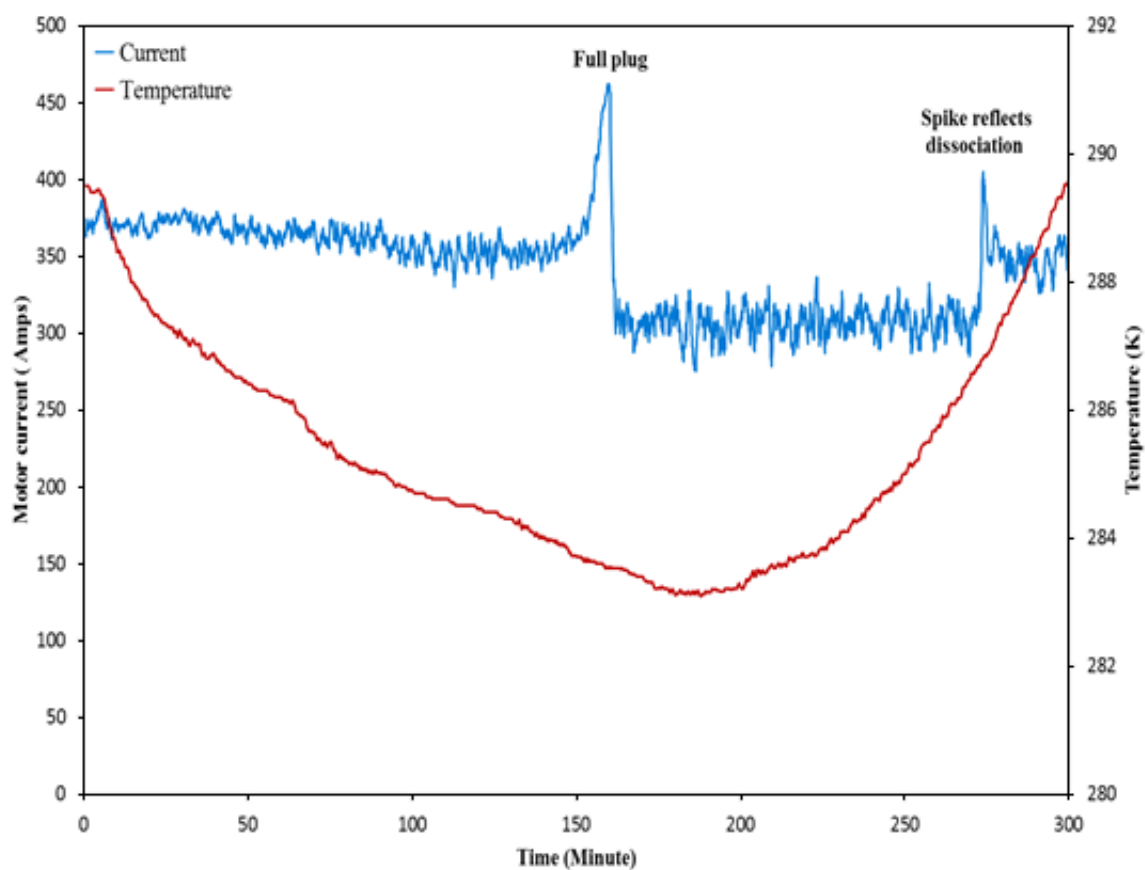
Figure 4-12 Motor current and temperature vs time during hydrate formation/dissociation process for a 16% CO$_2$ + 84% CH$_4$ gas mixture at a pressure of 10 MPa
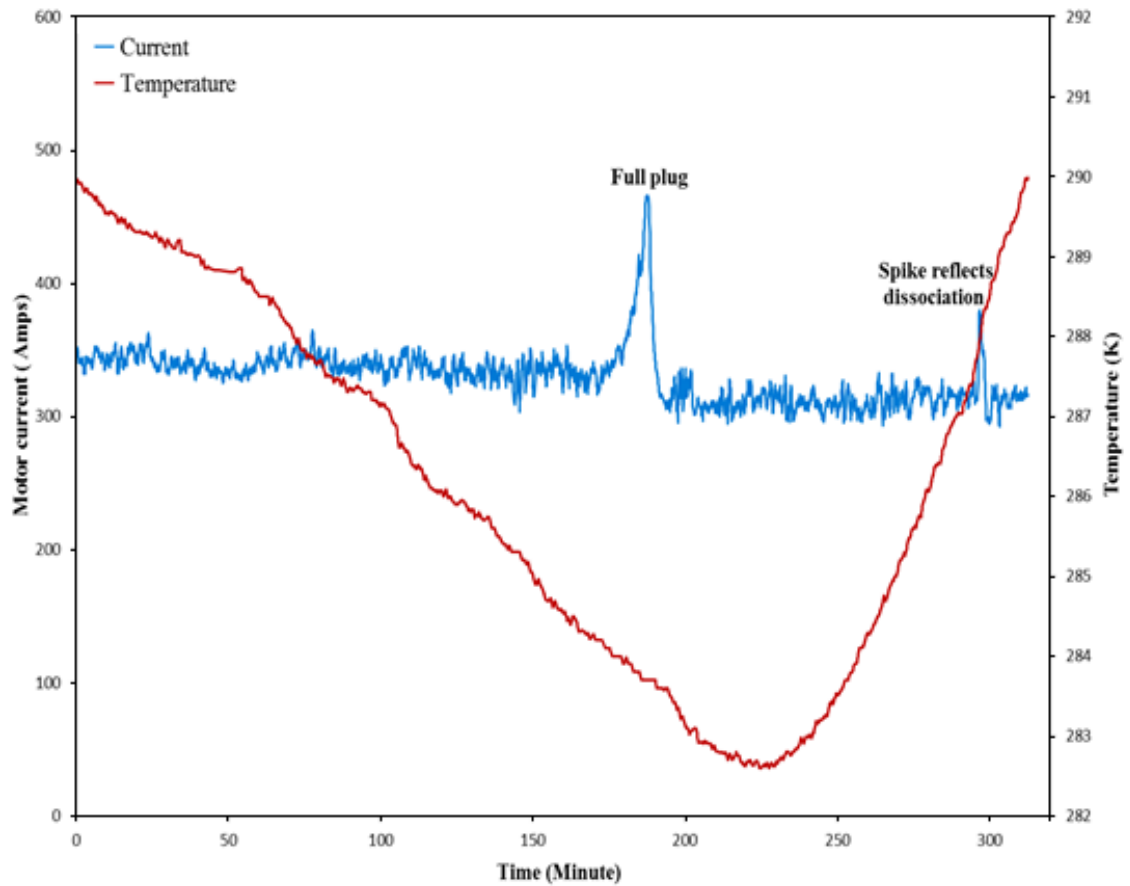
Figure 4-13 Motor current and temperature vs time during hydrate formation/dissociation process for a 80% CH$_4$ + 20% CO$_2$ gas mixture at a pressure of 10 MPa

Figure 4-14 shows a series of images that were captured during the hydrate formation process in the PVT sapphire cell. During cooling and when the temperature reached 2–4 degrees below the hydrate dissociation temperature, hydrate formation started at the liquid-gas interface (Figure 4-14a), which is consistent with Tohidi et al. (2001) and Ueno et al. (2015).

With continuing progress of the experiment, hydrate particles grew gradually on the surface area and then built up towards the centre (Figure 4-14b). Later, the hydrate particles increased in size and migrated into the liquid phase, which shrank due to hydrate growth (Figure 4-14c-e). However, the PVT cell content was still flowing and no apparent change in the motor current was observed during this period. Gas hydrates continued to grow until all liquid was consumed. At this stage, the motor current began to increase dramatically until it reached the maximum value. Once the solid hydrate

plug was sharply formed (Figure 4-14f), the magnetic stirrer stopped moving, and the hydrate completely blocked the system causing a rapid decrease in the current. During the heating process, the gas hydrate started dissociating and gas bubbles appeared in the solid phase (Figure 4-14g). At this point, the stirrer started to move again, and a small increase in the current was measured.

Start formation

a

t= 5 mins

b

t= 10 mins

c

t= 20 mins

d

t= 60 mins

e

t= 74 mins

f

Start dissociation

g
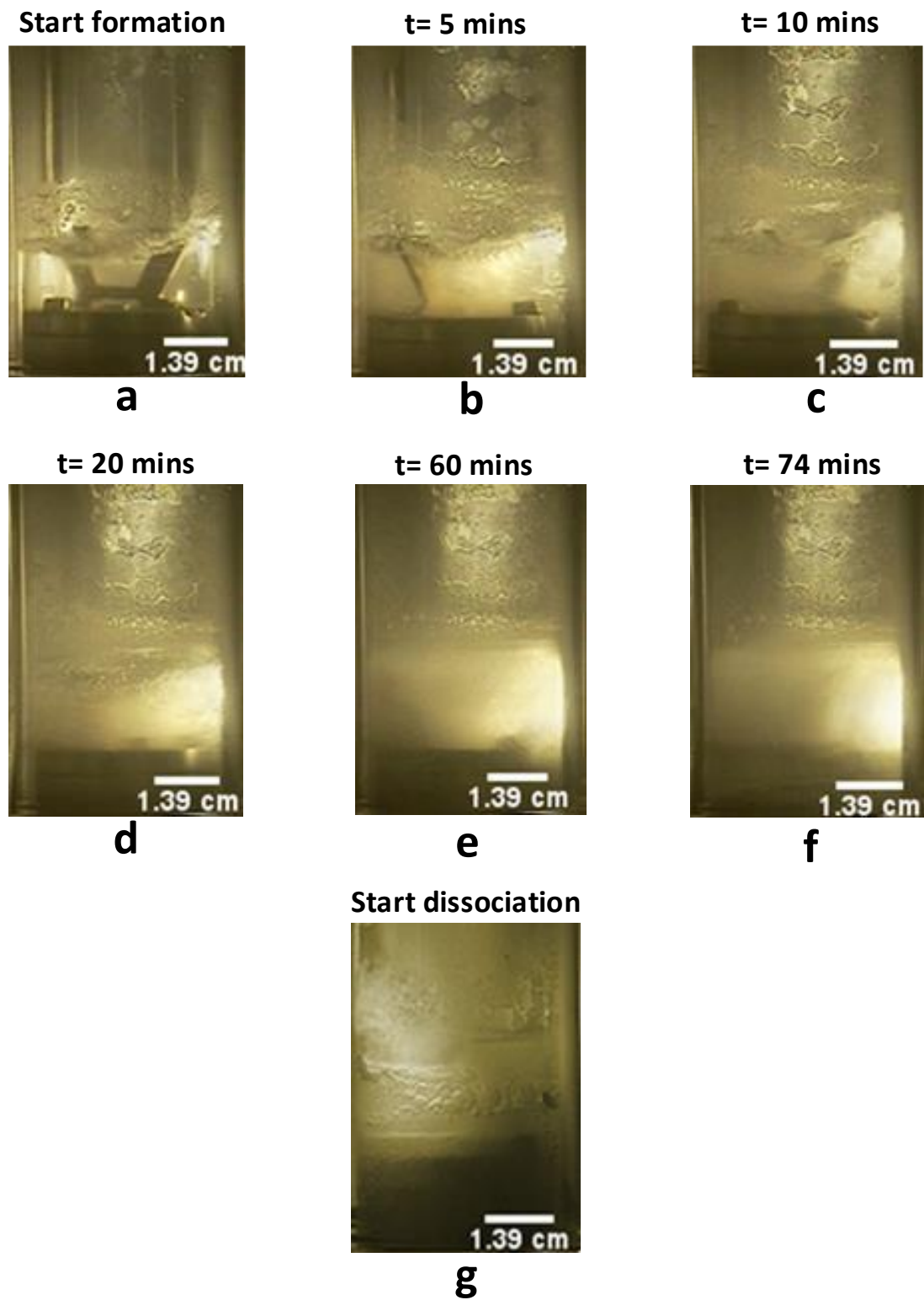
Figure 4-14 Images captured during the experiments

4.5 Conclusions

The gas hydrate equilibrium conditions are of major significance in the energy sector due to the importance of gas hydrates as a potential alternative energy resource, as a means of CO_2 sequestration, as a factor in global climate change and as a threat to flow assurance and gas production systems. Thus, in the present study, the hydrate equilibrium data for the carbon dioxide + methane + water, nitrogen + methane + water and carbon dioxide + nitrogen + water systems were experimentally measured in the PVT sapphire cell apparatus. Experiments were conducted at temperatures varying from 275.75K to 293.95K and pressures ranging from 5 MPa to 25 MPa. An acceptable agreement was found between the obtained experimental data and the literature data (Jhaveri and Robinson 1965, Adisasmito et al. 1991, Dholabhai and Bishnoi 1994, Servio et al. 1999, Seo et al. 2001, Nakamura et al. 2003, Mohammadi et al. 2005, Beltrán and Servio 2008a, Lu and Sultan 2008, Sabil et al. 2014). Specifically, we observed that at any given pressure the hydrate equilibrium temperature increased with increasing CO_2 mole percentage in the $CO_2 + CH_4$ and $CO_2 + N_2$ gas mixtures, whereas increasing the N_2 mole fraction in the $N_2 + CH_4$ gas mixture reduced the hydrate equilibrium temperature at any given pressure. Furthermore, motor current measurements were performed during the gas hydrate formation and dissociation process, which showed that the motor current could be used as a gas hydrate formation and dissociation criterion, particularly in the cases where visual observations are not possible.

Chapter 5   Thermodynamic Modelling and Empirical Correlation for the Prediction of Gas Hydrate Equilibrium Conditions*

5.1   Summary

Following on from chapter 4 where experimental hydrate equilibrium measurements for carbon dioxide + methane, nitrogen + methane and carbon dioxide + nitrogen were determined, this chapter seeks to present approaches for modelling gas hydrate equilibrium conditions. As mentioned previously, gas hydrate formation represents one of the main problems facing the oil and gas industry as it poses a significant threat to the production, processing and transportation of natural gas. Here, gas hydrate particles can agglomerate and build up gradually so that a large mass of hydrate is formed, which can block flowlines, valves, chokes and other production equipment. Thus, accurate predictions of gas hydrate equilibrium conditions are essential requirements for designing gas production systems at safe operating conditions and mitigating the problems caused by the formation of hydrates. Thus, in this chapter, first, a thermodynamic model for gas hydrate equilibrium conditions and cage occupancies for the gas mixtures containing methane, carbon dioxide and nitrogen at different compositions are proposed. The van der Waals-Platteeuw thermodynamic theory coupled with the Peng-Robinson equation of state and Langmuir adsorption model are employed in the proposed model. The experimental measurements generated in chapter 4 are used to evaluate the accuracy of this model. The results are discussed extensively in the discussion section.

Second, a new hydrate empirical correlation for predicting gas hydrate equilibrium conditions was obtained for the same hydrate mixtures. The new correlation was proposed for a wide range of pressures, temperatures and gas specific gravities. The nonlinear regression technique was applied to develop the correlation based on 142 experimental data points collected from the literature, validated by 85 data points not

*References:

1. Sadeq et al. (2017) in One Curtin International Postgraduate Conference, Miri, Sarawak, Malaysia, 10-12 December 2017.
2. Sadeq et al. (2018) in Offshore Technology Conference Asia held in Kuala Lumpur, Malaysia, 20-23 March 2018.

previously used for developing this correlation. The statistical parameters analysis showed an average absolute error of 0.2183, a squared correlation coefficient (R^2) of 0.9978 and standard deviation of 0.2483. In addition, comparing the new correlation results with the experimental data and with those calculated by other correlations showed an excellent performance for the investigated range.

5.2   Introduction

Natural gas hydrates (clathrate hydrates) are nonstoichiometric solid ice-like compounds that are composed mainly of water molecules, which physically encage small gas molecules. Methane, carbon dioxide, nitrogen, ethane and propane are examples of gas hydrate formers (Sloan and Koh 2008, Delli and Grozic 2014). Generally, depending on the arrangement of the water molecules and the size of the gas molecules, gas hydrates have been found to form the following three structures: sI, sII and sH (Sloan 2003, Carroll 2014). Typically, gas hydrate formation is expected whenever a system of gas hydrate former (i.e. gas) and water molecules exist at specific conditions of high pressure and low temperatures (usually pressure above 0.6 MPa and temperatures above the freezing point of water up to 300 K (Sloan and Koh 2008)).

The importance of gas hydrates in the oil and gas industry became apparent in the 1930s when Hammerschmidt (1934) discovered that solid hydrates were plugging the oil and gas transmission pipelines. Since then, gas hydrates have been considered as a flow assurance problem in the oil and gas industry. In addition, gas hydrates could have severe consequences to the oil and gas production facilities regarding safety and cost. Moreover, gas hydrate technology has many applications in the industry due to the high stability and storage capacity (up to 180 m^3 of gas can be stored in 1 m^3 of hydrates at standard conditions) (Sloan and Koh 2008). Therefore, gas hydrates can be considered as a secure and convenient method for gas storing and transportation (Taheri et al. 2014) and as a potential energy resource (Makogon 2010). Thus, accurate prediction of hydrate equilibrium conditions is essential for designing gas production systems at safe operating conditions, and for investigating the feasibility of gas hydrate as a storage and transportation medium. The best method for determining the hydrate

equilibrium conditions is to measure them experimentally. However, experimental measurements of hydrate temperatures and pressures for a wide range of gas compositions are not feasible. Thus, in the present study we first applied the Langmuir adsorption model coupled with van der Waals-Platteeuw theory (van der Waals and Platteeuw 1959) and the Peng-Robinson equation of state (Peng and Robinson 1976) to describe the CO_2 + CH_4, N_2 + CH_4 and N_2 + CO_2 hydrate equilibrium conditions compared to the experimental measurements conducted in the cryogenic sapphire cell for the temperature and pressure ranges of 275.5K to 292.95 K and 5 MPa to 25 MPa, respectively. Moreover, the cage occupancies for the gas mixtures in each cavity of hydrate were evaluated. Second, a new hydrate empirical correlation for predicting hydrate equilibrium conditions for different gas mixtures containing methane, nitrogen and carbon dioxide was established for the pressure range of 1.7–450 MPa and temperature range of 273–320 K for specific gravities of 0.533–1. The results acquired using the new correlation were compared with the literature data and computational results from other widely used industrial empirical correlations.

5.3   Methodology

5.3.1   Theoretical Model Prediction

The occupancies of the sI hydrate cavities were evaluated based on the fact that at equilibrium the chemical potential of water in the hydrate phase (μ_w^H) equates to the chemical potential of water in the liquid phase (μ_w^L) as per Equation 5-1 below:

$$\mu_w^H = \mu_w^L \qquad\qquad\qquad 5\text{-}1$$

Therefore, the chemical potential difference of water in the hydrate phase was equal to the chemical potential difference of water in the liquid phase. Water molecules adopt the formation of a lattice due to a lowering value of Gibbs free energy, hence the change in chemical potential from a hypothetical empty hydrate lattice (superscript β) to an occupied lattice (i.e. hydrate, superscript (H)) can be expressed using Equation 5-2 as:

$$\Delta\mu_w^H = \Delta\mu_w^L = \mu_w^H - \mu_w^\beta = \mu_w^\beta - \mu_w^L \qquad\qquad 5\text{-}2$$

The fractional occupancy of each hydrate cavity type was calculated based on the Langmuir adsorption approach. The occupancy of hydrate former 'i' in cavity type 'j' is a function of the fugacity of 'i', f_i (evaluated with the Peng-Robinson equation of state), and the Langmuir constant for a specified $i - j$ combination, $C_{i,j}$, as shown in Equation 5-3:

$$\theta_{i,j} = \frac{C_{i,j}f_i}{1 + \sum_i C_{i,j}f_i} \qquad\qquad 5\text{-}3$$

Using the Lennard-Jones-Devonshire cell potential theory, a relationship describing $C_{i,j}$ in terms of the cell potential, $\omega(r)$, Equation 5-4 was put forward by van der Waals and Platteeuw (van der Waals and Platteeuw 1959):

$$C_{i,j} = \frac{4\pi}{kT}\int_0^R \exp\left(\frac{\omega(r)}{kT}\right)r^2 dr \qquad\qquad 5\text{-}4$$

The Lennard-Jones-Devonshire theory takes the average of the potential between the solute (i.e. hydrate former) and the water. It also considers the coordination of the solute to water molecules for a particular cavity type, z_j, which is 20 for the small 5^{12} cavities and 24 for the large $5^{12}6^2$ cavity (Sloan and Koh 2008). Parameters k and T represent the Boltzmann constant and temperature, respectively. The cell potential is given according to Equation 5-5 and Equation 5-6:

$$\omega(r) = 2z_j e\left[\frac{\sigma^{12}}{R_j^{11}r}\left(\delta^{10} + \frac{a}{R_j}\delta^{11}\right) - \frac{\sigma^6}{R_j^5 r}\left(\delta^4 + \frac{a}{R_j}\delta^5\right)\right] \qquad\qquad 5\text{-}5$$

$$\delta^N = \frac{1}{N} \left[\left(1 - \frac{r}{R_j} - \frac{a}{R_j} \right)^{-N} - \left(1 + \frac{r}{R_j} - \frac{a}{R_j} \right)^{-N} \right]$$ 5-6

Cell potential is a function of the distance, r, between the guest molecule and the centre of the cavity. The constants a, e and σ are experimentally fitted parameters, or Kihara parameters, that are unique for every hydrate former and R_j is the radius of the cavity 'j'. Values of 3.95 and 4.33 Å are used for the small and large cavities, respectively (Lederhos et al. 1993). The remaining parameter values used in the present study are given in Table 5-1 (Erickson 1983).

The change in the chemical potential of water from an unoccupied water lattice to a hydrate structure can be used with the previous equations to calculate occupancies at the experimentally determined equilibrium conditions. This chemical potential change is given by Equation 5-7:

$$\Delta\mu_w^H = \mu_w^H - \mu_w^\beta = RT \sum_j v_j \ln\left(1 - \sum_i \theta_{i,j}\right)$$ 5-7

where, v_j is the number of 'j' cavities per water molecule ($v_j = 1/23$ and $v_j = 3/23$ for small cavities and large cavities, respectively) (Sloan and Koh 2008). Experimentally determined estimates of $\Delta\mu_w^H$ have previously been suggested. A value of -1264 J/mol provided by Erickson (1983) has been applied in the present study, permitting the evaluation of methane and carbon dioxide occupancies.

Table 5-1 Kihara potential parameters

Guest	a, Å	σ, Å	e/k, K
CH$_4$	0.3834	3.14393	155.593
CO$_2$	0.6805	2.97638	175.405
N$_2$	0.3526	3.13512	127.426

5.3.2 Empirical Correlation Prediction

Several methods have been proposed to predict hydrate equilibrium conditions. Historically, the K-value method was the first one used for predicting the hydrate formation conditions depending on using empirically estimated equilibrium constants (Carson and Katz 1942). Subsequently, Katz (1945) proposed the gas gravity method by generating charts relating the hydrate pressure and temperature to gas gravity defined as the molecular weight. This method represents a simple tool for predicting the gas hydrate conditions but has a limitation that methane is the primary gas with respect to other gases in the mixture (such as ethane, propane and butane). Later, the regression analysis method was employed by many researchers to correlate the hydrate equilibrium conditions as a function of gas gravity. Some of the correlations based on this method are Hammerschmidt (1936), Berge (1986), Motiee (1991) and Salufu and Nwakwo (2013).

The gas gravity method has been widely used in the gas processing industry as a simple tool for the initial estimation of the hydrate equilibrium conditions. This method was established as a chart that related the hydrate formation temperature and pressure with the gas mixtures specific gravity. The main limitation of this method is that the gas mixture mainly consists of methane, which results in a 50% error in the calculated hydrate conditions (Elgibaly and Elkamel 1998). This error was generated because the method predicts using the same hydrate conditions for different gas mixtures having equal specific gravities. In this context, various hydrate correlations have been proposed to predict the hydrate conditions for gas mixtures as a function of the specific gravity. In the present study, a comparison was conducted with some of the available correlations of the gas gravity method. Hammerschmidt (1936) proposed a simple relation for estimating the initial hydrate temperature as follows in Equation 5-8:

$$T = 8.9 \times P^{0.285} \tag{5-8}$$

This correlation was developed for pressures less than 2000 psi (13.7 MPa) and a temperature less than 60 °F (288.7 K).

Motiee (1991) developed Equation 5-9, which contains six parameters using a regression method and correlated hydrate temperature, pressure and specific gravity:

$$T = -124951 + 48.98387 \times log(P) + 2.66303 \times (log(P))^2 + 176.9101 \\ \times S_g \pm 75.5873 \times S_g{}^2 \pm 10.45 \ S_g \times log(P)$$ 5-9

Motiee's (1991) correlation has a limitation in that it is not applicable to gas mixtures containing non-hydrocarbon gases.

Salufu and Nwakwo (2013) proposed a correlation that required pressure and specific gravity to predict the hydrate equilibrium temperature as defined in Equation 5-10:

$$T = A[ln \, P - ln(B \times S_g)]$$ 5-10

where, P, T and S_g are the pressure in psi, the temperature in °F and the specific gravity of gas mixture, respectively, while A and B are the Salufu correlation constants given as follow:

A = 10.9529 and B = 2.4196 for the specific gravity range of 0.85–1
A = 12.1212 and B = 8.7511 for the specific gravity range of 0.6–0.84
A = 16.2602 and B = 105.358 for the specific gravity range of 0.1–0.559

In the new correlation, the hydrate temperature was correlated as a function of pressure and gas specific gravity (i.e. the temperature was a dependent variable whereas the pressure and specific gravity were independent variables). A simple mathematical formula was proposed as shown in Equation 5-11:

$$T = a_1 \times P^{a_2} + \frac{a_3}{a_4 - S_g} - a_5$$ 5-11

where, T is the calculated temperature in Kelvins, P is the pressure in MPa, S_g is the gas specific gravity and a_1-a_5 are the correlation coefficients given in Table 5-2. A total number of 227 experimental data points for different gas mixtures containing methane, carbon dioxide and nitrogen were collected from the literature as shown in Table 5-3 to develop the correlation. The nonlinear regression technique was applied to provide a strong relationship for correlating the hydrate equilibrium temperature to the equilibrium pressure and gas specific gravity. First, out of the collected experimental dataset, 142 data points were employed to obtain the fitting parameters for the correlation as listed in Table 5-2. Then, the remaining 85 data points were used to check the validity of the new correlation. The hydrate equilibrium temperature given by Equation 5-11 was correlated for a pressure range of 1.7–330 MPa and temperature range of 273–320 K and covered gas mixtures containing methane, carbon dioxide and nitrogen for a specific gravity range of 0.553 to 1.

Table 5-2 Coefficient values of the new correlation, Equation 5-11

Coefficients	Values
a_1	99.49483
a_2	0.069881
a_3	7271.546
a_4	38.76813
a_5	22.02004

Table 5-3 Experimental data collected from the literature used to construct the new correlation

Source	Temperature range, K	Pressure range, MPa	Specific gravity range	No. of data points
Unruh and Katz (1949)	277–281	2.84–5.1	0.621–0.88	6
Jhaveri and Robinson (1965)	273.2–295.2	2.65–34.33	0.553–0.85	35
Adisasmito et al. (1991)	273.7–287.6	1.81–10.95	0.63–0.987	29
Dholabhai and Bishnoi (1994)	274.1–284.84	2.36–7.53	0.74688	4
Mei et al. (1996)	273.7–285.3	2.99–10.1	0.5975	8
Servio et al. (1999)	274–278.26	2.315–3.4	0.7468	4
Nakano et al. (1999)	305.9–320.54	98–330	0.533	16
Seo et al. (2001)	273.1–281.46	2–5	0.75–0.96	12
Seo and Lee (2001)	274.36–282.6	2–5	0.746	3
Beltrán and Servio (2008b)	279.2–285.34	3.24–7.47	0.7468	3
Belandria et al. (2010)	279.1–284.2	3.6–5.29	0.81–0.815	4
Belandria et al. (2011)	277.9–285.5	4.03–8.27	0.75–1	6
Herri et al. (2011)	273.4–286.4	2.68–10.27	0.553–0.9	13
Lee et al. (2012)	274–278	1.71–4.24	0.553–1	11
Le Quang et al. (2016)	275.35–282.1	2.91–5.6	0.77–0.785	13
Sadeq et al. (2017)	276.8–293.95	5–25	0.553–0.75	53
Kastanidis et al. (2017)	274.3–278.7	2.63–4.01	0.7991	7

5.4 Results and Discussion

5.4.1 Theoretical Model Prediction

Fractional occupancies were calculated for $CO_2 + CH_4$ mixtures (Table 5-4), $N_2 + CH_4$ mixtures (Table 5-5) and $N_2 + CO_2$ mixtures (Table 5-6) for each cavity using Equation 5-3. Table 5-4 shows that the guest/cavity size ratio for methane in the small cavity was 0.867 and was 0.744 in the large cavity. For carbon dioxide, the ratios were1.018 and 0.874 for the small and large cavities, respectively (Lederhos et al. 1993). Given that the carbon dioxide guest size exceeds that of the small cavity, carbon dioxide adsorption is unlikely to occur. However, previous studies have shown that carbon dioxide occupation of the small cavity can occur with pure carbon dioxide gas (Ripmeester and Ratcliffe 1998, Circone et al. 2003). Methane has a far greater propensity towards the cavity due to its optimal guest/cavity ratio and its concentration far exceeds the carbon dioxide concentration in all gas mixtures. Methane was therefore assumed to dominate the occupation of small cavities; hence, the occupation of carbon dioxide was negated.

An interesting observation was the greater overall occupation of large cavities. This was particularly noticeable at lower pressures. Methane and carbon dioxide were both capable of stabilising the large cavity, as evidenced by their guest/cavity ratios, although carbon dioxide offered greater stability. It makes sense that with two capable guests for the large cavity compared to one for the small cavity, $\theta_{i,l}$ would be greater than $\theta_{i,s}$. Methane has been shown to occupy the large cavity to a greater extent in the absence of carbon dioxide (Lee et al. 2013). It is likely that due to the relatively higher number of large cavities in sI hydrates (6 to 2 in a unit cell), methane will prefer the large cage. With more possible sites for methane guests to fill relative to small cages, a higher methane occupancy of large cages than small cages will result in greater free energy changes and therefore greater lattice stabilisation.

Results also demonstrated an increase in $\theta_{i,j}$ for both sI cavities with pressure, which is in accordance with Equation 5-3. The filling of small cavities decreased with increased carbon dioxide concentration due to the accompanying reduction in methane partial pressure (and fugacity). Similarly, carbon dioxide filling of large cavities increased with CO_2 concentration and the small cavity occupation by methane decreased to a minor extent. Likewise, the extent of large cavity occupation by carbon

dioxide increased drastically and appeared to be proportional to CO_2 concentration. This increase ultimately reduced the filling of large cavities by methane. Greater inclusion of carbon dioxide in the lattice stabilises the hydrate structure because CO_2-water interactions are stronger than CH_4-water interactions in the large cage (Sloan and Koh 2008). Therefore, the increase in $\theta_{CO2,l}$ promoted hydrate equilibrium conditions.

For $N_2 + CH_4$ hydrates, the cage occupancy ratio of CH_4, θ_l/θ_s was greater than 1, which indicated that the small cages were less occupied than the large cages. CH_4 molecules occupy the large and small cavities of sI (Sum et al. 1997), whereas N_2 molecules prefer to occupy the small cages (Seo and Lee 2004). Thus, the methane molecules mainly occupy large cages and compete with nitrogen molecules for the best occupancy of small cages. The results also indicated that the occupancy of methane in both large and small cavities, $\theta_{CH4,l}$ and $\theta_{CH4,s}$, respectively, decreased with increased N_2 concentration in the mixture. This reduction caused an increase in N_2 occupancy and explained the dilution effect of nitrogen. For $N_2 + CO_2$, the nitrogen filling of small cavities increased drastically with N_2 concentration, which decreased CO_2 occupation of small cavities. This might explain the structural transformation phenomenon of mixed $N_2 + CO_2$ hydrates, which will be discussed later on. Furthermore, the results also demonstrated an increase in the occupancy for both the small and large cavities of $N_2 + CH_4$ and $N_2 + CO_2$ hydrates with pressure, which is in accordance with Equation 5-3.

The comparison of the experimental data presented in chapter 4 and the model calculations for various $CO_2 + CH_4$, $N_2 + CH_4$ and $N_2 + CO_2$ hydrates are illustrated in Figure 5-1, Figure 5-2 and Figure 5-3, respectively. Figure 5-1 shows that the model results using the Kihara parameters were in good agreement with the experimental results at low to mid pressures. However, at higher pressures, the experimental equilibrium points were noticeably further to the right (higher temperature). This discrepancy could potentially be a consequence of the assumption that CO_2 does not occupy small cages. Therefore, results indicated that the model was accurate at lower pressures (<10 MPa), while it had considerable deviation at extreme high pressures where CO_2 has the propensity (however small) to occupy the large cavities of sI.

Figure 5-2 and Figure 5-3 shows that the modelling results are in good agreement with the experimental data for N_2 + CH_4 hydrates and 64 mol% N_2 + 36 mol% CO_2. However, the experimental equilibrium points were not consistent with the modelling results. This variation could possibly be due to the structural conversion of sI/sII. Nitrogen, as the smallest hydrate former, can stabilise small cavities of sII, while carbon dioxide is well known to form sI (Kang et al. 2001). Literature studies revealed that the structure of N_2 + CO_2 hydrates could either be of sI or sII depending on the amount of nitrogen and carbon dioxide filled in the small and large cavities (Kang and Lee 2000). Therefore, the structural transition possibly occurs for the mixed N_2 + CO_2 hydrates. Further investigations with direct observations using appropriate techniques such as NMR and X-ray diffraction is recommended to study the potential structure transition of N_2 + CO_2 hydrates.

Table 5-4 Cage occupancy calculations for CO_2 + CH_4 mixtures in small and large cavities

CO_2 (mol%)	P (MPa)	$\theta_{CH_4,l}$	$\theta_{CH_4,s}$	$\theta_{CO2,l}$	$\theta_{i,s}$	$\theta{i,l}$
10	5.0	0.8468	0.8322	0.1288	0.8468	0.9611
	7.5	0.8924	0.8437	0.1300	0.8924	0.9737
	10	0.9172	0.8498	0.1303	0.9172	0.9802
	15	0.9434	0.8564	0.1303	0.9434	0.9867
	20	0.9573	0.8604	0.1297	0.9573	0.9901
	25	0.9659	0.8628	0.1293	0.9659	0.9921
16	5.0	0.8376	0.7605	0.2014	0.8376	0.9619
	7.5	0.8855	0.7712	0.2030	0.8855	0.9742
	10	0.9118	0.7771	0.2035	0.9118	0.9806
	15	0.9396	0.7831	0.2039	0.9396	0.9870
	20	0.9545	0.7874	0.2029	0.9545	0.9903
	25	0.9636	0.7908	0.2015	0.9636	0.9923
20	5.0	0.8306	0.7144	0.2479	0.8306	0.9623
	7.5	0.8806	0.7241	0.2505	0.8806	0.9746
	10	0.9077	0.7300	0.2508	0.9077	0.9808
	15	0.9368	0.7362	0.2509	0.9368	0.9872
	20	0.9523	0.7409	0.2495	0.9523	0.9904
	25	0.9619	0.7446	0.2478	0.9619	0.9924

Subscripts 's' and 'l' refer to small and large cavities, respectively.

Subscripts 'CH_4' and 'CO_2' refer to methane and carbon dioxide, respectively.

Table 5-5 Cage occupancy calculations for N$_2$ + CH$_4$ mixtures in small and large cavities

N$_2$ (mol%)	P (MPa)	$\theta_{CH_4,s}$	$\theta_{CH_4,l}$	$\theta_{N_2,s}$	$\theta_{N_2,l}$	$\theta_{i,s}$	$\theta_{i,l}$
10	5	0.8272	0.8626	0.0855	0.0603	0.9127	0.9229
	7.5	0.8327	0.8705	0.0930	0.0656	0.9258	0.9361
	10	0.8356	0.8748	0.0996	0.0702	0.9352	0.9450
	15	0.8337	0.8758	0.1120	0.0790	0.9457	0.9548
	20	0.8319	0.8759	0.1214	0.0857	0.9533	0.9616
	25	0.8290	0.8747	0.1294	0.0914	0.9584	0.9661
20	7.5	0.7432	0.8013	0.1843	0.1341	0.9276	0.9354
	10	0.7410	0.8017	0.1953	0.1423	0.9363	0.9440
	15	0.7326	0.7974	0.2151	0.1573	0.9477	0.9548
	20	0.7238	0.7918	0.2314	0.1698	0.9552	0.9616
	25	0.7178	0.7878	0.2437	0.1792	0.9614	0.9670
31	5	0.6505	0.7210	0.2664	0.2000	0.9168	0.921
	7.5	0.6458	0.7208	0.2832	0.2134	0.9290	0.9342
	10	0.6401	0.7182	0.2979	0.2252	0.9380	0.9433
	15	0.6271	0.7094	0.3222	0.2449	0.9493	0.9543
	20	0.6158	0.7009	0.3414	0.2607	0.9572	0.9616
	25	0.6072	0.6943	0.3558	0.2727	0.9630	0.9670
36	5	0.6072	0.6836	0.3100	0.2364	0.9172	0.9200
	7.5	0.6032	0.6837	0.3290	0.2520	0.9322	0.9357
	10	0.5971	0.6805	0.3439	0.2643	0.9411	0.9447
	15	0.5825	0.6698	0.3698	0.2860	0.9523	0.9559
	20	0.5696	0.6596	0.3895	0.3029	0.9591	0.9625
	25	0.5590	0.6509	0.4057	0.3169	0.9647	0.9678

Subscripts 's' and 'l' refer to small and large cavities, respectively.

Subscripts 'CH_4' and 'N_2' refer to methane and nitrogen, respectively.

Table 5-6 Cage occupancy calculations for N_2 + CO_2 mixtures in small and large cavities

N_2 (mol%)	P (MPa)	$\theta_{CO_2,s}$	$\theta_{CO_2,l}$	$\theta_{N_2,s}$	$\theta_{N_2,l}$	$\theta_{i,s}$	$\theta_{i,l}$
64	5	0.2458	0.9042	0.6447	0.0780	0.8996	0.9822
	7.5	0.2335	0.8956	0.6881	0.0897	0.9216	0.9852
	10	0.2121	0.8846	0.7227	0.1022	0.9348	0.9868
	15	0.1751	0.8597	0.7758	0.1287	0.9509	0.9885
	20	0.1492	0.8361	0.8111	0.1533	0.9603	0.9894
74	5	0.1864	0.8640	0.7230	0.1147	0.9094	0.9787
	7.5	0.1695	0.8522	0.7588	0.1299	0.9283	0.9821
	10	0.1549	0.8396	0.7849	0.1444	0.9398	0.9840
	15	0.1298	0.8118	0.8245	0.1745	0.9543	0.9863
	20	0.1125	0.7867	0.8507	0.2010	0.9632	0.9877

Subscripts '*s*' and '*l*' refer to small and large cavities, respectively.

Subscripts '*N_2*' and '*CO_2*' refer to nitrogen and carbon dioxide, respectively.
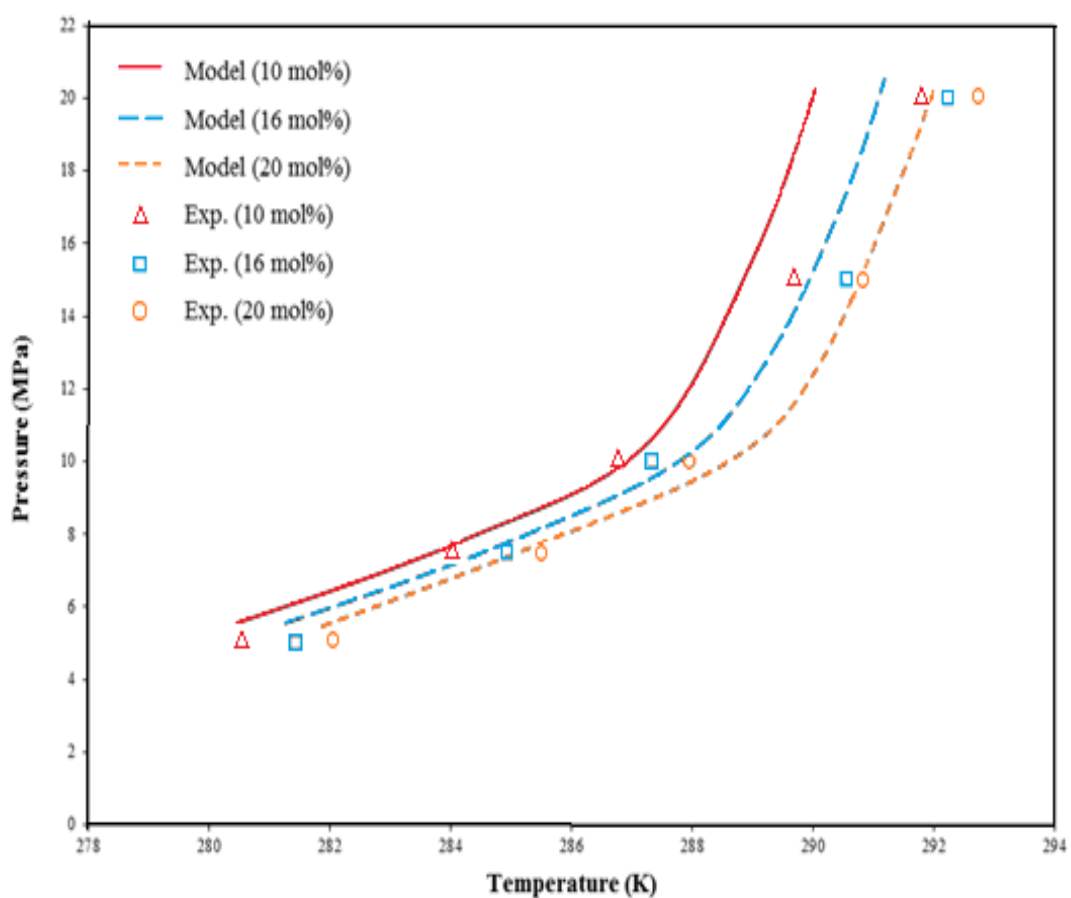
Figure 5-1 Comparison of experimental methane – carbon dioxide hydrate dissociation points with model data. Numbers indicate CO_2 mole percentage in the mixture. Average relative deviations between the experimental data and the model results are 0.21%, 0.18% and 0.13% for the 10% CO_2 + 90% CH_4, 16% CO_2 + 84% CH_4 and 20% CO_2 + 80% CH_4 gas mixtures, respectively
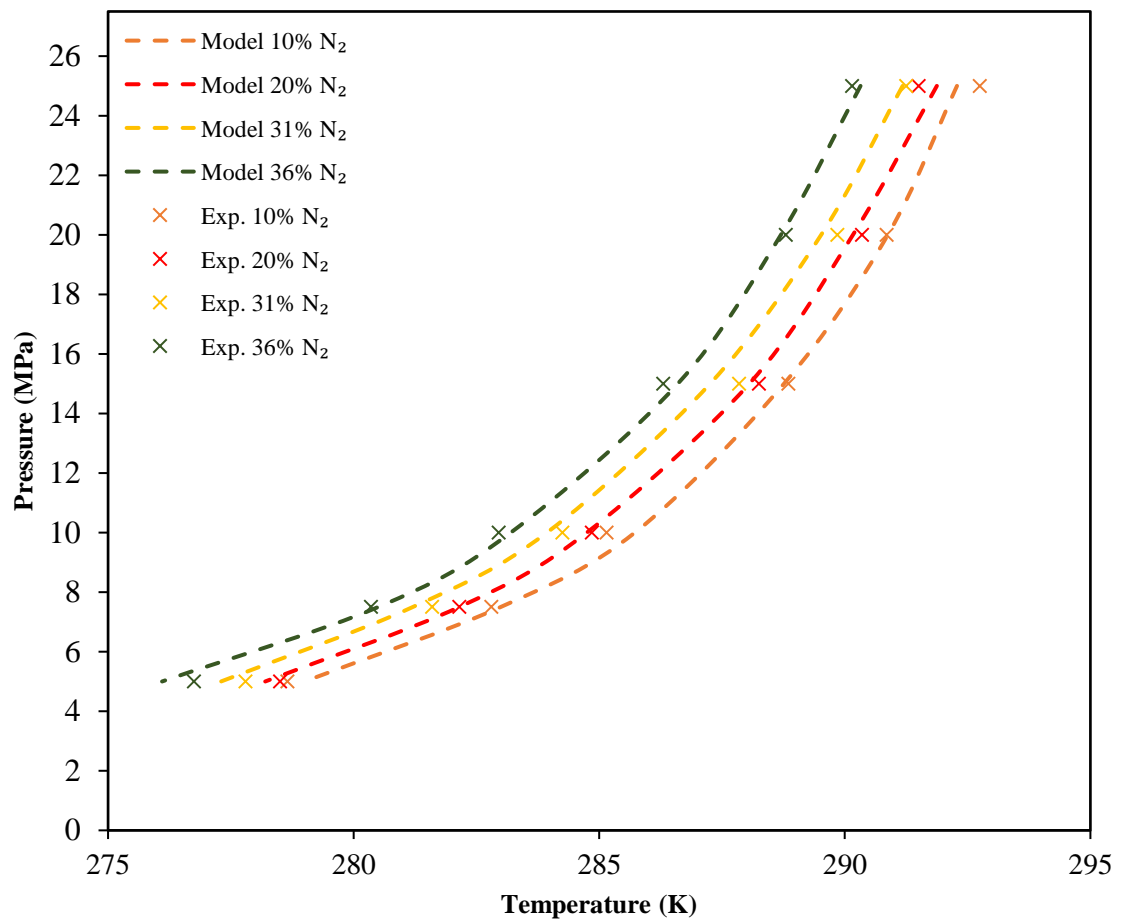
Figure 5-2 Comparison of experimental N_2 + CH_4 hydrates with model predictions. Numbers indicate N_2 mole percentage in the mixture. Average relative deviations between the experimental data and the model results are 0.087%, 0.054%, 0.15% and 0.12% for the 10% N_2 + 90% CH_4, 20% N_2 + 80% CH_4, 31% N_2 + 69% CH_4 and 36% N_2 + 64% CH_4 gas mixtures, respectively
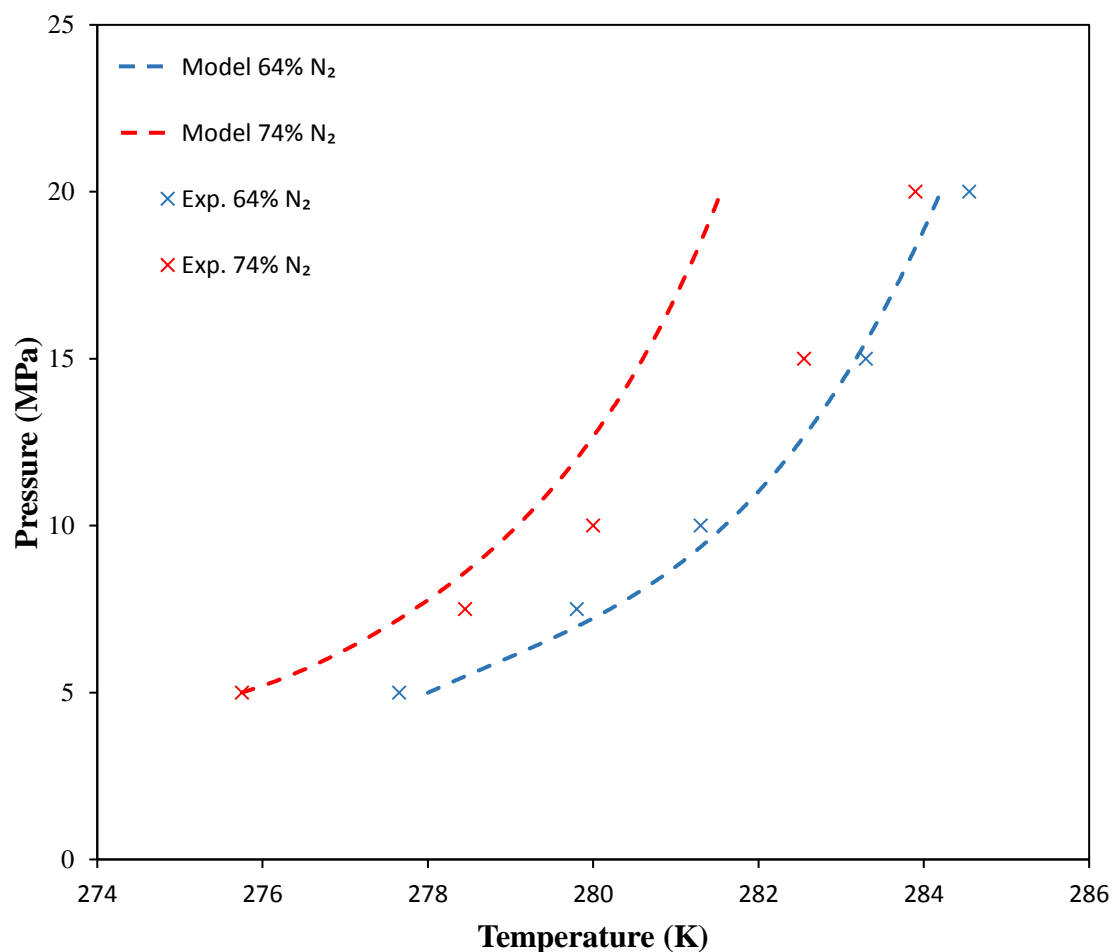
Figure 5-3 Comparison of experimental N₂ + CO₂ hydrates with model predictions. Numbers indicate N₂ mole percentage in the mixture. Average relative deviations between the experimental data and the model results are 0.07% and 0.58% for the 36% CO₂ + 64% N₂ and 26% CO₂ + 74% N₂, respectively

5.4.2   Empirical model prediction

The performance and accuracy of the new correlation, Equation 5-11, were checked by applying the statistical error analysis to 85 data points that were not used in the correlation development. Statistical parameters of the new correlation, including average deviation, average absolute deviation, standard deviation, average absolute percentage error, root mean square errors and correlation coefficient (R^2) are

calculated. These statistical parameters are defined in Equations 5-12 to 5-18 as follows:

$$AD = \frac{1}{n} \sum_{i=1}^{n} (T_{EXP(i)} - T_{Cal(i)}) \qquad\qquad 5\text{-}12$$

$$AAD = \frac{1}{n} \sum_{i=1}^{n} |T_{EXP(i)} - T_{Cal(i)}| \qquad\qquad 5\text{-}13$$

$$SD = \sqrt[2]{\frac{\sum_{i=1}^{n}(x - avg.x)}{n}} \qquad\qquad 5\text{-}14$$

$$SAAPE = \frac{1}{n} \sum_{n=1}^{i} \left[\left| \frac{\left(T_{cal.}(i) - T_{exp.}(i)\right)}{T_{exp.}(i)} \times 100 \right| \right] \qquad\qquad 5\text{-}15$$

$$RMS = \sqrt[2]{\frac{\sum_{i=1}^{n}(T_{cal.}(i) - T_{exp.}(i))^2}{n}} \qquad\qquad 5\text{-}16$$

$$RMS = \sqrt[2]{\frac{\sum_{i=1}^{n}(T_{cal.}(i) - T_{exp.}(i))^2}{n}} \qquad\qquad 5\text{-}17$$

$$R^2 = \left[\frac{n\sum_{i=1}^{n}T_{exp.}(i) \times T_{cal.}(i) - \left(\sum_{i=1}^{n}T_{exp.}(i)\right)\left(\sum_{i=1}^{n}T_{cal.}(i)\right)}{\sqrt[2]{n\sum_{i=1}^{n}\left(T_{exp.}(i)\right)^2 - \left(\sum_{i=1}^{n}T_{exp.}(i)\right)^2} \times \sqrt[2]{n\sum_{i=1}^{n}\left(T_{cal.}(i)\right)^2 - \left(\sum_{i=1}^{n}T_{cal.}(i)\right)^2}} \right]^2 \qquad 5\text{-}18$$

where, n is the number of points in the dataset, $T_{cal.}$ is the calculated hydrate equilibrium temperature, $T_{exp.}$ is the experimental hydrate equilibrium temperature and x is defined as $\left| \frac{\left(T_{cal.}(i) - T_{exp.}(i)\right)}{T_{exp.}(i)} \times 100 \right|$.

The correlation results were also compared with the experimental data and with the predictions calculated by Hammerschmidt (1936), Motiee (1991), and Salufu (2013). Table 5-7 shows statistical parameters of the proposed correlation compared with the other correlations. According to Table 5-7, the new correlation had the highest value of squared correlation coefficient ($R^2 = 0.9978$) and lowest absolute percentage error (0.2183) compared to the other correlations. In addition, the new correlation showed a standard deviation and root mean square errors less than 1, which indicates the ability of the new correlation to predict the hydrate equilibrium temperature correctly for the assumed range of conditions. In addition, Table 5-7 shows that the Hammerschmidt correlation had lower performance (highest statistical parameters) than that of the other correlations.

The accuracy of the proposed correlation was also checked by comparing the calculated temperatures with the experimental data shown in Figure 5-4, and our calculated temperatures were in good agreement with the experimental data for gas mixtures with a specific gravity in the range of 0.553 to 1. The cross plots shown in Figure 5-5, compare the measured hydrate equilibrium temperatures with those calculated by our correlation (a), Hammerschmidt (b), Motiee (c) and Salufu (d). As demonstrated, an excellent agreement was shown between the measured and calculated results for our correlation compared with other correlations.

Table 5-7 Statistical analysis parameters for the new correlation compared with other correlations

Analysis parameter	This work	Hammerschmidt (1936)	Motiee (1991)	Salufu (2013)
AD	0.0127	-13.1245	-4.7073	-5.3278
AAD	0.6203	13.1245	8.6390	5.4487
SD	0.1381	4.0165	1.1501	1.0296
AAPE	0.2183	4.3963	3.0223	1.9469
RMS	0.7239	18.5168	9.2604	6.1317
R^2	0.9978	0.8792	0.8887	0.9783

AD: Average deviation

AAD: Average absolute deviation

SD: Standard deviation

AAPE: Average absolute percentage error

RMS: Root mean square error

R^2: Squared correlation coefficient
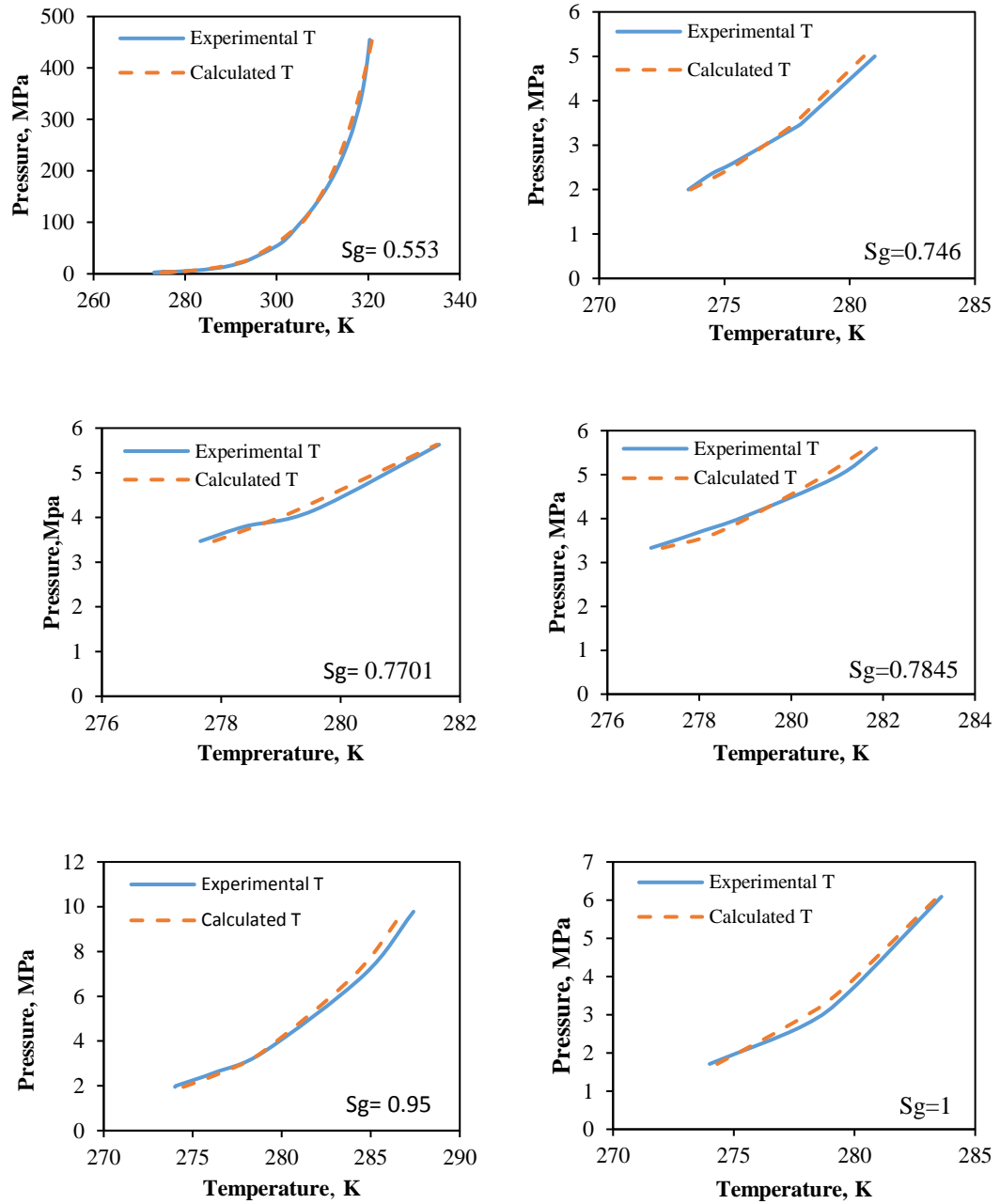
Figure 5-4 Comparison of the new correlation results with the experimental data for gas mixtures with specific gravities (Sg) of 0.553, 0.746, 0.7701, 0.7845, 0.95 and 1
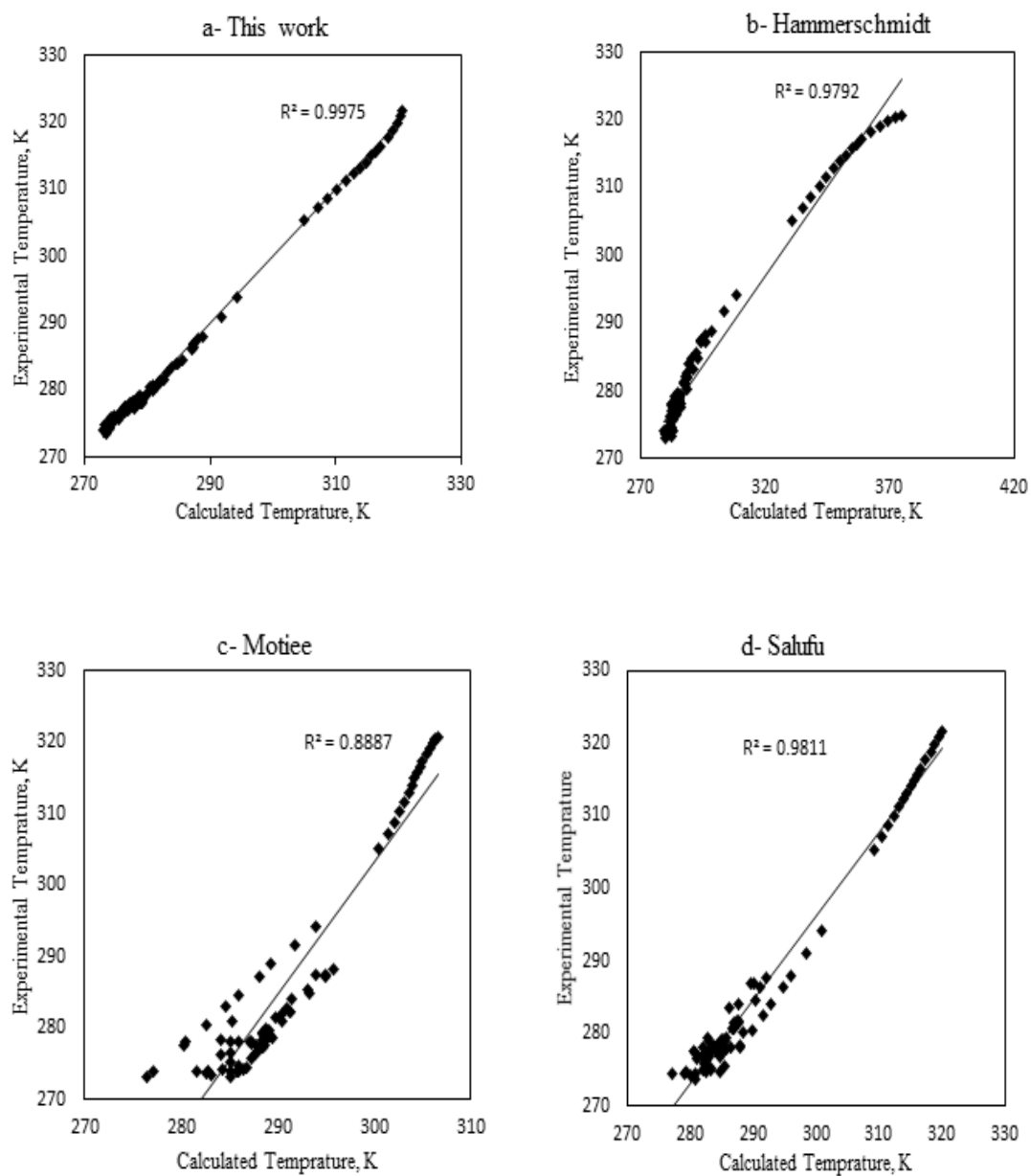
Figure 5-5 Cross plots of the experimental and predicted equilibrium temperatures calculated by the new correlation (a), Hammerschmidt (b), Motiee (c) and Salufu (d) correlations

5.5   Conclusions

The gas hydrate equilibrium conditions are of significance in the energy sector and have extensive applications in industry because of their role either as a potential energy source or as a threat to flow assurance. Thus, in the present study, we first proposed a thermodynamic model for gas hydrate equilibrium conditions and cage occupancies for $CO_2 + CH_4$, $N_2 + CH_4$ and $CO_2 + N_2$, at different compositions. The occupancy calculations for the $CO_2 + CH_4$ hydrate system have shown that CO_2 stabilises the sI hydrate. Results also demonstrated that an increase in CO_2 gas composition resulted in higher CO_2 hydrate equilibrium conditions. This confirms and explains the observed promotion of hydrate equilibrium conditions with increasing CO_2 gas composition. The validity of the proposed model was tested by comparison with the experimental data. A comparison between the experimental data and the model calculations for carbon dioxide + methane hydrates shows that the model can acceptably predict the hydrate equilibria at pressures lower than 10 MPa. For $N_2 + CH_4$ and 64 mol% N_2 + 36 mol% CO_2 hydrate systems, an acceptable agreement was found between the experimental and model results. However, a considerable deviation was noticed between the experimental data and model prediction for 74 mol% N_2 + 26 mol% CO_2 hydrate. Therefore, we investigated a potential structural transformation that occurs for this mixed hydrate.

Second, a new correlation was developed for accurate prediction of hydrate equilibrium temperatures for different gas mixtures containing methane, nitrogen and carbon dioxide. The new correlation was applicable for the temperature range of 273–320 K, pressure range of 1.7–330 MPa, and for gas mixtures containing methane, carbon dioxide and nitrogen with specific gravity range of 0.553 to 1. The statistical parameters showed that the new correlation has an excellent performance compared with Hammerschmidt, Motiee and Salufu correlations. In addition, the correlation results showed good agreement with the experimental measurements within the investigated range. Consequently, the new correlation represents a simple, accurate, low-cost and direct method for predicting gas hydrate equilibrium conditions in a system that meets the above operating conditions.

Chapter 6   Experimental Pore-scale Analysis of Carbon Dioxide Hydrate in Sandstone via X-Ray Micro-Computed Tomography*

6.1   Summary

Carbon dioxide geo-sequestration (CGS) into sediments in the form of (gas) hydrates is one of the proposed methods for reducing anthropogenic carbon dioxide emissions to the atmosphere and, thus reducing global warming and climate change. However, there is a serious lack of understanding as to how such CO_2 hydrate forms and exists in sediments. We thus imaged CO_2 hydrate distribution in sandstone, and investigated the hydrate morphology and cluster characteristics via X-ray micro-computed tomography (μCT) in 3D in-situ. A substantial amount of gas hydrate (~17% saturation) was observed, and the stochastically distributed hydrate clusters followed the power-law relations with respect to their size distributions and surface area-volume relationships. The layer-like hydrate configuration is expected to reduce CO_2 mobility in the reservoir, and the smaller than expected hydrate surface-area/volume ratio would reduce methane production and CO_2 storage capacities. These findings will aid large-scale implementation of industrial CGS projects via the hydrate route.

6.2   Introduction

Carbon dioxide emissions into the atmosphere have increased significantly over the past decades (IPCC 2005, Pachauri et al. 2014). This is coupled with massive growth in fossil fuel consumption, where CO_2 is also emitted (IEA 2016). Such high CO_2 concentrations, however, lead to rising global temperatures (global warming), and thus climate change (Houghton et al. 2001). Indeed, CO_2 contributes approximately 60 percent to this global warming (Yang et al. 2008). Decreasing the level of CO_2 emissions is thus crucial for mitigating climate change. One solution suggested for achieving this is to capture and sequester CO_2 in permafrost areas (e.g. Alaska North Slope; Schoderbek and Boswell 2011), onshore Arctic regions (e.g. Alberta portion,

Canada; Cote and Wright 2010; Zatsepina et al. 2014) and deep ocean environments (White et al. 2003, Yamasaki 2003, Orr 2009). The thermo-physical conditions prevailing in such marine environments are clearly within the CO_2 hydrates stability zone (Clennell et al. 1999, Tohidi et al. 2010, Park et al. 2014). In addition, as hydrate formation within the porous medium blocks the pores and causes a reduction in sediment permeability, and could provide an additional seal by self-sealing (Kvamme et al. 2007, Tohidi et al. 2010). However, sequestration of CO_2 in such environments will lead to the dissociation of the in-situ natural gas hydrates, thus releasing the methane inside them. Problematically, methane released into the atmosphere causes further global warming (hydrate gun hypothesis; Kennett et al. 2003).

At the same time, the demand for energy sources (e.g. for natural gas) is increasing (Dudley 2013, Al-Fatlawi et al. 2017), which led to the proposal that natural gas hydrates (the main gas here is methane) can be a potential energy source (Makogon 2010). Thus, the sequestration of CO_2 in the form of hydrates may be combined with methane production via CO_2-CH_4 replacement in methane hydrate-bearing sediments (Graue et al. 2008, Ohgaki et al. 1994)

Furthermore, hydrate morphology, distribution and saturation in sediments significantly affect seismic velocities (compressional and shear velocities) and petro-physical properties (such as permeability, electrical conductivity, and shear strength; Waite et al. 2009). Thus, gas hydrate exploration and monitoring depend on the distribution and morphology of the hydrates in the pore space (Dai, Banik, et al. 2008, Dai, Snyder, et al. 2008) and multiple pore-scale models (free floating, cementing sediments and contacting but not cementing sediments; (Helgerud et al. 1999, Jones et al. 2007)) have been hypothesized to correlate the hydrate distribution with seismic velocities.

Consequently, pore-scale characterisation of hydrates in their host sediments is essential for exploration, monitoring and implementation of hydrate-CGS and hydrate exploitation as an energy source. However, experimental data for CO_2-hydrate formation and existence in sediments is limited despite their vital importance (Tohidi et al. 2010, Ta et al. 2015) and most of the previous studies, imaged hydrate formation in unconsolidated sediments. Thus, we thus imaged CO_2 hydrate formation and

dissociation via X-ray (μCT) at high resolution in 3D in-situ and analysed the corresponding hydrate microstructures.

6.3 Experimental Methodology

6.3.1 Materials and Experimental Set-up

A small cylindrical Bentheimer sandstone plug (5 mm in diameter and 15 mm in length) was drilled and used in these experiments. Bentheimer is a clean, homogeneous sandstone consisting mainly of quartz (99 wt%) with high permeability and porosity (Rahman et al. 2016). Porosity and permeability of 22.1% and 2370 mD, respectively, were measured precisely with a nitrogen permeameter-porosimeter (AP-608 with accuracy ±0.1%) on a sister plug drilled from the same block. Carbon dioxide (purity 99.9 mol%, supplied by BOC Australia) was used as a hydrate-forming gas. Sodium iodine brine solution was prepared by mixing 6% by weight of NaI into deionised water; this brine was used as the aqueous phase (note that iodide is needed to ensure sufficient X-ray contrast (Lusic and Grinstaff 2012)), see below. A high-pressure X-ray transparent vessel (Iglauer et al. 2011, Rahman et al. 2016, Lebedev et al. 2017, Iglauer and Lebedev 2017) was used as a core holder for hydrate formation and X-ray μCT imaging. The small Bentheimer plug was mounted inside the core holder, and the core holder was connected to the hydrate formation setup as shown in Figure 6-1. In addition to the high-pressure (core-holder) flow cell, the setup consisted of three high precision syringe pumps (ISCO 500D with an accuracy of 0.1%); the first two pumps were used for CO_2 and brine injection, respectively, and the third pump provided confining pressure by compressing the deionised water. A thermocouple was installed in the flow cell to monitor the temperature during the hydrate formation process with a precision of ± 0.5 K. The cooling temperatures required for hydrate formation were achieved by circulating an antifreeze liquid containing ethylene glycol via a thermo-refrigerated bath (Alpha RA8, Lauda, Germany). A high-resolution μCT scanner (Xradia VersaXRM) was then used to image the core plug in 3D at a high resolution of $(3.43 \text{ μm})^3$. μCT is an efficient and nondestructive method that is commonly used to investigate the pore-scale structure of rock samples (Blunt et al. 2013, Cnudde and Boone 2013, Wildenschild and Sheppard 2013, Iglauer and Lebedev 2017).
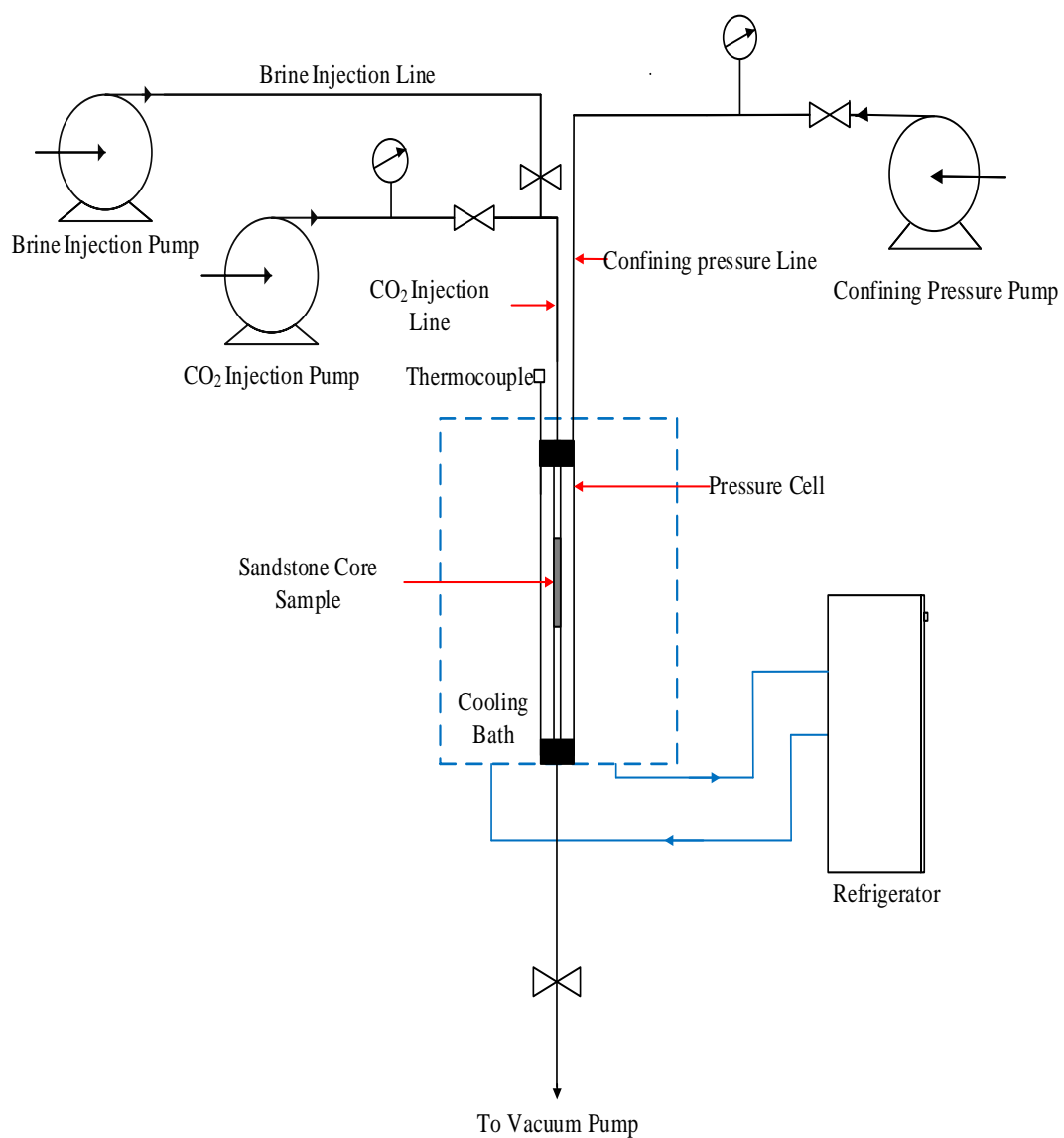
Figure 6-1 Experimental apparatus used for forming CO₂ hydrate in a Bentheimer sandstone plug (at 3 MPa and 274 K)

6.3.2   Experimental Procedure

Initially, the flow cell and flow lines were vacuumed for 24 h to remove any air from the system, and the confining pressure and pore pressure were increased to 8 MPa and 3 MPa, respectively. The sample was then completely saturated with doped brine (6 wt% NaI in deionised water) by injecting more than 1000 pore volumes (PV) of brine. Subsequently, 50 PV of CO_2 gas was injected into the core at the same pressure conditions at a flow rate of 0.1 mL/min (capillary number = 5×10^{-6}) to obtain a partially (brine) saturated porous medium. These steps were performed at an ambient laboratory temperature (294 K). Hydrate formation was then started by decreasing the temperature to 274 K (1 °C; which is below the CO_2 hydrate equilibrium temperature; note that the CO_2-hydrate formation temperature in sediments is ~ 8 °C at 3 MPa) (Yang et al. 2012). Cooling was achieved by circulating the coolant continuously through a copper coil wrapped around the core holder. Because the CO_2 injection pump was set to maintain a constant pressure of 3 MPa, gas consumption in the injection pump over time indicated hydrate formation (Sloan and Koh 2008). Hydrate conditions (3 MPa pore pressure and 274 K) were maintained for 48 h to let the hydrate nucleate and grow inside the sample. Thus, the entire hydrate formation process was considered complete when no further gas was injected into the system (from the injection pump reservoir). The core holder was then placed inside the μCT scanner and an image of the hydrate-bearing core was acquired at a high resolution of $(3.43 \ \mu m)^3$.

The core holder with the core sample was then left in the scanner for 24 h at room temperature (294 K), and the plug was again imaged μCT by imaged at the same high resolution of $(3.43 \ \mu m)^3$, i.e. after hydrate dissociation. All μCT images were filtered with a 3D non-local mean algorithm (Buades et al. 2005, Buades et al. 2008) and segmented with a watershed algorithm (Schlüter et al. 2014) for subsequent analysis.

6.4   Results and Discussion

6.4.1 Visualisation and Morphology of CO₂ Hydrate

The CO_2 hydrate formed inside the Bentheimer plug is visualised in Figure 6-2,
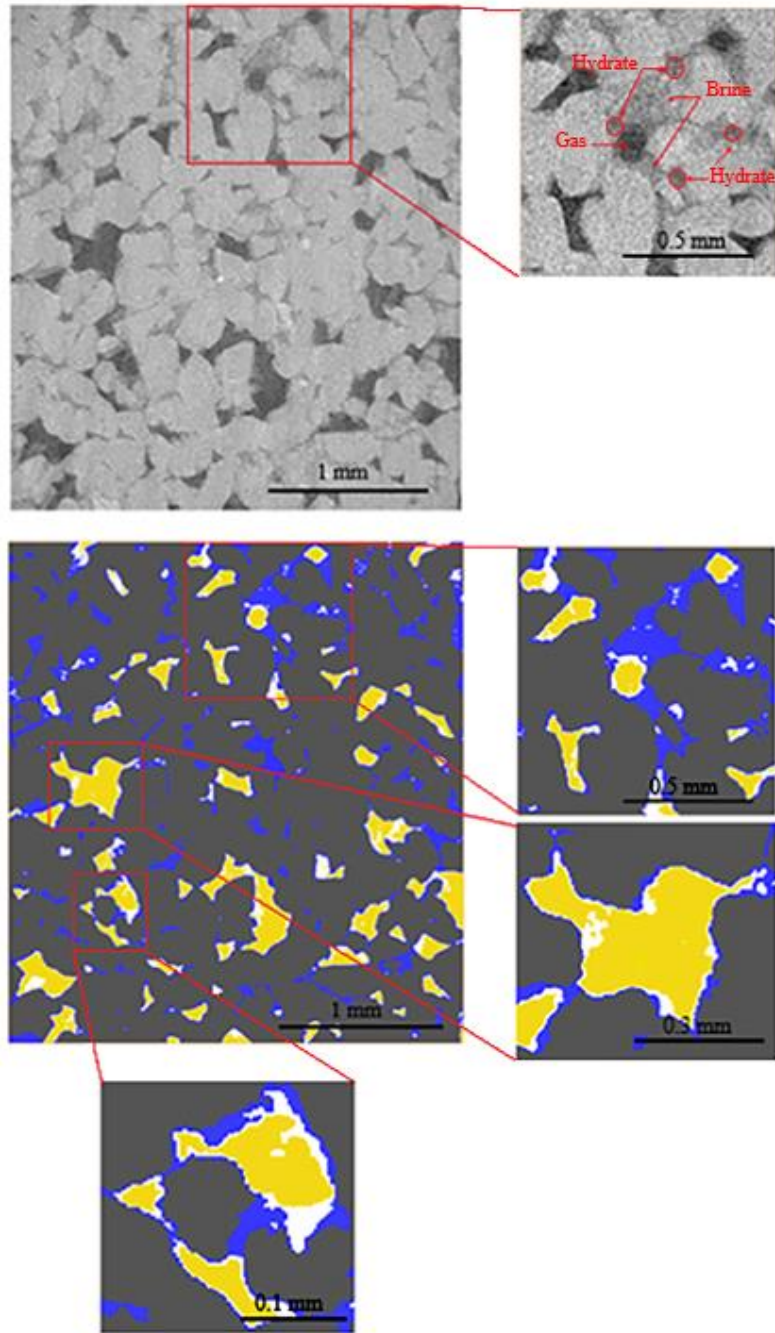
Figure 6-2 Raw (top) and segmented (bottom) 2D slices through the CO_2 hydrate-bearing core (3 MPa, 274K) . In the raw images, CO_2 is black while hydrate is dark grey, brine is slightly lighter grey, and sandstone is light grey. In the segmented images, grain particles are dark grey, hydrates are white, brine is blue, and CO_2 gas is yellow
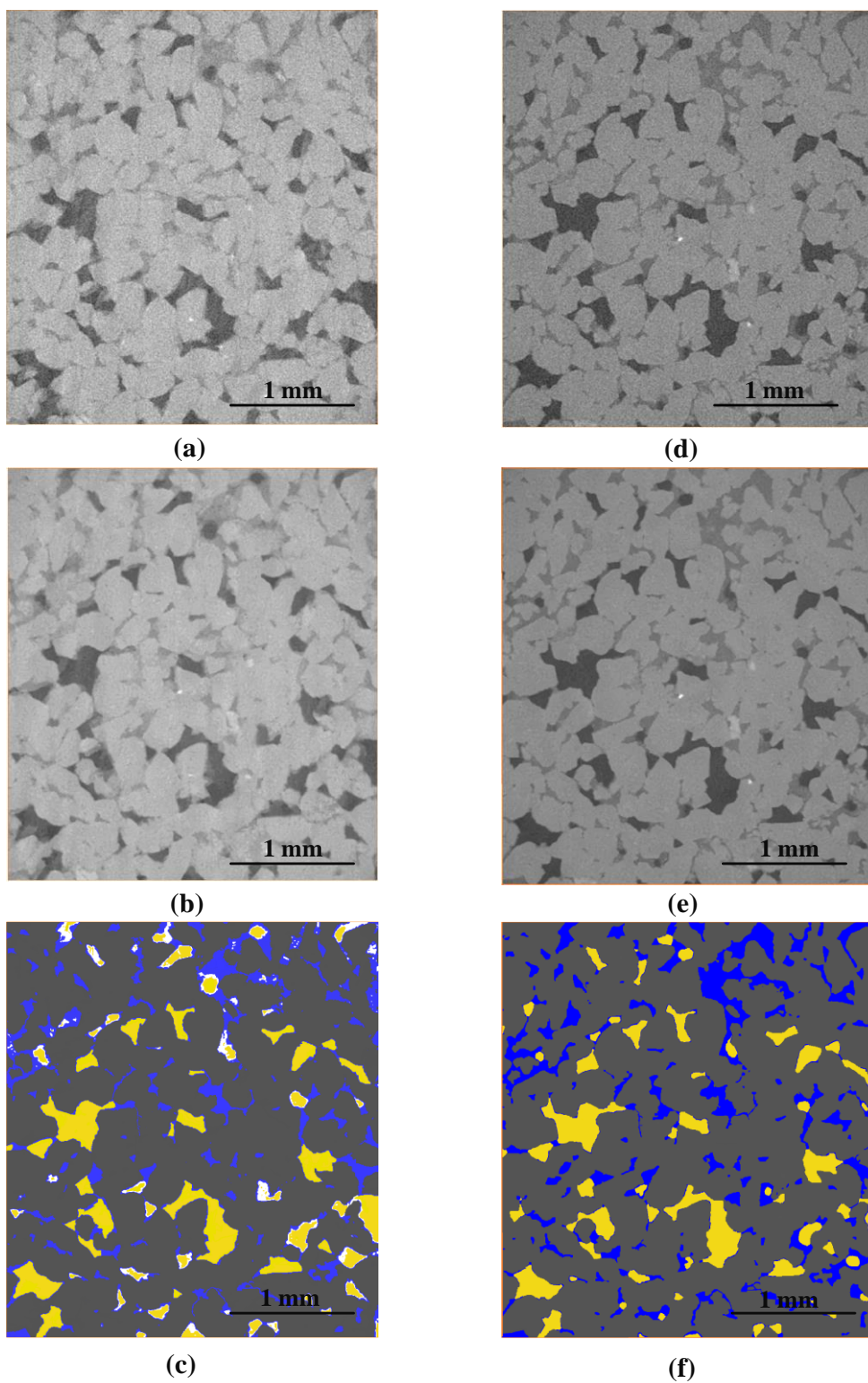
Figure 6-3 Raw (a,d), filtered (b,e) and segmented (c,f) 2D slices through the hydrate-bearing core (a-c) and the core after hydrate dissociation (d-f). In the segmented images, grain particles are dark grey, hydrates clusters are white, brine is blue, and CO₂ gas is yellow

Hydrate-bearing sandstone
Brine

Sandstone after hydrate dissociation

CO$_2$ Gas

Hydrate

(a) (d) (b) (e) (c)
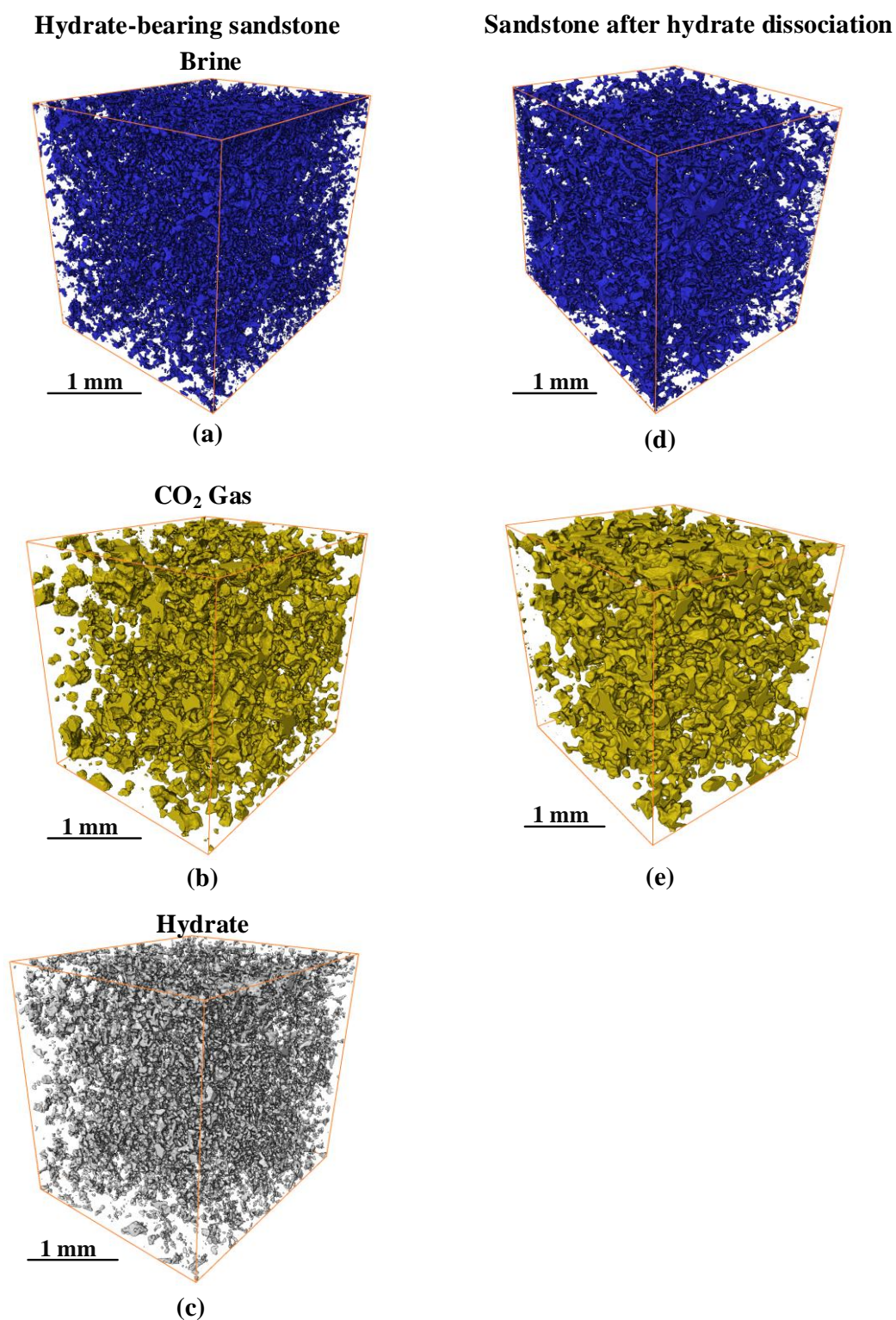
Figure 6-4 Three-dimensional segmented images showing each phase. The left-hand side shows the phases for the hydrate-bearing sample (3 MPa, 274K), while the right side shows the phases after hydrate dissociation (3 MPa, 294K). Blue is brine; yellow is CO$_2$ gas and grey is CO$_2$-hydrate

The μCT images thus provide information about the distribution of various sample components. Precisely, four components (grains, brine, CO_2 gas, and hydrate), each with a different gray scale value, can be determined from the images. The different grey scales correlate with the X-ray mass attenuation coefficient μ_x, which is proportional to a product of the bulk density ρ_b, the effective atomic number Z (i.e. the chemical composition) and the beam energy E (which is kept constant here at 90 keV); $\mu_x \sim \rho_b(a + b \times Z^{3.8}/E^{3.2})$, where a is the Klein-Nishina coefficient and, b is a constant (Vinegar and Wellington 1987, Van Geet et al. 2000, Jin et al. 2004, Sato et al. 2005). Different materials thus produce a contrast in X-ray attenuation and a distinctly different grey scale in the image. Black/dark grey regions indicate low X-ray attenuation while the light regions identify high attenuation. The bulk densities of the four components are as follows: grain density (quartz)= 2.65 g/cm^3 (Johnson and Olhoeft 1984), NaI brine (6 wt %) density= 1.04 g/cm^3, CO_2 gas density at 3 MPa and 1°C = 0.0766 g/cm^3 (Scalabrin et al. 2006) and CO_2 hydrate density = 1.1 g/cm^3 (Aya et al. 1997). Thus, the grains have a higher attenuation value and a lighter color in the μCT image, whereas the CO_2 gas with a lower attenuation is black. Hydrate and brine have greyscales in between, i.e. hydrate is dark grey and brine is slightly lighter because of the K_α-edge absorption of the iodine dissolved in the brine (doping agent), which is consistent with observations made for methane-hydrate (Sato et al. 2005, Jin et al. 2006).

We can thus distinctly differentiate CO_2 hydrates, CO_2 gas and brine in the pores, and thus determine their distribution and morphology. At the image (mm)scale, a random spatial hydrate distribution within the pore space was observed, which is consistent with natural hydrate occurrence in sands and glass beads (Dai et al. 2012, Kerkar et al. 2014). However, at pore (μm) scale, CO_2 hydrate resided mainly in the pore body of the sandstone, and it did not contact the grain surface. This is consistent with the free-floating model (Zhao et al. 2014, Zhao, Yang, et al. 2015). Instead, a layer of free brine was observed between the grain surface and hydrate as shown in Figure 6-2. This observation is consistent with the behaviour of carbon dioxide hydrate in etched glass micromodels (Tohidi et al. 2001), xenon hydrates in quartz sand and glass beads (Chaouachi et al. 2015), and molecular dynamics computations for methane hydrates in the presence of silica (Bagherzadeh et al. 2012). The presence of a brine film coating the grain surface indicates that the brine is the wetting phase (Iglauer 2017), although

hydrate migration to the grain surface may be kinetically inhibited. In addition, CO_2 hydrate formation occurred at the brine-CO_2 interface, indicating preferential hydrate nucleation and growth at the water-gas interface, as observed for CO_2- and methane-hydrate formation within a 2D porous silicon micromodel (Hauge et al. 2016, Almenningen et al. 2017) and methane hydrate in sands (Waite et al. 2004, Jin et al. 2012). Furthermore, the free CO_2 gas existed mainly in the pore centre which indicates that CO_2 is the non-wetting phase (Iglauer et al. 2015). Thus, the CO_2 hydrate did not completely plug the pores due to the existence of a wetting brine film.

However, hydrates substantially reduce permeability, i.e. hydrate formation obstructs the flow (Kneafsey et al. 2011, Almenningen et al. 2017). Consequentially, such pore-centred gas hydrate layers assist in vertical sealing and restrict the upwards CO_2 flux (Kvamme et al. 2007). However, such hydrate layers are also expected to reduce lateral CO_2 spreading in the reservoir, and thus reduce storage capacity. Moreover, CH_4 recovery rates (by CH_4-CO_2 hydrate exchange) are expected to be reduced, although the brine layers may act as paths for CH_4 flow (Kvamme et al. 2007). However, literature results showed that CH_4 recovery could be enhanced using different strategies such as injection of $CO_2 + N_2$ gas mixtures (Hauge et al. 2014), injection of chemical inhibitors (Hossainpour 2013, Khlebnikov et al. 2016) or CO_2 injection at high initial pressures(Zhao et al. 2012). These strategies would prevent hydrate formation near the production well, and thus increase storage capacity.

6.4.2 Hydrate Saturation in the Core Sample

Three-dimensional visualisations of each component within the CO_2 hydrate-bearing sample (a-c) and after hydrate dissociation (d and e) are shown in Figure 6-4. We first measured the porosity of the images by counting the number of pore voxels and divided them by the total number of voxels (i.e. the bulk volume). This μCT porosity was 21.1%, which is consistent with the 22.1% gas porosity measured pycnometrically (see above). The slightly higher experimental gas porosity was caused by limited spatial μCT resolution (clay pore space cannot be resolved at 3 μm resolution (Desrues et al. 2006)). Furthermore, the saturation of each component (volume fraction of each component in the pore space) was measured on the μCT images (Table 6-1). A

significant CO_2 hydrate saturation (17.8%) was observed, which was localised at the brine-gas interface and exhibited layer-like morphology (see Figure 6-2)

Table 6-1 Brine, CO₂, and hydrate saturations and statistical parameters in the hydrate-bearing sandstone before and after hydrate dissociation

Component	Saturation (%)		τ		p	
	Hydrate-bearing plug	After dissociation	Hydrate-bearing plug	After dissociation	Hydrate-bearing Plug	After dissociation
CO₂	59.0	64.2	1.375	1.15	0.764	0.74
Hydrate	17.8	-	1.58	-	0.791	-
Brine	23.2	35.8	-	-	-	-

6.4.3 Gas Hydrate Statistics - Cluster Size Distributions and Surface Area-Volume Relationships

CO_2 hydrate and free gas distributions in the pore space were statistically analysed before and after hydrate dissociation, (Figure 6-5). Power law relations were observed for the CO_2-gas and CO_2-hydrate cluster size distributions (Table 6-1); i.e. $N \propto V^{-\tau}$, where N is the number of clusters of size V counted and τ is the fitting exponent. A large number of small hydrate clusters was observed, which rapidly dropped with increasing size, and only a few large hydrate clusters were measured. These large clusters (Figure 6-6), ~ 1.5% of the total hydrate clusters), however, contributed most to the hydrate saturation and they spanned several pores. Fewer small CO_2 gas clusters were counted, and the largest gas clusters were larger than the largest hydrate clusters (the largest hydrate cluster had a volume of 205028 μm^3, wheareas the largest CO_2 cluster size had a volume of 407724 μm^3, approximately two times larger). This is reflected in the smaller τ values associated with the CO_2 gas cluster size distributions. τ was 1.375 in the hydrate-bearing sample, and τ decreased to 1.15 after hydrate

dissociation. Physically, CO_2 was released from the hydrates and coalesced with the CO_2 bubbles, thus increasing their sizes.

Moreover, the surface area (A) of the hydrate and CO_2 clusters were measured and plotted as a function of their volume (V,

Figure 6-7). A power-law relation was again observed ($A \propto V^{-p}$, Table 6-1). An exponent $p \sim 0.75$ indicates structures less compact than a sphere ($p = 2/3$), but more compact than a completely percolation-like ramified structure (where $p \sim 1$, Stauffer 1979). This implies a smaller surface area/volume ratio for each hydrate cluster than expected by the percolation theory. Such a smaller ratio has significant implications in terms of gas recovery via CO_2-CH_4 exchange and safe storage in hydrate-bearing sediments; because hydrate dissociation/formation rates are directly proportional to the cluster surface area (Kwon et al. 2008, Cheng et al. 2013). Smaller surface area/volume ratios lead to lower dissociation rates during the CO_2-CH_4 exchange process, and thus less production and overall lower CO_2 storage capacity.
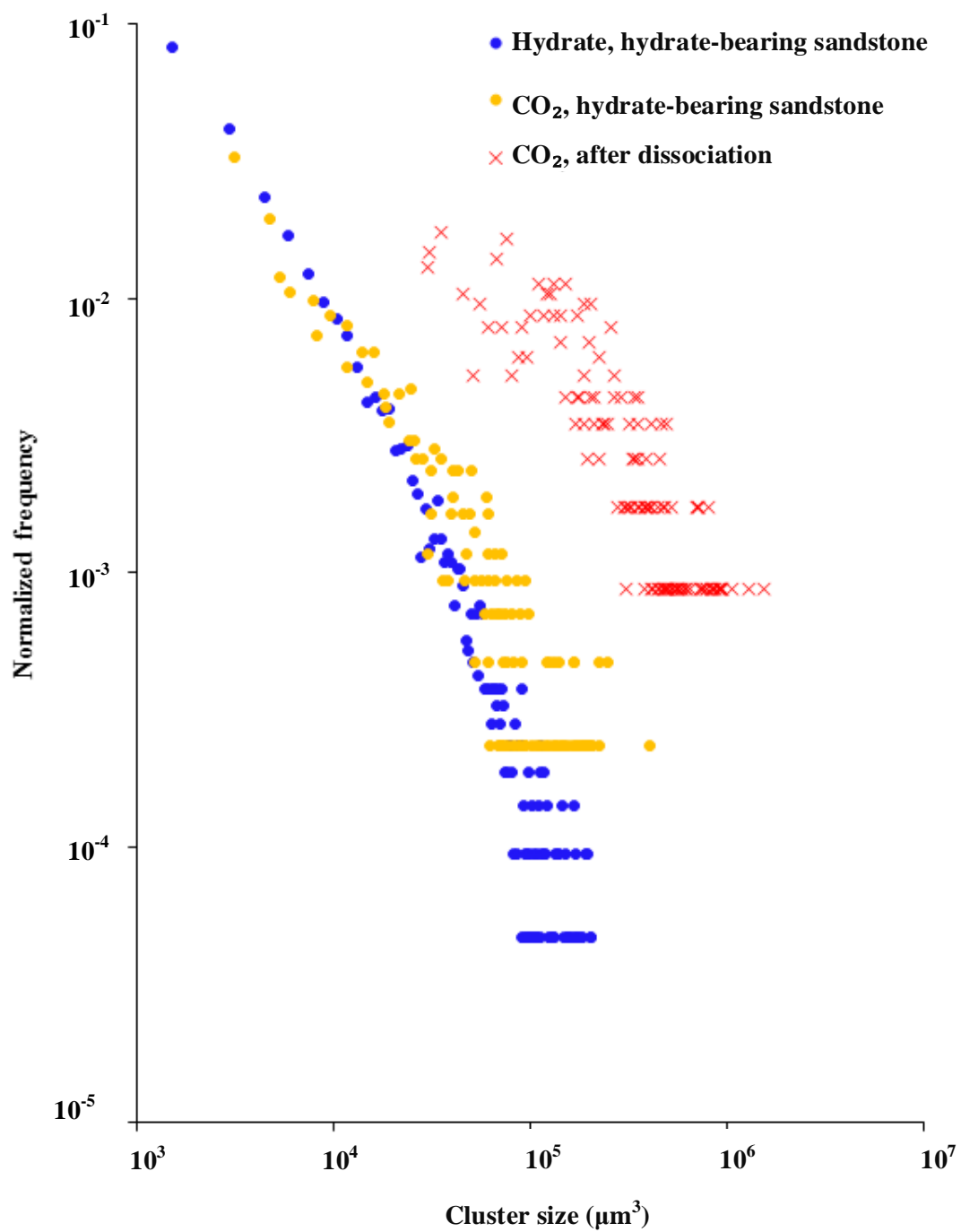
Figure 6-5 CO₂ hydrate and CO₂ gas clusters size distributions in Bentheimer sandstone before and after hydrate dissociation
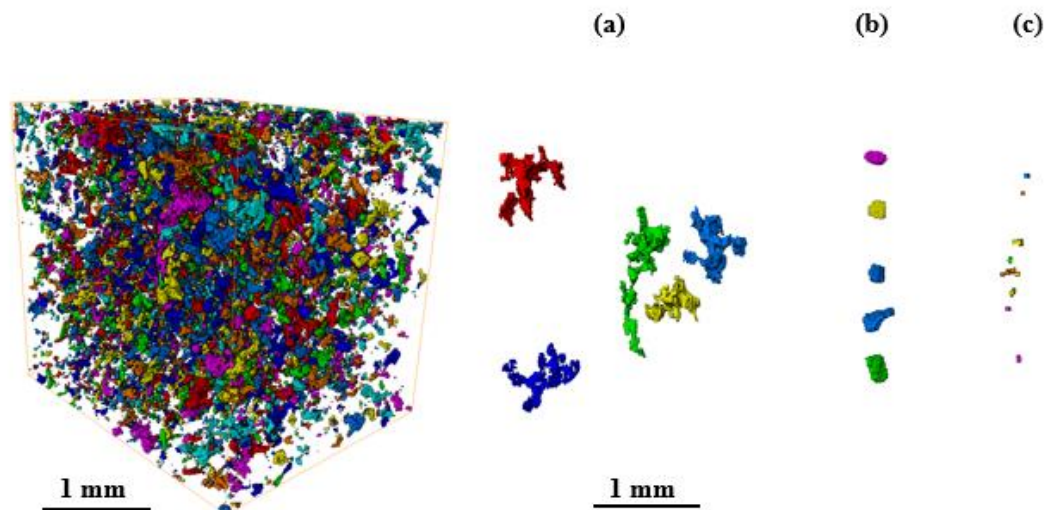
Figure 6-6 Hydrate clusters, (a) the largest hydrate clusters (size 204080–206590 μm³), (b) medium hydrate clusters (size 5227–7456 μm³) and (c) small hydrate clusters (size 40.5–121 μm³)
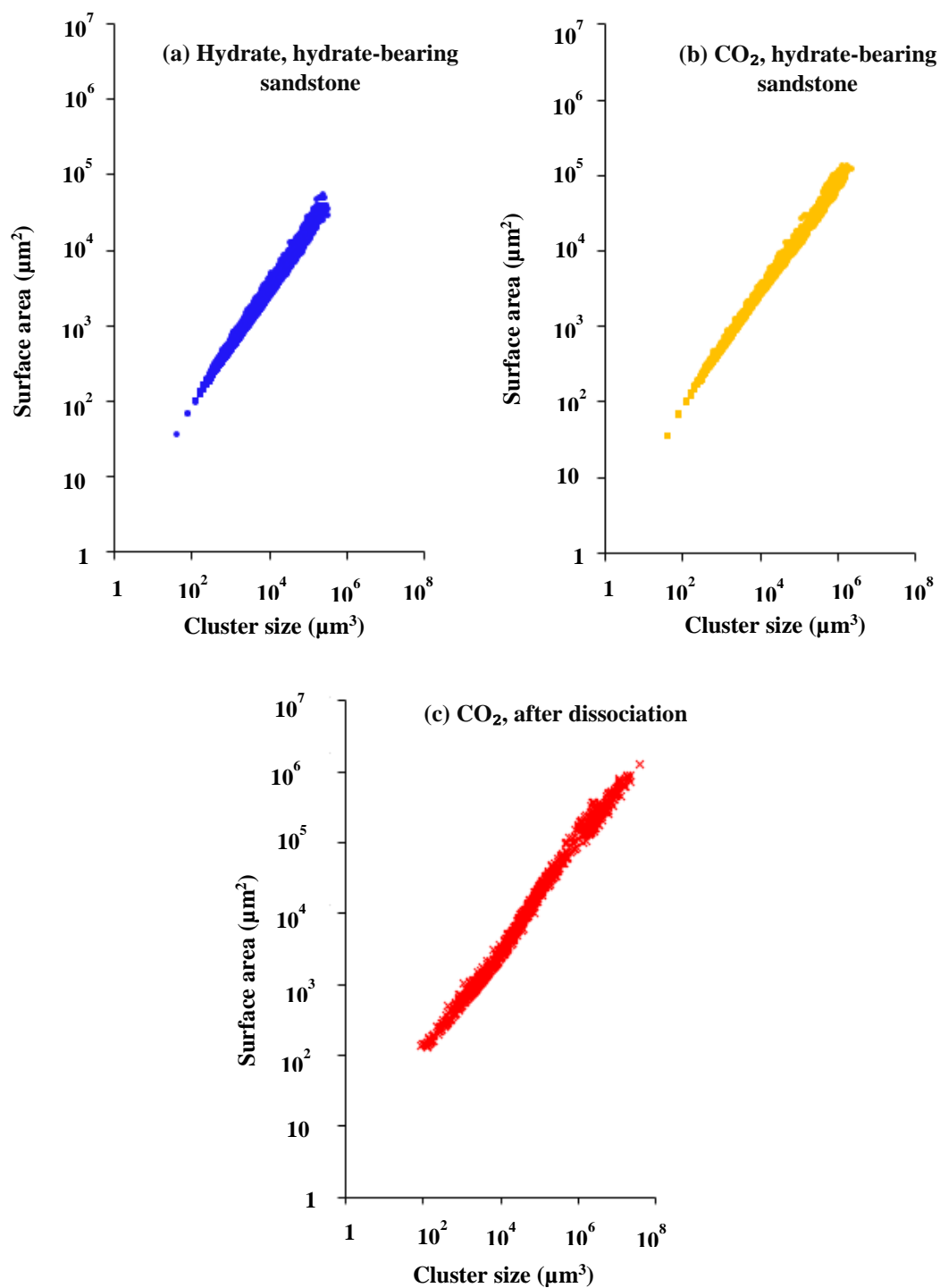
Figure 6-7 Surface area-volume relationships for (a) CO_2 hydrate, (b) CO_2 gas clusters before hydrate dissociation and (c) CO_2 gas clusters after hydrate dissociation in the Bentheimer sample

6.5 Conclusions

Detailed understanding of morphology, distribution and occurrence of gas hydrate in host sediments is crucial for CGS (CO_2 is stored as CO_2-hydrate), natural gas recovery from hydrate-bearing sediments by CO_2 injection and interpretation of seismic data (Waite et al. 2004, Graue et al. 2008, Rochelle et al. 2009). However, knowledge is limited for pore-scale (µm-scale) behaviour of CO_2 hydrate in sediments. Therefore, we imaged the distribution of CO_2 hydrates in sandstone via X-ray µCT and studied the hydrate morphology and cluster size characteristics in 3D at high resolution. Clearly, CO_2 hydrate mainly formed in the pores at the gas-water interface, without contacting the grain surface, which is consistent with the free-floating model (Zhao et al. 2014, Zhao, Yang, et al. 2015).

Statistically, the hydrate and CO_2 cluster size distributions followed power-law relations ($N \propto V^{-\tau}$, where N is the number of clusters of size V counted and τ is the fitting exponent). A τ value of 1.375 for the hydrate cluster size distribution indicates that only a few large hydrate clusters were present; τ decreased to 1.15 after hydrate dissociation due to CO_2 being liberated from the hydrates, which then coalesced with the existing CO_2 bubbles, thus increasing their sizes. A power law relationship ($A \propto V^{-p}$) was also observed for the surface area (A)-cluster volume (V) relationship. A p ~ 0.75 indicated structures less compact than a sphere, but more compact than percolation-like ramified structures (Stauffer 1979). This has important implications for safe storage in hydrate-bearing sediments and gas recovery via CO_2-CH_4 exchange; such a lower surface area-volume ratio results in less CH_4 production and overall lower CO_2 storage capacity. These results thus add to the fundamental understanding, planning and execution of industrial CGS projects via the hydrate-disposal route.

Chapter 7 Ultrasonic Measurements of Hydrate-bearing Sandstone*

7.1 Summary

A potential alternative energy resource to meet energy demands is the vast amount of gas stored in hydrate reserves. However, major challenges regarding exploration and production surround profitable and effective exploitation of these reserves. The measurement of acoustic velocity is a useful method for exploration of gas hydrate reserves and can be an efficient method to characterise the hydrate-bearing sediments. In this chapter, the compressional wave velocity (P-wave velocity) of consolidated sediments (Bentheimer) with and without THF and carbon dioxide hydrate-bearing pore fillings were measured using the pulse transmission method. The study found that the P-wave velocities of consolidated sediments increased with increasing hydrate formation and confining pressure. Of the samples tested, the increase in wave velocity of the dry and THF hydrate-bearing samples was 27.6 % and 31.9 %, respectively, while the P-wave velocities increased by 7%–8% after carbon dioxide hydrate formation in sandstone sample. Interestingly, at the initial stage of hydrate formation, there was no change in P-wave velocity, which was followed by a steady increase as the hydrate crystals began to agglomerate and then increased rapidly to a constant value confirming the test solution had converted to a hydrate solid.

7.2 Introduction

The search for cleaner and more abundant alternative energy resources continues as the world faces scarcity in traditional conventional resources (Ball and Wietschel 2009, Al-Fatlawi et al. 2017). An unconventional resource that has in recent years gained heightened attention is natural gas production from hydrate reserves (Makogon et al. 2007, Boswell and Collett 2011). Gas hydrates have gained such popularity because of the huge amount of trapped gas and the role they could play in global climate change and the carbon cycle (Dickens 2004, Giavarini and Hester 2011), the geological hazards surrounding them and the risk of seafloor instability (Dillon et al. 2001, Sultan et al. 2004, Best et al. 2006). The estimated amount of natural gas (mainly

methane) at standard conditions that is entrapped within hydrate deposits is approximately 5×10^{15} m^3, which surpasses the conventional resources by at least one order of magnitude (Meyer 1981, Kvenvolden 1988, Rice 2006, Dawe and Thomas 2007, Sloan and Koh 2008, Konno et al. 2010). Moreover, recently, carbon dioxide hydrate formation in sediments has received growing attention as it is regarded as a potential technology for carbon dioxide sequestration and storage in deep ocean sediments (Yamasaki 2003, White et al. 2003, Orr 2009); thus, reducing carbon dioxide emissions into the atmosphere. Simultaneously, CO_2 hydrate formation within the sediment pore space could provide an additional seal to natural geological seals by self-sealing (House et al. 2006, Kvamme et al. 2007, Tohidi et al. 2010)

Natural gas hydrates are non-stoichiometric, ice-like compounds formed when gas (such as methane, carbon dioxide, nitrogen and ethane) or volatile liquid (such as THF) molecules are encaged by the strong hydrogen bonds of water molecules (Sloan and Koh 2008, Carroll 2014, Sadeq, Iglauer, Lebedev, and Barifcani 2018). Thermodynamically, hydrates usually form and remain stable under favourable conditions of low temperature and high pressure(Sloan and Koh 2008, Carroll 2014), and 1 m^3 of natural gas hydrates can be stored in approximately 180 m^3 of natural gas (Veluswamy et al. 2014). These conditions are found in the permafrost regions and offshore marine sediments, which represent the ideal environment for gas hydrate formation. Typically, gas hydrates occur within the pore space of coarse-grain rocks, or along fractures in fine-grain rocks (Collett 1999, Schindler and Batzle 2015).

Knowledge of the physical properties of sediments bearing gas hydrates is vitally important to successfully characterise and commercialise the production of natural gas from these hydrate deposits. Common geophysical processes such as well logging and seismic surveying enable quantification of gas hydrate deposits, albeit this requires further development (Collett and Lee 2012). However, the resulting field measurements become meaningful after further studies are conducted in the laboratory, which then allow for interpretation and calibration. Seismic velocities (e.g. acoustic P-wave velocity) have been widely and effectively employed for detection and exploration of gas hydrates in their host sediments (Shipley et al. 1979, Prakash et al. 2010, Spence et al. 2010). Seismic velocities are influenced by the type and amount of pore filling; therefore, when hydrate forms in the sediments, the acoustic P-wave velocity increases significantly compared with the velocity of sediments containing

other pore fillings (Berge et al. 1999, Lee and Collett 2001, Winters et al. 2007). The compressional wave velocity (P-wave velocity) is considered to be a significant property, which can provide information about the lithology, distribution and in-situ conditions of hydrate-bearing sediments (Lee and Collett 2001, Carcione and Gei 2004, RyDZy and Batzle 2010). Furthermore, methane hydrate is the most common gas hydrate that exists in nature, and thus obtaining gas hydrate samples of it from the field are rare, because it is technically difficult to obtain and preserve them for laboratory studies (Yun et al. 2006, Waite et al. 2009), thus laboratory synthesis of hydrate-bearing samples is significant for acquiring essential knowledge about gas hydrates in their host sediments. However, it is difficult to synthesize methane hydrate in the laboratory, as it requires it to be cooled to -78.7 °C to be stabilized at atmospheric pressure (Sloan and Koh 2008) or it requires higher pressure conditions (Carroll 2014). In addition, it is difficult to form methane hydrates in aqueous solutions due to its low solubility in water (Lide and Frederikse 1995). Thus, in this study, we have used THF as the hydrate former in bentheimer samples due to easy laboratory synthesis. THF is completely soluble in water (Sloan and Koh 2008) and it is commonly used as a substitution to form hydrate from methane dissolved in water (Yun et al. 2005) Moreover, researchers have showed that THF and methane hydrates reveal analogous mechanical, electrical and thermal characteristics (Lee, Yun, et al. 2007). On the other hand, THF and methane form different hydrate structures (THF hydrate forms structure sII, while methane forms structure sI hydrate) (Sloan and Koh 2008). Additionally, there are small differences in the velocities for both structures compared with the variation in velocities resulting from the various pore-scale hydrate distributions (Sloan and Koh 2008)

Previous laboratory studies of ultrasonic measurements of hydrate-bearing sediments have been conducted on unconsolidated sediments such as sands and glass beads (Yun et al. 2005, RyDZy and Batzle 2010, Li et al. 2012). To date, limited studies investigate the effect of hydrate formation on the compressional velocities of consolidated sediments (e.g. Benthiemer sandstone)

In the present study, the effect of different pore space fillings on measured acoustic properties of Bentheimer sandstones were studied for a better understanding of the interaction between hydrates and their host sediments. The experiments were performed under low-temperature conditions (~ 1 °C) with a confining pressure range

of 2–20 MPa. THF and carbon dioxide were used as hydrate formers in the consolidated sediments. The P-wave velocities of different pore fillings such as dry, brine-saturated, THF brine-saturated, THF hydrate-bearing and CO_2 hydrate-bearing samples were obtained. These measurements can be used to identify the hydrate occurrence compared to other pore fillings and sediments. Compressional wave velocity data serve as a good basis for gas hydrate estimation in consolidated sediments that have not been previously studied. Furthermore, the present provided insight into the use of acoustic velocity measurements to address the concerns of hydrate formation in gas production pipelines.

7.3   Methodology

7.3.1 Experimental Setup

The schematic of the experimental set-up used for hydrate formation and measurement of P-wave velocity as a function of confining pressure is presented in Figure 7-1. The set-up comprises mainly of the following components: high-pressure cell, cooling system, high-performance liquid chromatography (HPLC) pump for liquid injection, hand oil pump for applying confining pressure and P-wave recording and measuring system. The signals were processed, displayed and digitised on a digital oscilloscope (model DS4022, RIGOL). The high-pressure cell was filled with hydraulic oil and the core sample was placed inside a rubber sleeve to control the ambient confining pressure. The pressure cell was submerged in a cooling bath. To allow for temperature control, the cooling and heating cycles were initiated by circulating coolant liquid using a controlled temperature liquid circulator (± 0.1 K, model Alpha RA8, LAUDA). The confining pressure was applied to the sample at a range of 2–20 MPa by a manual oil pump. Two piezo-electric transducers (1 MHz, A114S, OLYMPUS) were attached to the cell walls for transmitting and receiving P-wave signals through the samples. During each experiment, the P-waveforms were generated using the pulser/receiver (model 5072PR, OLYMPUS). The experimental set-up was the same for both THF and CO_2 hydrate experiments. However, in the CO_2 hydrate experiments, three high precision syringe pumps were included ((ISCO 500D with an accuracy of 0.1%); the first two pumps were used for CO_2 and brine injection and the third pump provided confining pressure by compressing deionised water (Figure 6-1, chapter 6).
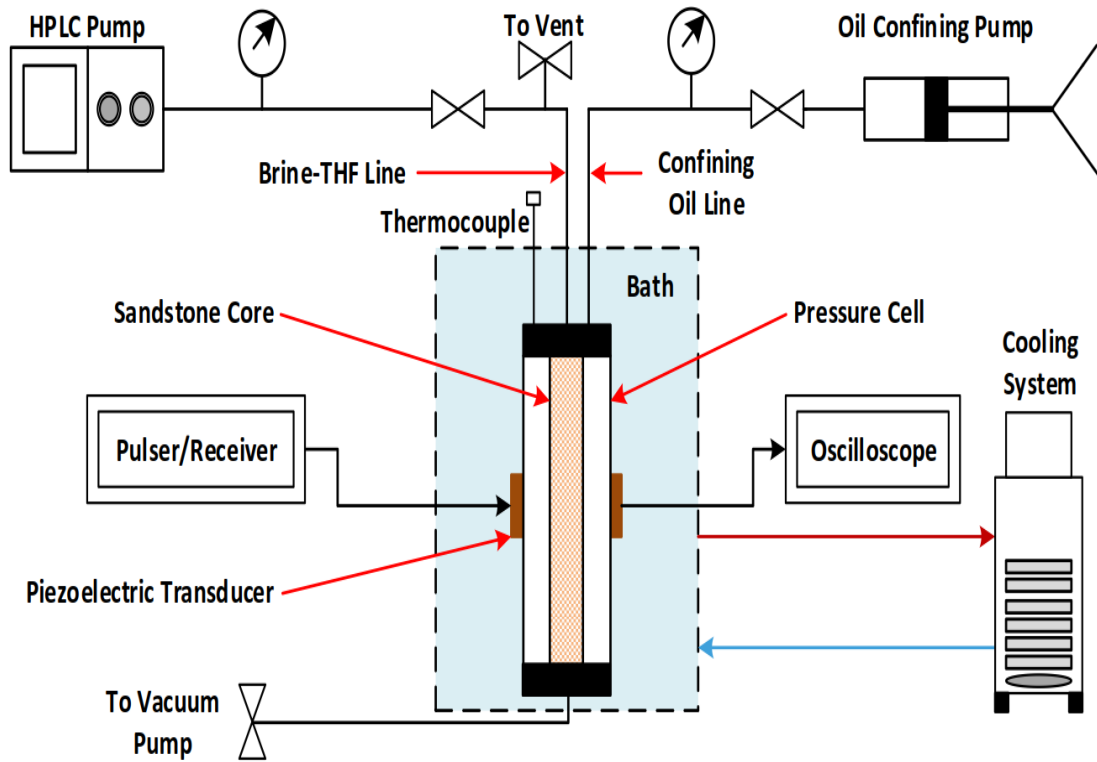
Figure 7-1 Experimental set-up for hydrate formation in sediments and P-wave velocity measurements

7.3.2 Materials

The materials utilised in the study are given in Table 7-1. Cylindrical Bentheimer sandstone samples from Kocurek Industries were used as the experimental porous medium for hydrate formation. Bentheimer is a homogenous clean sandstone mainly consisting of quartz with high permeability and average porosity of approximately 22%–25% (Rahman et al. 2016). The gas porosity and permeability of the Bentheimer samples were measured in the laboratory using a nitrogen automated permeameter-porosimeter (error of ± 0.1%, model AP-608). The properties of the sample are listed in Table 7-2. The THF testing solution was prepared from pure THF solution (Sigma-Aldrich, purity of 99.9 mol%) combined with NaCl (Sigma-Aldrich, purity of 99.5 mol%) as well as deionised water produced in the laboratory (17 MΩ·cm at 23.7 °C).

Carbon dioxide (purity 99.9 mol%, supplied by BOC Australia) was used as a hydrate-forming gas in the CO_2 hydrate experiment.

Table 7-1. Materials used in the study

Material	Purity	Supplier
Bentheimer sandstone	99 wt % quartz	Kocurek Industries
Tetrahydrofuran (THF)	99.9 mol%	Sigma-Aldrich
Carbon dioxide (CO_2)	99.9 mol%	BOC Australia
Methanol	99.8 mol%	Sigma-Aldrich
Sodium chloride (NaCl)	>99.5 mol%	Sigma-Aldrich

Table 7-2 Properties of the Bentheimer sandstone samples used in the study

Sample	B1	B2	B3
Length (cm)	8.1	8.1	8.1
Diameter (cm)	3.8	3.8	3.8
Pore volume (cm^3)	22.23	21.90	21.1
Porosity (%)	24.13	23.60	22.1
Permeability (md)	3371	3152	2370

7.3.3 Experimental Procedure

The Bentheimer samples were cleaned using methanol and then dried in an oven for 24 h at 60 °C. The dry samples were then mounted inside a rubber sleeve and tightly assembled in the high-pressure core holder within the cell. A K-type thermocouple with a precision of (± 0.5 °C) was attached to the core holder to measure the temperature during the hydrate formation/dissociation process. The cell was then placed firmly inside the cooling bath, and the HPLC pump, confining oil pump and transducers were connected. The entire system was then vacuumed prior to saturating the sample with a brine solution, to ensure the sample had undergone complete

saturation. A confining pressure of 10 MPa was applied to the core sample while several pore volumes of brine were injected into the cell via a tube connected from the top of the cell. The HPLC pump was then activated to inject the hydrate formers.

In the THF hydrate formation experiment, brine and THF testing solutions were injected at the desired concentrations at a constant flow rate of 2 mL/min. The ultrasonic measurements were conducted on dry and brine saturated samples as a function of confining pressure at room temperature. Several volumes of the stoichiometric THF testing solution were then injected into the brine saturated sample to displace the brine and to saturate the sample with THF testing solution. Following the injection of the solution, the inlet and outlet of the cell were closed so that no solution could move out of the sample. The hydrate formation process was initiated by circulation of the coolant liquid from the cooling system. The cell temperature was gradually decreased to 1 °C.

In the CO_2 hydrate formation experiment, after the Bentheimer core sample was completely saturated with brine, 50 PV of CO_2 gas was injected into the core at a pore pressure of 3 MPa and a flow rate of 0.1 mL/min (capillary number = 5×10^{-6}) to obtain a partially (brine) saturated porous medium. Hydrate formation was then started by decreasing the temperature to 274 K (1 °C, which is below the CO_2 hydrate equilibrium temperature; note that the CO_2-hydrate formation temperature in sediments is ~ 8 °C at 3 MPa Yang et al., 2012). More details on CO_2 hydrate formation process and experimental set up were presented in chapter 6.

During the THF and CO_2 hydrate formation process, the transmitted P-waves from the piezo-electric transducers that were attached to the outer wall of the pressure cell were recorded, and the temperature was maintained at 1 °C. The P-waves travelled through the cell wall, the confining fluid, the rubber sleeve, the core sample and finally, to the receiver. An increase in the compressional wave velocities indicated that hydrate formation had occurred. The system was maintained at these conditions for a further 24 h to allow for complete hydrate formation after which a cycles of confining pressures (2–20 MPa) were applied, and the P-waves were recorded. The cooling process was stopped when there was no change in the compressional wave velocities with time. Later, hydrate dissociation was achieved by gradually heating the cell to room temperature.

P-wave velocities were measured via the pulse transmission method (Birch 1960), i.e. by sending a P-wave signal through the cell and sample material and measuring signal travel time. Signal waveforms (of the compressional waves) were measured before, during and after hydrate formation. The core was cooled from 294 K to 274 K by a circulating cooling bath, and signal waveforms were measured for each 1 K interval. Subsequently, the temperature was kept constant at 274 K until the compressional wave velocity stabilised. First arrival times were measured on the waveforms before and after hydrate formation, and the P-wave velocity was then calculated following the methodology described by Birch (1960). The P-wave velocities of the core samples were then calculated using Equation 7-1 from the measured arrival time and the sample diameter:

$$V_P = \frac{L}{t - t_d} \qquad\qquad 7\text{-}1$$

Where, V_P is the P-wave velocity of the core sample in m/s, L is the diameter of the core sample in m, t is the total measured travel time in s, and t_d is the dead travel time of the pulse through the cell wall and the rubber sleeve in s.

Furthermore, since changes in temperature will influence the elastic properties of the rubber sleeve, a relationship for t_d had to be developed to cater for this dependency on temperature. Thus, t_d was calibrated as a function of temperature (T) and confining pressure (P_{con}) using an aluminum sample of known P-wave velocity. Figure 7-2 shows t_d through the cell wall and the rubber sleeve as a function of temperature and confining pressure. The relationship for t_d can then be developed through regression analysis as shown in Equation 7-2 where the R-squared value is 0.9779.

$$t_d = (-0.0003T - 0.0128)P_{con} + 0.0661 + 20.35 \qquad\qquad 7\text{-}2$$
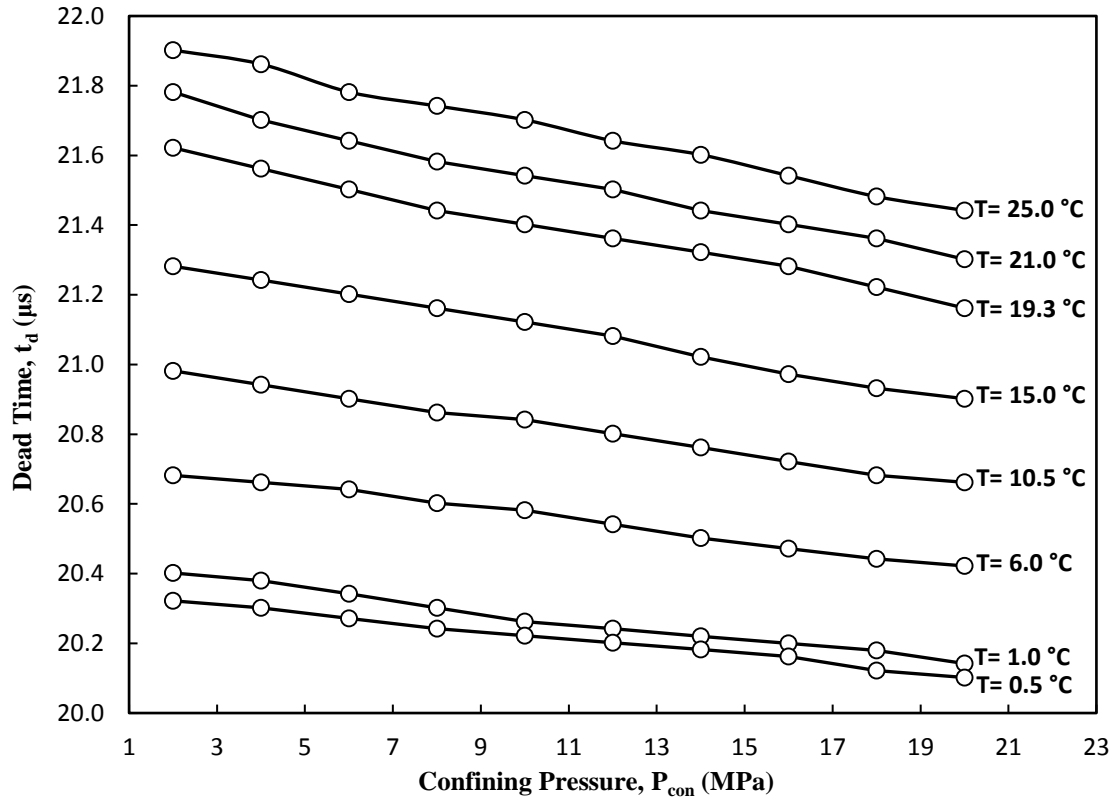
Figure 7-2 Dead time (*t_d*) as a function of temperature and confining pressure

7.4 Results and Discussions

7.4.1 THF Hydrate Formation in Sandstone

THF was chosen for hydrate formation in the present study due to its simple process and application in experiments. It also helps to overcome the difficulties surrounding the use of methane hydrates in the laboratory such as the high pressures and longer formation times required for hydrate stability. THF is thus used as the hydrate guest former as a substitution for methane gas as it can form a hydrate out of solution at ambient pressure and at a temperature of ~3.9 °C (Gough and Davidson 1971, Pearson et al. 1986, Lee, Yun, et al. 2007, Yun et al. 2007, Strobel et al. 2009, Xue et al. 2012). In addition, THF is ideally miscible with water and the amount of water in the solution allows for control of the hydrate concentration (hydrate saturation) in the pore space (Yun et al. 2005). Thus, a mixture containing THF at a concentration of 15 wt % and balance being pure water will yield a hydrate saturation of 100% (Yun et al. 2005). In the present study, the test solution contained 15 wt% THF and 85 wt% brine (81.5 wt% water and 3.5 wt% NaCl) to yield a hydrate saturation of approximately 80 wt%.

The P-waveforms produced from a Bentheimer sample containing different pore fillings is shown in Figure 7-3 where the arrows refer to the arrival times for the measured P-waves. The travel path of the P-wave was measured with an accuracy of 0.1%. The uncertainty in measurements of wave arrival was thus 0.3%. The resulting waveforms clearly show a change as the pore fillings vary in content from dry, brine-saturated, THF brine-saturated, and finally to THF hydrate-bearing. Evidently, the speed and amplitude of the measured P-wave for the hydrate-bearing sample is the highest amongst the other samples and pore fillings.
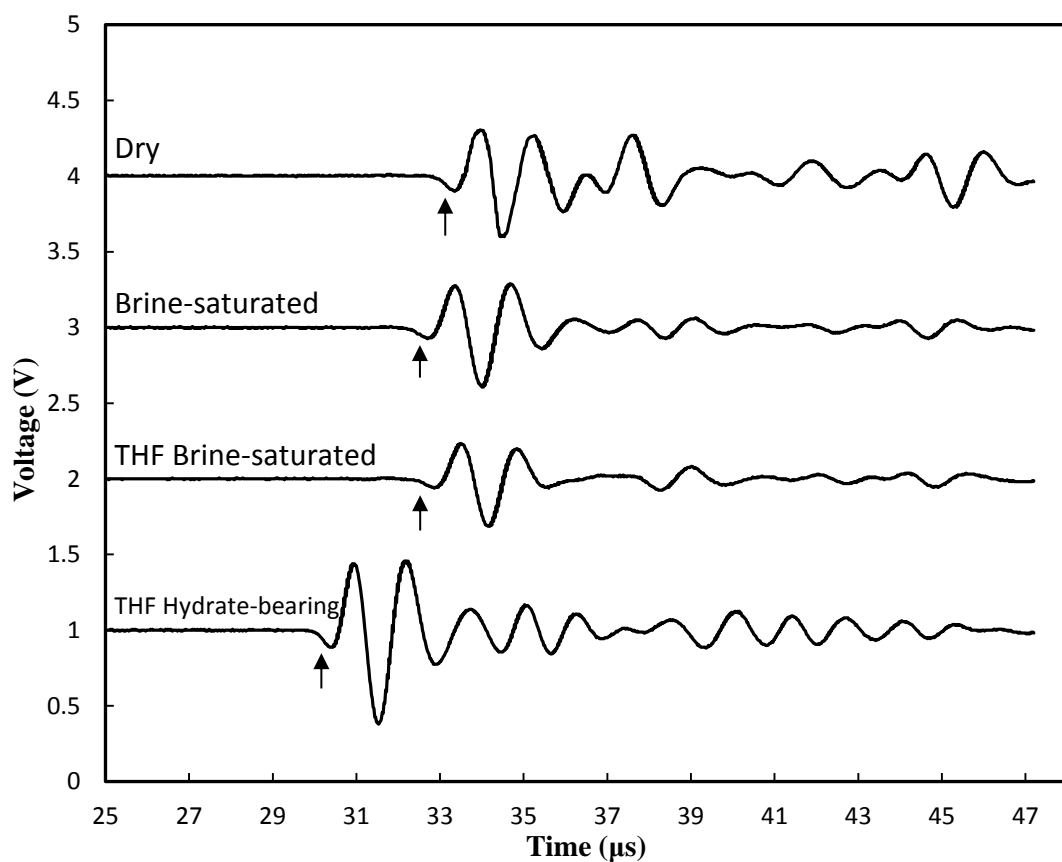
Figure 7-3 Typical P-waveforms recorded for different pore fillings of Bentheimer samples

The measured compressional wave velocities in the dry samples are presented in Figure 7-4 as a function of confining pressure in comparison to the literature data (Tao et al. 1995, Mayr and Burkhardt 2006). As the confining pressure increased, the compressional wave velocities increased due to the compression, which represent normal behaviour in rock samples. The experimental data from the present study have

the same trend as the literature data. A variation of 6.6% was observed between the measured data and that in the literature. This variation is due to the different sandstone used in the literature (i.e. Berea sandstone) and the differences in sample properties such as the distribution of grain size and pore space network characteristics.
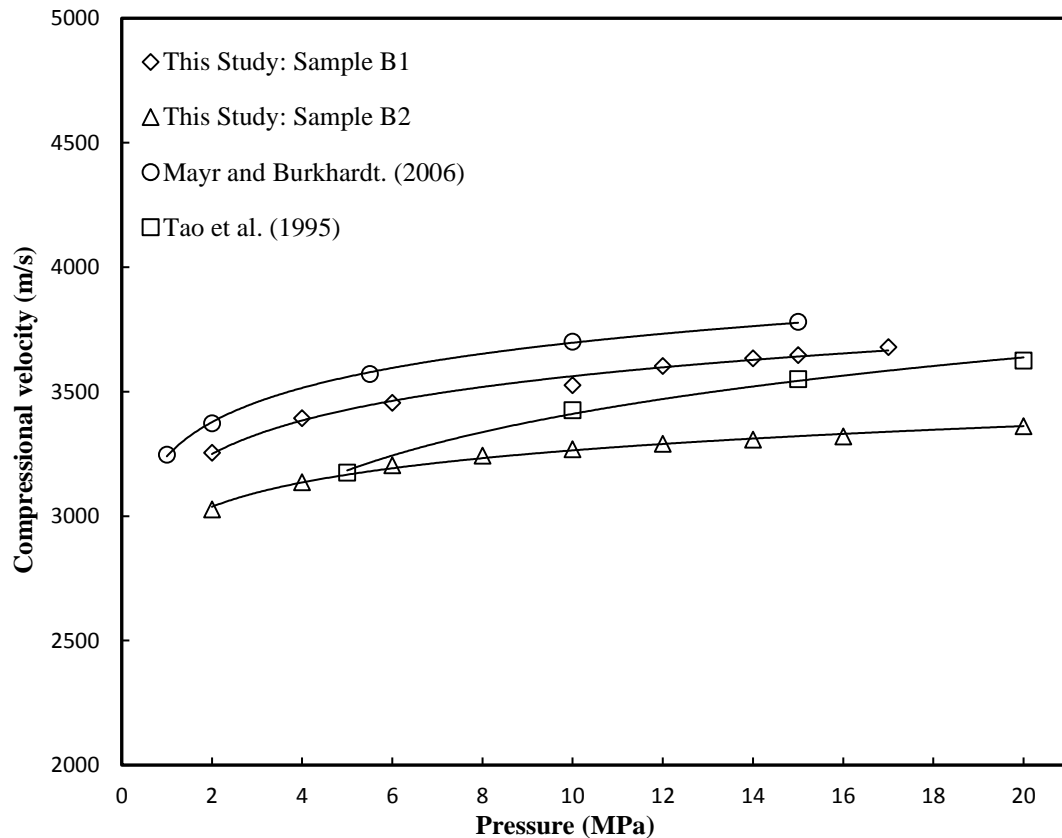
Figure 7-4 Compressional wave velocity in dry Bentheimer sample as a function of confining pressure compared to the literature (Tao et al. 1995, Mayr and Burkhardt 2006). The lines are fitted logarithmic trend-lines

The corresponding P-wave velocities for the different pore fillings for B1 and B2 Bentheimer sandstone samples were calculated and are shown in Table 7-3, Figure 7-5 and Figure 7-6. These results represent the compressional wave velocities across different pore fillings (dry, brine-saturated, THF brine-saturated and THF hydrate-bearing) as a function of pressure. For all pore filling types, the compressional wave velocities increased as the confining pressure increased. The compressional wave velocity in the dry sample was lower than that in the brine saturated and THF brine-

saturated samples for the studied pressure range. The same behaviour was reported by Mayr and Burkhardt (2006) for the dry and partially water saturated Bentheimer sandstone samples. The compressional wave velocity was significantly higher for the hydrate-bearing sediment than that of the other samples. An average increase of 964.9 m/s and 1028 m/s was observed in the dry and hydrate-bearing sediment samples of B1 and B2, respectively, which corresponds to a percentage increase in compressional wave velocity of 27.6% for sample B1 and 31.9% for sample B2. This general increase in compressional wave velocity can be explained by the fact that the formation of hydrate solids in pore spaces leads to a decrease in the P-wave travel time (Figure 7-3), which translates to an increase in compressional wave velocity. The higher increase in compressional wave velocity observed in sample B2 may be attributed to its lower porosity and pore volume, which means a greater number of cracks were closed compared to sample B1 due to the applied confining pressure (Mayr and Burkhardt 2006). Thus, under the hydrate formation conditions, the compressional wave velocity increased in Bentheimer sandstone samples (B1 and B2) due to the plugging caused by hydrate solids as well as the closing of cracks due to the applied pressure.
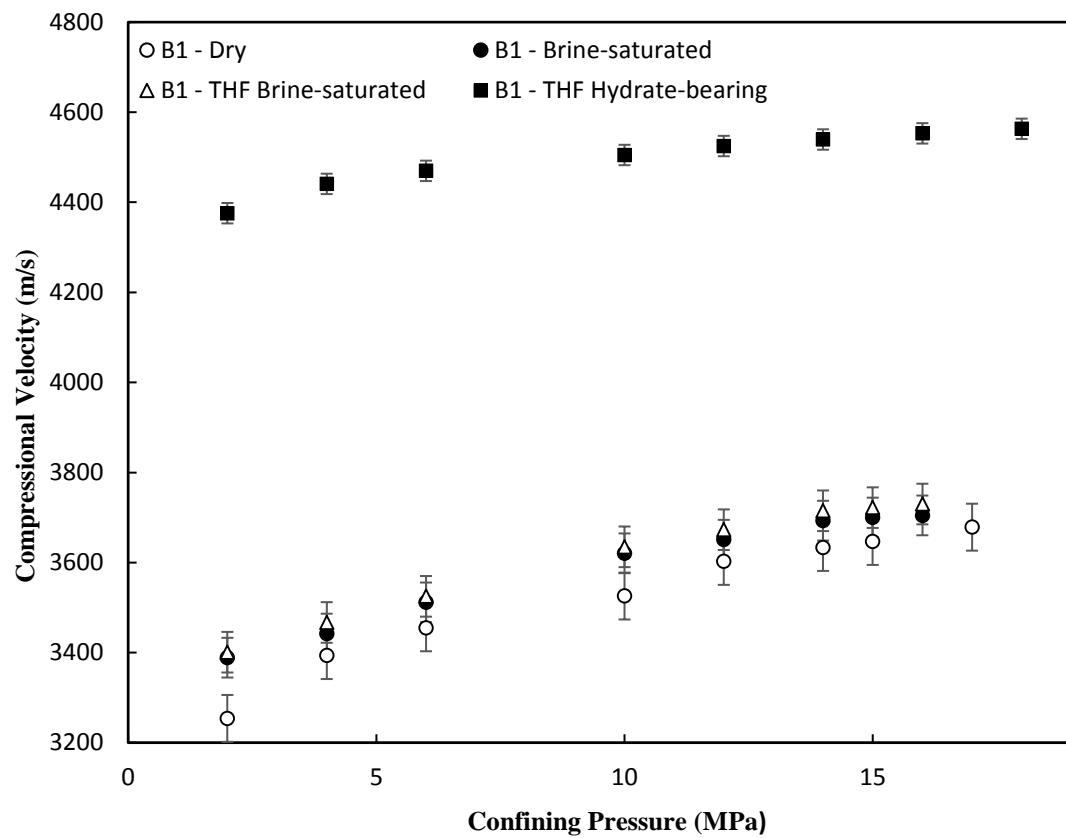
Figure 7-5 Compressional wave velocity as a function of confining pressure for different pore fillings in sample B1
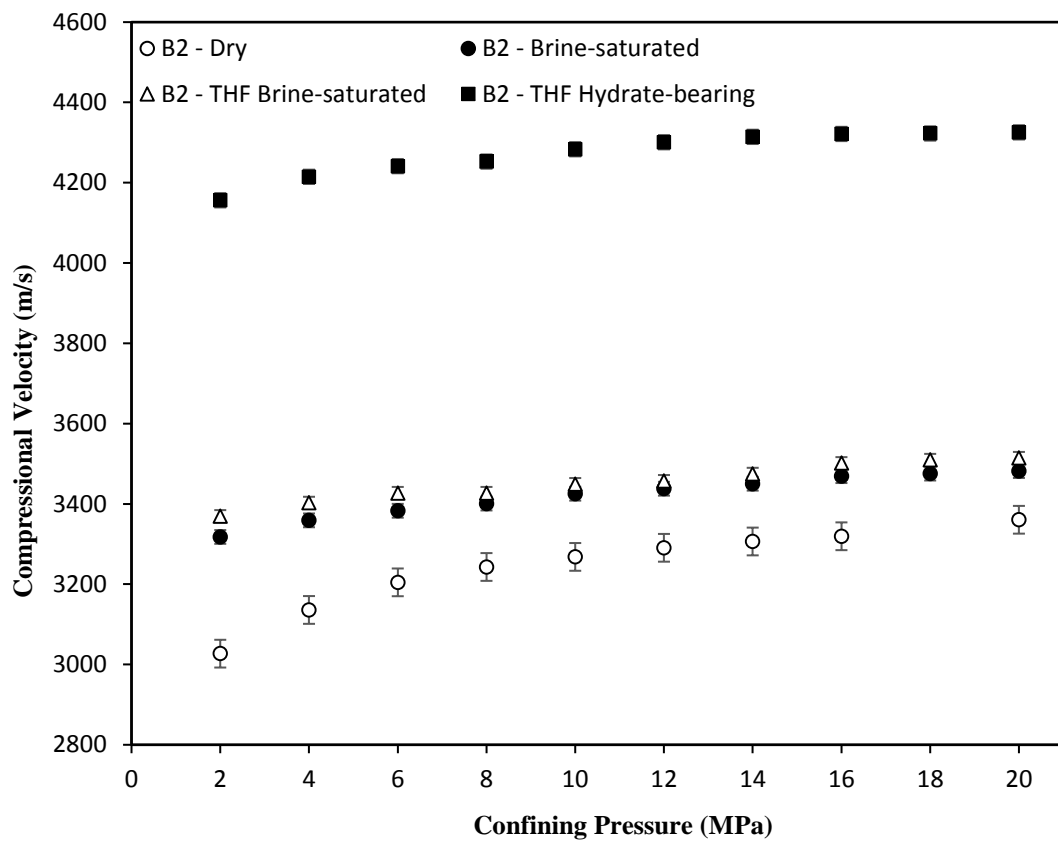
Figure 7-6 Compressional wave velocity as a function of confining pressure for different pore fillings in sample B2

Table 7-3 Experimentally measured compressional velocities for different pore fillings in Bentheimer samples as a function of confining pressure

Sample	P_{con} (MPa)	V_P (m/s)			
		Dry	Brine-saturated	THF Brine-saturated	THF Hydrate-bearing
B1	2	3254	3389	3401	4376
	4	3393	3442	3467	4441
	6	3455	3512	3525	4470
	10	3526	3621	3635	4505
	12	3602	3651	3673	4525
	14	3634	3693	3715	4539
	15	3647	3700	3722	-
	16	-	3704	3730	4553
	17	3679	-	-	-
B2	2	3026.97	3317.67	3358.96	4156
	4	3135.83	3358.96	3402.57	4215
	6	3204.58	3382.88	3427.12	4241
	8	3242.87	3400.81	3427.12	4253
	10	3267.97	3425.33	3449.21	4283
	12	3290.61	3437.731	3463.04	4301
	14	3306.36	3450.21	3474.76	4314
	16	3319.35	3469.11	3501.33	4321
	18	-	3475.46	3509.420	4323
	20	3360.45	3481.83	3514.288	4325

The evolution of compressional wave velocity during the cooling process (THF hydrate formation) at 14 MPa is shown in Figure 7-7. It can be seen that the compressional wave velocity remained constant at ~3474 m/s for the first 20 h. However, the temperature began to decrease below the hydrate equilibrium temperature of the THF solution (~3.9 °C) at ~11 h indicating that hydrate formation had initiated, while there was no change seen in the compressional wave velocity for the next 9 h as the temperature steadily dropped to 1 °C. This behaviour was due to hydrate formation occurring initially as thin hydrate films forming at the pore surface, then progressing into a water-hydrate slurry followed by a slow solid crystallisation stage (Beltrán and Servio 2008a, Alef et al. 2018). The velocity then increased steadily from t = 20-24 h to ~3510 m/s while the temperature was kept constant at 1 °C. This apparent increase in compressional wave velocity was due to initial hydrate crystals starting to agglomerate in the pore spaces. During the next 10 h, the velocity increased rapidly to ~3830 m/s. This rapid increase may be due to the rapid hydrate crystallisation occurring in the pore spaces. Lastly, there was no noticeable change occurring in the compressional wave velocity and the recorded velocity approaches to the approximately constant value of ~3,860 m/s. Therefore, the hydrate formation process had finished and the THF testing solution has been converted into a hydrate solid.
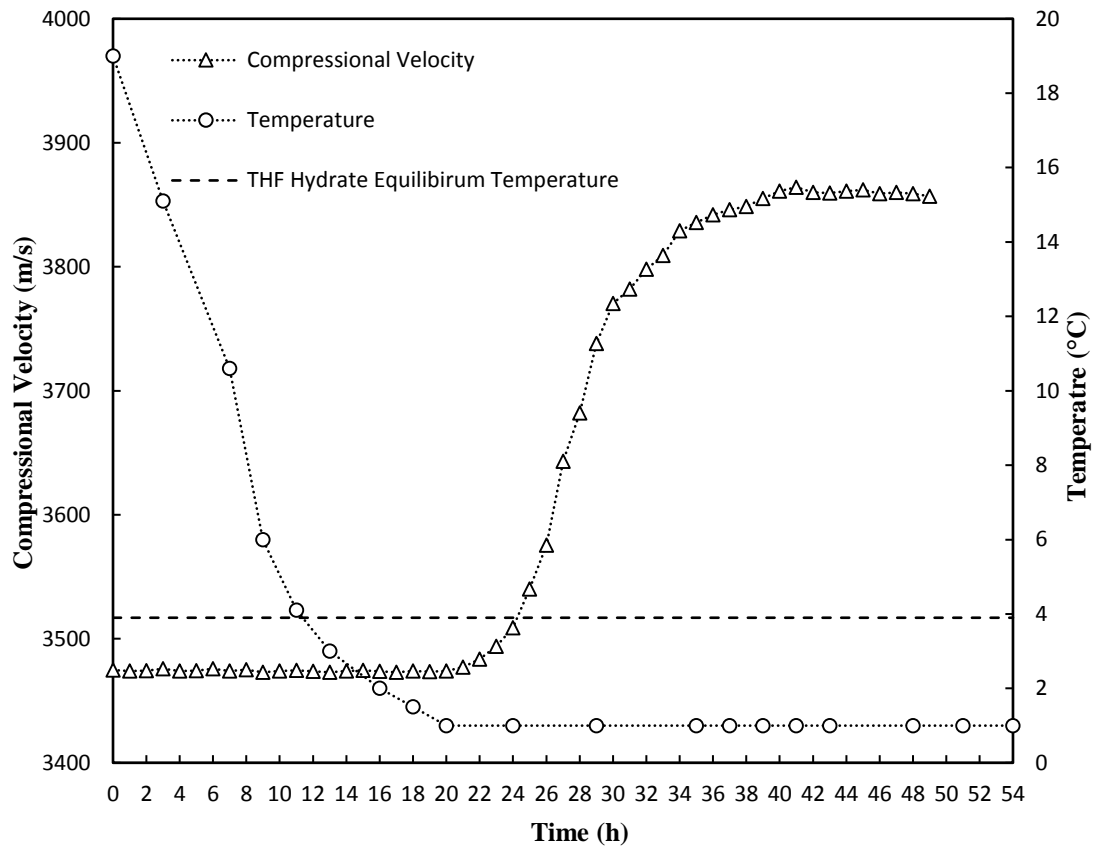
Figure 7-7 Evolution of compressional wave velocity during THF hydrate formation at confining pressure of 14 MPa in sample B2

In contrast, gas hydrate formation in production pipelines from gas reservoirs is a major concern. Hydrate formation in pipelines can result in safety concerns for operation personnel, environmental issues in the case of a leak, production downtime, increased maintenance and repair costs (Chatti et al. 2005, Sloan 2005, Alef et al. 2018). The monitoring of compressional wave velocity along pipelines can be used to detect hydrate formation and serve as a warning system to operators. As can be seen from Figure 7-7, a window of 4 h can be achieved before a rapid increase in compressional wave velocity is observed. During this time, the operator may take precautionary measures such as the injection of hydrate inhibitors to lower the risk of hydrate promotion and agglomeration.

7.4.2 CO$_2$ hydrate formation in sandstone

Following on from the μCT experiment for imaging the CO$_2$ hydrate formation in Bentheimer sandstone, measurements of the compressional wave velocities were conducted using the same materials and procedures used in the μCT experiments, see chapter 7. However, a large Bentheimer core (B3; Table 7-2) was used as the host sediment. P-wave velocities through sample B3 were calculated before and after CO$_2$ hydrate formation and are reported in Table 7-4 and Figure 7-8. Compressional wave velocities increased by 7%-8% after CO$_2$ hydrate formation (e.g. from 2880 m/s to 3100 m/s at 8 MPa confining pressure; Figure 7-8). This observation is consistent with the free-floating model (Helgerud et al. 1999, Waite et al. 2009). In this model, the floating hydrate is considered part of the pore fluid (and not the rock matrix), thus only the bulk modulus of the pore fluid changes (but not that of the rock skeleton) (Waite et al. 2009). The free-floating model is applicable for hydrate saturations up to 40% (Spangenberg et al. 2005); recall that in μCT experiments the hydrate saturation was ~ 17%. This conclusion is consistent with the μCT images, where hydrate layers between water and CO$_2$ gas were observed. CO$_2$ hydrate thus has no effect on the stiffness of the sedimentary matrix (Brugada et al. 2010).

During the first stage, the velocity remained stable and did not show a significant change until CO$_2$ hydrate nucleation began (Figure 7-9). Increasing velocities demonstrated that the hydrate had formed in the pore space. The hydrate formation process was completed when the velocities stabilised. The measured P-wave velocities before and after hydrate formation are listed in Table 7-4.
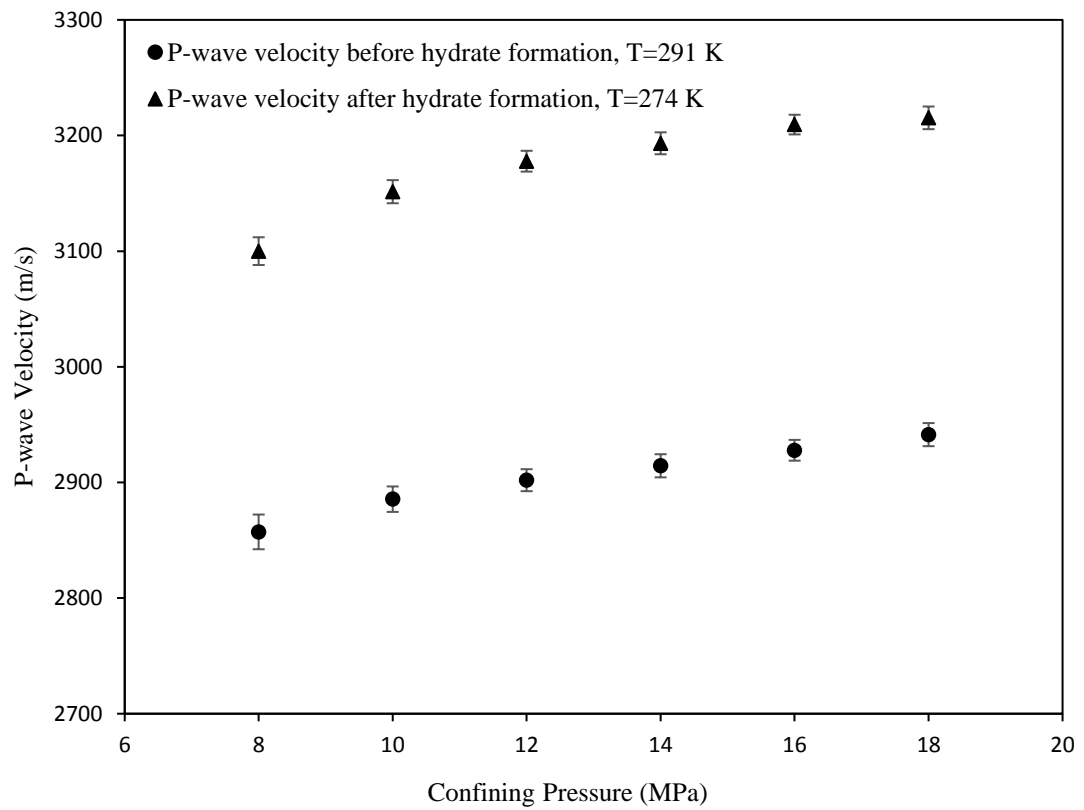
Figure 7-8 P-wave velocities measured through sample B3 before and after CO₂ hydrate formation as a function of confining pressure (pore pressure = 3 MPa)

Table 7-4 P-wave velocities before and after CO₂ hydrate formation in sample B3

Confining Pressure, MPa	P-wave velocity before hydrate formation, m/s	P-wave velocity after hydrate formation, m/s
8	2857	3100
10	2886	3146
12	2902	3167
14	2914	3193
16	2928	3209
18	2941	3226
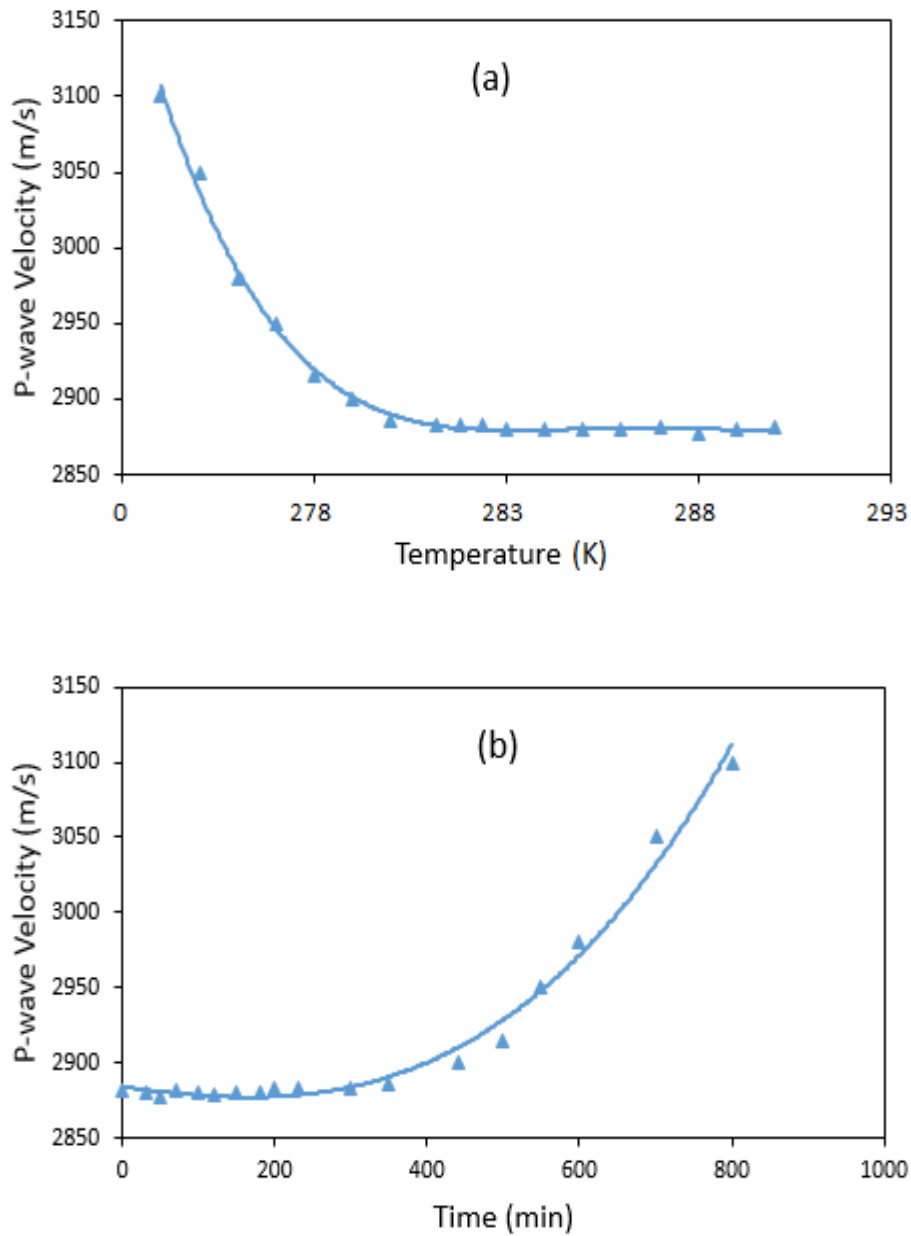
Figure 7-9 Evolution of P-wave velocity during CO_2 hydrate formation in sample B3 as a function of (a) temperature and (b) time at 8 MPa confining pressure

7.5   Conclusions

Hydrate reserves are currently classified as an unconventional energy resource although they have the potential to become an alternative resource to meet the growing demands. The acoustic method is an important method for the exploration of gas hydrate reserves and can be an efficient method to characterise hydrate-bearing

sediments. In the present study, the pulse transmission method was used to determine the compressional wave velocities of three Bentheimer samples. Thus, new compressional wave velocity measurements have been reported for multiple pore fillings ranging from dry, brine-saturated, THF brine-saturated, THF hydrate-bearing and CO_2 hydrate-bearing as a function of confining pressure in consolidated sediments. The THF hydrate formation in the pore spaces is indicated by a significant increase in velocities; typically they increased by 27.6% and 31.9% compared to a dry sample for B1 and B2, respectively.

Furthermore, P-wave velocities increased by 7%−8% after CO_2 hydrate formation, which confirms the hydrate free-floating behaviour. This conclusion is consistent with the μCT images of CO_2 hydrate-bearing sandstone (see chapter 6). These free-floating hydrates have no significant contribution to the stiffness of the host sediments.

At the initial stage of hydrate formation, there was no change in the compressional wave velocity, which was followed by a steady increase as the hydrate crystals began to agglomerate and then increased rapidly to a constant value suggesting that the test solution had converted to a hydrate solid. The experimental data of the present study will aid in the formulation of geophysical models to determine hydrate content in consolidated sediments. Furthermore, the study has given an insight into the use of compressional wave velocity to detect hydrate formation in gas production pipelines. A window of 4 h was found before high-risk hydrate formation would form that can potentially blocking the gas pipelines could occur.

Chapter 8   Conclusions and Recommendations

This chapter introduces the overall conclusions from the studies presented in the previous chapters and gives recommendations for potential future research work.

8.1   Conclusions

Gas hydrates have continued to be an area of increasing attention because of their role as the main flow assurance problem in natural gas production and their importance as a potential energy resource. This thesis presents experimental measurements and modelling of gas hydrate equilibrium conditions for different gas mixtures containing methane, carbon dioxide and nitrogen. In addition, the CO_2 existing in consolidated sandstone samples have been studied in terms of hydrate morphology, distribution and hydrate cluster characteristics. Another study was performed to investigate the effect of hydrate formation on compressional wave velocities of consolidated sandstone samples.

Experimental studies using PVT sapphire cell, ultrasonic measurements set-up and X-ray µCT were conducted to achieve the targets and objectives of this thesis. The study consists of five chapters, which are summarised below.

8.1.1 Experimental Determination of Hydrate Phase Equilibrium for Different Gas Mixtures Containing Methane, Carbon Dioxide and Nitrogen with Motor Current Measurements

- New hydrate equilibrium measurements of the systems of carbon dioxide + methane + water, nitrogen + methane + water and carbon dioxide + nitrogen + water were reported at varying temperature and pressure conditions.
- The comparison between the obtained experimental data and the literature data (Jhaveri and Robinson 1965, Adisasmito et al. 1991, Dholabhai and Bishnoi 1994, Servio et al. 1999, Seo et al. 2001, Nakamura et al. 2003, Mohammadi et al. 2005, Beltrán and Servio 2008a, Lu and Sultan 2008, Sabil et al. 2014) showed good consistency.
- Results indicated that the hydrate equilibrium conditions for gas mixtures vary depending upon the type of gases in the mixture and their concentrations.

Specifically, the hydrate equilibrium temperature increased with increasing CO_2 concentration in the $CO_2 + CH_4$ and $CO_2 + N_2$ gas mixtures at any given pressure. However, increasing N_2 concentration in the $N_2 + CH_4$ gas mixture reduced the hydrate equilibrium temperature at any given pressure.

- Motor current measurements conducted during the experimental processes (formation and dissociation) indicated that the motor current could be effectually used as a gas hydrate formation and dissociation parameter, particularly in the cases when visual observations are inaccessible.

8.1.2 Thermodynamic Modelling and Empirical Correlation for the Prediction of Gas Hydrate Equilibrium Conditions

- A thermodynamic model was developed for hydrate equilibrium conditions and cage occupancies for varying gas mixtures containing CH_4, CO_2 and N_2. The occupancy results showed that the CO_2 stabilised the sI hydrate in the $CO_2 + CH_4$ hydrate system, which confirmed the promotion of hydrate conditions with increasing CO_2 gas concentration. The proposed model was validated by comparison with experimental measurements. The comparison results demonstrated that the model could acceptably predict the hydrate equilibria at pressures lower than 10 MPa in the $CO_2 + CH_4$ hydrate system. Moreover, for $N_2 + CH_4$ and 64 mol% N_2 + 36 mol% CO_2 hydrate systems, the model results showed good performance when tested with the experimental data. However, for 74 mol% N_2 + 26mol% CO_2 hydrate, a considerable deviation was observed between the experimental data and model predictions. Therefore, a potential structural transformation could occur for this mixed hydrate.

- A new empirical correlation was developed that can be used for accurate prediction of the hydrate equilibrium temperatures. This correlation is applicable for a wide range of temperatures, pressures and for gas mixtures containing CH_4, CO_2 and N_2 with specific gravities up to 1. This correlation showed excellent accuracy compared with the published experimental data and results obtained from other hydrate correlations. Thus, it represents a simple, accurate and direct

tool for predicting gas hydrate equilibrium conditions in the system that meets the above operating conditions.

8.1.3 Experimental Pore-scale Analysis of Carbon Dioxide Hydrate in Sandstone via X-Ray Micro-Computed Tomography

- We studied CO_2 hydrate distribution in sandstone and investigated the hydrate morphology and cluster characteristics to determine the role that CO_2 hydrate plays in CGS and natural gas recovery from hydrate-bearing sediments. CO_2 hydrates in Bentheimer were imaged via X-ray µCT. It was found that CO_2 hydrate mainly formed in the centre of the pore bodies, without contacting the grain surface, which is consistent with the free-floating model (Zhao et al. 2014, Zhao, Yang, et al. 2015).

- A brine layer existed between the hydrate and the grain surface indicating that brine is the wetting phase.

- CO_2 hydrate saturation (17.8%) was observed, which was localised at the brine-gas interface and exhibited layer-like morphology.

- It has been shown for the first time how CO_2 hydrate clusters are formed, distributed and shaped within a sandstone at in-situ conditions of pore-scale. The stochastically distributed hydrate clusters followed power-law relations in terms of their size distributions ($N \propto V-\tau$, where N is the number of clusters of size V counted and τ is the fitting exponent) and surface area-volume relationships ($A \propto V-p$, where A is the surface area and V is the cluster volume).

- A τ value of 1.375 for the hydrate cluster size distribution indicated that only a few large hydrate clusters were present; τ decreased to 1.15 after hydrate dissociation due to CO_2 being liberated from the hydrates, which then coalesced with the existing CO_2 bubbles, thus increasing their size.

- An exponent $p \sim 0.75$ indicated structures less compact than a sphere ($p = 2/3$), but more compact than percolation-like ramified structures where $p \sim 1$ (Stauffer 1979). This has important implications for safe storage in hydrate-bearing sediments and gas recovery via CO_2-CH_4 exchange; such a lower surface area-volume ratio results in less CH_4 production and overall lower CO_2 storage capacity.

- In summary, this study provided a significant contribution to current knowledge as it adds to the fundamental understanding, planning and execution of industrial CGS projects via the hydrate-disposal route.

8.1.4 Ultrasonic Measurements of Hydrate-bearing Sandstone

- The acoustic method is an important method for the exploration of gas hydrate reserves and can be used as an efficient method to characterise hydrate-bearing sediments.

- The compressional wave velocities were measured for multiple pore filling sandstone samples: dry, brine-saturated, THF brine-saturated, THF hydrate-bearing and CO_2 hydrate-bearing. All velocities were reported as a function of confining pressure.

- The hydrate formation in the pore space was indicated by the significant increase in compressional wave velocities.

- P-wave velocities increased by 27.6% and 31.9% in the THF hydrate-bearing sandstone as compared to a dry sample for two sandstone samples.

- P-wave velocities increased by 7%–8% after CO_2 hydrate formation, which confirms the hydrate free-floating behaviour. This conclusion is consistent with the μCT images of CO_2 hydrate-bearing sandstone. These free-floating hydrates have no significant contribution to the stiffness of the host sediments.

- At the first stage of hydrate formation, no change in P-wave velocity was observed. However, this stage was followed by a steady increase in the velocity as the hydrate crystals began to agglomerate and then increased rapidly to a constant value indicating that the test solution had converted to a hydrate solid.

- The results presented in this study will aid in the formulation of geophysical models to determine the hydrate content in consolidated sediments. Furthermore, the study has given an insight into the use of compressional wave velocity to detect hydrate formation in gas production pipelines.

8.2 Potential Future Research Work

On the basis of the findings in this thesis, a number of recommendations are proposed for future research work:

- Further investigation should be conducted to measure gas hydrate equilibrium conditions for other types of gas mixtures for a broader range of operating conditions (temperature and pressures).

- Studying the memory effect on the equilibrium conditions of gas hydrate containing gas mixtures could explain the reduction in the induction time prior to hydrate nucleation process. Various experiments are recommended to investigate the memory effect of mixed hydrates under varying conditions for hydrate forming methods (isobaric and isochoric).

- Studying the potential structural transition of some types of mixed hydrates (e.g. N_2-CO_2) using high-speed visualisation techniques such as NMR and X-ray diffraction.

- In the present thesis, we studied CO_2 hydrate formation in sandstone. More research is needed on the formation and dissociation of multi-component hydrate systems in sediments.

- Studying the influence of wetting properties (contact angle) between gas hydrates, liquid and the mineral surface of the hydrate hosting sediments and thus their effects on the hydrate nucleation rate.

- A further study is recommended to use the compressional wave velocity to detect hydrate formation in gas production pipelines before blocking the pipeline could occur.

References

Adeleke, Najeem A. 2010. "Blockage Detection in Natural Gas Pipelines by Transient Analysis."

Adeyemo, Adebola, Rajnish Kumar, Praveen Linga, John Ripmeester, and Peter Englezos. 2010. "Capture of carbon dioxide from flue or fuel gas mixtures by clathrate crystallization in a silica gel column." *International Journal of Greenhouse Gas Control* 4 (3):478-485.

Adisasmito, Sanggono, Robert J Frank, and E Dendy Sloan 1991. "Hydrates of carbon dioxide and methane mixtures." *Journal of Chemical and Engineering Data* 36 (1):68-71.

Akin, S, and AR Kovscek. 2003. "Computed tomography in petroleum engineering research." *Geological Society, London, Special Publications* 215 (1):23-38.

Al-Fatlawi, Omar, Md Mofazzal Hossain, and Jake Osborne. 2017. "Determination of best possible correlation for gas compressibility factor to accurately predict the initial gas reserves in gas-hydrocarbon reservoirs." *International Journal of Hydrogen Energy* 42 (40):25492-25508.

Alef, Khalid, Stefan Iglauer, and Ahmed Barifcani. 2018. "Effect of Dissolved Oxygen, Sodium Bisulfite, and Oxygen Scavengers on Methane Hydrate Inhibition." *Journal of Chemical & Engineering Data* 63 (5):1821-1826.

AlHarooni, Khalifa, Ahmed Barifcani, David Pack, Rolf Gubner, and Varun Ghodkay. 2015. "Inhibition effects of thermally degraded MEG on hydrate formation for gas systems." *Journal of Petroleum Science and Engineering*.

Almenningen, Stian, Josef Flatlandsmo, Anthony R Kovscek, Geir Ersland, and Martin A Fernø. 2017. "Determination of pore-scale hydrate phase equilibria in sediments using lab-on-a-chip technology." *Lab on a Chip* 17 (23):4070-4076.

Arora, Amit, and Swaranjit Singh Cameotra. 2015. "Natural Gas Hydrate as an Upcoming Resource of Energy." *Journal of Petroleum & Environmental Biotechnology* 6 (01).

Aya, I, K Yamane, and H Nariai. 1997. "Solubility of CO_2 and density of CO_2 hydrate at 30 MPa." *Energy* 22 (2-3):263-271.

Bagherzadeh, S Alireza, Peter Englezos, Saman Alavi, and John A Ripmeester. 2012. "Molecular modeling of the dissociation of methane hydrate in contact with a silica surface." *The Journal of Physical Chemistry B* 116 (10):3188-3197.

Baldwin, BA, A Moradi-Araghi, and JC Stevens. 2003. "Monitoring hydrate formation and dissociation in sandstone and bulk with magnetic resonance imaging." *Magnetic resonance imaging* 21 (9):1061-1069.

Baldwin, Bernard A, Jim Stevens, James J Howard, Arne Graue, Bjorn Kvamme, Erick Aspenes, Geir Ersland, Jarle Husebø, and David R Zornes. 2009. "Using magnetic resonance imaging to monitor CH_4 hydrate formation and spontaneous conversion of CH_4 hydrate to CO_2 hydrate in porous media." *Magnetic resonance imaging* 27 (5):720-726.

Ball, Michael, and Martin Wietschel. 2009. "The future of hydrogen–opportunities and challenges." *International journal of hydrogen energy* 34 (2):615-627.

Barrer, R.M., and WI Stuart. 1957. "Non-stoicheiometric clathrate compounds of water." Proc. R. Soc. Lond. A.

Beget, James E, and Jason A Addison. 2007. "Methane gas release from the Storegga submarine landslide linked to earlyHolocene climate change: a speculative hypothesis." *The Holocene* 17 (3):291-295.

Belandria, Veronica, Ali Eslamimanesh, Amir H Mohammadi, Pascal Théveneau, Hervé Legendre, and Dominique Richon. 2011. "Compositional analysis and hydrate dissociation conditions measurements for carbon dioxide+methane+water system." *Industrial & Engineering Chemistry Research* 50 (9):5783-5794.

Belandria, Veronica, Amir H Mohammadi, and Dominique Richon. 2010. "Phase equilibria of clathrate hydrates of methane+ carbon dioxide: New experimental data and predictions." *Fluid Phase Equilibria* 296 (1):60-65.

Beltrán, JG, and P Servio. 2008a. "Morphology studies on gas hydrates interacting with silica gel.//paper presented at Sixth International Conference on Gas Hydrate." *British Columbia, Canada*.

Beltrán, Juan G, and Phillip Servio. 2008b. "Equilibrium studies for the system methane+ carbon dioxide+ neohexane+ water." *Journal of Chemical and Engineering Data* 53 (8):1745-1749.

Benesh, Matthew E. 1942. The use of gas hydrates in improving the load factor of gas supply systems. Google Patents.

Berge, BK. 1986. "Hydrate predictions on a microcomputer." Petroleum Industry Application of Microcomputers.

Berge, Lars Inge, Kjell Arne Jacobsen, and Arne Solstad. 1999. "Measured acoustic wave velocities of R11 (CCl3F) hydrate samples with and without sand as a function of hydrate concentration." *Journal of Geophysical Research: Solid Earth* 104 (B7):15415-15424.

Berndt, Christian, Stefan Bünz, Trevor Clayton, Jürgen Mienert, and Martin Saunders. 2004. "Seismic character of bottom simulating reflectors: examples from the mid-Norwegian margin." *Marine and Petroleum Geology* 21 (6):723-733.

Best, Angus I, Jeffrey A Priest, Christopher RI Clayton, and Emily VL Rees. 2013. "The effect of methane hydrate morphology and water saturation on seismic wave attenuation in sand under shallow sub-seafloor conditions." *Earth and Planetary Science Letters* 368:78-87.

Best, Angus I, Michael D Richardson, Bernard P Boudreau, Alan G Judd, Ira Leifer, Anthony P Lyons, Christopher S Martens, Danial L Orange, and Simon J Wheeler. 2006. "Shallow seabed methane gas could pose coastal hazard." *Eos* 87 (22):213-217.

Birch, Francis. 1960. "The velocity of compressional waves in rocks to 10 kilobars: 1." *Journal of Geophysical Research* 65 (4):1083-1102.

Bishnoi, P Raj, and V Natarajan. 1996. "Formation and decomposition of gas hydrates." *Fluid phase equilibria* 117 (1):168-177.

Blanco, Gabriel, Reyer Gerlagh, Sangwon Suh, John Barrett, Heleen C de Coninck, CF Diaz Morejon, Ritu Mathur, Nebojsa Nakicenovic, Alfred Ofosu Ahenkorah, and Jiahua Pan. 2014. "Drivers, trends and mitigation."

Blunt, Martin J, Branko Bijeljic, Hu Dong, Oussama Gharbi, Stefan Iglauer, Peyman Mostaghimi, Adriana Paluszny, and Christopher Pentland. 2013. "Pore-scale imaging and modelling." *Advances in Water Resources* 51:197-216.

Bohrmann, Gerhard, Jens Greinert, Erwin Suess, and Marta Torres. 1998. "Authigenic carbonates from the Cascadia subduction zone and their relation to gas hydrate stability." *Geology* 26 (7):647-650.

Bohrmann, Gerhard, and Marta E Torres. 2006. "Gas hydrates in marine sediments." In *Marine geochemistry*, 481-512. Springer.

Booth, James S, Mary M Rowe, and Kathleen M Fischer. 1996. *Offshore gas hydrate sample database: with an overview and preliminary analysis*: Citeseer.

Booth, JS, WJ Winters, William P Dillon, MB Clennell, and MM Rowe. 1998. "Major occurrences and reservoir concepts of marine clathrate hydrates: implications of field evidence." *Geological Society, London, Special Publications* 137 (1):113-127.

Boswell, R., K. Yamamoto, S.-R. Lee, T. S. Collett, P. Kumar, and S. Dallimore. 2014. "Chapter 8. Methane Hydrates." In *Future Energy*, edited by T. M. Letcher, 159−178. New York: Elsevier Publishing.

Boswell, Ray, and Tim Collett. 2006. "The gas hydrates resource pyramid." *Natural Gas & Oil* 304:285-4541.

Boswell, Ray, and Timothy S Collett. 2011. "Current perspectives on gas hydrate resources." *Energy and environmental science* 4 (4):1206-1215.

Boswell, Ray, Timothy S Collett, Matthew Frye, William Shedd, Daniel R McConnell, and Dianna Shelander. 2012. "Subsurface gas hydrates in the northern Gulf of Mexico." *Marine and Petroleum Geology* 34 (1):4-30.

Brewer, Peter G, Franklin M Orr Jr, Gernot Friederich, Keith A Kvenvolden, Daniel L Orange, James McFarlane, and William Kirkwood. 1997. "Deep-ocean field test of methane hydrate formation from a remotely operated vehicle." *Geology* 25 (5):407-410.

Brownstein, S, DW Davidson, and D Fiat. 1967. "Proton resonance spectra of some gas hydrates." *The Journal of Chemical Physics* 46 (4):1454-1459.

Brugada, J, YP Cheng, K Soga, and JC Santamarina. 2010. "Discrete element modelling of geomechanical behaviour of methane hydrate soils with pore-filling hydrate distribution." *Granular Matter* 12 (5):517-525.

Bruusgaard, Hallvard, Juan G Beltrán, and Phillip Servio. 2008. "Vapor− liquid water− hydrate equilibrium data for the system $N_2+CO_2+H_2O$." *Journal of Chemical and Engineering Data* 53 (11):2594-2597.

Buades, Antoni, Bartomeu Coll, and J-M Morel. 2005. "A non-local algorithm for image denoising." Computer Vision and Pattern Recognition, 2005. CVPR 2005. IEEE Computer Society Conference on.

Buades, Antoni, Bartomeu Coll, and Jean-Michel Morel. 2008. "Nonlocal image and movie denoising." *International Journal of Computer Vision* 76 (2):123-139.

Buffett, Bruce A. 2000. "Clathrate hydrates." *Annual Review of Earth and Planetary Sciences* 28 (1):477-507.

Byk, S Sh, and Valentina Ivanovna Fomina. 1968. "Gas hydrates." *Russian Chemical Reviews* 37 (6):469.

Cailletet, L, and R Bordet. 1882. "Sur divers hydrates qui se forment par la pression et la détente." *CR Hebd. Seances' Acad. Sci* 95:58-61.

Camargo, RMT, MAL Gonçalves, JRT Montesanti, CABR Cardoso, and K Minami. 2004. "A perspective view of flow assurance in deepwater fields in Brazil." Offshore Technology Conference.

Carcione, Jose M, and Davide Gei. 2004. "Gas-hydrate concentration estimated from P-and S-wave velocities at the Mallik 2L-38 research well, Mackenzie Delta, Canada." *Journal of Applied Geophysics* 56 (1):73-78.

Carroll, John. 2014. *Natural gas hydrates: a guide for engineers*: Gulf Professional Publishing.

Carson, Don B, and Donald L Katz. 1942. "Natural gas hydrates." *Transactions of the AIME* 146 (01):150-158.

Castaldi, Marco J, Yue Zhou, and Tuncel M Yegulalp. 2007. "Down-hole combustion method for gas production from methane hydrates." *Journal of petroleum Science and Engineering* 56 (1-3):176-185.

Chaouachi, Marwen, Andrzej Falenty, Kathleen Sell, Frieder Enzmann, Michael Kersten, David Haberthür, and Werner F Kuhs. 2015. "Microstructural evolution of gas hydrates in sedimentary matrices observed with synchrotron X-ray computed tomographic microscopy." *Geochemistry, Geophysics, Geosystems* 16 (6):1711-1722.

Chatti, Imen, Anthony Delahaye, Laurence Fournaison, and Jean-Pierre Petitet. 2005. "Benefits and drawbacks of clathrate hydrates: a review of their areas of interest." *Energy conversion and management* 46 (9-10):1333-1343.

Cheng, ChuanXiao, JiaFei Zhao, YongChen Song, ZiHao Zhu, WeiGuo Liu, Yi Zhang, MingJun Yang, and XiChong Yu. 2013. "In-situ observation for formation and dissociation of carbon dioxide hydrate in porous media by magnetic resonance imaging." *Science China Earth Sciences* 56 (4):611-617. doi: 10.1007/s11430-012-4570-5.

Chong, Zheng Rong, She Hern Bryan Yang, Ponnivalavan Babu, Praveen Linga, and Xiao-Sen Li. 2015. "Review of natural gas hydrates as an energy resource: prospects and Challenges." *Applied Energy*.

Circone, Susan, Laura A Stern, Stephen H Kirby, William B Durham, Bryan C Chakoumakos, Claudia J Rawn, Adam J Rondinone, and Yoshinobu Ishii. 2003. "CO_2 hydrate: synthesis, composition, structure, dissociation behavior, and a comparison to structure I CH_4 hydrate." *The Journal of Physical Chemistry B* 107 (23):5529-5539.

Claypool, George E, and IR Kaplan. 1974. "The origin and distribution of methane in marine sediments." In *Natural gases in marine sediments*, 99-139. Springer.

Claypool, George E, and Keith A Kvenvolden. 1983. "Methane and other hydrocarbon gases in marine sediment." *Annual Review of Earth and Planetary Sciences* 11 (1):299-327.

Clayton, CRI, JA Priest, and EVL Rees. 2010. "The effects of hydrate cement on the stiffness of some sands." *Géotechnique* 60 (6):435.

Clennell, M Ben, Martin Hovland, James S Booth, Pierre Henry, and William J Winters. 1999. "Formation of natural gas hydrates in marine sediments: 1. Conceptual model of gas hydrate growth conditioned by host sediment properties." *Journal of Geophysical Research: Solid Earth* 104 (B10):22985-23003.

Cnudde, Veerle, and Matthieu Nicolaas Boone. 2013. "High-resolution X-ray computed tomography in geosciences: A review of the current technology and applications." *Earth-Science Reviews* 123:1-17.

Collett, T. S. 1993. "Natural gas hydrates of the Prudhoe Bay and Kuparuk River area, North Slope, Alaska." *American Association of Petroleum Geologists Bulletin* 77 (5):793-812.

Collett, Tim, Jang-Jun Bahk, Rick Baker, Ray Boswell, David Divins, Matt Frye, Dave Goldberg, Jarle Husebø, Carolyn Koh, and Mitch Malone. 2014. "Methane Hydrates

in Nature: Current Knowledge and Challenges." *Journal of chemical & engineering data* 60 (2):319-329.

Collett, Timothy S. 1999. "Natural Gas Hydrates: Resource of the 21st Century?" *AAPG Bulletin* 83 (12).

Collett, Timothy S. 2000. "Natural gas hydrate as a potential energy resource." In *Natural Gas Hydrate*, 123-136. Springer.

Collett, Timothy S. 2001. "AAPG Memoir 74, Chapter 7: Natural-Gas Hydrates, Resource of the Twenty-First Century?".

Collett, Timothy S. 2002. "Energy resource potential of natural gas hydrates." *AAPG bulletin* 86 (11):1971-1992.

Collett, Timothy S. 2013. "Gas Hydrate Reservoir Properties."

Collett, Timothy S, Arthur H Johnson, Camelia C Knapp, and Ray Boswell. 2009. "Natural gas hydrates: a review."

Collett, Timothy S, and Myung W Lee. 2012. "Well log characterization of natural gas-hydrates." *Petrophysics* 53 (05):348-367.

Collett, TS, M Riedel, J Cochran, R Boswell, J Presley, P Kumar, A Sathe, A Sethi, M Lall, and V Sibal. 2008. "National Gas Hydrate Program (NGHP) Expedition 01 Initial Reports." *Directorate General of Hydrocarbons, New Delhi*.

Conrad, Heiko. 2009. "Tetrahydrofuran clathrate hydrate formation studied by X-ray Raman scattering." *Faculty of Physics, Technique University Dortmund*.

Crampin, Stuart. 1977. "A review of the effects of anisotropic layering on the propagation of seismic waves." *Geophysical Journal International* 49 (1):9-27.

Dai, Jianchun, Niranjan Banik, Diana Gillespie, and Nader Dutta. 2008. "Exploration for gas hydrates in the deepwater, northern Gulf of Mexico: Part II. Model validation by drilling." *Marine and Petroleum Geology* 25 (9):845-859.

Dai, Jianchun, Fred Snyder, Diana Gillespie, Adam Koesoemadinata, and Nader Dutta. 2008. "Exploration for gas hydrates in the deepwater, northern Gulf of Mexico: Part I. A seismic approach based on geologic model, inversion, and rock physics principles." *Marine and Petroleum Geology* 25 (9):830-844.

Dai, Sheng, J Carlos Santamarina, William F Waite, and Timothy J Kneafsey. 2012. "Hydrate morphology: Physical properties of sands with patchy hydrate saturation." *Journal of Geophysical Research: Solid Earth* 117 (B11).

Dallimore, SR. 2005. "Summary and implications of the Mallik 2002 gas hydrate production research well program." *Scientific Results from the Mallik 2002 Gas Hydrate Production Well Program, Mackenzie Delta, Northwest Territories, Canada*:1-36.

Dangayach, S, DN Singh, P Kumar, SK Dewri, B Roy, C Tandi, and J Singh. 2015. "Thermal instability of gas hydrate bearing sediments: Some issues." *Marine and Petroleum Geology* 67:653-662.

Daraboina, Nagu, Igor L. Moudrakovski, John A. Ripmeester, Virginia K. Walker, and Peter Englezos. 2013. "Assessing the performance of commercial and biological gas hydrate inhibitors using nuclear magnetic resonance microscopy and a stirred autoclave." *Fuel* 105:630-635. doi: https://doi.org/10.1016/j.fuel.2012.10.007.

Dashti, Hossein, Leonel Zhehao Yew, and Xia Lou. 2015. "Recent advances in gas hydrate-based CO_2 capture." *Journal of Natural Gas Science and Engineering* 23:195-207.

Davy, Humphry. 1811. "The Bakerian Lecture. On some of the combinations of oxymuriatic gas and oxygene, and on the chemical relations of these principles, to inflammable bodies." *Philosophical Transactions of the Royal Society of London* 101:1-35.

Dawe, RA, and S Thomas. 2007. "A large potential methane source—Natural gas hydrates." *Energy Sources, Part A* 29 (3):217-229.

De Forcrand, R. 1902. "Sur la composition des hydrates de gaz." *Compt. rend* 135:959-961.

De Forcrand, R. 1925. "L'hydrate de Xénon." *Compt. rend* 181:15.

de Forcrand, R, and Sully Thomas. 1897. *Compt. Rend.*:109.

De la Rive, A. 1829. "Observations sur le liquide que l'on obtient par la condensation du gaz acide sulfureux." Annales de Chimie et de Physique. Paris.

Deaton, WM, and EM Frost Jr. 1946. Gas hydrates and their relation to the operation of natural-gas pipe lines. Bureau of Mines, Amarillo, TX (USA). Helium Research Center.

Delli, Mohana L, and Jocelyn LH Grozic. 2014. "Experimental determination of permeability of porous media in the presence of gas hydrates." *Journal of Petroleum Science and Engineering* 120:1-9.

Demirbas, Ayhan. 2010a. *Methane gas hydrate*: Springer Science & Business Media.

Demirbas, Ayhan. 2010b. "Processes for methane production from gas hydrates." *Methane Gas Hydrate*:161-181.

Desrues, Jacques, Gioacchino Viggiani, and Pierre Besuelle. 2006. *Advances in X-ray Tomography for Geomaterials*. Vol. 118. London: Wiley-ISET.

Dholabhai, Pankaj D, and P Raj Bishnoi. 1994. "Hydrate equilibrium conditions in aqueous electrolyte solutions: mixtures of methane and carbon dioxide." *Journal of Chemical and Engineering Data* 39 (1):191-194.

Dickens, Gerald R. 2004. "Global change: Hydrocarbon-driven warming." *Nature* 429 (6991):513-515.

Dillon, William P, Jeffrey W Nealon, Michael H Taylor, Myung W Lee, Rebecca M Drury, and Christopher H Anton. 2001. "Seafloor collapse and methane venting associated with gas hydrate on the blake ridge: causes and implications to seafloor stability and methanerelease." *Natural gas hydrates: Occurrence, distribution, and detection*:211-233.

Dong, Zhenzhen, Stephen Holditch, Duane McVay, and Walter B Ayers. 2012. "Global unconventional gas resource assessment." *SPE Economics & Management* 4 (04):222-234.

Du Frane, Wyatt L, Laura A Stern, Karen A Weitemeyer, Steven Constable, and Jeffery J Roberts. 2011. Electrical properties of methane hydrate+ sediment mixtures. Lawrence Livermore National Laboratory (LLNL), Livermore, CA.

Dudley, B. 2013. "Statistical review of world energy." *BP plc, London*.

Dvorkin, Jack, Michael B Helgerud, William F Waite, Stephen H Kirby, and Amos Nur. 2000. "Introduction to physical properties and elasticity models." In *Natural Gas Hydrate*, 245-260. Springer.

Dvorkin, Jack, and Amos Nur. 1996. "Elasticity of high-porosity sandstones: Theory for two North Sea data sets." *Geophysics* 61 (5):1363-1370.

Dvorkin, Jack, Manika Prasad, Akio Sakai, and Dawn Lavoie. 1999. "Elasticity of marine sediments: Rock physics modeling." *Geophysical research letters* 26 (12):1781-1784.

Dyadin, Yuri A, Eduard G Larionov, Andrei Y Manakov, Fridrich V Zhurko, Eugeny Y Aladko, Tamara V Mikina, and Vladislav Y Komarov. 1999. "Clathrate hydrates of hydrogen and neon." *Mendeleev communications* 9 (5):209-210.

Egawa, Kosuke, Toshiko Furukawa, Tatsuo Saeki, Kiyofumi Suzuki, and Hideo Narita. 2013. "Three-dimensional paleomorphologic reconstruction and turbidite distribution prediction revealing a Pleistocene confined basin system in the northeast Nankai Trough area." *AAPG bulletin* 97 (5):781-798.

Elgibaly, Ahmed A, and Ali M Elkamel. 1998. "A new correlation for predicting hydrate formation conditions for various gas mixtures and inhibitors." *Fluid Phase Equilibria* 152 (1):23-42.

Englezos, Peter. 1993. "Clathrate hydrates." *Industrial & Engineering Chemistry Research* 32 (7):1251-1274.

Erickson, Dale D. 1983. "Development of a natural gas hydrate prediction computer program." Colorado School of Mines. Arthur Lakes Library.

Ersland, Geir, Jarle Husebø, Arne Graue, and Bjørn Kvamme. 2009. "Transport and storage of CO2 in natural gas hydrate reservoirs." *Energy Procedia* 1 (1):3477-3484.

Eslamimanesh, Ali, Amir H Mohammadi, Dominique Richon, Paramespri Naidoo, and Deresh Ramjugernath. 2012. "Application of gas hydrate formation in separation processes: a review of experimental studies." *The Journal of Chemical Thermodynamics* 46:62-71.

Falser, S, S Uchida, AC Palmer, K Soga, and TS Tan. 2012. "Increased gas production from hydrates by combining depressurization with heating of the wellbore." *Energy & fuels* 26 (10):6259-6267.

Falser, Simon, Andrew C Palmer, Khoo Boo Cheong, and Tan Thiam Soon. 2013. "Temperature increase during the depressurization of partially hydrate-saturated formations within the stability region." *Energy & Fuels* 27 (2):796-803.

Fan, Shuan-Shi, and Tian-Min Guo. 1999. "Hydrate formation of CO_2-rich binary and quaternary gas mixtures in aqueous sodium chloride solutions." *Journal of Chemical and Engineering Data* 44 (4):829-832.

Fan, Shuanshi, Yuzhen Zhang, Genlin Tian, Deqing Liang, and Dongliang Li. 2006. "Natural gas hydrate dissociation by presence of ethylene glycol." *Energy & fuels* 20 (1):324-326.

Faraday, Michael, and Humphry Davy. 1823. "On fluid chlorine." *Philosophical Transactions of the Royal society of London* 113:160-165.

Floodgate, GD, and AG Judd. 1992. "The origins of shallow gas." *Continental Shelf Research* 12 (10):1145-1156.

Fowler, DL, WV Loebenstein, DB Pall, and Charles A Kraus. 1940. "Some unusual hydrates of quaternary ammonium salts." *Journal of the American Chemical Society* 62 (5):1140-1142.

Fujii, Tetsuya, Masaru Nakamizu, Yoshihiro Tsuji, Takatoshi Namikawa, Toshiharu Okui, Masayuki Kawasaki, Koji Ochiai, Mizue Nishimura, and Osamu Takano. 2009. "Methane-hydrate occurrence and saturation confirmed from core samples, eastern Nankai Trough, Japan."

Gabitto, Jorge F, and Costas Tsouris. 2010. "Physical properties of gas hydrates: A review." *Journal of Thermodynamics* 2010.

Giavarini, Carlo, and Keith Hester. 2011. *Gas hydrates: Immense energy potential and environmental challenges*: Springer Science & Business Media.

Ginsburg, G.D. 1969. "Hydrogeology of the North Yenisei Region." *Natural Gas Crystalline Hydrate Formation in the Interior of the Earth* 1:109-128.

Goel, Naval. 2006. "In situ methane hydrate dissociation with carbon dioxide sequestration: Current knowledge and issues." *Journal of petroleum science and engineering* 51 (3):169-184.

Gough, SR, and DW Davidson. 1971. "Composition of tetrahydrofuran hydrate and the effect of pressure on the decomposition." *Canadian Journal of Chemistry* 49 (16):2691-2699.

Graue, Arne, B Kvamme, Bernie Baldwin, Jim Stevens, James J Howard, Eirik Aspenes, Geir Ersland, Jarle Husebo, and D Zornes. 2008. "MRI visualization of

spontaneous methane production from hydrates in sandstone core plugs when exposed to CO_2." *SPE Journal* 13 (02):146-152.

Gudmundsson, J. S., and A. Borrehaug. 1996. "Frozen hydrate for transport of natural gas." Proceedings of the 2nd International Conference of Natural Gas Hydrates, Toulouse, France, 1996.

Haghighi, Hooman, Antonin Chapoy, Rod Burgess, and Bahman Tohidi. 2009. "Experimental and thermodynamic modelling of systems containing water and ethylene glycol: Application to flow assurance and gas processing." *Fluid Phase Equilibria* 276 (1):24-30.

Hammerschmidt, EG. 1934. "Formation of gas hydrates in natural gas transmission lines." *Industrial & Engineering Chemistry* 26 (8):851-855.

Hammerschmidt, EG. 1936. "Gas hydrates." *Am. Gas Assoc. Mon* 18 (7):273-276.

Handa, YP, RE Hawkins, and JJ Murray. 1984. "Calibration and testing of a Tian-Calvet heat-flow calorimeter Enthalpies of fusion and heat capacities for ice and tetrahydrofuran hydrate in the range 85 to 270 K." *The Journal of Chemical Thermodynamics* 16 (7):623-632.

Hartmann, D.L., A.M.G. Klein Tank, M. Rusticucci, L.V. Alexander, S. Brönnimann, Y. Charabi, F.J. Dentener, E.J. Dlugokencky, D.R. Easterling, A. Kaplan, B.J. Soden, P.W. Thorne, M. Wild, and P.M. Zhai. 2013. "Observations: Atmosphere and Surface." In *Climate Change 2013: The Physical Science Basis. Contribution of Working Group I to the Fifth Assessment Report of the Intergovernmental Panel on Climate Change*, edited by T.F. Stocker, D. Qin, G.-K. Plattner, M. Tignor, S.K. Allen, J. Boschung, A. Nauels, Y. Xia, V. Bex and P.M. Midgley, 159–254. Cambridge, United Kingdom and New York, NY, USA: Cambridge University Press.

Hau-Riege, Stefan P. 2012. *High-Intensity X-rays-Interaction with Matter: Processes in Plasmas, Clusters, Molecules and Solids*: John Wiley & Sons.

Hauge, LP, KA Birkedal, G Ersland, and A Graue. 2014. "Methane production from natural gas hydrates by CO2 replacement-review of lab experiments and field trial." SPE Bergen One Day Seminar.

Hauge, LP, J Gauteplass, MD Høyland, G Ersland, A Kovscek, and MA Fernø. 2016. "Pore-level hydrate formation mechanisms using realistic rock structures in high-pressure silicon micromodels." *International Journal of Greenhouse Gas Control* 53:178-186.

Helgerud, MB, J Dvorkin, A Nur, A Sakai, and T Collett. 1999. "Elastic-wave velocity in marine sediments with gas hydrates: Effective medium modeling." *Geophysical Research Letters* 26 (13):2021-2024.

Herri, J-M, A Bouchemoua, Matthias Kwaterski, Amara Fezoua, Yamina Ouabbas, and Ana Cameirao. 2011. "Gas hydrate equilibria for CO_2–N_2 and CO_2–CH_4 gas mixtures—Experimental studies and thermodynamic modelling." *Fluid Phase Equilibria* 301 (2):171-190.

Hester, KC, RM Dunk, Sheri N White, Peter G Brewer, Edward T Peltzer, and ED Sloan. 2007. "Gas hydrate measurements at Hydrate Ridge using Raman spectroscopy." *Geochimica et Cosmochimica Acta* 71 (12):2947-2959.

Hossainpour, Reza. 2013. "Catalysts for Enhanced CO_2-CH_4 Exchange in Natural Gas Hydrates. An experimental feasibility study of exchange enhancement by use of chemical additives." The University of Bergen.

Houghton, John Theodore, YDJG Ding, David J Griggs, Maria Noguer, Paul J van der Linden, Xiaosu Dai, Kathy Maskell, and CA Johnson. 2001. *Climate Change 2001:The Scientific Basis*: The Press Syndicate of the University of Cambridge.

House, Kurt Zenz, Daniel P. Schrag, Charles F. Harvey, and Klaus S. Lackner. 2006. "Permanent carbon dioxide storage in deep-sea sediments." *Proceedings of the National Academy of Sciences* 103 (33):12291-12295. doi: 10.1073/pnas.0605318103.

IEA. 2016. "Decoupling of Global Emissions and Economic Growth Confirmed." Accessed 23 March. www.iea.org/newsroom/news/2016/march/decoupling-of-global-emissions-and-economic-growth-confirmed.html.

Iglauer, Stefan. 2017. "CO_2–Water–Rock Wettability: Variability, Influencing Factors, and Implications for CO_2 Geostorage." *Accounts of Chemical Research* 50 (5):1134-1142.

Iglauer, Stefan, and Maxim Lebedev. 2017. "High pressure-elevated temperature x-ray micro-computed tomography for subsurface applications." *Advances in Colloid and Interface Science*.

Iglauer, Stefan, Adriana Paluszny, Christopher H Pentland, and Martin J Blunt. 2011. "Residual CO_2 imaged with X-ray micro-tomography." *Geophysical Research Letters* 38 (21).

Iglauer, Stefan, CH Pentland, and A Busch. 2015. "CO_2 wettability of seal and reservoir rocks and the implications for carbon geo-sequestration." *Water Resources Research* 51 (1):729-774.

IPCC. 2005. "IPCC, 2005: IPCC special report on carbon dioxide capture and storage."

Islam, MR. 1994. "A new recovery technique for gas production from Alaskan gas hydrates." *Journal of petroleum Science and Engineering* 11 (4):267-281.

Jhaveri, Jaysukh, and Donald B Robinson. 1965. "Hydrates in the methane-nitrogen system." *Canadian Journal of Chemical Engineering* 43 (2):75-78.

Jin, Shigeki, Jiro Nagao, Satoshi Takeya, Yusuke Jin, Junko Hayashi, Yasushi Kamata, Takao Ebinuma, and Hideo Narita. 2006. "Structural investigation of methane hydrate sediments by microfocus X-ray computed tomography technique under high-pressure conditions." *Japanese Journal of Aplied Physics* 45 (7L):L714.

Jin, Shigeki, Satoshi Takeya, Junko Hayashi, Jiro Nagao, Yasushi Kamata, Takao Ebinuma, and Hideo Narita. 2004. "Structure analyses of artificial methane hydrate

sediments by microfocus X-ray computed tomography." *Japanese Journal of Applied Physics* 43 (8R):5673.

Jin, Yusuke, Yoshihiro Konno, and Jiro Nagao. 2012. "Growth of methane clathrate hydrates in porous media." *Energy and Fuels* 26 (4):2242-2247.

John, VT, KD Papadopoulos, and GD Holder. 1985. "A generalized model for predicting equilibrium conditions for gas hydrates." *AIChE Journal* 31 (2):252-259.

Johnson, A. H. 2013. "Unconventional Energy Resources: 2013 Review." *Natural Resources Research* 23 (1):19-98. doi: 10.1007/s11053-013-9224-6.

Johnson, GR, and GR Olhoeft. 1984. "Density of rocks and minerals." In *CRC handbook of physical properties of rocks*, edited by R.S. Carmichael, 38. Boca Raton, FL: CRC Press.

Jones, Emrys, Tom Latham, Daniel Russell McConnell, Matt Frye, Jesse Hunt, William Shedd, Dianna Shelander, Ray Boswell, Kelly Rose, and Carolyn Ruppel. 2008. "Scientific objectives of the Gulf of Mexico gas hydrate JIP Leg II drilling." Offshore Technology Conference.

Jones, KW, PB Kerkar, D Mahajan, WB Lindquist, and H Feng. 2007. "Microstructure of natural hydrate host sediments." *Nuclear Instruments and Methods in Physics Research Section B: Beam Interactions with Materials and Atoms* 261 (1):504-507.

Jung, Jong-Won, and J Carlos Santamarina. 2012. "Hydrate formation and growth in pores." *Journal of Crystal Growth* 345 (1):61-68.

Kang, S-P, H Lee, C-S Lee, and W-M Sung. 2001. "Hydrate phase equilibria of the guest mixtures containing CO_2, N_2 and tetrahydrofuran." *Fluid Phase Equilibria* 185 (1):101-109.

Kang, Seong-Pil, and Huen Lee. 2000. "Recovery of CO_2 from flue gas using gas hydrate: thermodynamic verification through phase equilibrium measurements." *Environmental science & technology* 34 (20):4397-4400.

Kastanidis, Panagiotis, George E Romanos, Athanassios K Stubos, Ioannis G Economou, and Ioannis N Tsimpanogiannis. 2017. "Two-and three-phase equilibrium experimental measurements for the ternary CH_4+ CO_2+ H_2O mixture." *Fluid Phase Equilibria* 451:96-105.

Katsuki, Daisuke, Ryo Ohmura, Takao Ebinuma, and Hideo Narita. 2006. "Formation, growth and ageing of clathrate hydrate crystals in a porous medium." *Philosophical magazine* 86 (12):1753-1761.

Katz, Donald L. 1945. "Prediction of conditions for hydrate formation in natural gases." *Transactions of the AIME* 160 (01):140-149.

Katz, Donald La Verne. 1959. *Handbook of natural gas engineering*: McGraw-Hill.

Kelkar, SK, MS Selim, and ED Sloan. 1998. "Hydrate dissociation rates in pipelines." *Fluid Phase Equilibria* 150:371-382.

Kelland, Malcolm A. 2006. "History of the Development of Low Dosage Hydrate Inhibitors." *Energy & Fuels* 20 (3):825-847. doi: 10.1021/ef050427x.

Kerkar, Prasad B, Kristine Horvat, Keith W Jones, and Devinder Mahajan. 2014. "Imaging methane hydrates growth dynamics in porous media using synchrotron X-ray computed microtomography." *Geochemistry, Geophysics, Geosystems* 15 (12):4759-4768.

Kerkar, Prasad, Keith W Jones, Robert Kleinberg, W Brent Lindquist, Stan Tomov, Huan Feng, and Devinder Mahajan. 2009. "Direct observations of three dimensional growth of hydrates hosted in porous media." *Applied physics letters* 95 (2):024102.

Khlebnikov, VN, SV Antonov, AS Mishin, DA Bakulin, IV Khamidullina, Meng Liang, VA Vinokurov, and PA Gushchin. 2016. "A new method for the replacement of CH_4 with CO_2 in natural gas hydrate production." *Natural Gas Industry B* 3 (5):445-451.

Kim, Do-Youn, Tae-Won Uhm, Huen Lee, Young-Joo Lee, Byong-Jae Ryu, and Ji-Hoon Kim. 2005. "Compositional and structural identification of natural gas hydrates collected at Site 1249 on Ocean Drilling Program Leg 204." *Korean Journal of Chemical Engineering* 22 (4):569-572.

Kim, Gil Young, B Narantsetseg, B-J Ryu, D-G Yoo, JY Lee, HS Kim, and Michael Riedel. 2013. "Fracture orientation and induced anisotropy of gas hydrate-bearing sediments in seismic chimney-like-structures of the Ulleung Basin, East Sea." *Marine and Petroleum Geology* 47:182-194.

Kim, Sun Hyung, Myoung Do Seo, Jeong Won Kang, and Chul Soo Lee. 2011. "Hydrate-containing phase equilibria for mixed guests of carbon dioxide and nitrogen." *Fluid Phase Equilibria* 306 (2):229-233.

King, A. D. 2004. "The solubility of ethane, propane, and carbon dioxide in aqueous solutions of sodium cumene sulfonate." *Journal of Colloid and Interface Science* 273 (1):313-319. doi: https://doi.org/10.1016/j.jcis.2003.11.042.

Kleinberg, RL, C Flaum, DD Griffin, PG Brewer, GE Malby, ET Peltzer, and JP Yesinowski. 2003. "Deep sea NMR: Methane hydrate growth habit in porous media and its relationship to hydraulic permeability, deposit accumulation, and submarine slope stability." *Journal of Geophysical Research: Solid Earth* 108 (B10).

Kneafsey, Timothy J, Yongkoo Seol, Arvind Gupta, and Liviu Tomutsa. 2011. "Permeability of laboratory-formed methane-hydrate-bearing sand: measurements and observations using X-ray computed tomography." *SPE Journal* 16 (01):78-94.

Kneafsey, Timothy J, Liviu Tomutsa, George J Moridis, Yongkoo Seol, Barry M Freifeld, Charles E Taylor, and Arvind Gupta. 2007. "Methane hydrate formation and dissociation in a partially saturated core-scale sand sample." *Journal of Petroleum Science and Engineering* 56 (1-3):108-126.

Koh, Carolyn A. 2002. "Towards a fundamental understanding of natural gas hydrates." *Chemical Society Reviews* 31 (3):157-167.

Koh, Carolyn A, and E Dendy Sloan. 2007. "Natural gas hydrates: Recent advances and challenges in energy and environmental applications." *AIChE journal* 53 (7):1636-1643.

Koh, Carolyn A, E Dendy Sloan, Amadeu K Sum, and David T Wu. 2011. "Fundamentals and applications of gas hydrates."

Konno, Yoshihiro, Yoshihiro Masuda, Yosuke Hariguchi, Masanori Kurihara, and Hisanao Ouchi. 2010. "Key factors for depressurization-induced gas production from oceanic methane hydrates." *Energy & fuels* 24 (3):1736-1744.

Kuhs, WF, B Chazallon, PG Radaelli, and F Pauer. 1997. "Cage occupancy and compressibility of deuterated N2-clathrate hydrate by neutron diffraction." *Journal of inclusion phenomena and molecular recognition in chemistry* 29 (1):65-77.

Kumar, Anjani, Brij Maini, PR Bishnoi, Matthew Clarke, Olga Zatsepina, and Sanjay Srinivasan. 2010. "Experimental determination of permeability in the presence of hydrates and its effect on the dissociation characteristics of gas hydrates in porous media." *Journal of Petroleum Science and Engineering* 70 (1-2):114-122.

Kvamme, B, A Graue, T Buanes, T Kuznetsova, and G Ersland. 2007. "Storage of CO_2 in natural gas hydrate reservoirs and the effect of hydrate as an extra sealing in cold aquifers." *International Journal of Greenhouse gas control* 1 (2):236-246.

Kvenvolden, KA. 1998. "A primer on the geological occurrence of gas hydrate." *Geological Society, London, Special Publications* 137 (1):9-30.

Kvenvolden, Keith A. 1988. "Methane hydrate—a major reservoir of carbon in the shallow geosphere?" *Chemical geology* 71 (1-3):41-51.

Kvenvolden, Keith A. 1993. "Gas hydrates—geological perspective and global change." *Reviews of geophysics* 31 (2):173-187.

Kvenvolden, Keith A. 1999. "Potential effects of gas hydrate on human welfare." *Proceedings of the National Academy of Sciences* 96 (7):3420-3426.

Kvenvolden, Keith A, LA Barnard, and DH Cameron. 1983. "Pressure core barrel-application to the study of gas hydrates, deep-sea drilling project site-533, leg-76." *Initial Reports of the Deep Sea Drilling Project* 76 (NOV):367-375.

Kvenvolden, Keith A, and Leo A Barnard. 1982. "Hydrates of Natural Gas in Continental Margins: Environmental Processes: Model Investigations of Margin Environmental and Tectonic Processes."

Kvenvolden, Keith A, and Thomas D Lorenson. 2001. "Global occurrences of gas hydrate." The Eleventh International Offshore and Polar Engineering Conference.

Kvenvolden, Keith A, and Mark A McMenamin. 1980. "Hydrates of natural gas: a review of their geologic occurrence."

Kvenvolden, Keith A, and Bruce W Rogers. 2005. "Gaia's breath—global methane exhalations." *Marine and Petroleum Geology* 22 (4):579-590.

Kwon, Tae-Hyuk, and Gye-Chun Cho. 2009. "Evolution of compressional wave velocity during CO_2 hydrate formation in sediments." *Energy & Fuels* 23 (11):5731-5736.

Kwon, Tae-Hyuk, Gye-Chun Cho, and J Carlos Santamarina. 2008. "Gas hydrate dissociation in sediments: Pressure-temperature evolution." *Geochemistry, Geophysics, Geosystems* 9 (3).

Le Quang, Duyen, Baptiste Bouillot, Jean-Michel Herri, Philippe Glénat, and Pierre Duchet-Suchaux. 2016. "Experimental procedure and results to measure the composition of gas hydrate, during crystallization and at equilibrium, from N_2–CO_2–CH_4–C_2H_6–C_3H_8–C_4H_{10} gas mixtures." *Fluid Phase Equilibria* 413:10-21.

Leaist, DG, JJ Murray, ML Post, and DW Davidson. 1982. "Enthalpies of decomposition and heat capacities of ethylene oxide and tetrahydrofuran hydrates." *The Journal of Physical Chemistry* 86 (21):4175-4178.

Lebedev, Maxim, Yihuai Zhang, Vassili Mikhaltsevitch, Stefan Inglauer, and Taufiq Rahman. 2017. "Residual trapping of supercritical CO_2: direct pore-scale observation using a low cost pressure cell for micro computer tomography." *Energy Procedia* 114:4967-4974.

Lederhos, JP, RL Christiansen, and ED Sloan. 1993. "A first order method of hydrate equilibrium estimation and its use with new structures." *Fluid phase equilibria* 83:445-454.

Lee, Jong-Won, Do-Youn Kim, and Huen Lee. 2006. "Phase behavior and structure transition of the mixed methane and nitrogen hydrates." *Korean Journal of Chemical Engineering* 23 (2):299-302.

Lee, JY, J Carlos Santamarina, and C Ruppel. 2010. "Volume change associated with formation and dissociation of hydrate in sediment." *Geochemistry, Geophysics, Geosystems* 11 (3).

Lee, JY, TS Yun, JC Santamarina, and C Ruppel. 2007. "Observations related to tetrahydrofuran and methane hydrates for laboratory studies of hydrate-bearing sediments." *Geochemistry, Geophysics, Geosystems* 8 (6).

Lee, Myung W, and Timothy S Collett. 2001. "Elastic properties of gas hydrate-bearing sediments." *Geophysics* 66 (3):763-771.

Lee, Myung W, and William F Waite. 2008. "Estimating pore-space gas hydrate saturations from well log acoustic data." *Geochemistry, Geophysics, Geosystems* 9 (7).

Lee, Sangyong, Junshe Zhang, Raxit Mehta, T. K. Woo, and Jae W. Lee. 2007. "Methane Hydrate Equilibrium and Formation Kinetics in the Presence of an Anionic Surfactant." *The Journal of Physical Chemistry C* 111 (12):4734-4739. doi: 10.1021/jp0667590.

Lee, Seungmin, Youngjun Lee, Sungwon Park, Yunju Kim, Inuk Cha, and Yongwon Seo. 2013. "Stability conditions and guest distribution of the methane+ ethane+

propane hydrates or semiclathrates in the presence of tetrahydrofuran or quaternary ammonium salts." *The Journal of Chemical Thermodynamics* 65:113-119.

Lee, Sung-Rock. 2011. "2nd ulleung basin gas hydrate expedition (UBGH2): findings and implications." *Fire in the Ice* 11 (1):6-9.

Lee, Yun-Je, Taro Kawamura, Yoshitaka Yamamoto, and Ji-Ho Yoon. 2012. "Phase equilibrium studies of tetrahydrofuran (THF)+ CH_4, THF+ CO_2, CH_4+ CO_2, and THF+ CO_2+ CH_4 Hydrates." *Journal of Chemical & Engineering Data* 57 (12):3543-3548.

Li, Feng-Guang, Chang-Yu Sun, Sheng-Li Li, Guang-Jin Chen, Xu-Qiang Guo, Lan-Ying Yang, Heng Pan, Shi Li, and Ke Zhang. 2012. "Experimental studies on the evolvement of electrical resistivity during methane hydrate formation in sediments." *Energy & Fuels* 26 (10):6210-6217.

Lide, DR, and HPR Frederikse. 1995. "Handbook of Chemistry and Physics, CRC Press, Inc." *Boca Raton, FL.*

Linga, Praveen, Adebola Adeyemo, and Peter Englezos. 2007. "Medium-pressure clathrate hydrate/membrane hybrid process for postcombustion capture of carbon dioxide." *Environmental Science & Technology* 42 (1):315-320.

Loh, Matilda, Simon Falser, Ponnivalavan Babu, Praveen Linga, Andrew Palmer, and Thiam Soon Tan. 2012. "Dissociation of fresh-and seawater hydrates along the phase boundaries between 2.3 and 17 MPa." *Energy & Fuels* 26 (10):6240-6246.

Long, Jinping. 1994. "Gas hydrate formation mechanism and kinetic inhibition." Colerado School of Mines.

Löwig, Carl. 1828. "Ueber einige Bromverbindungen und über Bromdarstellung." *Annalen der Physik* 90 (11):485-499.

Lu, Shyi-Min. 2015. "A global survey of gas hydrate development and reserves: Specifically in the marine field." *Renewable and Sustainable Energy Reviews* 41 (C):884-900.

Lu, Zhengquan, and Nabil Sultan. 2008. "Empirical expressions for gas hydrate stability law, its volume fraction and mass-density at temperatures 273.15 K to 290.15 K." *Geochemical Journal* 42 (2):163-175.

Lusic, Hrvoje, and Mark W Grinstaff. 2012. "X-ray-computed tomography contrast agents." *Chemical Reviews* 113 (3):1641-1666.

Macintosh, N. 2000. "FlowAssurance Still Leading Concern Among Producers. sl: Offshore."

Makogon, IŪriĭ Fedorovich. 1997. *Hydrates of hydrocarbons*: Pennwell Books.

Makogon, IŪriĭ Fedorovich, and Yuri F Makogon. 1997. *Hydrates of hydrocarbons*: Pennwell Books.

Makogon, YF. 1965. "A gas hydrate formation in the gas saturated layers under low temperature." *Gas Industry* 5:14-15.

Makogon, YF, SA Holditch, and TY Makogon. 2007. "Natural gas-hydrates—A potential energy source for the 21st Century." *Journal of Petroleum Science and Engineering* 56 (1):14-31.

Makogon, Yu F. 1982. "Perspectives for the development of gas hydrate deposits." Gas hydrates and permafrost: Proceedings of the 4th Canadian Permafrost Conference.

Makogon, Yuri F. 2010. "Natural gas hydrates–A promising source of energy." *Journal of Natural Gas Science and Engineering* 2 (1):49-59.

Malone, R.D. 1985. Gas Hydrates Topical Report–DOE. US: METC/SP-218 (DE85001986): Morgantown (DOE, Morgantown Energy Technology Center).

Maslin, Mark, Matthew Owen, Richard Betts, Simon Day, Tom Dunkley Jones, and Andrew Ridgwell. 2010. "Gas hydrates: past and future geohazard?" *Philosophical Transactions of the Royal Society of London A: Mathematical, Physical and Engineering Sciences* 368 (1919):2369-2393.

Mavko, Gary, Tapan Mukerji, and Jack Dvorkin. 2009. *The rock physics handbook: Tools for seismic analysis of porous media*: Cambridge university press.

Max, Michael D, Arthur H Johnson, and William P Dillon. 2005. *Economic geology of natural gas hydrate*. Vol. 9: Springer Science & Business Media.

Max, Michael D, Arthur H Johnson, and William P Dillon. 2013. *Natural Gas Hydrate-Arctic Ocean Deepwater Resource Potential*: Springer.

Mayr, Sibylle I, and Hans Burkhardt. 2006. "Ultrasonic properties of sedimentary rocks: Effect of pressure, saturation, frequency and microcracks." *Geophysical Journal International* 164 (1):246-258.

McGuire, Patrick L. 1981. Methane hydrate gas production by thermal stimulation. Los Alamos Scientific Lab., NM (USA).

Mehta, Ajay P, and E Dendy Sloan. 1994. "A thermodynamic model for structure-H hydrates." *AIChE journal* 40 (2):312-320.

Mehta, Ajay P, and E Dendy Sloan Jr. 1994. "Structure H hydrate phase equilibria of paraffins, naphthenes, and olefins with methane." *Journal Of Chemical And Engineering Data* 39 (4):887-890.

Mei, Dong-Hai, Jian Liao, Ji-Tao Yang, and Tian-Min Guo. 1996. "Experimental and modeling studies on the hydrate formation of a methane+ nitrogen gas mixture in the presence of aqueous electrolyte solutions." *Industrial and engineering chemistry research* 35 (11):4342-4347.

Mekala, Prathyusha, Ponnivalavan Babu, Jitendra S Sangwai, and Praveen Linga. 2014. "Formation and dissociation kinetics of methane hydrates in seawater and silica sand." *Energy & Fuels* 28 (4):2708-2716.

Meyer, RF. 1981. "Speculations on oil and gas resources in small fields and unconventional deposits." *Long-term energy resources*:49-72.

Misyura, S Ya. 2013. "Effect of heat transfer on the kinetics of methane hydrate dissociation." *Chemical Physics Letters* 583:34-37.

Mohammadi, Amir H, Ross Anderson, and Bahman Tohidi. 2005. "Carbon monoxide clathrate hydrates: equilibrium data and thermodynamic modeling." *AIChE journal* 51 (10):2825-2833.

Mohebbi, V., A. Naderifar, R. M. Behbahani, and M. Moshfeghian. 2012. "Investigation of kinetics of methane hydrate formation during isobaric and isochoric processes in an agitated reactor." *Chemical Engineering Science* 76:58-65. doi: https://doi.org/10.1016/j.ces.2012.04.016.

Moon, Changman, Paul C Taylor, and P Mark Rodger. 2003. "Molecular dynamics study of gas hydrate formation." *Journal of the American Chemical Society* 125 (16):4706-4707.

Moridis, George J. 2008. "Toward production from gas hydrates: current status, assessment of resources, and simulation-based evaluation of technology and potential." *Lawrence Berkeley National Laboratory*.

Moridis, George J, Timothy S Collett, Ray Boswell, Masanori Kurihara, Matthew T Reagan, Carolyn Koh, and E Dendy Sloan. 2009. "Toward production from gas hydrates: current status, assessment of resources, and simulation-based evaluation of technology and potential." *SPE Reservoir Evaluation & Engineering* 12 (05):745-771.

Mork, Marit, Grethe Schei, and Roar Larsen. 2000. "NMR imaging study of hydrates in sediments." *Annals of the New York Academy of Sciences* 912 (1):897-905.

Motiee, M. 1991. "Estimate possibility of hydrates." *Hydrocarbon processing* 70 (7):98-99.

Najibi, Hesam, Antonin Chapoy, Hooman Haghighi, and Bahman Tohidi. 2009. "Experimental determination and prediction of methane hydrate stability in alcohols and electrolyte solutions." *Fluid Phase Equilibria* 275 (2):127-131.

Nakajima, Yasuharu, Tatsuya Takaoki, Kazunari Ohgaki, and Susumu Ota. 2002. "Use of hydrate pellets for transportation of natural gas-II-proposition of natural gas transportation in form of Hydrate pellets." Proc. 4th Int. Conf. Gas Hydrates.

Nakamura, Toshiyuki, Takashi Makino, Takeshi Sugahara, and Kazunari Ohgaki. 2003. "Stability boundaries of gas hydrates helped by methane—structure-H hydrates of methylcyclohexane and cis-1, 2-dimethylcyclohexane." *Chemical engineering science* 58 (2):269-273.

Nakano, Shinya, Masato Moritoki, and Kazunari Ohgaki. 1999. "High-pressure phase equilibrium and Raman microprobe spectroscopic studies on the methane hydrate system." *Journal of Chemical & Engineering Data* 44 (2):254-257.

Ng, Heng-Joo, and Donald B Robinson. 1976. "The measurement and prediction of hydrate formation in liquid hydrocarbon-water systems." *Industrial & Engineering Chemistry Fundamentals* 15 (4):293-298.

Obanijesu, Emmanuel O, Ahmed Barifcani, Vishnu K Pareek, and Moses O Tade. 2014. "Experimental study on feasibility of H_2 and N_2 as hydrate inhibitors in natural gas pipelines." *Journal of Chemical & Engineering Data* 59 (11):3756-3766.

Ohgaki, K. 1994. "A proposal for gas storage on the bottom of the ocean using gas hydrates." *Int. Chem. Eng.* 34:417-419.

Ohgaki, Kazunari, Yoshihiro Makihara, and Kiyoteru Takano. 1993. "Formation of CO_2 Hydrate in Pure and Sea Waters." *Journal of chemical engineering of Japan* 26 (5):558-564.

Ohgaki, Kazunari, Kiyoteru Takano, and Masato Moritoki. 1994. "Exploitation of CH_4 Hydrates under the Nankai Trough in Combination with CO_2 Storage." *Kagaku Kogaku Ronbunshu* 20:121-121.

Ohmura, Ryo, Toru Shigetomi, and Yasuhiko H Mori. 1999. "Formation, growth and dissociation of clathrate hydrate crystals in liquid water in contact with a hydrophobic hydrate-forming liquid." *Journal of crystal growth* 196 (1):164-173.

Orr, Franklin M. 2009. "Onshore geologic storage of CO_2." *Science* 325 (5948):1656-1658.

Pachauri, Rajendra K, Myles R Allen, Vicente R Barros, John Broome, Wolfgang Cramer, Renate Christ, John A Church, Leon Clarke, Qin Dahe, and Purnamita Dasgupta. 2014. *Climate change 2014: synthesis report. Contribution of Working Groups I, II and III to the fifth assessment report of the Intergovernmental Panel on Climate Change*: IPCC.

Park, Kyeong-nam, Sang Yeon Hong, Jin Woo Lee, Kyung Chan Kang, Young Cheol Lee, Myung-Gyu Ha, and Ju Dong Lee. 2011. "A new apparatus for seawater desalination by gas hydrate process and removal characteristics of dissolved minerals (Na^+, Mg^{2+}, Ca^{2+}, K^+, B^{3+})." *Desalination* 274 (1):91-96.

Park, Taehyung, Daeseung Kyung, and Woojin Lee. 2014. "Effect of organic matter on CO_2 hydrate phase equilibrium in phyllosilicate suspensions." *Environmental Science and Technology* 48 (12):6597-6603.

Parkes, Ronald John, BA Cragg, JC Fry, RA Herbert, and JWT Wimpenny. 1990. "Bacterial biomass and activity in deep sediment layers from the Peru margin." *Phil. Trans. R. Soc. Lond. A* 331 (1616):139-153.

Parrish, William R, and John M Prausnitz. 1972. "Dissociation pressures of gas hydrates formed by gas mixtures." *Industrial & Engineering Chemistry Process Design and Development* 11 (1):26-35.

Paull, C., W.S. Reeburgh, S.R. Dallimore, G. Enciso, C.A. Koh, K.A. Kvenvolden, C. Mankin, and M. Riedel. 2010. *Realizing the energy potential of methane hydrate for the United States*. Washington DC: National Research Council of the National Academies.

Pearson, C, J Murphy, and R Hermes. 1986. "Acoustic and resistivity measurements on rock samples containing tetrahydrofuran hydrates: laboratory analogues to natural gas hydrate deposits." *Journal of Geophysical Research: Solid Earth* 91 (B14):14132-14138.

Pearson, CF, PM Halleck, PL McGuire, R Hermes, and M Mathews. 1983. "Natural gas hydrate deposits: A review of in situ properties." *The Journal of Physical Chemistry* 87 (21):4180-4185.

Peng, Ding-Yu, and Donald B Robinson. 1976. "A new two-constant equation of state." *Industrial & Engineering Chemistry Fundamentals* 15 (1):59-64.

Perrin, Andrea, Osama M. Musa, and Jonathan W. Steed. 2013. "The chemistry of low dosage clathrate hydrate inhibitors." *Chemical Society Reviews* 42 (5):1996-2015. doi: 10.1039/C2CS35340G.

Pickering, Spencer Umfreville. 1893. "X.—The hydrate theory of solutions. Some compounds of the alkyl-amines and ammonia with water." *Journal of the Chemical Society, Transactions* 63:141-195.

Prakash, Anand, BG Samanta, and NP Singh. 2010. "A seismic study to investigate the prospect of gas hydrate in Mahanadi deep water basin, northeastern continental margin of India." *Marine Geophysical Researches* 31 (4):253-262.

Priest, Jeffrey A, Angus I Best, and Christopher RI Clayton. 2005. "A laboratory investigation into the seismic velocities of methane gas hydrate-bearing sand." *Journal of Geophysical Research: Solid Earth* 110 (B4).

Priest, Jeffrey A, Emily VL Rees, and Christopher RI Clayton. 2009. "Influence of gas hydrate morphology on the seismic velocities of sands." *Journal of Geophysical Research: Solid Earth (1978–2012)* 114 (B11).

Rabbel, Wolfgang. 2006. "Seismic methods." In *Groundwater geophysics*, 23-83. Springer.

Rahman, Taufiq, Maxim Lebedev, Ahmed Barifcani, and Stefan Iglauer. 2016. "Residual trapping of supercritical CO_2 in oil-wet sandstone." *Journal of Colloid and Interface Science* 469:63-68.

Rees, Emily VL, Jeffery A Priest, and Chris RI Clayton. 2011. "The structure of methane gas hydrate bearing sediments from the Krishna–Godavari Basin as seen from Micro-CT scanning." *Marine and Petroleum Geology* 28 (7):1283-1293.

Rice, Warren. 2006. "Hydrogen production from methane hydrate with sequestering of carbon dioxide." *International Journal of Hydrogen Energy* 31 (14):1955-1963.

Ripmeester, John A, S Tse John, Christopher I Ratcliffe, and Brian M Powell. 1987. "A new clathrate hydrate structure." *Nature* 325 (6100):135-136.

Ripmeester, John A, and Christopher I Ratcliffe. 1998. "The diverse nature of dodecahedral cages in clathrate hydrates as revealed by 129Xe and 13C NMR spectroscopy: CO_2 as a small-cage guest." *Energy & fuels* 12 (2):197-200.

Rochelle, CA, AP Camps, D Long, A Milodowski, K Bateman, D Gunn, P Jackson, MA Lovell, and J Rees. 2009. "Can CO_2 hydrate assist in the underground storage of carbon dioxide?" *Geological Society, London, Special Publications* 319 (1):171-183.

Röntgen, Wilhelm Conrad. 1896. "On a new kind of rays." *Science* 3 (59):227-231.

Roozeboom, HW. 1885. "Sur la dissociation des hydrates de l'acide sulfureux, du chlore et du brome." *Recueil des Travaux Chimiques des Pays-Bas* 4 (2):65-73.

Rydzy, Marisa B, and Michael L Batzle. 2010. "Ultrasonic velocities in laboratory-formed gas hydrate-bearing sediments." 23rd EEGS Symposium on the Application of Geophysics to Engineering and Environmental Problems.

Sabil, Khalik M, Qazi Nasir, Bezhad Partoon, and Akbar A Seman. 2014. "Measurement of H–LW–V and Dissociation Enthalpy of Carbon Dioxide Rich Synthetic Natural Gas Mixtures." *Journal of Chemical and Engineering Data* 59 (11):3502-3509.

Sadeq, Dhifaf, Stefan Iglauer, Maxim Lebedev, and Ahmed Barifcani. 2018. "Prediction of Hydrate Phase Equilibrium Conditions for Different Gas Mixtures." Offshore Technology Conference Asia.

Sadeq, Dhifaf, Stefan Iglauer, Maxim Lebedev, Taufiq Rahman, Yihuai Zhang, and Ahmed Barifcani. 2018. "Experimental pore-scale analysis of carbon dioxide hydrate in sandstone via X-Ray micro-computed tomography." *International Journal of Greenhouse Gas Control* 79:73-82.

Sadeq, Dhifaf, Stefan Iglauer, Maxim Lebedev, Callum Smith, and Ahmed Barifcani. 2017. "Experimental determination of hydrate phase equilibrium for different gas mixtures containing methane, carbon dioxide and nitrogen with motor current measurements." *Journal of Natural Gas Science and Engineering* 38:59-73.

Saito, Shozaburo, and Riki Kobayashi. 1965. "Hydrates at high pressures: Part III. Methane-argon-water, argon-nitrogen-water system." *AIChE Journal* 11 (1):96-99.

Salufu, Samuel O, and Princess Nwakwo. 2013. "New Empirical Correlation for Predicting Hydrate Formation Conditions." SPE Nigeria Annual International Conference and Exhibition.

Santamarina, J Carlos, and Carolyn Ruppel. 2010. "The impact of hydrate saturation on the mechanical, electrical, and thermal properties of hydrate-bearing sand, silts, and clay." *Geophysical Characterization of Gas Hydrates, Geophys. Dev. Ser* 14:373-384.

Sassen, R, SL Losh, L Cathles III, HH Roberts, JK Whelan, AV Milkov, ST Sweet, and DA DeFreitas. 2001. "Massive vein-filling gas hydrate: relation to ongoing gas migration from the deep subsurface in the Gulf of Mexico." *Marine and Petroleum Geology* 18 (5):551-560.

Sassen, Roger, and Ian R MacDonald. 1994. "Evidence of structure H hydrate, Gulf of Mexico continental slope." *Organic Geochemistry* 22 (6):1029-1032.

Sato, Mitsutaka, Satoshi Takeya, Jiro Nagao, Shigeki Jin, Yasushi Kamata, Hideki Minagawa, Takao Ebinuma, and Hideo Narita. 2005. "Distribution of hydrate saturation ratios in artificial methane hydrate sediments measured by high-speed X-ray computerized tomography." *Japanese Journal of Applied Physics* 44 (1R):473.

Scalabrin, G, P Marchi, F Finezzo, and R Span. 2006. "A reference multiparameter thermal conductivity equation for carbon dioxide with an optimized functional form." *Journal of physical and chemical reference data* 35 (4):1549-1575.

Schicks, Judith M, Erik Spangenberg, Ronny Giese, Bernd Steinhauer, Jens Klump, and Manja Luzi. 2011. "New approaches for the production of hydrocarbons from hydrate bearing sediments." *Energies* 4 (1):151-172.

Schindler, Mandy, and Michael L Batzle. 2015. "Pore-Scale Investigations of Hydrate Bearing Sediments." In *Pore Scale Phenomena: Frontiers in Energy and Environment*, 115-133. World Scientific.

Schindler, Mandy, Michael L Batzle, and Manika Prasad. 2017. "Micro X-Ray computed tomography imaging and ultrasonic velocity measurements in tetrahydrofuran-hydrate-bearing sediments." *Geophysical Prospecting* 65 (4):1025-1036.

Schlüter, Steffen, Adrian Sheppard, Kendra Brown, and Dorthe Wildenschild. 2014. "Image processing of multiphase images obtained via X-ray microtomography: a review." *Water Resources Research* 50 (4):3615-3639.

Schoderbek, David, and Ray Boswell. 2011. "Iġnik sikumi# 1, gas hydrate test well, successfully installed on the Alaska North slope." *Natural Gas & Oil* 304:285-4541.

Schon, JH. 1998. "Physical properties of rocks: Fundamentals and principles of petrophysics." *Handbook of geophysical exploration*.

Seo, Yu-Taek, Seong-Pil Kang, Huen Lee, Chul-Soo Lee, and Won-Mo Sung. 2000. "Hydrate phase equilibria for gas mixtures containing carbon dioxide: a proof-of-concept to carbon dioxide recovery from multicomponent gas stream." *Korean Journal of Chemical Engineering* 17 (6):659-667.

Seo, Yu-Taek, and Huen Lee. 2001. "Multiple-phase hydrate equilibria of the ternary carbon dioxide, methane, and water mixtures." *The Journal of Physical Chemistry B* 105 (41):10084-10090.

Seo, Yu-Taek, and Huen Lee. 2004. "Structure and guest distribution of the mixed carbon dioxide and nitrogen hydrates as revealed by X-ray diffraction and 13C NMR spectroscopy." *The Journal of Physical Chemistry B* 108 (2):530-534.

Seo, Yu-Taek, Huen Lee, and Ji-Ho Yoon. 2001. "Hydrate phase equilibria of the carbon dioxide, methane, and water system." *Journal of Chemical and Engineering Data* 46 (2):381-384.

Seol, Yongkoo, and Evgeniy Myshakin. 2011. "Experimental and numerical observations of hydrate reformation during depressurization in a core-scale reactor." *Energy & Fuels* 25 (3):1099-1110.

Servio, Phillip, Fritz Lagers, Cor Peters, and Peter Englezos. 1999. "Gas hydrate phase equilibrium in the system methane–carbon dioxide–neohexane and water." *Fluid phase equilibria* 158:795-800.

Sfaxi, Imen Ben Attouche, Veronica Belandria, Amir H Mohammadi, Rafael Lugo, and Dominique Richon. 2012. "Phase equilibria of $CO_2 + N_2$ and $CO_2 + CH_4$ clathrate hydrates: Experimental measurements and thermodynamic modelling." *Chemical Engineering Science* 84:602-611.

Shaw, George H. 1986. "Elastic properties and equation of state of high pressure ice." *The Journal of chemical physics* 84 (10):5862-5868.

Shipley, Thomas H, Mark H Houston, Richard T Buffler, F Jeanne Shaub, Kenneth J McMillen, John W Ladd, and J Lamar Worzel. 1979. "Seismic evidence for widespread possible gas hydrate horizons on continental slopes and rises." *AAPG bulletin* 63 (12):2204-2213.

Sira, JH, SL Patil, and VA Kamath. 1990. "Study of hydrate dissociation by methanol and glycol injection." SPE Annual technical conference and exhibition.

Sloan , E Dendy. 2003. "Fundamental principles and applications of natural gas hydrates." *Nature* 426 (6964):353.

Sloan, E Dendy. 2005. "A changing hydrate paradigm—from apprehension to avoidance to risk management." *Fluid Phase Equilibria* 228:67-74.

Sloan, E Dendy, and Carolyn Koh. 2008. *Clathrate hydrates of natural gases*. 3rd ed. New York: CRC press.

Sloan, E Dendy, Carolyn Ann Koh, and Amadeu Sum. 2010. *Natural gas hydrates in flow assurance*: Gulf Professional Publishing.

Sloan, ED, and F Fleyfel. 1991. "A molecular mechanism for gas hydrate nucleation from ice." *AIChE Journal* 37 (9):1281-1292.

Smith, Callum, Ahmed Barifcani, and David Pack. 2015. "Gas hydrate formation and dissociation numerical modelling with nitrogen and carbon dioxide." *Journal of Natural Gas Science and Engineering* 27:1118-1128.

Smith, Callum, Ahmed Barifcani, and David Pack. 2016. "Helium substitution of natural gas hydrocarbons in the analysis of their hydrate." *Journal of Natural Gas Science and Engineering* 35:1293-1300.

Song, Yongchen, Chuanxiao Cheng, Jiafei Zhao, Zihao Zhu, Weiguo Liu, Mingjun Yang, and Kaihua Xue. 2015. "Evaluation of gas production from methane hydrates using depressurization, thermal stimulation and combined methods." *Applied Energy* 145:265-277.

Spangenberg, E, J Kulenkampff, R Naumann, and J Erzinger. 2005. "Pore space hydrate formation in a glass bead sample from methane dissolved in water." *Geophysical Research Letters* 32 (24).

Spangenberg, Erik, and Johannes Kulenkampff. 2006. "Influence of methane hydrate content on electrical sediment properties." *Geophysical Research Letters* 33 (24).

Spangenberg, Erik, Mike Priegnitz, Katja Heeschen, and Judith M Schicks. 2014. "Are laboratory-formed hydrate-bearing systems analogous to those in nature?" *Journal of Chemical & Engineering Data* 60 (2):258-268.

Spence, GD, RR Haacke, and RD Hyndman. 2010. "Seismic indicators of natural gas hydrate and underlying free gas." In *Geophysical Characterization of Gas Hydrates*, 39-71. Society of Exploration Geophysicists.

Stauffer, Dietrich. 1979. "Scaling theory of percolation clusters." *Physics Reports* 54 (1):1-74.

Strizhov, I. N., and I. E. Khodanovich. 1946. "Gas Production. Gostoptekhizdat. Moscow, Russia. ."

Strobel, Timothy A, Carolyn A Koh, and E Dendy Sloan. 2009. "Thermodynamic predictions of various tetrahydrofuran and hydrogen clathrate hydrates." *Fluid Phase Equilibria* 280 (1):61-67.

Suess, Erwin, Gerhard Bohrmann, Jens Greinert, and Erwin Lausch. 1999. "Flammable ice." *Scientific American* 281 (5):76-83.

Sultan, Nabil, Pierre Cochonat, J-P Foucher, and J Mienert. 2004. "Effect of gas hydrates melting on seafloor slope instability." *Marine geology* 213 (1):379-401.

Sum, Amadeu K, Robert C Burruss, and E Dendy Sloan. 1997. "Measurement of clathrate hydrates via Raman spectroscopy." *The Journal of Physical Chemistry B* 101 (38):7371-7377.

Sun, Shi-Cai, Chang-Ling Liu, and Qing-Guo Meng. 2015. "Hydrate phase equilibrium of binary guest-mixtures containing CO_2 and N_2 in various systems." *The Journal of Chemical Thermodynamics* 84:1-6.

Sun, Zhi-gao, Ruzhu Wang, Rongsheng Ma, Kaihua Guo, and Shuanshi Fan. 2003. "Natural gas storage in hydrates with the presence of promoters." *Energy Conversion and Management* 44 (17):2733-2742.

Ta, Xuan Hien, Tae Sup Yun, Balasingam Muhunthan, and Tae-Hyuk Kwon. 2015. "Observations of pore-scale growth patterns of carbon dioxide hydrate using X-ray

computed microtomography." *Geochemistry, Geophysics, Geosystems* 16 (3):912-924.

Taheri, Zahra, Mohammad Reza Shabani, Khodadad Nazari, and Ali Mehdizaheh. 2014. "Natural gas transportation and storage by hydrate technology: Iran case study." *Journal of Natural Gas Science and Engineering* 21:846-849.

Takeishi, Reiji. 2014. "Japan's Energy Policy in the Asian Region." *Public Policy Review* 10 (1):153-187.

Tao, G, MS King, and M Nabi-Bidhendi. 1995. "Ultrasonic wave propagation in dry and brine-saturated sandstones as a function of effective stress: laboratory measurements and modelling 1." *Geophysical Prospecting* 43 (3):299-327.

Thomas, Sydney, and Richard A Dawe. 2003. "Review of ways to transport natural gas energy from countries which do not need the gas for domestic use." *Energy* 28 (14):1461-1477.

Tohidi, Bahman, Ross Anderson, M Ben Clennell, Rod W Burgass, and Ali B Biderkab. 2001. "Visual observation of gas-hydrate formation and dissociation in synthetic porous media by means of glass micromodels." *Geology* 29 (9):867-870.

Tohidi, Bahman, Jinhai Yang, Manoochehr Salehabadi, Ross Anderson, and Antonin Chapoy. 2010. "CO_2 hydrates could provide secondary safety factor in subsurface sequestration of CO_2." *Environmental Science and Technology* 44 (4):1509-1514.

Tohidi, Burgass, RW Burgass, A Danesh, KK Østergaard, and AC Todd. 2000. "Improving the accuracy of gas hydrate dissociation point measurements." *Annals of the New York Academy of Sciences* 912 (1):924-931.

Torres, ME, Ann M Trehu, N Cespedes, M Kastner, UG Wortmann, J-H Kim, P Long, A Malinverno, JW Pohlman, and Michael Riedel. 2008. "Methane hydrate formation in turbidite sediments of northern Cascadia, IODP Expedition 311." *Earth and Planetary Science Letters* 271 (1):170-180.

Trehu, Ann M, Philip E Long, ME Torres, GRRF Bohrmann, FR Rack, TS Collett, DS Goldberg, AV Milkov, Michael Riedel, and P Schultheiss. 2004. "Three-dimensional distribution of gas hydrate beneath southern Hydrate Ridge: constraints from ODP Leg 204." *Earth and Planetary Science Letters* 222 (3):845-862.

Tse, JS, BM Powell, VF Sears, and YP Handa. 1993. "The lattice dynamics of clathrate hydrates. An incoherent inelastic neutron scattering study." *Chemical physics letters* 215 (4):383-387.

Uchida, Takashi, Scott Dallimore, and JUN Mikami. 2000. "Occurrences of Natural Gas Hydrates beneath the Permafrost Zone in Mackenzie Delta: Visual and X-ray CT Imagery." *Annals of the New York Academy of Sciences* 912 (1):1021-1033.

Udachin, KA, CI Ratcliffe, GD Enright, and JA Ripmeester. 1997. "Structure H hydrate: A single crystal diffraction study of 2, 2-dimethylpentane· 5 (Xe, H2S)· 34H2O." *Supramolecular Chemistry* 8 (3):173-176.

Ueno, Hiroki, Hotaka Akiba, Satoru Akatsu, and Ryo Ohmura. 2015. "Crystal growth of clathrate hydrates formed with methane+ carbon dioxide mixed gas at the gas/liquid interface and in liquid water." *New Journal of Chemistry* 39 (11):8254-8262.

Unruh, Carl H, and Donald L Katz. 1949. "Gas hydrates of carbon dioxide-methane mixtures." *Journal of Petroleum Technology* 1 (04):83-86.

Van Cleeff, A, and GAM Diepen. 1960. "Gas hydrates of nitrogen and oxygen." *Recueil des Travaux Chimiques des Pays-Bas* 79 (6):582-586.

van der Waals, JH, and JC Platteeuw. 1959. "Clathrate solutions." *Advances in Chemical Physics* 2:1-57.

Van Geet, Maarten, Rudy Swennen, and Martine Wevers. 2000. "Quantitative analysis of reservoir rocks by microfocus X-ray computerised tomography." *Sedimentary Geology* 132 (1):25-36.

Veluswamy, Hari Prakash, Weng Inn Chin, and Praveen Linga. 2014. "Clathrate hydrates for hydrogen storage: the impact of tetrahydrofuran, tetra-n-butylammonium bromide and cyclopentane as promoters on the macroscopic kinetics." *International Journal of Hydrogen Energy* 39 (28):16234-16243.

Villard, P. 1890. "Sur l'hydrate et la composition des hydrates de gaz." *C.R. Acad. Sci., Paris* 119:368-371.

Villard, P. 1896. "Combination de l'argon avec l'eau." *Comptes Rendus Hebdomadaires des Seances de l'Academie des Sciences* 123:377-380.

Villard, Paul. 1888. "Sur quelques nouveaux hydrates de gaz." *Compt. rend* 106:1602-1603.

Vinegar, Harold J, and Scott L Wellington. 1987. "Tomographic imaging of three-phase flow experiments." *Review of Scientific Instruments* 58 (1):96-107.

von Stackelberg, M, and HR Müller. 1954. "Feste Gas Hydrate II." *Zeitschrift fuer Elektrochem* 58:25-31.

Von Stackelberg, Mv. 1954. "Fete Gashydrate II. Struktur and Raumchemie." *Zeit. F. Elektro.* 58:25.

Waite, William F, Timothy J Kneafsey, William J Winters, and DH Mason. 2008. "Physical property changes in hydrate-bearing sediment due to depressurization and subsequent repressurization." *Journal of Geophysical Research: Solid Earth* 113 (B7).

Waite, William F, J Carlos Santamarina, Douglas D Cortes, Brandon Dugan, DN Espinoza, J Germaine, Jaewon Jang, JW Jung, Timothy J Kneafsey, and H Shin. 2009. "Physical properties of hydrate-bearing sediments." *Reviews of Geophysics* 47 (4).

Waite, William F, and E Spangenberg. 2013. "Gas hydrate formation rates from dissolved-phase methane in porous laboratory specimens." *Geophysical Research Letters* 40 (16):4310-4315.

Waite, William F, William J Winters, and DH Mason. 2004. "Methane hydrate formation in partially water-saturated Ottawa sand." *American Mineralogist* 89 (8-9):1202-1207.

Wang, Yi, Xiao-Sen Li, Gang Li, Ning-Sheng Huang, and Jing-Chun Feng. 2014. "Experimental study on the hydrate dissociation in porous media by five-spot thermal huff and puff method." *Fuel* 117:688-696.

Wenji, Song, Xiao Rui, Huang Chong, He Shihui, Dong Kaijun, and Feng Ziping. 2009. "Experimental investigation on TBAB clathrate hydrate slurry flows in a horizontal tube: Forced convective heat transfer behaviors." *international journal of refrigeration* 32 (7):1801-1807.

Whiffen, BL, H Kiefte, and MJ Clouter. 1982. "Determination of acoustic velocities in xenon and methane hydrates by Brillouin spectroscopy." *Geophysical Research Letters* 9 (6):645-648.

White, Curt M, Brian R Strazisar, Evan J Granite, James S Hoffman, and Henry W Pennline. 2003. "Separation and capture of CO_2 from large stationary sources and sequestration in geological formations—coalbeds and deep saline aquifers." *Journal of the Air and Waste Management Association* 53 (6):645-715.

Whiticar, Michael J, Eckard Faber, and Martin Schoell. 1986. "Biogenic methane formation in marine and freshwater environments: CO_2 reduction vs. acetate fermentation—isotope evidence." *Geochimica et Cosmochimica Acta* 50 (5):693-709.

Wilcox, Willard I, DB Carson, and DL Katz. 1941. "Natural gas hydrates." *Industrial & Engineering Chemistry* 33 (5):662-665.

Wildenschild, Dorthe, and Adrian P Sheppard. 2013. "X-ray imaging and analysis techniques for quantifying pore-scale structure and processes in subsurface porous medium systems." *Advances in Water Resources* 51:217-246.

Winters, William J, Ingo A Pecher, William F Waite, and David H Mason. 2004. "Physical properties and rock physics models of sediment containing natural and laboratory-formed methane gas hydrate." *American Mineralogist* 89 (8-9):1221-1227.

Winters, William J, William F Waite, DH Mason, LY Gilbert, and IA Pecher. 2007. "Methane gas hydrate effect on sediment acoustic and strength properties." *Journal of Petroleum Science and Engineering* 56 (1):127-135.

Winters, William, Michael Walker, Robert Hunter, Timothy Collett, Ray Boswell, Kelly Rose, William Waite, Marta Torres, Shirish Patil, and Abhijit Dandekar. 2011. "Physical properties of sediment from the Mount Elbert gas hydrate stratigraphic test well, Alaska North Slope." *Marine and Petroleum Geology* 28 (2):361-380.

Wood, David A. 2015. "Gas hydrate research advances steadily on multiple fronts: A collection of published research (2009–2015)." *Journal of Natural Gas Science and Engineering* (24):A1-A8.

Worthington, Paul F. 2010. "Petrophysical evaluation of gas-hydrate formations." *Petroleum Geoscience* 16 (1):53-66.

Wróblewski, Zygmunt Florenty. 1882. *Sur la combinaison de l'acide carbonique et de l'eau*.

Xie, Yingming, Gang Li, Daoping Liu, Ni Liu, Yingxia Qi, Deqing Liang, Kaihua Guo, and Shuanshi Fan. 2010. "Experimental study on a small scale of gas hydrate cold storage apparatus." *Applied Energy* 87 (11):3340-3346.

Xu, Wenyue, and Carolyn Ruppel. 1999. "Predicting the occurrence, distribution, and evolution of methane gas hydrate in porous marine sediments." *Journal of Geophysical Research: Solid Earth* 104 (B3):5081-5095.

Xue, Kaihua, Jiafei Zhao, Yongchen Song, Weiguo Liu, Weihaur Lam, Yiming Zhu, Yu Liu, Chuanxiao Cheng, and Di Liu. 2012. "Direct observation of THF hydrate formation in porous microstructure using magnetic resonance imaging." *Energies* 5 (4):898-910.

Yamamoto, Koji, Yoshihiro Terao, Tesuya Fujii, Terumichi Ikawa, Makoto Seki, Maki Matsuzawa, and Takayuki Kanno. 2014. "Operational overview of the first offshore production test of methane hydrates in the Eastern Nankai Trough." Offshore Technology Conference.

Yamasaki, Akihiro. 2003. "An overview of CO_2 mitigation options for global warming—emphasizing CO_2 sequestration options." *Journal of Chemical Engineering of Japan* 36 (4):361-375.

Yang, Hongqun, Zhenghe Xu, Maohong Fan, Rajender Gupta, Rachid B Slimane, Alan E Bland, and Ian Wright. 2008. "Progress in carbon dioxide separation and capture: A review." *Journal of Environmental Sciences* 20 (1):14-27.

Yang, Mingjun, Yongchen Song, Xuke Ruan, Yu Liu, Jiafei Zhao, and Qingping Li. 2012. "Characteristics of CO_2 Hydrate Formation and Dissociation in Glass Beads and Silica Gel." *Energies* 5 (4):925-937.

You, Kehua, Timothy J Kneafsey, Peter B Flemings, Peter Polito, and Steven L Bryant. 2015. "Salinity-buffered methane hydrate formation and dissociation in gas-rich systems." *Journal of Geophysical Research: Solid Earth* 120 (2):643-661.

Yun, Tae Sup, FM Francisca, J Carlos Santamarina, and C Ruppel. 2005. "Compressional and shear wave velocities in uncemented sediment containing gas hydrate." *Geophysical Research Letters* 32 (10).

Yun, Tae Sup, J Carlos Santamarina, and C Ruppel. 2007. "Mechanical properties of sand, silt, and clay containing tetrahydrofuran hydrate." *Journal of geophysical research: solid earth* 112 (B4).

Yun, TS, GA Narsilio, JC Santamarina, and C Ruppel. 2006. "Instrumented pressure testing chamber for characterizing sediment cores recovered at in situ hydrostatic pressure." *Marine Geology* 229 (3-4):285-293.

Zarinabadi, Soroush, and Amir Samimi. 2012. "Problems of hydrate formation in oil and gas pipes deals." *Journal of American Science* 8 (8).

Zatsepina, Olga Ye, Hassan Hassanzadeh, and Mehran Pooladi-Darvish. 2014. "Geological Storage of CO2 as Hydrate in a McMurray Depleted Gas Reservoir." *Gas Injection for Disposal and Enhanced Recovery*:311-329.

Zhao, Jiafei, Kun Xu, Yongchen Song, Weiguo Liu, Weihaur Lam, Yu Liu, Kaihua Xue, Yiming Zhu, Xichong Yu, and Qingping Li. 2012. "A review on research on replacement of CH_4 in natural gas hydrates by use of CO_2." *Energies* 5 (2):399-419.

Zhao, Jiafei, Lei Yang, Yu Liu, and Yongchen Song. 2015. "Microstructural characteristics of natural gas hydrates hosted in various sand sediments." *Physical Chemistry Chemical Physics* 17 (35):22632-22641.

Zhao, Jiafei, Lei Yang, Kaihua Xue, Weihaur Lam, Yanghui Li, and Yongchen Song. 2014. "In situ observation of gas hydrates growth hosted in porous media." *Chemical Physics Letters* 612:124-128.

Zhao, Jiafei, Lei Yao, Yongchen Song, Kaihua Xue, Chuanxiao Cheng, Yu Liu, and Yi Zhang. 2011. "In situ observations by magnetic resonance imaging for formation and dissociation of tetrahydrofuran hydrate in porous media." *Magnetic resonance imaging* 29 (2):281-288.

Zhao, Jiafei, Zihao Zhu, Yongchen Song, Weiguo Liu, Yi Zhang, and Dayong Wang. 2015. "Analyzing the process of gas production for natural gas hydrate using depressurization." *Applied Energy* 142:125-134.

APPENDIX A: Measured hydrate dissociation data of $CO_2 + CH_4$, $N_2 + CH_4$ and $N_2 + CO_2$

Table A- 1 Measured hydrate dissociation data of $CO_2 + CH_4$ gas mixture in water

P/MPa	T/K CO_2 mol%= 0	T/K CO_2 mol%=10	T/K CO_2 mol%=16	T/K CO_2 mol%=20
5	279.45	280.55	281.45	282.05
7.5	283.25	283.95	284.95	285.55
10	285.75	286.75	287.35	287.95
15	289.05	289.65	290.55	290.85
20	291.18	291.8	292.25	292.75
25	292.95	293.35	293.5	293.95

Table A- 2 Measured hydrate dissociation data of N$_2$ + CH$_4$ gas mixture in water

P/ MPa	T/K N$_2$ mol%= 0	T/K N$_2$ mol%=10	T/K N$_2$ mol%=20	T/K N$_2$ mol%=31	T/K N$_2$ mol%=36
5	279.45	278.65	-	277.8	276.75
7.5	283.25	282.8	282.15	281.6	280.35
10	285.75	285.15	284.85	284.25	282.95
15	289.05	288.85	288.25	287.85	286.3
20	291.18	290.85	290.35	289.85	288.8
25	292.95	292.75	291.5	291.25	290.15

Table A- 3 Measured hydrate dissociation data of N$_2$ + CO$_2$ gas mixture in water

P/ MPa	T/K N$_2$ mol%= 64	T/K N$_2$ mol%=74
5	277.8	275.75
7.5	280.1	278.65
10	281.6	280.6
15	283.3	282.75
20	284.45	283.9

APPENDIX B: Official Permissions and Copyrights

Copyright Clearance Center

RightsLink®

Home | Account Info | Help
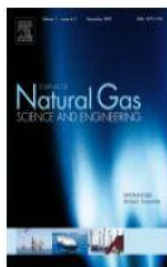
Title: Experimental determination of hydrate phase equilibrium for different gas mixtures containing methane, carbon dioxide and nitrogen with motor current measurements

Author: Dhifaf Sadeq, Stefan Iglauer, Maxim Lebedev, Callum Smith, Ahmed Barifcani

Publication: Journal of Natural Gas Science and Engineering

Publisher: Elsevier

Date: February 2017

© 2016 Elsevier B.V. All rights reserved.

Logged in as:
Dhifaf Sadeq
Curtin University

LOGOUT

BACK | CLOSE WINDOW

Title:	Prediction of Hydrate Phase Equilibrium Conditions for Different Gas Mixtures	Logged in as: Dhifaf Sadeq Curtin University
Conference Proceedings:	Offshore Technology Conference Asia	Account #: 3001311520
Author:	Dhifaf Sadeq, Curtin University;Stefan Iglauer, Curtin University;Maxim Lebedev, Curtin University et al	LOGOUT
Publisher:	Society of Petroleum Engineers	
Date:	2018	
	2018. Offshore Technology Conference	

Order Completed

Thank you for your order.

This Agreement between Curtin University -- Dhifaf Sadeq ("You") and Society of Petroleum Engineers ("Society of Petroleum Engineers") consists of your license details and the terms and conditions provided by Society of Petroleum Engineers and Copyright Clearance Center.

Your confirmation email will contain your order number for future reference.

printable details

License Number	4422310999468
License date	Sep 05, 2018
Licensed Content Publisher	Society of Petroleum Engineers
Licensed Content Publication	SPE Proceedings
Licensed Content Title	Prediction of Hydrate Phase Equilibrium Conditions for Different Gas Mixtures
Licensed Content Author	Dhifaf Sadeq, Curtin University;Stefan Iglauer, Curtin University;Maxim Lebedev, Curtin University et al
Licensed Content Date	Jan 1, 2018
Type of Use	Thesis/Dissertation
Requestor type	author of the original work
SPE member	yes
SPE member number	4633660
Format	print and electronic
Portion	full article
Will you be translating?	no
Distribution	4
Order reference number	
Title of your thesis / dissertation	Gas Hydrates Investigation: Flow assurance for Gas Production and Effects on Hydrate-bearing Sediments
Expected completion date	Oct 2018
Estimated size (number of pages)	200
Requestor Location	Curtin University 26 Dick Perry Avenue Kensington
	Perth, WA 6151 Australia Attn: Dhifaf Sadeq
Billing Type	Invoice
Billing address	Curtin University 26 Dick Perry Avenue

205

Copyright Clearance Center

RightsLink®

Home   Account Info   Help   ✉

Title: Experimental pore-scale analysis of carbon dioxide hydrate in sandstone via X-Ray micro-computed tomography

Author: Dhifaf Sadeq,Stefan Iglauer,Maxim Lebedev,Taufiq Rahman,Yihuai Zhang,Ahmed Barifcani

Publication: International Journal of Greenhouse Gas Control

Publisher: Elsevier

Date: December 2018

© 2018 Elsevier Ltd. All rights reserved.

BACK   CLOSE WINDOW

Copyright Clearance Center

RightsLink®

Home | Account Info | Help

Title: Compressional wave velocity of hydrate-bearing bentheimer sediments with varying pore fillings

Author: Dhifaf Sadeq,Khalid Alef,Stefan Iglauer,Maxim Lebedev,Ahmed Barifcani

Publication: International Journal of Hydrogen Energy

Publisher: Elsevier

Date: 27 December 2018

© 2018 Hydrogen Energy Publications LLC. Published by Elsevier Ltd. All rights reserved.

Logged in as:
Dhifaf Sadeq
Curtin University
Account #:
3001311520

LOGOUT

BACK | CLOSE WINDOW

APPENDIX C: Attribution of Authorship

Paper: "Experimental determination of hydrate phase equilibrium for different gas mixtures containing methane, carbon dioxide and nitrogen with motor current measurements" Journal of Natural Gas Science and Engineering, 38, 59-73.

Authors and full affiliations: Dhifaf Sadeq[a,c], Stefan Iglauer[b], Maxim Lebedev [a], Callum Smith[a], Ahmed Barifcani[a].

[a] WA School of Mines: Minerals, Energy and Chemical Engineering, Curtin University, Bentley Western Australia 6102, Australia

[b] School of Engineering, Petroleum Engineering discipline, Edith Cowan University, Joondalup Western Australia 6027, Australia

[c] University of Baghdad, College of Engineering, Department of Petroleum Engineering, Baghdad, Iraq

	Conception and design	Acquisition of data and method	Data conditioning and manipulation	Analysis and statistical method	Interpretation and discussion	Final approval
Dr. Stefan Iglauer						×
I acknowledge that these represent my contribution to the above research output. Signature:						
Dr. Maxim Lebedev						×
I acknowledge that these represent my contribution to the above research output. Signature:						
Dr. Callum Smith				×	×	
I acknowledge that these represent my contribution to the above research output. Signature:						
Dr. Ahmed Barifcani	×					×
I acknowledge that these represent my contribution to the above research output. Signature:						

Conference Paper: "Hydrate Equilibrium Model and Cage Occupancies for $N_2 + CH_4$ and $N_2 + CO_2$ Gas Mixtures" in One Curtin International Postgraduate Conference, At Miri, Sarawak, Malaysia, 10-12 December (2017).

Authors and full affiliations: Dhifaf Sadeq[a,c], Stefan Iglauer[b], Maxim Lebedev [a], Callum Smith[a], Ahmed Barifcani[a].

[a] WA School of Mines: Minerals, Energy and Chemical Engineering, Curtin University, Bentley Western Australia 6102, Australia

[b] School of Engineering, Petroleum Engineering discipline, Edith Cowan University, Joondalup Western Australia 6027, Australia

[c] University of Baghdad, College of Engineering, Department of Petroleum Engineering, Baghdad, Iraq

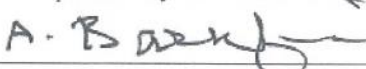|	Conception and design	Acquisition of data and method	Data conditioning and manipulation	Analysis and statistical method	Interpretation and discussion	Final approval
Dr. Stefan Iglauer						×
I acknowledge that these represent my contribution to the above research output. Signature: Igv						
Dr. Maxim Lebedev						×
I acknowledge that these represent my contribution to the above research output. Signature: Lebeda						
Dr. Callum Smith				×	×	
I acknowledge that these represent my contribution to the above research output. Signature: CSmith						
Dr. Ahmed Barifcani	×					×
I acknowledge that these represent my contribution to the above research output. Signature: A. Barifcani						

Conference Paper: "Prediction of Hydrate Phase Equilibrium Conditions for Different Gas Mixtures" in Offshore Technology Conference Asia. Offshore Technology Conference. Malaysia, 20 - 23 March (2018)

Authors and full affiliations: Dhifaf Sadeq[a,c], Stefan Iglauer[b], Maxim Lebedev [a], Ahmed Barifcani[a].

[a] WA School of Mines: Minerals, Energy and Chemical Engineering, Curtin University, Bentley Western Australia 6102, Australia

[b] School of Engineering, Petroleum Engineering discipline, Edith Cowan University, Joondalup Western Australia 6027, Australia

[c] University of Baghdad, College of Engineering, Department of Petroleum Engineering, Baghdad, Iraq

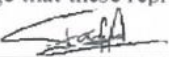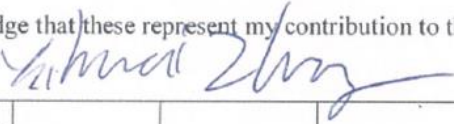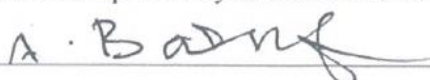|	Conception and design	Acquisition of data and method	Data conditioning and manipulation	Analysis and statistical method	Interpretation and discussion	Final approval
Dr. Stefan Iglauer						×
I acknowledge that these represent my contribution to the above research output. Signature:						
Dr. Maxim Lebedev						×
I acknowledge that these represent my contribution to the above research output. Signature: *lebedev*						
Dr. Ahmed Barifcani	×					×
I acknowledge that these represent my contribution to the above research output. Signature: A. Barif						

Paper: "Experimental Pore-scale Analysis of Carbon Dioxide Hydrate in Sandstone via X-Ray Micro-Computed Tomography" International Journal of Greenhouse Gas Control, 79, 73-82.

Authors and affiliations: Dhifaf Sadeq[a,c], Stefan Iglauer[b], Maxim Lebedev [a], Taufiq Rahman [a], Yihuai Zhang[a], Ahmed Barifcani[a].

[a] WA School of Mines: Minerals, Energy and Chemical Engineering, Curtin University, Bentley Western Australia 6102, Australia
[b] School of Engineering, Petroleum Engineering discipline, Edith Cowan University, Joondalup Western Australia 6027, Australia
[c] University of Baghdad, College of Engineering, Department of Petroleum Engineering, Baghdad, Iraq

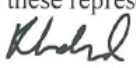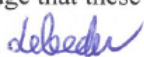|	Conception and design	Acquisition of data and method	Data conditioning and manipulation	Analysis and statistical method	Interpretation and discussion	Final approval
Dr. Stefan Iglauer	×			×	×	×
I acknowledge that these represent my contribution to the above research output. Signature:						
Dr. Maxim Lebedev		×	×			×
I acknowledge that these represent my contribution to the above research output. Signature:						
Taufiq Rahman				×		
I acknowledge that these represent my contribution to the above research output. Signature:						
Yihuai Zhang			×			
I acknowledge that these represent my contribution to the above research output. Signature:						
Dr. Ahmed Barifcani						×
I acknowledge that these represent my contribution to the above research output. Signature:						

Paper: "Compressional Wave Velocity of Hydrate-Bearing Bentheimer Sediments with Varying Pore Fillings" accepted for publication in the International Journal of Hydrogen Energy.

Authors and full affiliations: Dhifaf Sadeq[a,c], Khalid Alef[a], Stefan Iglauer[b], Maxim Lebedev [a], Ahmed Barifcani[a].

[a] WA School of Mines: Minerals, Energy and Chemical Engineering, Curtin University, Bentley Western Australia 6102, Australia

[b] School of Engineering, Petroleum Engineering discipline, Edith Cowan University, Joondalup Western Australia 6027, Australia

[c] University of Baghdad, College of Engineering, Department of Petroleum Engineering, Baghdad, Iraq

	Conception and design	Acquisition of data and method	Data conditioning and manipulation	Analysis and statistical method	Interpretation and discussion	Final approval
Khalid Alef					×	×
I acknowledge that these represent my contribution to the above research output. Signature:						
Dr. Stefan Iglauer						×
I acknowledge that these represent my contribution to the above research output. Signature:						
Dr. Maxim Lebedev		×	×			×
I acknowledge that these represent my contribution to the above research output. Signature:						
Dr. Ahmed Barifcani						×
I acknowledge that these represent my contribution to the above research output. Signature:						